

METALLURGICAL TRANSACTIONS

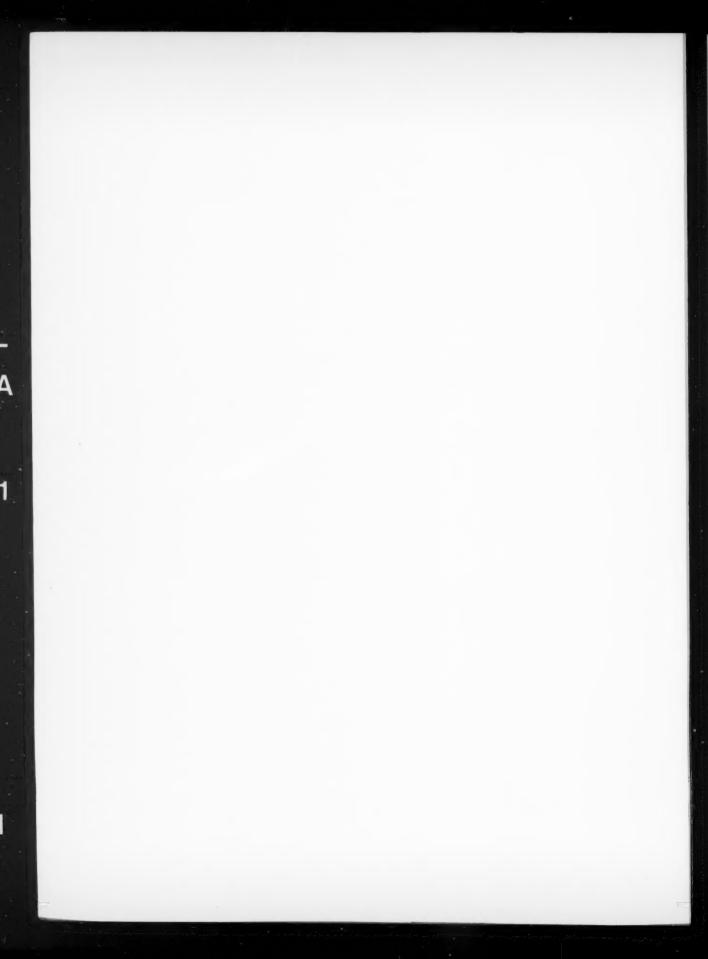
Volume 22A-No. 12

December 1991

1991 Index



TIMS
Minerals · Metals · Materials



Combined Author Index

Aaronson, H.I.

Abbaschian, R.

Abe. F. Ablitzer, D. Acharya, S. Adler, P.H. Advani, A.H. Agren, J.

Aikin, R.M., Jr. Akagi, S. Alam, M. Alcantara, N.G. Alexander, D.E. Allen, S.M.

Allen, W.P.

Allison, J.E Altstetter, C.J. An. Z.Z. Ando, S. Andrews, R.M.

Araki, H.

Ardell, A.J. Argyropoulos, S.A. Arsenault, R.J. Arzt. E. Asaki, Z.

Asaro, R.J Asayama, Y Asfahani R I Ashby, M.F.

Asundi, M.K. Aswath, P.B. Atkinson, C.

Atteridge, D.G. Attlegard, M. Awakura, Y.

Aver, R.

Bacon, D.J. Baek, w.-H Baragar, D. Baram, J.

Barlat, F. Barradas, R.G.

Basak, P.S Baskes, M.I. Bauer, E. Baxter, W.J Bayuzick, R.J.

Beatty, J.H. Becker, R. Beckermann, C Bernstein, I.M.

Berriche, R Bertero, G.A.

Beumler, H.W. Bewlay, B.P. Bhathena, N.M. Bhowai, P.R. Biegler, L.T.

Blanchard, P Bonnen, J.J. Bonnet, R. Borzone, G.

Bouchaud, E. Bowden, J.W. Boyer, A. Bray, J.W.

1341-1348A 1674-1678A 1259-12704 1271-1286A 2225-2235A

111-120B 259-261B 2237-2246A 677-688B

1745-1752A 1753-1759A 1381-1390A 142B 2181-2186A 1633-1646A 2863-2868A 2869-2876A 2877-2888A 2553-2563A 753-764A 765-773A 1007-1019

2605-2618A 261-264A 2393-2399A 2903-2915A 2309-2318A 125-128A 783-786A

2225-2235A 2061-2068A

417-427B 3013-3018A

837-851A

295-303B

631-639B

161-170A 2935-2945A 2959-2968A

2459-2466A

1211-12184

1247-1248A

1219-1224A

2917-2934A

569-574B

397-404B

1969-1978A

1185-1196A

2969-2974A 321-333A

2503-2514A

2515-2522A

1525-1534A

623-630B 3035-3039A

1311-1315A

1678-1680A

2713-2721A

675-683A

45-58A 349-361B 5-10A 1443-1451A

513-519A

521-529A

2445-2450A 357-366A

2713-2721A

2723-2732A

203-213A 2153-2156A

1999-20084

649-659B 3041-3050A 1535-1544A

1007-1019A

1145-1158A

2119-2123A

1945-1956A 1957-1967A

1021-10284

2947-2957A

2401-2405A

2277-2285A

641-648B

575-581B

915-9264

829-836A 817-828A

5-11B

Cantor, B. Cassada, W.A.

Brearley, W.H. Briant, C.L.

Brody, H.D.

Brooks, J.A. Brown, L.M.

Brungs, M.P. Bryant, J.D.

Burford, D.A. Burke, M.G.

Burkhart I F

Butler, J.F., Jr.

Cacciamani, G. Cahill, A.E. Caligiuri, R.D. Campbell, J.B. Campbell, P.C.

Butler, B.D.

Brimacombe J K

Catana, A. Chaigneau, R. Chakraborty, S. Chakravartty, J.K. Chan, K.S. Chan, S.L.I. Chandrasekharaiah,

Chang, S.N. Chang, Y.-B. Chang, Y.A.

Chang, Y.W. Chao, C.Y. Chapman, K.S. Chelakara, R. Chen, D. Chen, F.C. Chen, J.H. Chen, L. Chen, P.S.

Chen, S.-W.

Chen, S.I Chen, S.I. Chen, S.W. Chen, W. Chen, X. Chen, Y.-C. Chen, Y.S. Cheng, C.J. Cheng, L.

Cheruvu, N.S. Chiba, H. Chin, B.A. Cho, K. Cho, T.J. Choi, C.K.

Choi, J. Choi, Y.U. Chopra, M.A. Chou, J.S. Chou, K.-C. Christodoulou, L.

Chu, D. Chu, M.G. Chu, W.-Y. Chu, W.-Y. Chuang, T.H. Chuang, Y.-Y. Chun, B.S. Chun, Y-G. Cieslak, M.J. Clark, J.B.

Clevenger, E. Cohen, J.B. Colombie, C. Coltters, R.G. Combres, Y. Conrad, R.K. Cook DP

1287-1298A 129-137A 403-414A 2153-2156A

861-874B 2769-2778A

2779-2790A 2791-2805A 2761-2768A 915-926A 1159-11644 1693-1708A 305-307B 2009-2019A 447-4544 1775-1788A 455-468A 135-136B 2807-2809A 45-58A

2119-2123A 135-136B 2349-2357A 377-391A 2769-2778A 2779-2790A 2791-2805A 2487-2501A 287-297A 299-306A

1145-1158A 503-511B 429-437B 820-836A 2579-2586A 1937-1943A 685-695A

2645-2653A 2837-2848A 203-213A 267-271A 367-375A 1407-1415A 513-521B 2917-2934A 918-921B 2061-2068A 2287-2296A 2709-2711A 731-738A

203-213A 267-271A 653-656A 2837-2848A 499-506A 59-70A 1113-1115A 653-656A 225-234A 1945-1956A 1957-1967A

1811-1820A 499-502B 859-865A 367-375A 256-258A 1115-1119A 2587-2596A 2153-2156A 755-764B 2467-2473A 2265-2276A

27-31B 2009-2019A 1789-1799A 2837-2848A 71-81A 1801-1809A 2837-2848A 560-563B 2407-2414A 2429-2443A 2959-2968A 2039-2048A

Ferro, R. Field, R.D. 1721-1728A 2807-2809A 1535-1544A Fine, M.E. 661-668B Fink, J.L. 83-96A 121-134R Fleming, H.G.

11-18A 2173-2179A 927-934A

Daehn, G.S. Daeubler, M.A. Daniel, D.

Darken, L.S. Dave, N. Davenport, W.G. David, S.A.

Cortie, M.B.

Cotton, J.D.

Cullers, C.L.

Cutts, D.G.

Davidson, D.L.

Davis, L.C. de Bussac, A. de Keijser, Th.H. DeArdo, A.J. DebRoy, T.

Devadas, C.

Dève, H.E. Devine, T.M. Devletian, J.H. Dewing, E.W.

Dhers, J. Dimiduk, D.M. Dippenaar, R.J. Dixit, S.G. Dokiya, M. Dollar, M.

Domnanovitch, A. Doucet, A.B. Dragone, T.L. Dryden, J.R. Duffy, J. Durry, J. Duggan, B.J. Dunand, D.C. Dunning, J.S. Dutta, I.

Eady, J.A. Eagar, T.W.

Earthman, J.C. Easterling, K.E. Elangovan, S. Flfmark J Elzey, D.M. Enomoto, M.

Era. H.

Eric, R.H. Erlich, D.C. Eshelman, M.A. Euno, N. Evangelista, E. Evans, A.G.

Evans, J.W. Eyring, L.

Fabietti, L.M. Fang, H.S. Fang, Z. Fayeulle, S. Fedou, R. Felicelli, S.D. Ferreira, A.

Fitzner, K. Fleischer, R.L.

1595-1607A 623-627A

1113-1115A 513-519A 521-529A 2069-2076A

689-703E 225-232B 13-20B 677-688B 233-241B 243-257B 377-391A 97-112A 113-123A 3065-3067A 125-128A

1871-1880A 142B 219-224B 557-560B 307-319A 321-333A 335-349A 2975-2984A 2889-29024

177-182B 669-672B 2385-2392A 1573-1583A 775-781B 3075-3076A 2597-2603A 2445-2450A

2597-2603A 393-401A 1029-1036A 1159-1164A 367-375A 1126-1128A 2553-2563A

575-584A 65-71B 73-81B 2629-2635A 1071-1078A 1381-1390A 2297-2302A 837-851A 1235-1245A

1247-1248A 1341-1348A 251-253A 775-782A 53-63B 801-810B 2349-2357A 585-593A 441-446A 2257-2263A 2975-2984A 2107-2117A 121-134B

1323-1329A

1249-1258A 1674-1678A 19-23A 19-23A 1535-1544A 2133-2139A 847-859B 685-695A 2119-2123A 403-414A 1059-1070A 357-366A 264-267A

1103-1111A 129-137A

2156-2160A

403-414A

Flemings, M.C.

Foct, J. Frenk, A. Froet A.I Fruehan, R.J.

Fuiiwara, H. Fukunaka, Y.

Furuhara, T.

Gale, W.F. Ganesan, S Gangloff, R.P. Gao, Y.Y. Garcia, C.I. Garcia, J.C Garneau, S. Garrett, R.K., Jr.

Garrison, W.M., Geldenhuis, J.M.A. Génin, J.-M.R.

Gerberich, W.W. German, R.M. Ghali, E. Gillis, P.P.

Gingerich, K.A Giovanola, J.H. Girgis, M.

Goodwin, F.E. Gray, N.B. Gregolin, J.A.R. Greulich, F.A. Grieveson, P. Grinberg, Y. Grong, Ø. Gronsky, R. Grugel, R.N. Grujicic, M.

Gu. M.

Gupta, A.S. Gupta, S.K.

Ha, K.F. Hafley, J.L. Hajra, J.P.

Hales, S.J. Hall, E.L. Han, K.N. Han, Q. Han, Q. Hansen, S.S. Harris, T.M. Hawbolt, E.B.

Hayes, P.C. Heerema, R.H. Heinrich, J.C. Hellawell, A.

Hibi, T. Hillert, M. Hills C.R.

Hirato, T. Hirth, J.P.

Hjelen, J Ho, C.T. Hoadley, A.F.A. Hochman, R.F. Hoffman, M.A.

2761-2768A 2825-2828A 957-981A 269-294B 2385-2392A 139-141B 531-541A 33-38B 39-46B 481-489B 475-480B 629-631A 5-11B

631-639B 491-498B 1341-1348A

2451-2457A 889-900B 2415-2428A 1871-1880A 2401-2405A 623-630B 2959-2968A 938-941A 2039-2048A 2277-2285A 915-918B 1979-1991A 797-806A 59-70A 786-791A 623-630B 867-871A 807-815A 1937-1943A 2349-2357A 575-581B 623-630B 617-622A 13,20B 2181-2186A 915-926A 711-716B 467-473B 657-663A 2889-2902A 339-348B 2863-28684

261-264A 2553-2563A 593-605B 1037-1047A 427-439A 2619-2626A 755-764B 918-921B 2359-2374A 351-355A 307-319A 321-333A 335-3494 2769-2778A 2779-2790A 2791-2805A 211-217B 503-5118 847-859B 21-26B 641-648B

2695-2702A

1737-1743A

1887-1888

3035-3039A

711-716B

649-659B 397-404B 2187-2198A 2429-2443A 1049-1058A 569-574B 397-404B 1501-1510A 1331-1339A 657-663A 101-109B 139-141B 1453-1461A 1833-1840A

1841-1848A

Hofmeister, W.H.
Hogan, L.M. Hoglund, L. Hong, K.T. Hong, SH. Hong, S.J. Howe, J.M. Hsu, S.E. Hsu, T.J. Hsu, YF.
Hu, C.T. Hu, H. Hu, JH. Hu, Q.Z. Huang, F.H. Huang, JH. Huang, SC.
Huang, W. Hunt, J.D.
Hutchinson, B. Hwang, S.K. Hyman, M.E.
Ibaragi, M. Iksuchi, K. Incropera, F.P. Inoue, A. Inouye, T.K. Ipser, H. Irwin, D.W. Isaacs, J.A. Ishida, K. Ishihara, K.N. Ito, K.
Jackson, A.G. Jacob, K.T. Jacobson, D.L. Jain, N.C. Jamgotchian, H. Jani, S. Jansson, S.
Jardy, A. Jeannotte, D. Jeannotte, D.A. Jiang, R. Jiao, Q. Joarder, A. Johnson, W.C. Jonas, J.J.
Jones, J.W.
Jones, W.B. Jönsson, B.
Joshi, Y. Julsrud, S. Jung, WG. Jungling, T.L.
Kagawa, A. Kainuma, R. Kalcioglu, A.F. Kampe, S.L.
Kang, M. Kang, SJ.L. Kang, Y.S. Kang, Z. Karayaka, M. Katoh, M. Kaufman, M.J.
Kawada, T. Kawase, Y. Ke, W. Keller, K.W. Kelly, R.G. Kenik, E.A. Kho, Y.T.

2713-2721A

2723-2732A 575-584A

1745-1752A

935-937A 2969-2974A

415-425A 1287-1298A

1801-1809A

653-656A 1473-1478A

1479-1490A

Kim, Y.H.

Kimura, H. King, A.H. King, K.C. King, R.P.

Kinra, V.K.

Klein C.F.

Kieppa, O.J.

Kirkaldy, J.S. Kishitake, K.

25-33A 45-58A 27-31B Kluken, A.O. 723-729A 2049-2080A Kobayashi, S. Koczak, M.J. 2605-2618A 427-439A 2619-2626A 1911-1920A Konishi, Y. Korida, K. Kough, J.R. 941-945A 941-945A 1683-1687A Koyama, S. Kraus, H.G. 2681-2694A Kromp, W. 1647-1662A Kubin, L. Kumar, K.S. 2935-2945A Kumar, T.S.P. 2822-2825A Kundrat, D.M. Kung, S.-C. Kurz, W. 529-540R 2125-2132A 475-480B 1729-1736A Kwon, H. 575-584A 2855-2862A 441-446A 2849-2854A Kyllo, A.K. 439-445R 475-480B 839-845B Laasraoui, A. Lacaze, J. Laird, C. Laird, G., II 1721-1728A 607-616B Lake, J.S.H. Lalli, L.A. 1609-16134 2319-2325A 3041-3050A Lally, B. 1453-1461A Landes, J.D. 2975-2984A Laoui, T 2107-2117A Larson, R.S 111-120B Latanision, R.M. 1059-1070A Latreille, S Lawley, A. 357-366A 481-489B 183-192B Lawson, L. Le, H.M. 1811-18204 2565-2578A Lee, C.H. 2947-2957A 151-160A 1545-1558A Lee, C.S. Lee, D.-H. Lee, D.Y. 2069-20764 1633-1646A 1007-1019A 1049-1058A Lee, H.L. Lee, H.M. 2475-2485A 389B 831-837B Lee, J.C. 1103-1111A 2959-2968A 2039-2048A Lee JK Lee, S 569-574B 441-446A Lee, S.-C. 136-139B 2009-2019A Lee, S.-M. Lee, Y.T. 447-4544 Leta, D.P. 2969-2974A Leu, S.S. Levaillant, Ch. Levi, C.G. 783-786A 1323-1329A 697-707A 295-303B 2141-2152A Lewand Li, B.Q. Li, F. Li, H. Li, Q. Li, W.-B. Li, Z. 927-934A 3075-3076A 2935-2945A 2677-2680A 531-541A 253-255A 323-332B Liang, H. Liaw, P.K. Lin, D.W. Lin, X. Lin, Y. Lin, Y.L. 1889-1892A 139-149A 2629-2635A 323-332B Lipsitt, H.A. Liu, T.F. 2153-2156A 853-858A 1889-1892A 139-149A 2487-2501A Liu. Y.

3003-3011A 2393-2399A 1177-1183A 2199-2210A 53-63B 801-810B 641-651A 1511-1524A 251-253A 791-792A 775-782A 1969-1978A 1103-1111A 1680-1683A 657-663A 439-445R 2733-2745A 2747-2759A 1627-1631A 295-303B 629-631A 839-845B 243-257B 2597-2603A 1021-1028A 2733-2745A 2747-2759A 717-727B 363-383B 673-675B 3051-3057A 2523-2533A 1119-1122A 1115-1119A 2587-2596A 153-161B 151-160A 1545-1558A 2211-2223A -425A 1709-1720A 2156-2160A 641-648B

649-659B 455-468A 2141-2152A 523-527B 351-355A 3003-3011A 2733-2745A 2747-2759A 1059-1070A 2869-2876A 543.555A 1627-1631A 2637-2643A 935-937A 853-858A 1889-1892A 139-149A 755-764B 2579-2586A 2877-2888A 2818-28224 1197-1209A 853-858A 1889-1892A 139-149A 367-375A 1821-1831A 2645-2653A 2407-2414A 709-714A 1129A 1969-1978A 25-33A 83-96A 1647-1662A 121-134B 2849-2854A 2061-2068A 1126-1128A 1071-1078A 2695-2702A 2160-2162A 305-307B 455-468A 2069-2076A 2709-2711A 859-865A 1407-1415A 1721-1728A 1407-1415A 1417-1423A 2265-2276A 261-2644

1121-1125A 1745-1752A 1753-1759A 21-26B 1145-1158A 2077-2084A 677-688B 136-139B

469-477A

875-888B

569-574B

1001-1006A

2277-2285A

1595-1607A

1865-1869A

737-1743A

1887-1888A

1453-1461A

2523-2533A 2125-2132A

235-249A

489-498A

211-217B

469-477A

467-473B

11-18A

557-567A

593-605B

1559-1571A

3019-30244

1647-1662A

3025-3033A

938-941A

469-477A

867-871A

807-815A

633-640A

1079-1082A

557-560B 1037-1047A

1037-1047A

2303-2307A

1647-1662A 1721-1728A

1453-1461A

1573-1583A

2162-2165A

1680-1683A 685-695A

2667-2676A

2855-2862A

2309-2318A

2049-2060A 33-38B

715-721A 2535-2538A

783-786A

641-651A

73-81B

83-100B

1945-1956A

1957-1967A

2629-2635A 161-170A

1663-1672A

1789-1799A

2247-2256A 903-913A

1633-1646A

2855-2862A

1126-1128A

1225-1233A

1311-1315A

1305-1310A 2199-2210A 2917-2934A

689-703B 225-232B

569-574A 1466A

363-383B 783-786A

765-774B 873-877A

1709-1720A 1083-1091A

Machmeier, P.M. MacMillan, N.H. Maehara, Y. Mahapatra, R.B. Maiima, H.

Makhlouf M M Maloney, J.L. Mannan, S.K. Marcotte, V.C Marek, M.

Liu, Z. Liu, Z.-K.

Lograsso, T.A.

Loubradou, M. Luey, K. Lynch, D.C.

Margolin, H. Mason, J.T. Masumoto, T. Matsumara, O. Matthew, S.P. Matuszewski, T. Mauer, F.A. Mavrocordatos, C.E. Mayo, D.E. Mazumdar, B. McClung, R.C. McCormick, P.G. McCullough, C. McCune, R.A. McEvily, A.J.

McIntyre, J.F. McNallan, M.J. McNelley, T.R. McQueen, H.J.

Medrano, R.E.

Megill, R.W. Mehrabian, R. Mehrotra, G.M. Meletis, E.I. Mendiratta, M.G. Meschel, S.V.

Meyers, M.A. Mgaidi, A. Michaud, V.J. Miller, J.D. Miller, W.K Milligan, W.W. Mills, W.J. Min, D.J.

Minamino, Y. Misra, M.S. Mitra, U.

Mittemeijer, E.J.

Miwa, T. Mivamoto, Y Mohamed, F.A. Moran, B. Mori. N. Morland, P.T. Morris, J.W., Jr.

Morrison D.I. Mortensen, A.

Muan, A. Mullins, W.W.

Mundschau, M. Munir, Z.A. Mura, T. Murr, L.E.

Nakatani, M.

Nam, S.W.

Nakagawa, H. 543-555A Nakamura, S. 823-829B 2085-2095A 935-937A Nandapurkar, P.J. 889-900B 1775-1788A 2655-2665A

Naslain R Natarajan, S. Nava, Z. Neu, R.W. Newman, R.C. Ni, J. Nielsen, R.L. Nishikawa, K. Nishizawa, T. Nix, W.D. Noda, T. Noebe, R.D. Nomura, K. North, T.H.

Nardone, V. Nardone, V.C.

Norton, S.J. Notis, M.R. Nourbakhsh, S.

Ochiai S Ocken, H. Octor, H. Octor, H. Odegård, R. Ogawa, O. Ögi, K. Ohno, R. Ohriner F.K.

Okamoto, T. Okazaki, M. Olivares, R. Olson, G.B. Osamura, K.

Osseo-Asare, K. Otsubo, F.

Ozturk, B.

Pahi S K Padmavardhani, D.

Page, R.A. Pak, J.J. Palencia, I. Pan, Y.C. Pan, Z.-L.

Panchanadeeswaran, Park, I.-G. Paterson, E.A. Patterson, B.R.

Patwardhan, A.K. Pellerin, V. Perepezko, J.H.

Perng, T.-P. Perovic, V. Peters, M.

Peteves, S.D.

Pfeifer, M.J. Piascik, R.S. Piccone, T.J.

Pickering, H.W. Pinczolits, H. Pitchure, D. Plichta, M.R. Poirier, D.R.

Polonis, D.H. Pond, R.C. Potgieter, J.H. Pottore, N.S. Prabhu, K.N. Prasad, Y.V.R.K.

Prescott, P.J. Prewo, K.M. Puls, M.P. Purdy, G.R. Pvun, S.-I.

Qi, G. Qiu, C. Quenisset, J.M.

2107-2117A 171-182A 2133-2139A 33-38B 393-401A 661-668B 531-541A 349-361B 1709-1720A 5-11B 441-446A 1029-1036A 2225-2235A 1595-1607A 783-790B 1627-1631A 2822-2825A 467-473B 1737-1743A 3059-3064A

> 2085-2095A 983-991A 1021-1028A 831-837B 47-52B 1663-1672A 405-416B 447-465B 983-991A 783-786A 479-487A 1425-1434A 305-307B 2199-2210A 705-710B 323-332B 251-253A 791-792A 775-782A

3035-3039A 2985-2992A 2993-3001A 377-391A 765-774B 2818-2822A 1801-1809A 607-616A

1525-15344 1615-1626A 861-874B 19-23A 19-23A 2319-2325A 1535-1544A 753-764A 765-773A 1159-1164A 709-714A 1129A 1259-1270A 1921-1935A 2415-2428A 2761-2768A 2825-2828A 323-332B 2597-2603A 467-473B 1381-1390A 889-900B 847-859B 1049-1058A 1185-1196A 2173-2179A 1871-1880A 717-727B 2985-2992A 2993-3001A 829-836A 2339-2348A 529-540B 171-182A 2327-2337A

219-224B 2187-2198A 2133-2139A 807-815A

1159-1164A 2407-2414A

Kim, B.C.

Kim, H.-K.

Kim, H.S.

Kim, N.J.

Kim, W.T

Rabin, B.H. Rachev, I.P. Radhakrishnan, B. 277-286A

711-716B 513-521B

867-871A 191-202A

3071-3075A

1501-1510A 101-109B

2339-2348A

641-651A 3025-3033A 1901-1909A

2385-2392A

1849-1855A

1367-1380A 3059-3064A

163-175B 1525-1534A

153-161B

264-267A 193-209B 363-383B 607-616A

617-622A 191-202A

2385-2392A

2713-2721A

2723-2732A

2133-2139A

1435-1441A

2429-2443A

2503-2514A 2247-2256A

2257-2263A

2009-2019A 2257-2263A

3059-3064A

2125-2132A

3075-3076A

489-498A

163-175B

861-874B 875-888B

307-319A 321-333A

335-3494

333-338B

499-502B 823-829B

1721-17284

1122-1125A 1811-1820A

455-468A 1881-1886A

3019-3024A

2133-2139A

1029-1036A

2349-2357A 163-175B

1673-1674A

2429-2443A

1491-1500A

389B 585-593A

697-707A

791-799B

941-945A 941-945A

385-388B

1683-1687A

5-10A 1857-1864A

2809-2818A 2459-2466A 2703-2707A

1857-1864A 1287-1298A

1349-1365/

1165-1175A 287-297A

299-306A

1185-1196A

531-541A 2667-2676A

2947-2957A

1881-1886A

429-437B 309-321B 811-822B

5-10A 321-333A

879-886A

35-43A 633-640A

491-498B 541-555B

5-10A

333-338B 557-567A 887-902A 2277-2285A

Raghavan, K.S. Rajakumar, V. Ramadhyani, S. Ramon, J.T. Ramos Lucas, M.A. Rao, K.T.V. Rapp, R.A.

Rappaz, M. Ravichandran, N. Rawal, S.P. Rawers, J.C. Ray, R. Ray, S.Kr. Regnard, C Renon, H. Reuter, M.A Reynolds, A.P. Reynolds, W.T., Jr. Rhee, W.H. Richards, G.G.

Ricker, R.E. Ricou, R. Ritchie, I.G.

Ritchie, R.O. Robert, G. Robinson, M.B

Robinson, S.L. Rocher, J.P. Rohatgi, P.K. Romig, A.D., Jr. Roth, R.S. Ruddle, G. Ruhr, M. Ryoo, H.S. Ryum, N.

Sadler, P. Saetre, T.O. Sahai, Y.

Sahin, O Saida, J. Sakai, N Sakuma, Y. Samarasekera, I.V.

Samuel, F.H. Sandlin, A.C. Sano, N.

Sagib, M. Sarma, D.S.

Saxena, A Schaefer, R.J. Schaffer, G.B. Schamm, S. Schetky, L.M. Schlautmann, J.J. Schmidt, C.G. Scholey, K.E. Schrems, K.K. Schuster, J.C. Scully, J.R. Sedy, E.B. Seetharaman, V Sehitoglu, H.

Sekhar, J.A. Seo, K.W. Serra, A Shang, S.-S. Shangguan, D.

Shechtman, D. Shen, Y. Shenoy, R.N. Shercliff, H.R. Shewmon, P Shewmon, P.G. Shieh, P.-C. Shiflet, G.J. Shih, C.F. Shin, D.H. Shingu, P.H. Shoji, T. Siles, J.L.

Silvain, J.-F. Singh, V. Sismanis, P.G. Sission, R.D., Jr. Siwecki, T. Small, W.M. Smialek, J.I. Smith, D.M. Sohn, H.S. Sohn, H.Y.

Solheim A Soykan, O.

Spanos, G.

Speed, J.A. Sridhar, G. Srikanth, S. Srinivasan, A.V. Stadelmann, P. Starink, M.J. Starke, E.A., Jr.

Stefanescu, D.M. Stickney, M.J. Stobbs, W.M. Stoner, G.E. Stoop, P.M. Strife, J.R.

Sun, P.F. Sundararaian, G. Sundararaman, M. Sundman, B. Sunwoo, A.J. Suresh, S. Sutton, A.P. Suzuki, M.

Swięch, W. Szekely, J.

Tagaya, A. Taguchi, N. Takatsuka, K. Takechi, H Takeuchi, N. Tamura, K. Tanaka, E.

Tanaka, T. Taniuchi, M. Taricco, F Tawancy, H.M.

Taylor, K.A. Tedenac, J.C. Tewari, S.N. Thadhani, N.N. Themelis, N.J. Thi, H.N. Thiagarajan, S.

Thomas, G.J. Thompson, A.W.

Thompson, R.G.

Thoysen, K. Tiller, W.A. Tirupataiah, Y. Toguri, J.M Toker, N.Y.

Tokinori, K Tokuda, M. Tomita, Y. Trapaga, G. Trivedi, R.

Tseng, A.A. Tsu, I.-F. Tsukihashi, F. Turner, M.E., Jr.

161-170A Uen. G.C. 935-937A Ule, R.L. Ushio, R. 2849-2854A Uwakweh, O.N.C. 2097-2106A 1501-1510A 3003-3011A

797-806A

499-506A

417-427B

1001-1006A

2681-2694A

219-224B

730-752A

575-584A

737-754B

791-799R

560-563B

831-837B

801-810B

1674-1678A

1937-1943A

1122-1125A

1145-1158A 665-674A

607-616B

623-627A

287-2974

299-306A

385-388B

1937-1943A

1139-1144A

1849-1855A

1165-1175A

1767-1774A

2375-2384A

499-506A 2211-2223A

903-913A

817-828A

1185-1196A

2761-2768A

2825-2828A

1311-1315A

901-914B

499-502B

631-639B

489-498A

783-786A

631-639B

251-253A

791-792A

1425-1434A 629-631A

2855-2862A 3067-3071A

1463-1465A

2359-2374A

2401-2405A

2467-2473A

685-695A

183-192B

258-261A 258-261A

879-886A

1443-1451A

1615-1626A

2445-2450A

557-567A

887-902A

831-837B

1317-1322A

2375-2384A

617-621B

689-703B

225-232B

439-445B 1093-1102A

901-914B

235-249A

3051-3057A

1247-1248A

1249-1258A

2523-2533A

1767-1774A

215-224A

333-338B

499-502B

19-23A

2085-2095A

513-519A

521-529A

71-81A

171-182A

183-189A

53-63B

5-11B

Van Den Avyle, J.A. Van Der Merwe, J.H. van der Pers, N.M. Van Deventer, J.S.J. Van Mourik, P. Vandermeer, R.A.

Varin, R.A. Varma, S.K.

Vasudévan, A.K. Verhoeven, J.D. Vincent, L. Virk. I.S. Viskanta B Vitek, J.M.

Vivés, C. Vogt, J.-B. Vold, C.L. Voorhees, P.W.

Wada, T. Wadier, J.F. Wadley, H.N.G. Wagner, J.A. Wagnière, J.-D. Wagoner, R.H.

Wahi, R.P. Walker, N. Wall, R.N. Wallach, E.R. Walston, W.S. Wan, B.Y Wang, G.Z. Wang, L.

Wang, P. Wang, P.-C. Wang, W.-H.

Wang, Z.

Wang, Z.F. Wang, Z.G. Warren, G.W. Was, G.S. Watanabe, Y. Watson, K.D. Wayman, C.M.

Webb, G. Wei, Q. Weiss I. Weisch, G.

Weng, L.-C Whelan, E.P. Whittenberger, J.D. Wierszyllowski, I.A

Wilcox, B.C. Willis, C.F. Wilmott, P. Wisell, H. Won, C.W. Wren, G.G Wright, R.N. Wu, C.C

Wynblatt, P.

Xu, Y.B. Xue, Y.-H.

Yada, H. Yamada, Y. Yamanaka, R. Yamane, T. Yamatsuta, K. Yang, J.R. Yang, J.H. Yang, S.-C. Yang, Z. Yokokawa, H. Yoo, M.K. Yoon, D.N. You, C.P. Young, J.D.

1407-1415A 47-52B

2429-2443A 1165-1175A 1957-1967A 541-555B 665-674A 1367-1380A 2039-2048A 2545-2552A 258-261A 258-261A 264-267A

1979-1991A

797-806A

2523-2533A 1535-1544A 2545-2552A 513-521B 233-241B 243-257R 193-209B 2385-2392A 2039-2048A 2199-2210A

983-991A 111-120B 467-473R 2809-2818A 139-141B 3003-3011A 1775-1788A 2655-2665A 499-506A 861-874B 1609-1613A 2451-2457A 1443-1451A 765-774B 2287-2296A 723-729A 3013-3018A

2160-2162A 1678-1680A 1479-1490A 2287-2296A 2822-2825A

1585-1593A 2677-2680A 723-729A 521-529A 1633-1646A 2097-2106A 617-621B 1473-1478A 1479-1490A 125-128A 1761-1765A 1721-1728A 1121-1125A 709-714A

1129A

1821-1831A 983-991A 1595-1607A 993-999A 731-738A 2031-2038A 2889-2902A 1219-1224A 1391-1405A 560-563B 641-651A 277-286A 1407-14154 1417-1423A 2265-2276A

1833-1840A 1841-1848A

723-729A 2703-2707A

1674-16784 569-574B 839-845B 783-786A 2085-2095/ 2579-2586A 786-791A 1079-1082A 3075-3076A 2153-2156A 2969-2974A 2445-2450A Youzhashi A.A.

Zacharia, T. Zaiac, S Zee, R.H. Zhang, D.L. Zhang, G. Zhang, M.-X. Zhang, M.-Zhang, R.J. Zhang, W. Zhang, X. Zhang, Y. Zheng, M Zheng, X.

Zheng, Z. Zhou, D.S. Zhou, Y. Zhu, D.

Zhu, L. Zhu, Y.T. Zhu, Z. Zimmermann, M. Zocco, T.G. Zok, F. Zou H Zschack, P. Zuzanak, A.

775-781R

233-241B 243-257B 2681-2694A

859-865A 2487-2501A 2160-2162A 1865-1869A 1585-1593A 705-710B 918-921B 723-729A 507-511A 3071-3075A 507-511A 2160-2162A 1349-1365A 2822-2825A 309-321B 811-822B 2709-2711A 2287-2296A 1993-1998A 101-109B

1381-1390A

1511-15244

729B



Combined Subject Index

See Noise control		Adhesivity See Adhesion	
Aberration See Defects		Adsorption Knowledge-Based Simulation and Identification of Various	
Absolute temperature See Temperature		Metallurgical Reactors. Aerospace	541-555B
Absolute viscosity		Mechanical Properties of High Temperature Alloys of AIRu. Fracture of Single Crystals of the Nickel-Base Superalloy	403-414A
See Viscosity Absorbance		PWA 1480E in Helium at 22°C. Microstructural Evolution in Rapidly Solidified Al—Fe Alloys:	731-738A
See Absorption (energy) Absorbing		an Alternative Explanation. Strength and Ductile-Phase Toughening in the Two-Phase	927-934A
See Absorption (energy)		Nb/Ñb₅Si₃ Alloys. Aerospace engines	1573-1583A
Absorption (energy) In Situ Technique for Measuring the Absorption During Laser		See also Airplane engines	
Surface Remelting. Chlorosulfonated Polyethylene: a Versatile Polymer for Damping Acoustic Waves.	139-141B 633-640A	Aerospace engines, Materials selection Thermomechanical Fatigue of Particulate-Reinforced Aluminum 2xxx-T4.	697-707A
Absorption coefficient See Absorption (energy)		Age hardening See Aging	
Acicular structure The Origin of Transformation Textures in Steel Weld Metals Containing Acicular Ferrite.	657-663A	Aging (artificial) Aging (natural) Precipitation hardening	
Acid dissolution		Age hardening steels See Precipitation hardening steels	
The Dissolution Behavior of Metals From Ag/Cu and Ag/Au Alloys in Aidic and Cyanide Solutions. Acid leaching	755-764B	Ageing See Aging	
Reductive Ammonia Leaching of Manganese Nodules by Thiosulfate.	259-261B	Agents See Fluxes	
Dissolution of Malachite in Aqueous Ethylenediaminetetr- aacetate Solution.	569-574B	Reducing agents Stabilizers (agents)	
The Dissolution Behavior of Metals From Ag/Cu and Ag/Au Alloys in Aidic and Cyanide Solutions.	755-764B	Wetting agents	
Acidity See pH		Aging See also Aging (artificial) Aging (natural) Strike aging	
Acoustic emission Fracture Initiation at Hydrides in Zirconium. Acoustic emission testing	2327-2337A	Strain aging The Effect of Tungsten on Dislocation Recovery and Precipitation Behavior of Low-Activation Martensitic 9Cr Steels.	2225-2235A
Behavior of Acoustic Emission for Low-Strength Structural Steel During Fatigue and Corrosion Fatigue.	2677-2680A	Aging (artificial) See also Quench aging Electron Microscopy Study of the Aging and First Stage of	
Acoustic properties See Acoustic emission		Tempering of High-Carbon Fe—C Martensite. Aging Characteristics of Electron Beam and Gas Tungsten	797-806A
Actinide metals See Uranium		Arc Fusion Zones of Al—Cu—Li Alloy 2090. Phase Transformation in an Fe—9.0Al—29.5Mn—1.2Si	903-913A 1407-1415A
Activation energy Correction to "Literature Survey on Diffusivities of Oxygen Aluminum, and Vanadium in Alpha Titanium, Beta Titanium,		Alloy. A New Phase in an Fe—9.0AI—29.5Mn—1.2Si Alloy. Microstructural and Thermal Stability of a Ti—43Al Alloy Containing Dispersoids of Titanium Di-Boride.	1417-1423A 1721-1728A
and in Rutille". Activation Energy of δ-Γ ₁ Transformation in a Zn—Fe Electro- deposited Coating.	1121-1125A 1887-1888A	Phase Transformation in an Fe—10.1AI—28.6Mn—0.46C Alloy. Effect of Reinforcement on the Aging Response of Cast 6061	2265-2276A
Activation energy, pH effects Dissolution of Malachite in Aqueous Ethylenediaminetetr- aacetate Solution.	569-574B	Al—Al ₂ O ₃ Particulate Composites. Aging (natural)	2553-2563A
Activity (chemical)	000 01 10	Room-Temperature Aging of Hydrogen in α-Iron After Cathodic Charging.	261-264A
Activities of Boron in the Binary Ni—B and the Ternary Co— Fe—B Melts.	47-52B	Lattice Changes of Iron—Carbon Martensite on Aging at Room Temperature.	1957-1967A
Activities of Chromium in Molten Copper at Dilute Concentra- tions by Solid-State Electrochemical Cell. Thermodynamics of Aluminum—Barium Alloys. A Degenerate Electron Gas Model for Solutions of Aluminum	475-480B 607-616B	Morphology and Aging of the Martensite Induced by Cathodic Hydrogen Charging of High-Carbon Austenitic Steels. Agitation	1979-1991A
in Cryolite Melts. Thermochemical Nature of Minor Elements in Copper Smelt-	669-672B	See Bubbling	
ing Mattes. Phase Relations and Thermodynamics of the System Fe—	677-688B	Air arc melting See Electric arc melting	
Cr—O in the Temperature Range of 1600-1825°C (1873-2098K) Under Strongly Reducing Conditions.	689-703B	Air induction melting See Induction melting	
A Thermodynamic Study of the System Fe _x O + Al ₂ O ₃ + SiO ₂ at 1673K.	839-845B	Air melting See Melting	
A Reassesment of the Activity of Chromium in the Fe—Cr—O System at 1873K. Dissolution Equilibrium of Magnesium Vapor in Liquid Iron. An Experimental Study of Carbide/Austenite Equilibria in the	915-918B 918-921B	Aircraft components A New Phase in a Rapidly Solidified and Consolidated NbAis—1TiB> Alloy.	1901-1909A
High-Speed Steel Alloy System. Activity (chemical), Alloying effects	1391-1405A	Aircraft components, Joining Delayed Failure of PH13-8Mo Steel Plated With Aluminum-IVD.	2935-2945A
Effect of Phosphorus on Carbon Activity, Carbide Precipita- tion, and Coarsening in Ferritic Fe—C—P Alloys. Activity (chemical), Composition effects	35-43A	Aircraft engines See Aerospace engines	2300 23000
Thermodynamic Stability of Palladium Alloys. I. The Palladium—Niobium System.	1937-1943A	Aircraft equipment	
Activity coefficients See Activity (chemical)		See Aircraft components Airplane engines, Materials selection Shock Densification/Hot Isostatic Pressing of Titanium Alumi-	
Adhesion Development of Vibration-Damping Resins for Room- Temperature Application.	629-631A	nide. Alfven waves See Magnetohydrodynamics	2667-2676A
Adhesion, Impurity effects Effect of Sulfur Removal on Al ₂ O ₃ Scale Adhesion.	739-752A	Alkali metals See Lithium	
Adhesives See Binders (adhesives)		Potassium Sodium	

Alkaline earth metal alloys See Magnesium base alloys		Stress Concentration at a Notch Tip in Unidirectional Metal Matrix Composites.	2085-2095A
Alkaline earth metal compounds See Barium compounds		Chemical Stability of Zirconia-Stabilized Alumina Fibers Dur- ing Pressure Infiltration by Aluminum. Lorentz Force Infiltration of Fibrous Preforms.	2855-2862A 2903-2915A
Beryllium compounds		Aluminum, Diffusion	2500-25107
Alkaline earth metals See Barium Magnesium		Correction to "Literature Survey on Diffusivities of Oxygen Aluminum, and Vanadium in Alpha Titanium, Beta Titanium,	1121 1125A
Alkaline leaching Leaching Kinetics of Copper From Natural Chalcocite in Alka-		and in Rutile". Aluminum, Extraction	1121-1125A
line Na ₄ EDTA Solutions. Dissolution of Malachite in Aqueous Ethylenediaminetetr-	295-303B	Loss of Current Efficiency in Aluminum Electrolysis Cells. The Wettability of Carbon/TiB ₂ Composite Materials by Alu-	177-182B
aacetate Solution.	569-574B	minum in Cryolite Melts. A Thermodynamic and Experimental Study of the Electro-	617-621B
Alkalinity See pH		chemically Induced Cooling of the Anode in Hall—Heroult Cells.	831-837B
Alloy cast iron, Corrosion		Aluminum, Forming	
Modeling of the Corrosion Behavior and Its Interrelation With the Deformation Behavior and Microstructure in a Newly Developed 7.5Mn—5Cr—1.5Cu Alloy White Iron.	2319-2325A	Earing in Cup Drawing Face-Centered Cubic Single Crystals and Polycrystals. Aluminum, Mechanical properties	1525-1534A
Alloy cast iron, Mechanical properties On Thermal Shock Resistance of Austenitic Cast Irons.	1821-1831A	The Influence of Applied Stress, Crack Length, and Stress Intensity Factor on Crack Closure.	1559-1571A
Alloy cast iron, Metallography		Aluminum, Metal working	
Use of Differential Interference Contrast Microscopy to Detect Duplex Carbides in Alloy White Cast Irons.	1673-1674A	Dynamic Recrystallization During Hot Deformation of Aluminum: a Study Using Processing Maps.	2339-2348A
Alloy cast iron, Microstructure On the Nature of Eutectic Carbides in Cr—Ni White Cast		Aluminum, Reactions (chemical) The K ₂ ZrF ₈ Wetting Process: Effect of Surface Chemistry on	
Irons. Alloy plating	1709-1720A	the Ability of a SiC-Fiber Preform To Be Impregnated by Aluminum.	2133-2139A
The Effect of Continuous Heating on the Phase Transforma-		Aluminum, Rolling	
tions in Zinc—Iron Electrodeposited Coatings. Alloy steels	1737-1743A	Analysis of an Aluminum Single Crystal With Unstable Initial Orientation (001)[110] in Channel Die Compression.	45-58A
See also Chromium steels		Aluminum, Solubility	
High alloy steels High strength steels		A Degenerate Electron Gas Model for Solutions of Aluminum in Cryolite Melts.	669-672B
Low alloy steels Molybdenum steels		Solid Solubilities of Manganese and Titanium in Aluminum at 0.1 MPa and 2.1 GPa.	783-786A
Nickel steels		Aluminum, Ternary systems	
Precipitation hardening steels Tungsten steels		Calculation of Phase Diagrams and Solidification Paths of Aluminum-Rich Al—Li—Cu Alloys.	2837-2848A
Alloy steels, Steel making Distribution of Antimony Between Carbon-Saturated Iron and		Aluminum base alloys, Casting	
Synthetic Slags.	136-139B	Application of Thermodynamic Models to the Calculation of Solidification Paths of Aluminum-Rich Al—Li Alloys.	267-271A
Alloying See also Mechanical alloying		Behavior of Metal Alloys in the Semisolid State. Crystallization of a Faceted Primary Phase in a Stirred Slurry.	269-294B 575-584A
Microalloying		Heat Flux Transients at the Casting/Chill Interface During So-	
In Situ Technique for Measuring the Absorption During Laser Surface Remelting.	139-141B	lidification of Aluminum Base Alloys. Contribution to the Metal/Mold Interfacial Heat Transfer.	717-727B 729B
The Mass Transfer Kinetics of Niobium Solution Into Liquid Steel.	417-427B	Microstructural Evolution in Rapidly Solidified Al—Fe Alloys: an Alternative Explanation.	927-934A
Alloying elements		Behavior of Metal Alloys in the Semisolid State.	957-981A 2487-2501A
The Effect of Temperature and Nitrogen Content on the Parti- tioning of Alloy Elements in Duplex Stainless Steels.	2173-2179A	Nucleation of Solidification in Liquid Droplets. Aluminum base alloys, Composite materials	2407-2501A
Alloys		The Effect of Particulate SiC on Fatigue Crack Growth in a	97-112A
See Brazing alloys Dispersion hardening alloys		Cast-Extruded Aluminum Alloy Composite. Tensile Deformation and Fracture Toughness of	
Precipitation hardening alloys		2014 + 15 vol.% SiC Particulate Composite. Microstructurally Toughened Particulate-Reinforced Alumi-	113-123A
Shape memory alloys Spring alloys		num Matrix Cómposites. Dynamic Fracture Behavior of SiC Whisker-Reinforced Alu-	171-182A
Alpha annealing		minum Alloys.	367-375A
See Annealing Alphatizing		On the Influence of Ply-Angle on Damping and Modulus of Elasticity of a Metal-Matrix Composite. Thermomechanical Fatigue of Particulate-Reinforced Alumi-	641-651A
See Annealing		num 2xxx-T4.	697-707A
Alumina See Aluminum oxide		Fatigue Behavior of a 2xxx Series Aluminum Alloy Reinforced With 15 vol.% SiC _p .	1007-1019A
Aluminium		Tribological Behavior and Surface Analysis of Tribodeformed Al Alloy—50% Graphite Particle Composites.	1435-1441A
See Aluminum		Mechanical Behavior of Cast Particulate SiC/AL (A356) Metal Matrix Composites.	1585-1593A
Aluminum, Alloying elements In Situ Formation of Three-Dimensional TiC Reinforcements		The Mechanical Behavior of a Hybrid Metal Matrix Composite.	2107-2117A
in Ti-TiC Composites. Aluminum, Binary systems	859-865A	Microstructure Property Relationships and Hydrogen Effects	
Crystallographic Characterization of Some Intermetallic		in a Particulate-Reinforced Aluminum Composite. Effect of Reinforcement on the Aging Response of Cast 6061	2445-2450A
Compounds in the Al—Cr System. Thermodynamics of Aluminum—Barium Alloys.	5-10A 607-616B	Al—Al ₂ O ₃ Particulate Composites. Third-Order Bounds on the Elastic Moduli of Metal-Matrix	2553-2563A
The Al-Al _B Mo ₃ Section of the Binary System Aluminum— Molybdenum.	1729-1736A	Composites.	3065-3067A
Heats of Formation of Aluminum—Cerium Intermetallic Com- pounds.	2119-2123A	Aluminum base alloys, Corrosion On the Stress Corrosion Cracking of Al—Li Alloys: the Role	
Nonequilibrium Behavior in the Al-Ge Alloy Systems: In-		of Grain Boundary Precipitates. Pitting Corrosion Behavior of Powder Metallurgy Mechani-	264-267A
sights Into the Metastable Phase Diagram. Thermodynamic Equilibrium in the Low-Solute Regions of	2141-2152A	cally Alloyed IN-9052.	938-941A
Plutonium-Group IIIA Metal Binary Systems.	2237-2246A	Cleavage Crystallography of Liquid Metal Embrittled Alumi- num Alloys.	1849-1855A
Aluminum, Casting An Improved Mathematical Model for Electromagnetic Cast-		A Critical Evaluation of the Stress-Corrosion Cracking Mech- anism in High-Strength Aluminum Alloys.	2407-2414A
ers and Testing by a Physical Model. An Ultrasonic Method for Reconstructing the Two-Dimensional Liquid/Solid Interface in Solidifying Bodies.	121-134B 467-473B	Environmental Fatigue of an Al—Li—Cu Alloy. I. Intrinsic Crack Propagation Kinetics in Hydrogenous Environments.	2415-2428A
Aluminum, Coatings	401-4135	Aluminum base alloys, Crystal growth On the Rate of Dendrite Arm Coarsening.	569-574A
The Relationship Between Plastic Anisotropy of Steel Sheet and Temper Rolling Strain.	0456 04604	Diffusion-Controlled Kink Motion.	1219-1224A
Delayed Failure of PH13-8Mo Steel Plated With Aluminum-	2156-2160A	Correction to On the Rate of Dendrite Arm Coarsening". Modeling of Crystal Growth During Rapid Solidification. Thermodynamic Consideration of Grain Refinement of Alumi-	1466A 2475-2485A
IVD.	2935-2945A	Thermodynamic Consideration of Grain Refinement of Alumi- num Alloys by Titanium and Carbon.	3071-3075A
Aluminum, Composite materials Interface Structure in Infiltrated Composites of Aluminum Re- inforced With Alumina—Silica Fiber Preforms.	1106 11004	Aluminum base alloys, Directional solidification	
misroed With Aldinna—Silica Piper Preforms.	1126-1128A	Study on Formation of Channel-Type Segregation.	1663-1672A

A

1

Aluminum base alleys, Nechanical properties Causatitativa Assessment of the implications of Strain- folioside Microstructural Changes in Superplastivo, Causaticativa Changes in Superplastivo, Causativa Chan	Aluminum base alloys, Heat treatment In Situ Technique for Measuring the Absorption During Lase Surface Remelting.	er 139-141B	Aluminum compounds, Directional solidification Solidification Microporosity in Directionally Solidified Multi- component Nickel Aluminide.	225-234A
Fetigue Crack Trocognic on an Corpognic Fracture Tough- ness Behavior in Forder Measuring Juntimum—Limiting Analysis of Crack Tro Stelling Displacement in Anisotropic Growth. Charactrization of the Damping Properties of Disc-Cast Critical Control of the Damping Properties of Disc-Cast Fetigue and Fracture Selvative of an Authmium—Billian Aloy 800-Tip at Anisotra and Crycognic Temperature. Aloy After light Frameparks Exposure. Aloy After light Frameparks Exposure. Deciling and Dynamic Strain Alogin I Righty Solidita. Alor Jan Height Frameparks Exposure. Deciling and Dynamic Strain Alogin I Righty Solidita. Alor Jan Height Frameparks Exposure. Deciling and Dynamic Strain Alogin I Righty Solidita. The Deformation of an Aluminum—Billion Education July. The Effect of Copying Conditions. The Belleman of Long Strain Alogin I Righty Solidita. The Deformation of an Aluminum—Billion Soliditan July. The Effect of Dronger. Soliditan Alogin. The Effect of Dronger. Additions to Binary Tuk-Base Alors. The Effect of Dronger. Additions to Binary Tuk-Base Alors. The Effect of Dronger. Additions of Binary Tuk-Base Alors. The Effect of Dronger. Additions of Binary Tuk-Base Alors. The Effect of Dronger. Additions of Binary Tuk-Base Alors. The Effect of Dronger. Additions of Binary Tuk-Base Alors. The Effect of Dronger. Additions of Binary Tuk-Base Alors. The Effect of Dronger. Additions. The Effect of Dronger. Additions of Binary Tuk-Base Alors. The Effect of Dronger. Additions. The Effect of	Aluminum base alloys, Mechanical properties Quantitative Assessment of the Implications of Strain	1-	Aluminum compounds, Heat treatment Microstructural and Thermal Stability of a Ti43Al Alloy Con-	
Allorinum base alloys, Metal working The Effect of Copper, Chromium, Allory The Effect of Copper, Chromium, and Zirconium on the Microsophila and Metalonium phases of Allorinum base alloys, Metal working The Effect of Copper, Chromium, and Zirconium on the Microsophila and Metalonium phases of the Allorinum base allory, Metal working The Effect of Copper, Chromium, and Zirconium on the Microsophila and Metalonium on Allory The Effect of Copper, Chromium, and Zirconium on the Microsophila and Metalonium of Proporties of Allorinum base alloys, Metal working Decoration and Superplasticity at 300°C in an Aluminum base alloys, Metal working Experimental Deformisation of the Phase Equilibria of Monogalithrum hallors in the Allorinum and Aluminum base alloys, Metalonium on Aluminum base alloys, Metalonium base alloys, Metalonium base alloys, Metalonium base alloys, Metalonium on Aluminum base alloys, Metalonium base alloys,	Fatigue Crack Propagation and Cryogenic Fracture Tough	7-	Aluminum compounds, Mechanical properties	1/21-1/28A
Characterization of the Damping Properties of Dis-Cast Failigue and Fracture Behavior of an Aluminum—Lithour Alloy 800-71 et Aluminum Activation Aluminum Alloy 800-71 et Aluminum Alloy The Effect of Chromain Actions to Binary ThA-Base Al- To-Cast Activation Aluminum Date alloys, Microarticuture Development of Structure and Properties of a Rapidly Solidited Al- Landinum Alloy-800-71 et Aluminum Activation of the Aluminum Activation of the Services and Properties of a Rapidly Solidited Al- Landinum Date alloys, Microarticuture Development of Structure and Properties of a Rapidly Solidited Al- Landinum Date alloys, Microarticuture Development of Structure and Properties of a Rapidly Solidited Al- Landinum Date alloys, Microarticuture Development of Structure and Properties of a Rapidly Solidited Al- Landinum Date alloys, Microarticuture Development of Structure and Properties of a Rapidly Solidited Al- Landinum Date alloys, Microarticuture Development of Structure and Properties of a Rapidly Solidited Al- Landinum Date alloys, Microarticuture Development of Structure and Properties of a Rapidly Solidited Al- Landinum Date alloys, Brocketant Interded and Aluminum Date alloys,	Alloys. Analysis of Crack Tip Sliding Displacement in Anisotrop	191-202A ic	structure and Brittle Fracture Behavior in a Titanium Alumi-	71-81A
207-29. Alloy 800-71 et a fundered and Cycogenic Temperature. On the Entoritement of a Rajecily Solidified A1-Fe-V-Signary and Alloy 800-71 et a fundered and Cycogenic Temperature. On the Entoritement of a Rajecily Solidified A1-Fe-V-Signary and Alloy 800-71 et al. (1987-82). Surface You Nationation Under the Province Average Occasion and Alloy 800-71 et al. (1987-82). The Deformation of an Aluminum-Silcion Extract (1987-82). The Deformation of an Aluminum-Silcion Extract (1987-82). The Effect of Through-Thickness Anisotropy on the Cycogenic of Proceedings of Cycogenic Company. The Effect of Through-Thickness Anisotropy on the Cycogenic Ordination of Cycogenic Company. The Effect of Through-Thickness Anisotropy on the Cycogenic Ordination of Cycogenic Company. The Effect of Through-Thickness Anisotropy on the Cycogenic Cycogenic Cycog	Growth.	479-487A	A Model for the Strain-Rate Dependence of Yielding in Ni ₃ Al Alloys.	
Ally 2800-T6 at Ambient and Cryogenic Temperature. On the Stimmtonium of a Russian to History Title State Alloys. Surface Void Nuiseatroin United the Prower-law Cresp Condition in an Ambient and Cryose Condition in a Composition of the Ambient and Elevator Temperature Falips Action Convolution and Ambient Internation of Structure and Proprietties of Ambient and Structure and Proprietties of Ambient and Cryose Confirmation of Structure and Proprietties of Ambient and Cryose Confirmation and Superpleased (Ambient Confirmation and Superpleased Confirmation and Superpleas	Zinc—Aluminum Alloys.	617-622A	uminide Alloy.	
Augy After riggs: Isoniparative Exposure. No. 2019, Aller riggs: Isoniparative Applications. In 1975, 1976,	Alloy 8090-T6 at Ambient and Cryogenic Temperature. On the Embrittlement of a Rapidly Solidified Al—Fe—V—	723-729A	Plastic Deformation and Fracture of Binary TiAl-Base Alloys.	
Doublity and Dynamic Strian Aging in Rapidly Solidiled All- The Distriction of an Alluminum—Silicon Euterical 1911-1154. Material Effects of Presting Wear. Application to Iron, Tita- The Influence of Applied Stress, Crack Length, and Stress In- terially Factor On Place Closure. Alluminum Addition is Binary TIA-Base All 1958-1979. The Effect of Corporation, and Zirocolium on the Microstructure and Machinarial Properties of an All-Cu-l—Lz Alloy (Writage III (2007). The Copper Chromism, and Zirocolium on the Microstructure and Machinarial Properties of Alluminum Date alloys, Metallography and Corporation of Machinary and Stress In- terial Properties of an Alluminum Date alloys, Metallography and Stress In- terial Properties of Structural Properties of Alluminum Date alloys, Metallography and Properties of Alluminum Date alloys, Broad and Properties of Alluminum Date alloys, Plans Equilibria of Properties of Alluminum Date alloys, Plans Equilib	Surface Void Nucleation Under the Power-Law Creep Cond	li-	Microstructural Control. Microstructural Effects on Ambient and Elevated Tempera-	441-446A
The Deformation of an Aluminum—Silicon Euriceito Alloy Under Thems Oyeing Condition proposed to the Polyment of Control (1986) 11-11-11-11 (1986) 11-11-11-11 (1986) 11-11-11-11 (1986) 11-11-11-11 (1986) 11-11-11-11 (1986) 11-11-11-11 (1986) 11-11-11-11 (1986) 11-11-11-11-11 (1986) 11-11-11-11-11-11-11-11-11-11-11-11-11-	Ductility and Dynamic Strain Aging in Rapidly Solidified Al	u-	allics.	817-828A
Material Effects in Preting Wear. Application to Iron, Tita- mon, and Auminum Alogy. Material Fractor in Crack Closure. The Effect of Trincagh-Thickness Alisotropy on the Cryo- frinage it 2090-781. The Effect of Cromoim Additions to Binary Thi-Base A- The Effect of Cromoim Additions to Binary Thi-Base A- The Effect of Cromoim Additions to Binary Thi-Base A- The Effect of Cromoim Additions to Binary Thi-Base A- The Effect of Cromoim Additions to Binary Thi-Base A- The Effect of Cromoim Additions to Binary Thi-Base A- The Effect of Croport Chromium, and Zirocolum on the Mi- crostructure and Mechanized Properties of A — Zn—Mg- Aluminum base alloys, Metal working Aluminum base alloys, Metal working Aluminum—Magnesium Aloy. Aluminum—Magnesium Aloy. Aluminum—Magnesium Aloy. Aluminum—Magnesium Aloy. Aluminum—Sage alloys, Metal working Aluminum—Sage alloys, Metal working Aluminum—Base alloys, Metal working Aluminum—Magnesium Aloy. Aluminum—Base alloys, Metal working Aluminum—Sage alloys, Metal working Aluminum—Base alloys, Metalography The Use of Transmission Electron Microscopy for the As- sessment of Interphase Dourdaries. Aluminum—Base alloys, Metalography The Use of Transmission Electron Microscopy of the As- sessment of Interphase Dourdaries. Aluminum—Base alloys, Metalography The Cereation Deformation of the Phase Equilibria of Aluminum—Base alloys, Phases (state of matter) Aluminum—Base alloys, Metalography The Cereation Deformation of the Phase Equilibria of Aluminum—Base alloys, Metalography The Formation of Metalatable Phase Delaying Interphase Aluminum—Base alloys, Berelion on Alpound (Ir) Procipita- Aluminum—Base alloys, Berelion on Alpound (Ir) Procipita- Aluminum—Base alloys, Metalography T	The Deformation of an Aluminum—Silicon Eutectic Allo	у	Single-Crystalline and Polycrystalline B2 Ni—40Al.	
The Influence of Applied Stress, Crack Length, and Stress In The Effects of Chromium Additions to Binary TIA-Base Albys, 1090-1811, 1900-181, 1900	Material Effects in Fretting Wear: Application to Iron, Tit	a-	A Simple, Versatile Miniaturized Disk-Bend Test Apparatus	
genic Mechanical Properties of an Al—Cu—Li—Zr Alloy (firtigue) if 1909-178), (1789-1799A) (1799-1799A) (1789-1799A) (1789-1799A) (1789-1799A) (1789-1799A) (1799-1799A) (1789-1799A) (1799-179A) (tensity Factor on Crack Closure.	1559-1571A	The Effects of Chromium Additions to Binary TiAl-Base Al-	
The Effects of Chromium Additions to Binary TiAl-Base Al. loys. The Effect of Copper Chromium and Zirconium on the Mil- loys. The Effect of Copper Chromium and Zirconium on the Mil- loys. The Effect of Copper Chromium and Zirconium on the Mil- loys. The Effect of Copper Chromium and Zirconium on the Mil- Cu Alloys. Alluminum base alloys, Metal working Recrystalization and Superplasticity at 300°C in an Aluminum—Magnesium Alloy. The Use of Transmission Electron Microscopy for the As- The Use of Transmission Electron Microscopy for the As- Davisicophina of Structure and Processing of Transmission Electron Microscopy for the As- Davisicophina of Structure and Processing of Transmission Electron Microscopy for the As- Davisicophina of Structure and Processing of Transmission Electron Microscopy for the As- Davisicophina of Structure and Processing of Transmission Electron Microscopy for the As- Davisicophina of Structure and Processing of Transmission Electron Microscopy Aluminum base alloys, Phases (state of matter) Experimental Determination of the Phase Equilibria of Aluminum Base alloys, Phases (state of matter) Experimental Determination of the Phase Equilibria of Aluminum Base alloys, Powder technology Structure and Propersies of a Rapidly Solidified Al— Milloy France and Processing of Transmission Structure International Processing. The Formation of Metastable Phases by Mechanical Alloying Mechanism of Alcoult (Tr), Neptone alloys, Mechanical Alloying Mechanism of Alcoult (Tr), Neptone alloys, Wedding and Alloys	genic Mechanical Properties of an Al-Cu-Li-Zr Allo	ру		
The Effect of Copper, Chromium, and Zizonium on the Microstructure and Mechanical Properties of Al-Z—M-governal Mechanical Properties of Al-Z—M-governal Mechanical Properties of Al-Z—M-governal Mechanical Processing. 2545-2552A Aluminum base alloys, Metal working Recrystalization and Superplasticity at 300°C in an Aluminum—Magnesium Aloy. Aluminum—Magnesium Aloy. Aluminum—Magnesium Aloy. The Use of Transmission Electron Microscopy for the Assessment of Interphase Boundaries. Aluminum—Base alloys, Metallography The Use of Transmission Electron Microscopy for the Assessment of Interphase Boundaries. Aluminum—Base alloys, Metallography The Use of Transmission Electron Microscopy for the Assessment of Interphase Boundaries. Aluminum—Base alloys, Metallography The Use of Transmission Electron Microscopy for the Assessment of Interphase Boundaries. Aluminum—Base alloys, Metallography The Use of Transmission Electron Microscopy for the Assessment of Interphase Boundaries. Aluminum—Base alloys, Metallography The Use of Transmission Electron Microscopy for the Assessment of Interphase Boundaries. Aluminum—Base alloys, Phases (Istle of matter) Experimental Determination of the Phase Equilibria of Aluminum—Base alloys, Powder technology Synthesia of Interphase Double of Machine Processing. Aluminum base alloys, Phases (Istle of matter) Simulation of Metallography The Formation of Metallation Processing. The Formation of Metallation in Aluminum and Coppor System. The Effect of Plastic Detormation on Algoult (T), Procipital on the Aluminum and Coppor System. The Effect of Plastic Detormation on Algoult (T), Aluminum base alloys, Welding and Aluminum	The Effects of Chromium Additions to Binary TiAl-Base A	N-	phase Boundaries.	1145-1158A
Aluminum base alloys, Metallography The Use of Transmission Electron Microscopy for the Assessment of Nitrography Computations of Supering Strain of Hisraphse Boundaries. Aluminum base alloys, Microstructure Development of Structure and Proposity in Cast Al ₂ CuZ ₁₂ and Aluminum Base alloys, Plasaes (state of matter) Line Structure and Proposity in Cast Al ₂ CuZ ₁₂ and Aluminum Base alloys, Plasaes (state of matter) Aluminum Base alloys, Plasaes (state of matter) Line Structure and Proposity in Cast Al ₂ CuZ ₁₂ and Aluminum Compounds, Powder technology Structure and Properties of a Rapidly Solidified Al—Line Structure and Properties of a Rapidly Solidified Al—Immediated Properties of Aluminum Al	The Effect of Copper, Chromium, and Zirconium on the N crostructure and Mechanical Properties of Al—Zn—Mg-	li-	Development of Structure and Porosity in Cast Al ₅ CuZr ₂ and	2545-2552A
Aluminum—Bae alloys, Metallography The Use of Transmission Electron Microscopy for the Assessment of Interphase Boundaries. Aluminum base alloys, Microstructure Development of Structure and Proposity in Cast Al ₂ CuZ ₁₂ and Aluminum Date alloys, Planeas (state of matter) Line Aluminum Baes alloys, Planeas (state of matter) Aluminum—Bae alloys, Planeas (state of matter) Aluminum—Bae alloys, Planeas (state of matter) Aluminum—Bae alloys, Planeas (state of matter) Aluminum—Baes alloys, Planeas (state of matter) Structure and Properties of a Rapidly Solidified Al—Li- Gas Alominum and Opposition Processing. Structure and Properties of a Rapidly Solidified Al—Li- M——Z Alloy for High-Temperature Applications. II. Spray Alominum—Baes alloys, Planeas (state of matter) Structure and Properties of a Rapidly Solidified Al—Li- M——Z Alloy for High-Temperature Applications. II. Spray Alominum—Baes alloys, Planeas (state of matter) Structure and Properties of a Rapidly Solidified Al—Li- M——Z Alloy for High-Temperature Applications. II. Spray Alominum—Baes alloys, Planeas (state of Solidies) Structure and Properties of a Rapidly Solidified Al—Li- M——Z Alloy for High-Temperature Applications. II. Spray Aluminum baes alloys, Planeas (state of Solidies) Aluminum baes alloys, Planeas (state of Solidies) Aluminum baes alloys, Planeas (state of Solidies) Aluminum—Barian and Alloys (state of Solidies) Aluminum—Barian and Forest of Development of High-Temperature Applications. II. Interpediate of Solidies (state of Solidies) Aluminum—Barian and Forest of Solidies (st	Aluminum base alloys, Metal working		A New Phase in a Rapidly Solidified and Consolidated	1001 10001
The Use of Transmission Electron Microscopy for the Assessment of Interphase Boundaries. Aluminum base alloys, Microstructure Development of Structure and Proreptis from Lord Magnetic Compounds. Aluminum base alloys, Pases (state of matter) Experimental Determination of the Phase Equilibria of Aluminum base alloys, Pases (state of matter) Experimental Determination of the Phase Equilibria of Aluminum base alloys, Pases (state of matter) Experimental Determination of the Phase Equilibria of Aluminum Compounds (Marcompounds) Aluminum base alloys, Pases (state of matter) Experimental Determination of the Phase Equilibria of Aluminum Compounds (Marcompounds) Structure and Properties of a Rapidly Solidified Al—Lingham Compounds (Marcompounds) Aluminum base alloys, Pased treatment and Properties of a Rapidly Solidified Al—Lingham Compounds (Marcompounds) Aluminum base alloys, Pased Phases by Mechanian Alloying in the Aluminum and Copper System. Aluminum base alloys, Pased Phases by Mechanian Alloying in the Aluminum and Copper System. Aluminum base alloys, Pased Phases by Mechanian Alloying in the Aluminum Aluminum Compounds (Marcompounds) Chemical Potential Diagram of Al—Ti—Cystem Alega Formation on Tic Formed in Aluminum Aluminum Compounds (Marcompounds) Chemical Potential Diagram of Al—Ti—Cystem Aluminum Compounds (Marcompounds) Chemical Potential Diagram of Al—Ti—Cystem Aluminum Compounds (Marcompounds) Chemical Potential Diagram of Al—Ti—Cystem Aluminum Compounds (Marcompounds) Chemical Potential Diagram of Aluminum Compounds (Marcompounds) Chemical Potential Diagram o	Aluminum—Magnesium Alloy.			1901-1909A
Aluminum base alloys, Microstructure Development of Structure and Proprelly in Cast Al _Q Cuz's and Al _Q Mng/Zr ₂ intermetallic Compounds. Aluminum base alloys, Passes (latte of matter) Experimental Determination of the Phase Equilibria of Aluminum base alloys, Passes (latte of matter) Experimental Determination of the Phase Degram. Nonequilibrium Behavior in the Al—Ge Alloy Systems: Insights into the Metastable Phase Diagram. Nonequilibrium Behavior in the Al—Ge Alloy Systems: Insights into the Metastable Phase Diagram. Aluminum base alloys, Powder technology Structure and Proporties of a Rapidly Solidified Al—Limentary Min—Zr Alloy for High-Temperature Applications. I. Inert Cas Alomization Processing, The Formation of Metastable Phases by Mechanical Alloying in the Aluminum and Caper System. Aluminum base alloys, Reactions (chemical) Chemical Potential Diagram of Al—Ti—Cystem Al _C 2, Formation on Tier Potential Diagram of Al—Ti—Cystem Al _C 2, Formation on Tier Potential Diagram of Al—Ti—Cystem Al _C 2, Formation on Tier Potential Diagram of Al _C 2, If Type Composite materials Aluminum base alloys, Structural hardening Mechanism of Al _C 2, If Type Composite materials Aluminum Structure Al _C 2, Formation on Al _C 2, If Type Composite materials Aluminum Structure Al _C 2, Formation on Al _C 2, If Type Composite materials Aluminum Structure Al _C 2, Formation on Al _C 2, If Type Composite materials Aluminum Structure Al _C 2, Formation on Al _C 2, If Type Composite materials Aluminum Structure Al _C 2, Formation on Al _C 2, If Type Composite Materials with a Special Residence of Plastic Deformation on Al _C 2, If Type Composite Materials and Al _C 2, Aluminum Al _C 2	The Use of Transmission Electron Microscopy for the A		pounds.	2119-2123A
Aluminum base alloys, Passes (state of matter) Experimental Determination of the Phase Equilibria of Aluminum-Rich Alu—L—Cu Alloys Nonequilibrium Behavior in the Al—Ge Alloy Systems: Insights into the Metastable Phase Diagram. Aluminum base alloys, Powder technology Structure and Properties of a Rapidly Solidified Al—L—Mm—Zr Alloy for High-Temperature Applications. I. Inert and Properties of a Rapidly Solidified Al—L—Simm—Zr Alloy for High-Temperature Applications. I. Inert and Properties of a Rapidly Solidified Al—L—Simm—Zr Alloy for High-Temperature Applications. I. Inert and Properties of a Rapidly Solidified Al—L—Simm—Zr Alloy for High-Temperature Applications. I. Inert and Properties of the Effect of Texture on Limit Strain in Biaxially Structured Selection on Companies and Properties of Aluminum and Corpor System. Aluminum base alloys, Reactions (chemical) Thermodynamics of Aluminum—Barium Alloys. Aluminum Base alloys, Powder technology Structure and Properties of a Rapidly Solidified Al—L—Simm—Zr Alloy for High-Temperature Applications. I. Inert and Properties of Rapidly Solidified Al—L—Simm—Zr Alloy for High-Temperature Applications. I. Inert and Properties of Rapidly Solidified Al—L—Simm—Zr Alloy for High-Temperature Applications. I. Inert and Properties of Rapidly Solidified Al—L—Simm—Repeated Properties and Properties Aluminary Aluminum Aluminum Reposition of League. 115-124A 115-1252A 244-2552A 249-2854A 247-257A 247-257A 247-257A 247-257A 248-2552A 249-2854A 248-2854A 248-2854A 248-2854A 248-2854A 248-2854A 249-2854A 249-2854A 249-2854A 249-285	Aluminum base alloys, Microstructure		Synthesis of Iron Aluminides From Elemental Powders: Reac-	277-286A
Extractional Determination of the Phase Equilibria of Managemental Determination of the Phase Equilibria of Managemental Determination of the Phase Equilibria of Management of the All-Lambragement o	Al ₈₈ Mn ₉ Zr ₂₅ Intermetallic Compounds.	2545-2552A	Dynamic Compaction of Titanium Aluminides by Explosively	277-200N
Nonequilibrium Behavior in the Al—Ge Alloy Systems: Insights Into the Metastable Phase Diagrams. Aluminum base alloys, Powder technology Structure and Properties of a Rapidly Solidified Al—Liment and Properties of a Rapidly Solidified Al—Liment Aluminum	Experimental Determination of the Phase Equilibria		tems. Shock Densification/Hot Isostatic Pressing of Titanium Alumi-	
Structure and Properties of a Rapidly Solidified AI—LIMIGAS Allomization Professional Profession	Nonequilibrium Behavior in the Al-Ge Alloy Systems: I	n-	Aluminum compounds, Reactions (chemical)	
Min—Zr Alloy for High-Temperature Applications. I. Inert Gas Atomization Processing. Structure and Properties of a Rapidly Solidified Al—Lim Min—Zr Alloy for High-Temperature Applications. II. Spray Atomization and Deposition Processing. The Formation of Metastable Phases by Mechanical Alloying in the Aluminum and Copper System. Aluminum base alloys, Reactions (chemical) Chemical Potential Diagram of Al—TI—C System: Al ₄ C ₃ Formation on TiC Formed in Al—TI Liquids Containing Carbon. Aluminum base alloys, Structural hardening Mechanism of Al ₂ Cul (Tr) Nucleation and Growth. The Effect of Plastic Deformation on Al ₂ Cul (Tr) Precipitation. Aluminum base alloys, Structural hardening Mechanism of Al ₂ Cul (Tr) Nucleation and Growth. The Effect of Plastic Deformation on Al ₂ Cul (Tr) Precipitation. Aluminum of Lagor Particules. Computer Simulation of the Effect of Coherency Sirain on Cluster Growth Kinetics. Computer Simulation of the Effect of Coherency Sirain on Cluster Growth Kinetics. Aluminum base alloys, Welding Heat-Flow Simulation of the Effect of Coherency Sirain on Cluster Growth Kinetics. Aluminum base alloys, Welding Heat-Flow Simulation of Laser Remeiting With Experimental Validation. Aluminum base alloys, Welding Heat-Flow Simulation of Laser Remeiting With Experimental Validation. Aluminum base alloys, Welding Heat-Flow Simulation of Laser Remeiting With Experimental Validation. Aluminum compounds. See also Aluminum oxide Aluminum compounds, Composites materials NiAl-Base Alloys Ninth Aurinia. 101-1098 See also Aluminum oxide See also Aluminum oxide See also Aluminum oxide See also Aluminum oxide See also Aluminum and Ti—Al Alloys With Aurinia. 104-104-105-105-105-105-105-105-105-105-105-105		pum		607-6168
Mn—Zr Alloy for High-Temperature Applications. II. Spray Atomization and Deposition Processing 2515-2522A 2515-2522A 2515-2525A 2515-252A 2515-252	Mn—Zr Alloy for High-Temperature Applications. I. Inc Gas Atomization Processing.	ert 2503-2514A		2069-2076A
The Formation of Metastable Phases by Mechanical Alloying in the Aluminum and Copper System. Aluminum base alloys, Reactions (chemical) Chemical Diagram of Al—TI—C System: ALC ₃ Formation on TIC Formed in Al—TI—C System: ALC ₃ Formation on TIC Formed in Al—TI—C System: ALC ₃ Formation on TIC Formed in Al—TI—C System: ALC ₃ Formation on TIC Formed in Al—TI—Liquids Containing Carbon. Aluminum base alloys, Structural hardening Mechanism of Al ₂ CuLi (Ti), Nucleation and Growth. The Effect of Plastic Deformation on Al ₂ CuLi (Ti) Precipitation. A Calorimetric Study of Precipitation in an Al—Cu Alloy With Silicon Particles. On the Role of Elastic Interactions in the Nucleation and Growth of Leages. Computer Simulation of the Effect of Coherency Sirain on Cluster Growth Kinetics. Kinetic Equations for Concurrent Size and Shape Coarsening by the Ledge Mechanism Factor Associated With the Indentation of Work-Hardening Materials With a Spherical Ball. Aluminum base alloys, Welding Heat-Flow Simulation of Laser Remetiting With Experimental Validation. Align Chamical Stable Phases by Mechanical Aluminum compounds See also Aluminum conde Aluminum compounds, Casting Evolution of Boride Morphologies in TIAI—B Alloys. Aluminum compounds, Composite materials 101-1098 Aluminum base alloys, Welding Heat-Flow Simulation of Laser Remetiting With Experimental Validation. Align Chamical Stable Phases of the Composites of Electron Beam and Gas Tungsten Arc Fusion Zones of Al—Cu—Li Alloy 2090. Aluminum compounds, Casting Evolution of Boride Morphologies in TIAI—B Alloys. 101-1098 101-1098 101-1098 101-1098 101-1098 101-1098 102-1098 103-2084 103-209-2084 104-1099 104-1099 105-2084 105-2084 106-65-674A 106-67-74A 106-1099 106-1099 107-2094 107-2094 108-1099 109-3084 109-3194 109-3194 101-1098 101-1098 101-1098 101-1098 101-1098 101-1098 101-1098 101-1098 101-1098 101-1098 101-1098 101-1098 101-1098 101-1098 101-1098 101-1099 101-1099 101-1099 101-1099 101-1099 101-1099 101-1099	Mn—Zr Alloy for High-Temperature Applications. II. Spri	ау	The Relationship Between Plastic Anisotropy of Steel Sheet	
Aluminum base alloys, Reactions (chemical) Chemical Potential Diagram of Al—Ti—C System: Al ₄ C ₃ Formation on TiC Formed in Al—Ti—Liquids Containing Carbon. Aluminum base alloys, Structural hardening Mechanism of Al ₂ CuLI (T ₁) Nucleation and Growth. The Effect of Plastic Deformation on Al ₂ CuLI (T ₁) Precipitation. A Calorimetric Study of Precipitation in an Al—Cu Alloy With Silicon Particles. On the Role of Elastic Interactions in the Nucleation and Growth of Ledges. Computer Simulation of the Effect of Coherency Sirain on Cluster Growth Kinetics. On the Role of Elastic Interactions in the Nucleation and Growth Kinetics. On the Role of Elastic Interactions in the Nucleation and Growth Kinetics. On the Role of Elastic Interactions in the Nucleation and Growth Kinetics. On the Constraint Factor Associated With the Indentation of Work-Hardening Materials With a Spherical Ball. Aluminum base alloys, Welding Heat-Flow Simulation of Laser Remetting With Experimental Validation. Align Characteristics of Electron Beam and Gas Tungsten Arc Fusion Zones of Al—Cu—Li Alloy 2090. Aluminum bases alloys, Welding Heat-Flow Simulation of Laser Remetting With Experimental Validation. Aluminum bases alloys, Welding Heat-Flow Simulation of Laser Remetting With Experimental Validation. Aluminum bases alloys, Composite materials NiAl-Based Microstructurally Toughened Composites. 101-1098 See also Aluminum oxide Aluminum compounds, Composite materials NiAl-Based Microstructurally Toughened Composites. 1647-1682A Aluminum compounds, Composite materials NiAl-Based Microstructurally Toughened Composites. 1647-1682A Aluminum compounds, Composite materials NiAl-Based Microstructurally Toughened Composites. 1647-1682A Aluminum compounds, Composite materials NiAl-Based Microstructurally Toughened Composites. 1647-1682A 101-1098 See also Aluminum compounds, Composite materials NiAl-Based Microstructurally Toughened Composites. 1647-1682A 1647-1682A 1715-721A 175-721A 175-721A 175-721A 175-721A 175-721A 175-721A	The Formation of Metastable Phases by Mechanical Alloying	ng		2156-2160A
Aluminum base alloys, Structural hardening Mechanism of Al ₂ CuLi (T ₁) Nucleation and Growth. The Effect of Plastic Deformation on Al ₂ CuLi (T ₁) Precipitation. A Calorimetric Study of Precipitation in an Al—Cu Alloy With Silicon Particles. On the Role of Elastic Interactions in the Nucleation and Growth of Ledges. Computer Simulation of the Effect of Coherency Sirain on Cluster Growth Kinetics. Kinetic Equations for Concurrent Size and Shape Coarsening by the Ledge Mechanism. On the Constraint Factor Associated With the Indentation of Work-Hardening Materials With a Spherical Ball. Aluminum base alloys, Structural hardening Mechanism of Al ₂ CuLi (T ₁) Precipitation. A Galorimetric Study of Precipitation in an Al—Cu Alloy With Alloring Size of Electron Stress Concepts. Computer Simulation of the Effect of Coherency Sirain on Cluster Growth Kinetics. Kinetic Equations for Concurrent Size and Shape Coarsening by the Ledge Mechanism. On the Constraint Factor Associated With the Indentation of Work-Hardening Materials With a Spherical Ball. Aluminum base alloys, Welding Heat-Flow Simulation of Lager Remelting With Experimental Validation. Aging Characteristics of Electron Beam and Gas Tungsten Are Fusion Zones of Al—Cu—Li Alloy 2090. Aluminum brasses, Heat treatment The Aging Effect on Cu—Zn—Al Shape Memory Alloys With Low Contents of Aluminum. Aluminum compounds, Composite materials NiAl-Based Microstructurally Toughened Composites. See also Aluminum and Ti—Al Alloys With Alumina. Preliminary Studies on Tib2-Risinforced Near-y. Titanium Aluminudes. Reaction of Titanium and Ti—Al Alloys With Alumina. 1715-721A 1726-72A 287-297A 665-67-4A 665-67-4A 665-67-4A 197-1209A 2375-2384A 101-109B 903-913A 241-45-03 2475-2384A 2403-2915A 24803-2915A 2481-1990A 2475-284 24903-2915A 2481-1990A 24903-2915A 24903-2915A 24903-2915A 24903-2915A 24903-2916A 24903	Aluminum base alloys, Reactions (chemical)		Removal of Nitrogen From Steel Using Novel Fluxes.	783-790B
Mechanism of Al ₂ CuLi (T ₁) Nucleation and Growth. The Effect of Plastic Deformation on Al ₂ CuLi (T ₁) Precipitation. A Calorimetric Study of Precipitation in an Al—Cu Alloy With Silicon Particles. On the Role of Elastic Interactions in the Nucleation and Growth of Ledges. Computer Simulation of the Effect of Coherency Strain on Cluster Growth Kinetics. Kinetic Equations for Concurrent Size and Shape Coarsening by the Ledge Mechanism. On the Constraint Factor Associated With the Indentation of Work-Hardening Materials With a Spherical Ball. Aluminum base alloys, Welding Heat-Flow Simulation of Laser Remelting With Experimental Validation. Aging Characteristics of Electron Beam and Gas Tungsten Arc Fusion Zones of Al—Cu—Li Alloy 2090. Aluminum brasses, Heat treatment The Aging Effect on Cu—Zn—Al Shape Memory Alloys With Low Contents of Aluminum. Aluminum compounds See also Aluminum oxide Aluminum compounds, Casting Evolution of Boride Morphologies in TiAl—B Alloys. Aluminum compounds, Composite materials NiAl-Based Microstructurally Toughened Composites. Creep Deformation of TiB ₂ -Reinforced Nial-Groed Neal-Groed Neal	mation on TiC Formed in Al—Ti Liquids Containing Carbo	n. 3075-3076A	Reaction of Titanium and Ti—Al Alloys With Alumina. Interface Structure in Infiltrated Composites of Aluminum Re-	
tion. A Calorimetric Study of Precipitation in an Al—Cu Alloy With Silicon Particles. On the Role of Elastic Interactions in the Nucleation and Growth of Ledges. Computer Simulation of the Effect of Coherency Sirain on Cluster Growth Kinetics. Computer Simulation of the Effect of Coherency Sirain on Cluster Growth Kinetics. Not the Ledge Mechanism. On the Constraint Factor Associated With the Indentation of Work-Hardening Materials With a Spherical Ball. Aluminum base alloys, Welding Heat-Flow Simulation of Laser Remelting With Experimental Validation. Aging Characteristics of Electron Beam and Gas Tungsten Are Fusion Zones of All—Cu—Li Alloy 2090. Aluminum brasses, Heat treatment The Aging Effect on Cu—Zn—Al Shape Memory Alloys With Low Contents of Aluminum. Aluminum compounds See also Aluminum oxide Aluminum compounds, Composite materials NiAl-Based Microstructurally Toughened Composites. Creep Deformation of TiB2-Reinforced Near-y Titanium Aluminides. Reaction of Titanium and Ti—Al Alloys With Alumina. Presium 2 fusion 3 fusion 6 fusion 2 fusion 2 fusion 2 fusion 2 fusion 3 fusion 6 fusion 6 fusion 6 fusion 2 fus	Mechanism of Al ₂ CuLi (T ₁) Nucleation and Growth.	287-297A	Stress Concentration at a Notch Tip in Unidirectional Metal	
Silicon Particles. On the Role of Elastic Interactions in the Nucleation and Growth of Ledges. Computer Simulation of the Effect of Coherency Sirain on Cluster Growth Kinetics. Kinetic Equations for Concurrent Size and Shape Coarsening by the Ledge Mechanism. On the Constraint Factor Associated With the Indentation of Work-Hardening Materials With a Spherical Ball. Aluminum base alloys, Welding Heat-Flow Simulation of Laser Remelting With Experimental Validation. Aging Characteristics of Electron Beam and Gas Tungsten Arc Fusion Zones of Al—Cu—Li Alloy 2090. Aluminum brasses, Heat treatment The Aging Effect on Cu—Zn—Al Shape Memory Alloys With Low Contents of Aluminum. Aluminum compounds. See also Aluminum oxide Aluminum compounds, Casting Evolution of Boride Morphologies in TiAl—B Alloys. Aluminum compounds, Composite materials NiAl-Based Microstructurally Toughened Composites. Creep Deformation of Tib2-Reinforced Near-y Titanium Aluminides. Reaction of Titanium and Ti—Al Alloys With Alumina. Preliminary Studies on NiAl/Nb28n ₁ Reaction and Effectiveness of BoO as an Interfacial Reaction Barrier. Interfaces in XD Processed TiB ₂ /NiAl Composites. 197-129A Libratiano My Alumina Fibers and Na Pressure Casting of a Zirconia-Toughened Aluminan Fiber-Reinforced Near-y Titanium Aluminides. 101-109B 903-913A Aluminum compounds, Casting Evolution of Boride Morphologies in TiAl—B Alloys. Aluminum compounds, Composite materials NiAl-Based Microstructurally Toughened Composites. Creep Deformation of Tib2-Reinforced Near-y Titanium Aluminides. Reaction of Titanium and Ti—Al Alloys With Alumina. Preliminary Studies on NiAl/Nb28n ₁ Reaction and Effectiveness of BoO as an Interfacial Reaction Barrier. Interfaces in XD Processed TiB ₂ /NiAl Composites. 101-109B 101-109	tion.	299-306A	Effect of Reinforcement on the Aging Response of Cast 6061	
Growth of Ledges. Computer Simulation of the Effect of Coherency Sirain on Cluster Growth Kinetics. Kinetic Equations for Concurrent Size and Shape Coarsening by the Ledge Mechanism. On the Constraint Factor Associated With the Indentation of Work-Hardening Materials With a Spherical Ball. Aluminum base alloys, Welding Heat-Flow Simulation of Laser Remelting With Experimental Validation. Aging Characteristics of Electron Beam and Gas Tungsten Arc Fusion Zones of Al—Cu—Lu Alloy 2090. Aluminum brasses, Heat treatment The Aging Effect on Cu—2n—Al Shape Memory Alloys With Low Contents of Aluminum. Aluminum compounds See also Aluminum oxide Aluminum compounds, Composite materials NiAl-Based Microstructurally Toughened Composites. Creep Deformation of Tib2-Reinforced Near-y Titanium Aluminides. Reaction of Titanium and Ti—Al Alloys With Alumina. Preliminary Studies on NiAlNbg8ey Reaction and Effectiveness of BoO as an Interfacial Reaction Barrier. Interfaces in XD Processes Tib2, NiAl Composites. Composites. 197-1209A 198-13-1390A 199-13-14 275-2384A 101-109B	Silicon Particles.	665-674A	Chemical Stability of Zirconia-Stabilized Alumina Fibers Dur-	
Kinetic Equations for Concurrent Size and Shape Coarsening by the Ladge Mechanism. On the Constraint Factor Associated With the Indentation of Work-Hardening Materials With a Spherical Ball. Aluminum base alloys, Welding Heat-Flow Simulation of Laser Remelting With Experimental Validation. Aging Characteristics of Electron Beam and Gas Tungsten Arc Fusion Zones of All—Cu—Li Alloy 2090. Aluminum brasses, Heat treatment The Aging Effect on Cu—Zn—Al Shape Memory Alloys With Low Contents of Aluminum compounds See also Aluminum compounds See also Aluminum compounds, Casting Evolution of Boride Morphologies in TiAl—B Alloys. Aluminum compounds, Composite materials NiAl-Based Microstructurally Toughened Composites. Creep Deformation of TiB₂-Reinforced Near-γ Titanium Aluminides. Reaction of Titanium and Ti—Al Alloys With Alumina. Preliminary Studies on NiAl/Nb ₂ Be ₁₇ , Reaction and Effectiveness of BeO as an Interfacial Reaction Barrier. Interfaces in XD Processed TiB₂/NiAl Composites. Pressure Casting of a Zirconia-Toughened Aluminan Fiber-	Computer Simulation of the Effect of Coherency Strain of	on	Interfaces in XD Processed TiB ₂ /NiAl Composites.	
On the Constraint Factor Associated With the Indentation of Work-Hardening Materials With a Spherical Ball. Aluminum base alloys, Welding Heat-Flow Simulation of Laser Remelting With Experimental Validation. Aging Characteristics of Electron Beam and Gas Tungsten Are Fusion Zones of Al—Cu—Li Alloy 2090. Aluminum brasses, Heat treatment The Aging Effect on Cu—Zn—Al Shape Memory Alloys With Low Contents of Aluminum. Aluminum compounds See also Aluminum oxide Aluminum compounds, Casting Evolution of Boride Morphologies in TiAl—B Alloys. Aluminum compounds, Composite materials NiAl-Based Microstructurally Toughened Composites. Creep Deformation of TiBz-Reinforced Near-y Titanium Aluminides. Reaction of Titanium and Ti—Al Alloys With Alumina. Preliminary Studies on NiAl/NbzBe₁r Reaction and Effectiveness of BeO as an Interfacial Reaction Barrier. Interfaces in XD Processed TiBz/NiAl Composites. Pressure Casting of a Zirconia-Toughened Aluminan Fiber- Aluminum compounds See also Aluminum oxide, Reactions (cremical) The K-ZFF, Wetting Process: Effect of Surface Chemistry on the Ability of a SiC-Fiber Preform To Be Impregnated by Aluminum oxide, Selfect of Surface Chemistry on the Ability of a SiC-Fiber Preform To Be Impregnated by Aluminum oxide, Selfect of Surface Chemistry on the Ability of a SiC-Fiber Preform To Be Impregnated by Aluminum oxide, Selfect of Surface Chemistry on the Ability of a SiC-Fiber Preform To Be Impregnated by Aluminum oxide, Selfect of Surface Chemistry on the Ability of a SiC-Fiber Preform To Be Impregnated by Aluminum oxide, Selfect of Surface Chemistry on the Ability of a SiC-Fiber Preform To Be Impregnated by Aluminum oxide, Surface properties Effect of Sulfur Removal on Al ₂ O ₃ Scale Adhesion. Aluminum oxide, Search Surface properties Effect of Sulfur Removal on Al ₂ O ₃ Scale Adhesion. Aluminum oxide, Surface properties Effect of Sulfur Removal on Al ₂ O ₃ Scale Adhesion. Aluminum oxide, Surface properties Effect of Sulfur Removal on Al ₂ O ₃ Scale Adhesion. Aluminum oxid	Kinetic Equations for Concurrent Size and Shape Coarsening	ng	Reinforced NiAl Composite.	3059-3064A
Heat-Flow Simulation of Laser Remelting With Experimental Validation. Adjing Characteristics of Electron Beam and Gas Tungsten Arc Fusion Zones of Al—Cu—Li Alloy 2090. 903-913A	On the Constraint Factor Associated With the Indentation	of	Aluminum oxide, Reactions (chemical) The K ₂ ZrF ₆ Wetting Process: Effect of Surface Chemistry on	
Validation. Aging Characteristics of Electron Beam and Gas Tungsten Arc Fusion Zones of Al—Cu—Li Alloy 2090. Aluminum brasses, Heat treatment The Aging Effect on Cu—Zn—Al Shape Memory Alloys With Low Contents of Aluminum compounds See also Aluminum compounds See also Aluminum compounds, Casting Evolution of Boride Morphologies in TiAl—B Alloys. Aluminum compounds, Composite materials NiAl-Based Microstructurally Toughened Composites. Creep Deformation of TiB₂-Reinforced Near-γ Titanium Aluminides. Reaction of Titanium and Ti—Al Alloys With Alumina. Preliminary Studies on NiAlNb₂Be₁γ Reaction and Effectiveness of BeO as an Interfacial Reaction Barrier. Interfaces in XD Processed TiB₂/NiAl Composites. Pressure Casting of a Zirconia-Toughened Aluminar Fiber- Pressure Casting of a Zirconia-Toughened Aluminar Fiber- 101-109B Effect of Sulfur Removal on Al₂O₃ Scale Adhesion. 739-752A Ambient temperature See Temperature See Temperature See Temperature See Temperature See Temporature Ammoniac Pressive Behavior of Sintered Iron in Ammoniacal Armmonium Carbonate Solution. 323-332B Aluminum compounds, Composite materials NiAl-Based Microstructurally Toughened Composites. Creep Deformation of TiB₂-Reinforced Near-γ Titanium Aluminides. Reaction of Titanium and Ti—Al Alloys With Alumina. Pressure Casting of a Zirconia-Toughened Aluminar Fiber- 25-33A Aluminum compounds, Composite sation and Effective See Glass Analyzing See Failure analysis Mathematical analysis Stress analysis Aradicade method See Crystal growth Angles (geometry) See Contact angle Ammonium Carbonate Solution. 323-332B	Aluminum base alloys, Welding		the Ability of a SiC-Fiber Preform 10 Be Impregnated by Aluminum.	2133-2139A
Arc Fusion Zones of Al—Cu—Li Alloy 2090. Aluminum brasses, Heat treatment The Aging Effect on Cu—Zn—Al Shape Memory Alloys With Low Contents of Aluminum. Aluminum compounds See also Aluminum oxide Aluminum compounds, Casting Evolution of Boride Morphologies in TiAl—B Alloys. Aluminum compounds, Composite materials NiAl-Based Microstructurally Toughened Composites. Creep Deformation of TiB₂-Reinforced Near-γ Titanium Aluminides. Reaction of Titanium and Ti—Al Alloys With Alumina. Preliminary Studies on NiAlNb₂Be₁γ Reaction and Effectiveness of BeO as an Interfacial Reaction Barrier. Interfaces in XD Processed TiB₂/NiAl Composites. Pressure Casting of a Zirconia-Toughened Aluminar Fiber- Pressure Casting of a Zirconia-Toughened Aluminar Fiber- Ambient temperature See Temperature	Validation. Aging Characteristics of Electron Beam and Gas Tungst	101-109B	Aluminum oxide, Surface properties Effect of Sulfur Removal on Al ₂ O ₃ Scale Adhesion.	739-752A
The Aging Effect on Cu—Zn—Al Shape Memory Alloys With Low Contents of Aluminum. Aluminum compounds See also Aluminum oxide Aluminum compounds, Casting Evolution of Boride Morphologies in TiAl—B Alloys. Aluminum compounds, Composite materials NIAl-Based Microstructurally Toughened Composites. Creep Deformation of TiBg-Reinforced Near-y Titanium Aluminides. Reaction of Titanium and Ti—Al Alloys With Alumina. Pressure Casting of a Zirconia-Toughened Aluminar Fiber- Interfaces in XD Processed TiBg/NiAl Composites. Or Aluminum Compounds, Composites and See Glass Ammonia, Environment Active and Passive Behavior of Sintered Iron in Ammoniacal Ammonium Carbonate Solution. 323-332B Amorphous materials See Glass Mathematical analysis Mathematical analysis Stress analysis Andrade method See Crystal growth Angles (geometry) See Contact angle Ammonia, Environment Active and Passive Behavior of Sintered Iron in Ammoniacal Ammonium Carbonate Solution. 323-332B Amorphous materials See Glass Analyzing See Failure analysis Mathematical analysis Ma	Arc Fusion Zones of Al—Cu—Li Alloy 2090.		Ambient temperature See Temperature	
See also Aluminum oxide Aluminum compounds, Casting Evolution of Boride Morphologies in TiAl—B Alloys. Aluminum compounds, Composite materials NiAl-Based Microstructurally Toughened Composites. Creep Deformation of TiB₂-Reinforced Near-γ Titanium Aluminides. Reaction of Titanium and Ti—Al Alloys With Alumina. Preliminary Studies on NiAl/Nb₂8e₁-γ Reaction and Effectiveness of BeO as an Interfacial Reaction Barrier. Interfaces in XD Processed TiB₂/NiAl Composites. Pressure Casting of a Zirconia-Toughened Aluminar Fiber- Nandrade method See Crystal growth Angles (geometry) See Contact angle Analyzing See Failure analysis Mathematical analysis Stress analysis Andrade method See Crystal growth Angles (geometry) See Contact angle Analyzing See Failure analysis Mathematical analysis Stress analysis	The Aging Effect on Cu—Zn—Al Shape Memory Alloys Wi		Active and Passive Behavior of Sintered Iron in Ammoniacal	202 2225
Evolution of Boride Morphologies in TiAl—B Alloys. Aluminum compounds, Composite materials NiAl-Based Microstructurally Toughened Composites. Creep Deformation of TiB ₂ -Reinforced Near-y Titanium Alumindes. Reaction of Titanium and Ti—Al Alloys With Alumina. Presiminary Studies on NiAl/Nb ₂ Be ₁₇ Reaction and Effectiveness of BeO as an Interfacial Reaction Barrier. Interfaces in XD Processed TiB ₂ /NiAl Composites. 2535-2538A Interfaces in XD Processed TiB ₂ /NiAl Composites. 3013-3018A Pressure Casting of a Zirconia-Toughened Alumian Fiber-			Amorphous materials	323-3325
Autinium compounds, Composites materials NiAl-Based Microstructurally Toughened Composites. Creep Deformation of TiB ₂ -Reinforced Near-γ Titanium Aluminides. Reaction of Titanium and Ti—Al Alloys With Alumina. Preliminary Studies on NiAl/Nb ₂ Be _{1-γ} Reaction and Effectiveness of BeO as an Interfacial Reaction Barrier. Interfaces in XD Processed TiB ₂ /NiAl Composites. Pressure Casting of a Zirconia-Toughened Alumian Fiber- Mathematical analysis Stress analysis Andrade method See Crystal growth Angles (geometry) See Contact angle 3013-3018A	Aluminum compounds, Casting Evolution of Boride Morphologies in TiAl—B Alloys.	1647-1662A	Analyzing	
Creep Deformation of TiB ₂ -Reinforced Near- γ Titanium Aluminides. Reaction of Titanium and Ti—Al Alloys With Alumina. Preliminary Studies on NiAl/Nb ₂ Be _{1-γ} Reaction and Effectiveness of BeO as an Interfacial Reaction Barrier. Interfaces in XD Processed TiB ₂ /NiAl Composites. Pressure Casting of a Zirconian-Toughened Alumian Fiber- Pressure Casting of a Zirconian-Toughened Alumian Fiber-	Aluminum compounds, Composite materials	183-189A	See Failure analysis Mathematical analysis	
Reaction of Titanium and Ti—Al Alloys With Alumina. 715-721A Preliminary Studies on NiAl/Nb ₂ Be ₁₇ Reaction and Effectiveness of BeO as an Interfacial Reaction Barrier. Interfaces in XD Processed TiB ₂ /NiAl Composites. 2535-2538A 3013-3018A Pressure Casting of a Zirconia-Toughened Alumian Fiber-	Creep Deformation of TiB ₂ -Reinforced Near-γ Titanium in uminides.	447-454A	Andrade method	
Interfaces in XD Processed TiB ₂ (NiAl Composites. 3013-3018A Pressure Casting of a Zirconia-Toughened Alumian Fiber- Anisotropy	Reaction of Titanium and Ti—Al Alloys With Alumina. Preliminary Studies on NiAl/Nb ₂ Be ₁₇ Reaction and Effective	715-721A	See Crystal growth	
Reinforced NiAl Composite. 3059-3064A See also Elastic anisotropy	Interfaces in XD Processed TiB ₂ /NiAl Composites.	3013-3018A	See Contact angle	
	Reinforced NiAl Composite.			

4

Transformation of Retained Austenite in Carburized 4320 Steel.	1491-1500A	Attenuation See Damping	
The Effect of Through-Thickness Anisotropy on the Cryo- genic Mechanical Properties of an Al—Cu—Li—Zr Alloy		Austenite See also Retained austenite	
(Vintage III 2090-T81). Annealing See also Homogenizing	1789-1799A	The Thermal and Metallurgical State of Steel Strip During Hot Rolling. III. Microstructural Evolution. An Experimental Study of Carbide/Austenite Equilibria in the	335-349A
Spheroidizing Effects of Microalloying Elements and Heat Treatments on Tensile Properties in Cu—23Zn—3.4Al—1Ni—X Alloys. Mechanical Properties and Retained Austenite in Intercriti- cally Heat-Treated Bainite-Transformed Steel and Their	256-258A	High-Speed Steel Alloy System. Austenite, Alloying effects The Effect of Temperature and Nitrogen Content on the Partitioning of Alloy Elements in Duplex Stainless Steels.	1391-1405A 2173-2179A
Variation With Silicon and Manganese Additions. Microstructural Evolution of Modified 9Cr—1Mo Steel. Intermetallic Phase Formation and Breakdown of Molybde-	489-498A 1049-1058A 1501-1510A	Austenite, Cooling effects Nonequilibrium Austenite/c-Phase Eutectic Revealed in Rapidly Solidified High-Carbon Iron Alloy.	791-792A
num Diffusion Barriers in Ni—Mo—Cu Layers. Anodic dissolution New Observations on the Anodic Oxidation of Copper in Hot Acidified Copper Sulfate Solutions.	623-630B	Austenite, Phase transformations Morphology and Aging of the Martensite Induced by Cathodic Hydrogen Charging of High-Carbon Austenitic Steels.	1979-1991A
Anodic dissolution, pH effects Active and Passive Behavior of Sintered Iron in Ammoniacal Ammonium Carbonate Solution.	323-332B	Austenitic stainless steels, Chemical analysis Secondary Ion Mass Spectrometry Method for Distinguishing the State of Carbon in Steels Using Negative Molecular	1000 10701
Anodic polarization New Observations on the Anodic Oxidation of Copper in Hot _ Acidified Copper Sulfate Solutions.	623-630B	lons. Austenitic stainless steels, Coating The Chemistry and Structure of Wear-Resistant, Iron-Base	1969-1978A 983-991A
Environmental Fatigue of an Al—Li—Cu Alloy. I. Intrinsic Crack Propagation Kinetics in Hydrogenous Environments. Antifriction alloy a	2415-2428A	Hardfacing Alloys. Austenitic stainless steels, Composite materials NiAl-Based Microstructurally Toughened Composites.	183-189A
See Tin base alloys Antimony, Impurities Distribution of Antimony Between Carbon-Saturated Iron and		Austenitic stainless steels, Corrosion Accelerated Fracture Due to Tritium and Helium in 21-6-9 Stainless Steel.	879-886A
Synthetic Slags. Cathodic Copper Deposition at 65°C in the Absence and Presence of Bi ³⁺ and Sb ³⁺ Additives in Acidified CuSO ₄	136-139B	A Mechanistic Study of Transgranular Stress Corrosion Cracking of Type 304 Stainless Steel. Mechanisms of Deformation-Induced Grain Boundary Chro-	1453-1461A
Aqueous Solutions. Thermochemical Nature of Minor Elements in Copper Smelting Mattes.	575-581B 677-688B	mium Depletion (Sensitization) Development in Type 316 Stainless Steels.	2917-2934A
Antiphase boundaries The Mechanisms and Temperature Dependence of Superlat- tice Stacking Fault Formation in the Single-Crystal Superal-		Austenitic stainless steels, Mechanical properties Material Effects in Fretting Wear: Application to Iron, Titanium, and Aluminum Alloys.	1535-1544A
loy PWA 1480. Antiphase boundaries, Heating effects	2309-2318A	Low-Temperature Fatigue of 316L and 316LN Austenitic Stainless Steels. Internal Hydrogen-Induced Subcritical Crack Growth in Aus-	2385-2392A
Electron Microscopy Study of the Aging and First Stage of Tempering of High-Carbon Fe—C Martensite.	797-806A	tenitic Stainless Steels. High-Temperature Rupture of Microstructurally Unstable 304 Stainless Steel Under Uniaxial and Triaxial Stress States.	2605-2618A 2629-2635A
Arc melting See Electric arc melting		Delayed Failure of PH13-8Mo Steel Plated With Aluminum-IVD.	2935-2945A
Arc plasma welding See Plasma arc welding		Austenitic stainless steels, Powder technology Ultrasound Treatment of Centrifugally Atomized 316 Stain-	
Arc spraying See Plasma spraying		less Steel Powders. Austenitic stainless steels, Welding	3025-3033A
Arc welding See also Submerged arc welding Further Study on the Scattering of the Local Fracture Stress and Allied Toughness Value.	2287-2296A	Slag — Metal Reactions During Welding. I. Evaluation and Re- assessment of Existing Theories. Effect of Evaporation and Temperature-Dependent Material Properties on Weld Pool Development.	65-71B 233-241B
Arc welds See Welded joints	2201-2250A	Computational Modeling of Stationary Gas-Tungsten-Arc Weld Pools and Comparison to Stainless Steel 304 Experi- mental Results.	243-257B
Argon arc welding See Gas tungsten arc welding		Solidification Modeling and Solid-State Transformations in High-Energy Density Stainless Steel Welds.	915-926A
Arrhenius activation energy See Activation energy		Carbide Precipitation in Welds of Two-Phase Austenitic— Ferritic Stainless Steel.	2889-2902A
Arsenic, Impurities Thermochemical Nature of Minor Elements in Copper Smelting Mattes.	677-688B	Austenitic stainless steels, X ray analysis X-Ray Microanalysis of Phosphorus Segregation in Type 304L Stainless Steels.	253-255A
Artificial aging See Aging (artificial)	017-0005	Austenitizing Powder Metallurgy T15 Tool Steel. II. Microstructure and Properties After Heat Treatment.	2747-2759A
Astroceram See Ceramics		Auto oxidation See Oxidation	
Atmospheric temperature See Temperature		Autodiffusion See Diffusion	
Atomic diffusion See Diffusion		Autogenous smelting See Flash smelting	
Atomic properties See Atomic structure Electronic structure		Automobile components See Automotive components	
Atomic structure Electron Microscopy of Transformation Dislocations at Inter		Automotive bodies, Mechanical properties Vibration Damping Characteristics of Laminated Steel Sheet.	653-656A
phase Boundaries. Structural Ledges in Interphase Boundaries. The Crystallography and Atomic Structure of Line Defects in Twin Boundaries in Hexagonal-Close-Packed Metals.	1145-1158A 1165-1175A 1 1185-1196A	Automotive components See also Automotive bodies Automotive engines	
Atomic Structure of the Crystalline/Amorphous Interface in a Directionally Crystallized PdgoSigo Alloy. Real-Time Atomic-Level Observations of In Situ Chemical Re actions and Transformations Utilizing High-Resolution	1287-1298A	Automotive components, Materials selection Characterization of the Damping Properties of Die-Cast Zinc—Aluminum Alloys. The Deformation of an Aluminum—Silicon Eutectic Alloy Under Thermal Cycling Conditions.	617-622A
Electron Microscopy. Atomization See Atomizing	1323-1329A	Automotive components, Mechanical properties Development of Vibration-Damping Resins for Room-Temperature Application.	
Atomizing Structure and Properties of a Rapidly Solidified Al—Li— Mn—Zr Alloy for High-Temperature Applications. I. Iner	rt	Automotive engines, Materials selection Thermomechanical Fatigue of Particulate-Reinforced Aluminum 2xxx-T4.	
Gas Atomization Processing. Structure and Properties of a Rapidly Solidified AI—Li—Mn—Zr Alloy for High-Temperature Applications. II. Spra Atomization and Deposition Processing.	2503-2514A	Bacterial leaching, pH effects The Electrochemical Behavior of a Semiconducting Nautra Pyrite in the Presence of Bacteria.	

Bainite Discussion of "A Mechanism for the Formation of Lower Bai-		Blast furnace refractories See Refractories	
nite" and Authors' Reply. Ball milling The Formation of Metastable Phases by Mechanical Alloying	1674-1678A	Blast furnace slags Distribution of Antimony Between Carbon-Saturated Iron and Synthetic Slags.	136-139B
in the Aluminum and Copper System. Banded structure	2849-2854A	Heat-Transfer Phenomena in Water-Cooled Zinc-Furning Furnace Jackets.	163-175B
Modeling of Crystal Growth During Rapid Solidification. Banded structure, High temperature effects On the Embrittlement of a Rapidly Solidified Al—Fe—V—Si	2475-2485A	Blast furnaces The Influence of Specific Impurities on the Nucleation and Growth of Magnetite During Reduction of Artificially Prepared Hematite.	503-511B
Alloy After High-Temperature Exposure. Barium, Binary systems	853-858A	Body centered cubic lattice The Formation of Metastable Phases by Mechanical Alloying	
Thermodynamics of Aluminum—Barium Alloys. Barium compounds, Reactions (chemical)	607-616B	in the Aluminum and Copper System. Bohr model	2849-2854A
Thermodynamics of Aluminum—Barium Alloys. Basic electric furnaces	607-616B	See Atomic structure Bolting	
See Electric furnaces Basicity		Delayed Failure of PH13-8Mo Steel Plated With Aluminum-IVD.	2935-2945A
See pH Batch type furnaces		Boits, Mechanical properties Delayed Failure of PH13-8Mo el Plated With Aluminum-	
See Converters		IVD. Bomb reduction	2935-2945A
Bauschinger effect Hydrostatic Stresses and Their Effect on the Macroflow Behavior and Microfracture Mechanism of Two-Phase Alloys.	2695-2702A	See Reduction (chemical) Bombs (pressure vessels)	
Beams (structural) See Cantilever beams		See Pressure vessels Bonding	
Bend properties See Bend strength		Microstructural Development in Transient Liquid-Phase Bonding.	2451-2457A
Bend strength Powder Metallurgy T15 Tool Steel. II. Microstructure and	0747 07504	Borides, Composite materials Creep Deformation of TiB ₂ -Reinforced Near-γ Titanium Aluminides.	447-454A
Properties After Heat Treatment. Bend strength, Heating effects	2747-2759A	Interfaces in XD Processed TiB ₂ /NiAl Composites. Borides, Cooling effects	3013-3018A
Strength and Ductile-Phase Toughening in the Two-Phase Nb/Nb ₅ Si ₃ Alloys.	1573-1583A	Evolution of Boride Morphologies in TiAl—B Alloys. Borides, Synthesis	1647-1662A
Bend strength, Radiation effects A Simple, Versatile Miniaturized Disk-Bend Test Apparatus for Quantitative Yield-Stress Measurements.	2061-2068A	Enthalpies of Formation of Refractory Borides by High- Temperature Direct Synthesis Calorimetry: RuB _{1,1} and RhB _{1,1} .	1680-1683A
Bend tests Hydrogen-Assisted Ductile Fracture in Spheroidized 1520 Steel. II. Pure Bending. A Simple, Versatile Miniaturized Disk-Bend Test Apparatus	1615-1626A	Boron, Alloying elements Solidification Microporosity in Directionally Solidified Multi- component Nickel Aluminide. Evolution of Boride Morphologies in TIAI—B Alloys.	225-234A 1647-1662A
for Quantitative Yield-Stress Measurements. Bendability	2061-2068A	Boron, Composite materials Stress Concentration at a Notch Tip in Unidirectional Metal	
See Formability Bending strength		Matrix Composites. Boron, Dopants	2085-2095A
See Bend strength Bending tests		Grain Boundary Pest of Boron-Doped Ni ₃ Al at 1200°C. Ductilization of Ni—Ni₄Mo Alloys by Boron Additions.	1801-1809A 3067-3071A
See Bend tests Beryllium compounds, Composite materials Preliminary Studies on NiAl/Nb ₂ Be ₁₇ Reaction and Effective-		Boron, Powder technology The Effect of Reaction Condition on Composition and Properties of Ultrafine Amorphous Powders in (Fe,Co,Ni)—B Systems Prepared by Chemical Reduction.	2125-2132A
ness of BeO as an Interfacial Reaction Barrier. Binary systems, Phase transformations Thermodynamic Equilibrium in the Low-Solute Regions of	2535-2538A	Boron, Ternary systems Activities of Boron in the Binary Ni—B and the Ternary Co—	
Plutonium-Group IIIA Metal Binary Systems. Phase Equilibria in Alloys Displaying Diffusional and Displa-	2237-2246A	Fe—B Melts. Boron carbide, Composite materials	47-52B
cive Characteristics. Binary systems, Phases (state of matter)	2565-2578A	NiAl-Based Microstructurally Toughened Composites. Boron compounds	183-189A
Crystallographic Characterization of Some Intermetallic Compounds in the AI—Cr System. Thermodynamics of Binary Systems Using Interaction Pa-	5-10A	See also Borides Boron carbide	
rameters. Thermodynamics of Aluminum—Barium Alloys. The Al—Al ₈ Mo ₃ Section of the Binary System Aluminum—	593-605B 607-616B	Boron compounds, Alloying elements A New Phase in a Rapidly Solidified and Consolidated NbAl ₃ —1TiB ₂ Alloy.	1901-1909A
Molybdenum. Coherent Phase Equilibrium in Alloys With Congruent Points. Thermodynamic Stability of Palladium Alloys. I. The	1729-1736A 1921-1935A	Boundaries See Antiphase boundaries Grain boundaries	
Palladium—Niobium System. Heats of Formation of Aluminum—Cerium Intermetallic Compounds.	1937-1943A 2119-2123A	Phase boundary Boundary lubrication	
Nonequilibrium Behavior in the Al—Ge Alloy Systems: Insights Into the Metastable Phase Diagram.	2141-2152A	See Lubrication Brasses	
Binary systems, Reactions (chemical) Activities of Boron in the Binary Ni—B and the Ternary Co— Fe—B Melts.	47-52B	See also Aluminum brasses Brasses, Mechanical properties Quantitative Assessment of the Implications of Strain-	
Binders (adhesives) Interface Structure in Infiltrated Composites of Aluminum Re- inforced With Alumina—Silica Fiber Preforms.	1126-1128A	Induced Microstructural Changes in Superplasticity. Yielding Behavior of Prestrained Interstitial-Free Steel and 70/30 Brass.	83-96A 393-401A
Bismuth, Binary systems Thermodynamics of Binary Systems Using Interaction Parameters.		Brasses, Metal working Characterization of Hot Deformation Behavior of Brasses Using Processing Maps. I. a Brass. Characterization of Hot Deformation Behavior of Brasses	2985-2992A
Bismuth, Impurities Kinetics of Removal of Bismuth and Lead From Molten Copper Alloys in Vacuum Induction Melting.	447-465B	Using Processing Maps. II. β Brass and α — β Brass. Brasses, Phase transformations Effects of Thermal Cycling on the Martensitic Transformation	2993-3001A
Cathodic Copper Deposition at 65°C in the Absence and Presence of Bi ³⁺ and Sb ³⁺ Additives in Acidified CuSO ₄ Aqueous Solutions.	575-581B	in Two-Phase $\alpha \beta$ Brasses. The Shape Memory Effect and Superelasticity in Two-Phase Polycrystalline $\alpha \beta$ Brasses.	1473-1478A 1479-1490A
		B	
Thermochemical Nature of Minor Elements in Copper Smelt- ing Mattes. Blast furnace practice	677-688B	Braze See Brazing	

Brazed joints Effect of Grain Boundaries on Isothermal Solidification During Transient Liquid Phase Brazing.	1627-1631A	Coarsening Resistance of M ₂ C Carbides in Secondary Hard- ening Steels. II. Alloy Design Aided by a Thermochemical Database. Coarsening Resistance of M ₂ C Carbides in Secondary Hard-	2869-2876A
Brazing Modeling of Base Metal Dissolution Behavior During Tran-			2877-2888A
sient Liquid-Phase Brazing. Effect of Grain Boundaries on Isothermal Solidification During Transient Liquid Phase Brazing.	543-555A 1627-1631A	Carbon See also Graphite	
Brazing alloys Modeling of Base Metal Dissolution Behavior During Tran-		Carbon, Alloying elements Thermodynamic Consideration of Grain Refinement of Aluminum Alloys by Titanium and Carbon.	3071-3075A
sient Liquid-Phase Brazing. Bridgman method See Crystal growth	543-555A	Carbon, Quaternary systems Thermodynamic Properties of the Fe—Mn—V—C System.	1911-1920A
Brine		A Thermodynamic Assessment of the Fe—Cr—Ni—C System.	2187-2198A
See Salt water		Carbon, Ternary systems	0044 00004
Brittle fracture, Corrosion effects Brittle Fracture of an Au/Ag Alloy Induced by a Surface Film.	531-541A	An Assessment of the Fe—C—Si System. Carbon compounds	2211-2223A
Brittle fracture, Microstructural effects Effect of Hydrogen as a Temporary β Stabilizer on Microstructure and Brittle Fracture Behavior in a Titanium Aluminida Alloy.	71-81A	See Carbides Carbon steels See also High carbon steels	
Brittleness		Killed steels Low carbon steels	
See Temper brittleness		Medium carbon steels	
Bronzes, Phase transformations The Decomposition of the Beta Phase in the Copper—Tin System. Bubbles	11-18A	Carbon steels, Casting Optimization and Continuous Casting. I. Problem Formulation and Solution Strategy. Optimization and Continuous Casting. II. Application to In-	641-648B
Accelerated Fracture Due to Tritium and Helium in 21-6-9	970 998 A	dustrial Casters. Mold Behavior and Its Influence on Quality in the Continuous	649-659B
Stainless Steel. Discussion of "Evidence for the Existence of Potassium Bubbles in AKS-Doped Tungsten Wire" and Reply.	879-886A 2153-2156A	Casting of Steel Slabs. I. Industrial Trials, Mold Tempera- ture Measurements, and Mathematical Modeling.	861-874B
Bubbling Desulfurization Kinetics of Molten Copper by Gas Bubbling. Building materials	5-11B	Mold Behavior and Its Influence on Quality in the Continuous Casting of Steel Slabs. II. Mold Heat Transfer, Mold Flux Behavior, Formation of Oscillation Marks, Longitudinal Off- Corner Depressions, and Subsurface Cracks.	875-888B
See Construction materials Building up See Hard surfacing		Carbon steels, Diffusion Effect of Retained Austenite on the Hydrogen Content and Ef-	2579-2586A
Bulk modulus, Composition effects Third-Order Bounds on the Elastic Moduli of Metal-Matrix		fective Diffusivity of Martensitic Structure. Carbon steels, Mechanical properties High-Damping Metals and Alloys.	607-616A
Composites. Burdening	3065-3067A	Finite Element Prediction of the Fatigue Limit of Steel. Carbon steels, Rolling	1678-1680A
See Blast furnace practice Burning See Combustion		The Thermal and Metallurgical State of Steel Strip During Hot Rolling. III. Microstructural Evolution.	335-349A
CAD/CAM See Computer aided design		Carbonyl powders, Microstructure Microstructure of Ultrafine Carbonyl Iron Powder.	2709-2711A
CADAM		Carburization See Carburizing	
See Computer aided design Calculating		Carburizing See also Gas carburizing	
See Computation Computer programs		Transformation of Retained Austenite in Carburized 4320 Steel.	1491-1500A
Mathematical analysis Numerical analysis		Case carburizing See Carburizing	
Calculation See Computation		Case depth The Prediction of Case Depth in Laser Transformation Hard-	
Computer programs Mathematical analysis Numerical analysis		ening. Case hardening	2459-2466A
Calorimetry A Calorimetric Study of Precipitation in an Al—Cu Alloy With		See Carburizing	
Silicon Particles. Enthalpies of Formation of Refractory Borides by High- Temperature Direct Synthesis Calorimetry: RuB _{1.1} and	665-674A	Cast iron See also Alloy cast iron Gray iron	
RhB _{1.1} .	1680-1683A	White iron Cast iron, Casting	
Cantilever beams, Mechanical properties Thermal and Mechanical Considerations in Using Shape Memory Alloys to Control Vibrations in Flexible Structures.	623-627A	An Assessment of the Fe—C—Si System. Cast iron, End uses	2211-2223A
Carbides See also Boron carbide		Heat Flux Transients at the Casting/Chill Interface During Solidification of Aluminum Base Alloys.	717-727B
Metal carbides Silicon carbide		Casting See also Chill casting	
An Experimental Study of Carbide/Austenite Equilibria in the High-Speed Steel Alloy System.	1391-1405A	Continuous casting Pressure casting	
Use of Differential Interference Contrast Microscopy to Detect Duplex Carbides in Alloy White Cast Irons.	1673-1674A	Rheocasting Slab casting	
Thermodynamic Properties of the Fe—Mn—V—C System. A Thermodynamic Assessment of the Fe—Cr—Ni—C Sys-	1911-1920A	Squeeze casting An Improved Mathematical Model for Electromagnetic Cast-	
tem. Solute Distribution Around a Coherent Precipitate in a Multi-	2187-2198A	ers and Testing by a Physical Model.	121-134B
component Alloy. Powder Metallurgy T15 Tool Steel. I. Characterization of	2199-2210A	Castings See also Sand castings	
Powder and Hot Isostatically Pressed Material. Powder Metallurgy T15 Tool Steel. II. Microstructure and Properties After Heat Treatment.	2733-2745A 2747-2759A	Castings, Directional solidification Simultion of Freckles During Vertical Solidification of Binary Alloys.	847-859B
Carbide Precipitation in Welds of Two-Phase Austenitic— Ferritic Stainless Steel.	2889-2902A	Catalytic converters See Automotive components	O41-000D
Carbides, Alloying effects On the Nature of Eutectic Carbides in Cr—Ni White Cas Irons.	1709-1720A	Cathodic coatings (oxide)	
Solidification and Phase Equilibria in the Fe—C—Cr—NbC System.	2181-2186A	See Oxide coatings Causticity See by	
Carbides, Crystal growth Coarsening Resistance of M ₂ C Carbides in Secondary Hard	-	See pH Cavitation	
ening Steels. I. Theoretical Model for Multicomponen Coarsening Kinetics.	t 2863-2868A	Pitting Corrosion Behavior of Powder Metallurgy Mechani- cally Alloyed IN-9052.	938-941A

Cavitation, Stress effects High-Temperature Rupture of Microstructurally Unstable 304		Microstructural Evolution in Rapidly Solidified Al—Fe Alloys: an Alternative Explanation.	927-934A
Štainles's Steel Under Uniaxial and Triaxial Stress States. CCT curves See TTT curves	2629-2635A	Chlorides, Solubility Representation of the Solubility of Lead Chloride in Various Chloride Solutions With Pitzer's Model.	491-498B
Cells		Chlorine compounds See Chlorides	431-4305
See Electrolytic cells Cellular precipitates Growth-Speed Dependence of Primary Arm Spacings in Directionally Solidified Pb—10 wt.% Sn. Solute Distribution During Steady-State Cellular Growth.	2467-2473A 3035-3039A	Chromium, Alloying additive The Effects of Chromium Additions to Binary TiAl-Base Alloys. Chromium, Alloying elements	2619-2626A
Statistical Analysis of the Disorder of Two-Dimensional Cellu- lar Arrays in Directional Solidification.	3041-3050A	Solidification Microporosity in Directionally Solidified Multi- component Nickel Aluminide.	225-234A
Cementite The Role of Ledges in the Proeutectoid Ferrite and Proeutectoid Cementite Reactions in Steel.	1367-1380A	Ductility Enhancement in NIAI (B2)-Base Alloys by Microstructural Control. The Effect of Copper, Chromium, and Zirconium on the Microstructure and Mechanical Properties of AI—Zn—Mg—	441-446A
Ceramics See also Aluminum oxide Boron carbide		Cu Alloys. Chromium, Binary systems Crystallographic Characterization of Some Intermetallic	2809-2818A
Silicon carbide Titanium carbide		Compounds in the AI—Cr System. Chromium, Quaternary systems	5-10A
Ceramics, Joining Effect of Plastic Deformation on Residual Stresses in Ceramic/Metal Interfaces.	2822-2825A	A Thermodynamic Assessment of the Fe—Cr—Ni—C System.	2187-2198A
Cerium, Binary systems Heats of Formation of Aluminum—Cerium Intermetallic Compounds.	2119-2123A	Chromium, Reactions (chemical) Activities of Chromium in Molten Copper at Dilute Concentrations by Solid-State Electrochemical Cell. Kinetics of the Reduction of Bushveld Complex Chromite Ore	475-480B
Cerium compounds, Physical properties Heats of Formation of Aluminum—Cerium Intermetallic Com- pounds.	2119-2123A	at 1416°C. A Reassesment of the Activity of Chromium in the Fe—Cr—O System at 1873K.	801-810B 915-918B
CGF forging process See Forging	2115-2120A	Chromium, Ternary systems Representation of Excess Thermodynamic Properties of Ternary Systems Using Interaction Parameters.	583-591B
Chalcocite, Beneficiation Leaching Kinetics of Copper From Natural Chalcocite in Alka-		Chromium molybdenum nickel steels	303-3315
line Na₄EDTA Solutions. Chalcogenides See Sulfides	295-303B	See Nickel chromium molybdenum steels Chromium molybdenum steels See also Chromium molybdenum vanadium steels	
Charring See Combustion		Nickel chromium molybdenum steels Chromium molybdenum steels, Heat treatment	
Chatter See Vibration		Microstructural Evolution of Modified 9Cr—1Mo Steel. Chromium molybdenum steels, Nondestructive testing	1049-1058A
Chemical analysis See Microanalysis Surface analysis (chemical)		The Evaluation of In-Service Materials Degradation of Low- Alloy Steels by the Electrochemical Method. Chromium molybdenum steels, Structural hardening	2097-2106A
Chemical compounds See Cryolite		Coarsening Resistance of M ₂ C Carbides in Secondary Hard- ening Steels. III. Comparison of Theory and Experiment.	2877-2888A
Chemical equilibrium High-Temperature Thermodynamic Properties of the Vana- dium Carbides V ₂ C and VC _{0.73} Determined Using a Gal-		Chromium molybdenum steels, Welding Fracture Toughness Behavior of Ex-Service 2.25Cr—1Mo Steels From a 22-Year-Old Fossil Power Plant.	455-468A
vanic Cell Technique. A Degenerate Electron Gas Model for Solutions of Aluminum in Cryolite Melts.	661-668B	Chromium molybdenum vanadium steels, Forming Development of Deformation Instability in Hot Tensile Test Specimens.	2297-2302A
Phase Relations and Thermodynamics of the System Fe— Cr—O in the Temperature Range of 1600-1825°C (1873- 2098K) Under Strongly Reducing Conditions. Oxygen Pressure Dependence of Cu ₂ O—CuO—Gd ₂ O; Phase Diagram. Chemical Potential Diagram of Al—Ti—C System: Al ₄ C ₃ For	689-703B 705-710B	Chromium molybdenum vanadium steels, Mechanical properties Effect of Long-Term Service Exposure on Microstructure and Mechanical Properties of a CrMoV Steam Turbine Rotor Steel.	1811-1820A
mation on TiC Formed in AI—Ti Liquids Containing Carbon Chemical kinetics	. 3075-3076A	Chromium molybdenum vanadium steels, Nondestructive testing The Evaluation of In-Service Materials Degradation of Low-	
See Reaction kinetics Chemical potential Chemical Potential Chemical Research of Al. Ti. C. System: Al. C. For		Alloy Steels by the Electrochemical Method. Chromium nickel molybdenum steels	2097-2106A
Chemical Potential Diagram of Al—Ti—C System: Al ₄ C ₃ For mation on TiC Formed in Al—Ti Liquids Containing Carbon	. 3075-3076A	See Nickel chromium molybdenum steels Chromium nickel steels	
Chemical processes See Reactions (chemical)		See Nickel chromium steels Chromium ores, Reduction (chemical)	
Chemical processing equipment, Nondestructive testing The Evaluation of In-Service Materials Degradation of Low Alloy Steels by the Electrochemical Method.	2097-2106A	Kinetics of the Reduction of Bushveld Complex Chromite Ore at 1416°C.	801-810B
Chemical properties See Activity (chemical) Chemical potential		Chromium steels See also Chromium molybdenum steels Nickel chromium steels	
Chemical reactions See Reactions (chemical)		Chromium steels, Forming Influence of Microstructure on Centerburst Development in Steel Extrusions.	807-815A
Chemical reduction See Reduction (chemical)		Chromium steels, Mechanical properties Strain Distribution Effects on the Low-Cycle Fatigue Behavior	
Chemical vapor deposition Modeling Chemical Vapor Deposition of Silicon With Local	al	of Fe—C—Mo Steels. Chromium steels, Melting	675-683A
Equilibrium Consideration at the Substrate. Chemical Vapor Deposition Kinetics of Tungsten From WCI Onto Nickel Plate at Elevated Temperatures. Three-Dimensional Mathematical Model for Transport Phe	560-563B	Phase Relations and Thermodynamics of the System Fe- Cr-O in the Temperature Range of 1600-1825°C (1873- 2098K) Under Strongly Reducing Conditions.	
nomena in Horizontal Chemical Vapor Deposition Read tors. Chemistry	811-822B	Chromium steels, Metal working Torsional Hot Workability in 0.47C—0.86Mn—0.5Cr—E Steel From 650-870°C.	469-477A
See Electrochemistry Physical chemistry Surface chemistry Thermochemistry		Chromium steels, Steel making Phase Relations and Thermodynamics of the System Fe— Cr—O in the Temperature Range of 1600-1825°C (1873- 2098K) Under Strongly Reducing Conditions.	689-703B
Chill casting Heat Flux Transients at the Casting/Chill Interface During Solidification of Aluminum Base Allovs.)- 717-727B	Chromium steels, Structural hardening The Effect of Tungsten on Dislocation Recovery and Precipitation Behavior of Low-Activation Martensitic 9Cr Steels.	2225-2235A

Chromium vanadium steels		Columbium base alloys	
See Chromium molybdenum vanadium steels		See Niobium base alloys	
Cinematography Measurements of Rapid Solidification Rate in Highly Under- cooled Melts With a Video System.	2825-2828A	Columbium compounds See Niobium compounds	
Claddings, Corrosion Effects of Transformation on Texture and Iodine Stress Corrosion Cracking Resistance of Zircaloy Sheet.	2247-2256A	Columnar structure A Volume-Averaged Two-Phase Model for Transport Phenomena During Solidification.	349-361B
Cleavage		Combustion Anomalous Combustion Effects During Mechanical Alloying.	3019-3024A
Microstructure and Local Brittle Zone Phenomena in High- Strength Low-Alloy Steel Welds. Brittle Fracture of an Au/Ag Alloy Induced by a Surface Film.	139-149A 531-541A	Compacting See Explosive compacting	
Fracture of Single Crystals of the Nickel-Base Superalloy PWA 1480E in Hydrogen at 22°C.	2031-2038A	Compacts See Powder compacts	
Cleavage, Corrosion effects Cleavage Crystallography of Liquid Metal Embrittled Alumi-		Compatibility	
num Alloys.	1849-1855A	Reaction of Titanium and Ti—Al Alloys With Alumina. Compliance (elasticity)	715-721A
Cleavage, Microstructural effects Fracture of Single Crystals of the Nickel-Base Superalloy PWA 1480E in Helium at 22°C.	731-738A	See Modulus of elasticity Components	
Close packed hexagon See Hexagonal lattice		See Aircraft components Automotive components	
Clustering		Nuclear reactor components Pressure vessel components	
Computer Simulation of the Effect of Coherency Strain on Cluster Growth Kinetics.	1197-1209A	Rotors Shafts (power)	
The Role of Ledges in Stress Tensor-Mediated Surface Pro- cesses for Silicon and GaAs.	1317-1322A	Composite materials	
Lattice Changes of Iron—Carbon Martensite on Aging at		See also Fiber composites	
Room Temperature. Clustering, Heating effects	1957-1967A	Laminates Particulate composites Whisker composites	
Electron Microscopy Study of the Aging and First Stage of Tempering of High-Carbon Fe—C Martensite.	797-806A	Composite materials, Mechanical properties	
Coating See Continuous coating		Expressions for Predicting the Elasticity Modulus of Materials Reinforced by Second-Phase Grains.	507-511A
Surfacing		Composite materials, Reactions (chemical)	
Coatings See Electrocoatings		Preliminary Studies on NiAl/Nb ₂ Be ₁₇ Reaction and Effectiveness of BeO as an Interfacial Reaction Barrier.	2535-2538A
Oxide coatings Protective coatings		Compounds See Aluminum compounds	
Weld deposited coatings		Intermetallics	
Cobalt, Alloying elements Ductility Enhancement in NiAl (B2)-Base Alloys by Microstructural Control.	441-446A	Compression casting See Pressure casting	
Cobalt, Powder technology	441-440M	Compression strength See Compressive strength	
The Effect of Reaction Condition on Composition and Properties of Ultrafine Amorphous Powders in (Fe,Co,Ni)—B Systems Prepared by Chemical Reduction.	2125-2132A	Compressive modulus See Modulus of elasticity	
Cobalt, Ternary systems Activities of Boron in the Binary Ni—B and the Ternary Co—		Compressive properties See also Compressive strength	
Fe—B Melts.	47-52B	Mechanical, Elastic, and Structural Properties of Alloys of	129-137A
Cobalt base alloys, Mechanical properties High-Damping Metals and Alloys.	607-616A	Ru—Ta High-Temperature Intermetallic Compounds. Mechanical Properties of High Temperature Alloys of AIRu. 1000 to 1200K Time-Dependent Compressive Deformation of	403-414A
See Crack opening displacement		Single-Crystalline and Polycrystalline B2 Ni—40Al. Compressive strength	1595-1607A
Coefficient of expansion		Modeling of the Corrosion Behavior and Its Interrelation With the Deformation Behavior and Microstructure in a Newly	
See Thermal expansion Coefficient of friction		Developed 7.5Mn—5Cr—1.5Cu Alloy White Iron.	2319-2325A
See Friction		Compressive yield strength See Compressive strength	
Coefficient of thermal expansion See Thermal expansion		Computation	
Coil coating See Continuous coating		Correction to "A New Technique for Three-Dimensional Tran- sient Heat Transfer Computations of Autogenous Arc Welding".	389B
Cold aging See Aging (natural)		Computer aided design	
Cold cracking (welds)		Modeling Chemical Vapor Deposition of Silicon With Local Equilibrium Consideration at the Substrate.	309-321B
See Weld defects Cold deformation		Heat Flux Transients at the Casting/Chill Interface During So- ildification of Aluminum Base Alloys. Three-Dimensional Mathematical Model for Transport Phe-	717-727B
See Deformation Cold ductility		nomena in Horizontal Chemical Vapor Deposition Reactors.	811-822B
See Ductility Cold formability		Computer programs Heat Flux Transients at the Casting/Chill Interface During So-	
See Formability		lidification of Aluminum Base Alloys. Coarsening Resistance of M ₂ C Carbides in Secondary Hard-	717-727B
Cold forming See Cold working		ening Steels. II. Alloy Design Aided by a Thermochemical Database.	2869-2876A
Cold reduction See Cold working		Computer simulation Role of Near-Wall Node Location on the Prediction of Melt	
Cold rolling		Flow and Residence Time Distribution in Tundishes by	
Effects of Microalloying Elements and Heat Treatments o Tensile Properties in Cu—23Zn—3.4AL—1Ni—X Alloys.	256-258A	Mathematical Modeling. Dynamic Compaction of Titanium Aluminides by Explosively Generated Shock Waves: Experimental and Materials Sys-	
High Strain Rate Superplasticity of a 25 wt.% Cr—7 wt. Ni—3 wt.% Mo—0.14 wt.% N Duplex Stainless Steel.	1083-1091A	tems.	685-695A
Thermal Behavior of Steel Rolling With Nonconventions Rolls.	1767-1774A	Computer Simulation of the Effect of Coherency Strain on Cluster Growth Kinetics.	1197-1209A
Cold stretching		Macroscopic Description of Interface Migration by Ledge and Kink Motion Controlled by Volume Diffusion.	1225-1233A
See Stretching Cold working		Computer Simulation of Morphological Changes of Grain Boundary Precipitates Growing by the Ledge Mechanism. Report on Panel Discussion. II. Critical Problems in the Math-	1235-1245A
See also Cold rolling The Effect of Plastic Deformation on Al ₂ CuLi (T ₁) Precipits		ematics of Ledgewise Growth.	1247-1248A
tion.	299-306A	Thickening of Grain-Boundary α Allotriomorphs in a Ti—Ci Alloy by Multiple Sets of Ledges.	1341-1348A
Columbium See Niobium		Prediction of Steel Flow Stresses at High Temperatures and Strain Rates.	

An Experimental and Theoretical Study of Cementite Dissolu- tion in an Fe—Cr—C Alloy. Simulation of Subgrain Growth by Subgrain Rotation: a One- Dimensional Model.	1745-1752A 2257-2263A	Microstructural Engineering Applied to the Controlled Cool- ing of Steel Wire Rod. II. Microstructural Evolution and Me- chanical Properties Correlations. Microstructural Engineering Applied to the Controlled Cool- ing of Steel Wire Rod. III. Mathematical Model—	2779-2790A
Modeling of Crystal Growth During Rapid Solidification. Microstructural Engineering Applied to the Controlled Cool- ing of Steel Wire Rod. I. Experimental Design and Heat	2475-2485A	Formulation and Predictions.	2791-2805A
Transfer. Computers	2769-2778A	Copper, Alloying elements The Effect of Copper, Chromium, and Zirconium on the Mi-	
Growth Path Envelope Analysis of Ostwald Ripening. Correction to "Growth Path Envelope Analysis of Ostwald Ri-	19-23A	crostructure and Mechanical Properties of Al—Zn—Mg—Cu Alloys.	2809-2818A
pening". Computing	19-23A	Copper, Binary systems Thermodynamics of Binary Systems Using Interaction Parameters.	593-605B
See Computation Concast See Continuous casting		Copper, Crystal growth The Role of Ledges in Vapor/Solid Phase Transformations	
Concentration (stress)		Observed by Low-Energy Electron Microscopy and Photo- emission Electron Microscopy.	1311-1315A
See Stress concentration Concentration cell corrosion		Copper, Diffusion Intermetallic Phase Formation and Breakdown of Molybde- num Diffusion Barriers in Ni—Mo—Cu Layers.	1501-1510A
See Pitting (corrosion) Condensation (process)		Copper, End uses Mold Behavior and its Influence on Quality in the Continuous	1001-10101
See Condensing Condensing Observations of the Formation and Kinetics of Surface Steps	4000 40044	Casting of Steel Slabs. II. Mold Heat Transfer, Mold Flux Behavior, Formation of Oscillation Marks, Longitudinal Off- Corner Depressions, and Subsurface Cracks.	875-888B
During Evaporation and Condensation. Conducting sheet analog	1299-1304A	Copper, Extraction The Kinetics of S ³⁵ Exchange Between SO ₂ /CO/CO ₂ Gas	
See Heat transmission Conductivity		Mixtures and Copper Sulfide Melts at 1523K. Dissolution of Malachite in Aqueous Ethylenediaminetetr- aacetate Solution.	211-217B 569-574B
See Thermal conductivity Constitutional diagrams		Mathematical Modeling of Sulfide Flash Smelting Process. III. Volatilization of Minor Elements.	791-799B
See Phase diagrams Construction		Copper, Forming Dislocation Cell Structures and Mechanical Properties of	
See Sandwich construction Shipbuilding		Oxygen-Free High-Conductivity Copper During Wire Draw- ing at Various Speeds. Correction to "Dislocation Cell Structures and Mechanical	258-261A
Construction materials, Mechanical properties Development of Vibration-Damping Resins for Room- Temperature Application.	629-631A	Properties of Oxygen-Free High-Conductivity Copper Dur- ing Wire Drawing at Various Speeds".	258-261A
Contact angle The Wettability of Carbon/TiB ₂ Composite Materials by Aluminum in Cryolite Melts.	617-621B	Copper, Joining Effect of Plastic Deformation on Residual Stresses in Ceramic/Metal Interfaces.	2822-2825A
Nucleation of Solidification in Liquid Droplets. Contact bonding	2487-2501A	Copper, Mechanical properties A Simple, Versatile Miniaturized Disk-Bend Test Apparatus	
See Bonding Continuous casting		for Quantitative Yield-Stress Measurements. Effect of Grain Size on High Strain Rate Deformation of Copper.	2061-2068A 2349-2357A
An Ultrasonic Method for Reconstructing the Two- Dimensional Liquid/Solid Interface in Solidifying Bodies. Optimization and Continuous Casting. I. Problem Formulation	467-473B	Copper, Reactions (chemical) Activities of Chromium in Molten Copper at Dilute Concentrations by Solid-State Electrochemical Cell.	475-480B
and Solution Strategy. Optimization and Continuous Casting. II. Application to Industrial Casters.	641-648B 649-659B	Copper, Recovering The Dissolution Behavior of Metals From Ag/Cu and Ag/Au	
Mold Behavior and Its Influence on Quality in the Continuous Casting of Steel Slabs. I. Industrial Trials, Mold Tempera	3	Alloys in Aidic and Cyanide Solutions. Copper, Refining	755-764B
ture Measurements, and Mathematical Modeling. Mold Behavior and its Influence on Quality in the Continuous Casting of Steel Slabs. II. Mold Heat Transfer, Mold Flu Behavior, Formation of Oscillation Marks, Longitudinal Off	K	Desulfurization Kinetics of Molten Copper by Gas Bubbling. Desulfurization and Deoxidation of Cu—S—O Alloy in Induc- tion Melting and Solidification Under Argon and Their Rates	3
Corner Depressions, and Subsurface Cracks.	875-888B	of Elimination in Vacuum Induction Melting. Kinetics of Removal of Bismuth and Lead From Molten Cop- per Alloys in Vacuum Induction Melting.	405-416B 447-465B
Continuous coating Monitoring of Slag Composition Changes by Density Mea surements.	305-307B	Cathodic Copper Deposition at 65°C in the Absence and Presence of Bi ³⁺ and Sb ³⁺ Additives in Acidified CuSO ₄	
Control See Noise control		Aqueous Solutions. New Observations on the Anodic Oxidation of Copper in Ho	575-581B
Process control Controllability		Acidified Copper Sulfate Solutions. Deoxidation Rate of Copper Droplet Levitated in Ar—H ₂ Gas Stream.	
See Stability Controlled atmospheres		Thermochemical Nature of Minor Elements in Copper Smelt ing Mattes.	677-688B
See Inert atmospheres Controlled rolling		Copper, Rolling Analysis of an Aluminum Single Crystal With Unstable Initia Orientation (001)[110] in Channel Die Compression.	45-58A
Effects of Vanadium and Processing Parameters on th Structures and Properties of a Direct-Quenched Low Carbon Mo—B Steel.		Copper, Structural hardening	f 2375-2384A
Converters A Mathematical Model of the Nickel Converter. I. Model Development and Verification.	153-161B	Copper, Ternary systems Calculation of Phase Diagrams and Solidification Paths o Aluminum-Rich Al—Li—Cu Alloys.	of 2837-2848A
Cooling See Splat cooling Supercooling		Copper base alloys See also Brasses Bronzes	
Cooling rate Numerical Simulation of a Solidifying Pb—Sn Alloy: the E fects of Cooling Rate on Thermosolutal Convection and	ıd	Copper base alloys, Alloy development Effects of Microalloying Elements and Heat Treatments or	n 256-258A
Macrosegregation. Crystallization of a Faceted Primary Phase in a Stirred Slurr Solidification of Undercooled Sn—Sb Peritectic Alloys.			
Microstructural Evolution. Solidification of Undercooled Sn—Sb Peritectic Alloys. Heterogeneous Nucleation.	753-764A II. 765-773A	Copper base alloys, End uses Heat Flux Transients at the Casting/Chill Interface During So	
Mold Behavior and Its Influence on Quality in the Continuor Casting of Steel Siabs. II. Mold Heat Transfer, Mold Flu Behavior, Formation of Oscillation Marks, Longitudinal Of Corner Depressions, and Subsurface Cracks.	JX	lidification of Aluminum Base Alloys. Copper base alloys, Mechanical properties Faceted Fatigue Fracture and Its Relation to the Crystallo	>
Study on Formation of Channel-Type Segregation. Microstructural Engineering Applied to the Controlled Coding of Steel Wire Rod. I. Experimental Design and He	1663-1672A		415-425A 607-616A
Transfer.	2769-2778		1165-1175A

Copper base alloys, Powder technology	10.024	Crack closure, Stress effects	
Growth Path Envelope Analysis of Ostwald Ripening. Correction to "Growth Path Envelope Analysis of Ostwald Ripening".	19-23A 19-23A	The Effect of Particulate SiC on Fatigue Crack Growth in a Cast-Extruded Aluminum Alloy Composite. The Influence of Applied Stress, Crack Length, and Stress In-	97-112A
The Formation of Metastable Phases by Mechanical Alloying in the Aluminum and Copper System.	2849-2854A	tensity Factor on Crack Closure. Crack growth	1559-1571A
Copper base alloys, Structural hardening On the Constraint Factor Associated With the Indentation of		See Crack propagation	
Work-Hardening Materials With a Spherical Ball. Copper base alloys, Surface properties	2375-2384A	Crack initiation Microstructure and Local Brittle Zone Phenomena in High- Strength Low-Alloy Steel Welds.	139-149A
Surface Composition of Ternary Cu—Ag—Au Alloys. I. Experimental Results.	1833-1840A	Dynamic Fracture Behavior of SiC Whisker-Reinforced Alu-	367-375A
Surface Composition of Ternary Cu-Ag-Au Alloys. II. A		minum Alloys. The Initiation and Growth of Fatigue Cracks in a Titanium Al-	
Comparison of Experiment With Theoretical Models. Copper compounds, Microstructure	1841-1848A	uminide Alloy. Fatigue Behavior in the Potentiostatic Passive Corrosion Re-	377-391A
Development of Structure and Porosity in Cast Al ₅ CuZr ₂ and Al ₆₈ Mn ₉ Zr ₂₅ Intermetallic Compounds.	2545-2552A	gime of the Iron-Base Superalloy A-286. Modeling of Corrosion Fatigue Crack Initiation Under Passive Electrochemical Conditions.	513-519A 521-529A
Copper compounds, Physical properties Note on the Enthalpies of Formation of Cu ₃ Si and Cu ₃ Ge.	2162-2165A	Crack Initiation and Propagation During High-Temperature Fatigue of Oxide Dispersion-Strengthened Superalloys.	837-851A
Copper mattes Mathematical Modeling of Sulfide Flash Smelting Process. III. Volatilization of Minor Elements.	791-799B	Fatigue Behavior of a 2xxx Series Aluminum Alloy Reinforced With 15 vol.% SiC _p . Material Effects in Fretting Wear: Application to Iron, Tita-	1007-1019A
Copper mattes, Reduction (chemical) Thermochemical Nature of Minor Elements in Copper Smelt-	791-7990	nium, and Aluminum Alloys. The Mechanical Behavior of a Hybrid Metal Matrix Compos- ite.	1535-1544A 2107-2117A
ing Mattes.	677-688B	Further Study on the Scattering of the Local Fracture Stress	
Copper ores See also Chalcocite		and Allied Toughness Value.	2287-2296A
Copper ores, Reduction (chemical)		Crack initiation, Microstructural effects Surface Void Nucleation Under the Power-Law Creep Condi-	
Dissolution of Malachite in Aqueous Ethylenediaminetetr- aacetate Solution.	569-574B	tion in an AI—3 at.% Mg Solid Solution Alloy. Fracture Initiation at Hydrides in Zirconium.	935-937A 2327-2337A
Mathematical Modeling of Sulfide Flash Smelting Process. III. Volatilization of Minor Elements.	791-799B	Crack initiation, Stress effects Hydrostatic Stresses and Their Effect on the Macroflow Be- havior and Microfracture Mechanism of Two-Phase Alloys.	2695-2702A
Core hardness See Hardness		Crack opening displacement	EGGG ETGET
Corex process See Ironmaking		Further Study on the Scattering of the Local Fracture Stress and Allied Toughness Value.	2287-2296A
Corrodents		Crack opening displacement, Microstructural effects Micromechanics of Shear Ligament Toughening.	2021-2029A
See Corrosion environments Corrosion		A Comparison of the Fracture Behavior of Two Commercially Produced Heats of HY180 Steel Differing in Sulfide Type.	2277-2285A
See Stress corrosion cracking Transgranular corrosion		Crack propagation	
Corrosion cracking		The Kinetics and Micromechanics of Hydrogen-Assisted Cracking in Fe—3% Si Single Crystals.	59-70A
See Stress corrosion cracking Corrosion environments		Effects of Material Rate Sensitivity and Void Nucleation on Fracture Initiation in a Circumferentially Cracked Bar. The Initiation and Growth of Fatigue Cracks in a Titanium Al-	161-170A
Brittle Fracture of an Au/Ag Alloy Induced by a Surface Film. A Mechanistic Study of Transgranular Stress Corrosion	531-541A	uminide Alloy.	377-391A
Cracking of Type 304 Stainless Steel. Delayed Hydride Cracking Behavior for Zircaloy-2 Tubing.	1453-1461A 2049-2060A	Faceted Fatigue Fracture and its Relation to the Crystallo- graphic Slip Systems in Cu—16 at.% Al Single Crystals. Analysis of Crack Tip Sliding Displacement in Anisotropic	415-425A
Corresion latigue Fatigue Behavior in the Potentiostatic Passive Corrosion Re-		Elastic Media and Its Application to Stage I Fatigue Crack Growth.	479-487A
gime of the Iron-Base Superalloy A-286. Modeling of Corrosion Fatigue Crack Initiation Under Passive	513-519A	Fatigue Behavior in the Potentiostatic Passive Corrosion Regime of the Iron-Base Superalloy A-286.	513-519A
Electrochemical Conditions.	521-529A	Thermomechanical Fatigue of Particulate-Reinforced Aluminum 2xxx-T4.	697-707A
Environmental Fatigue of an Al—Li—Cu Alloy. I. Intrinsic Crack Propagation Kinetics in Hydrogenous Environments.	2415-2428A	Crack Initiation and Propagation During High-Temperature	
Behavior of Acoustic Emission for Low-Strength Structural Steel During Fatigue and Corrosion Fatigue. Corrosion mechanisms	2677-2680A	Fatigue of Oxide Dispersion-Strengthened Superalloys. Dynamic Fatigue Experiments on Optical Fibers. Thermomechanical Fatigue of a Lead Alloy.	837-851A 867-871A 1059-1070A
The Kinetics and Micromechanics of Hydrogen-Assisted		The Growth of Short Fatigue Cracks Under Compressive	1079-1082A
Cracking in Fe—3% Si Single Crystals. On the Stress Corrosion Cracking of Al—Li Alloys: the Role	59-70A	and/or Tensile Cyclic Loading. On the Mechanism of Fatigue Crack Growth in Silicon Nitride. A Critical Evaluation of the Stress-Corrosion Cracking Mech-	1425-1434A
of Grain Boundary Precipitates. Accelerated Fracture Due to Tritium and Helium in 21-6-9	264-267A	anism in High-Strength Aluminum Allovs.	2407-2414A
Stainless Steel. Pitting Corrosion Behavior of Powder Metallurgy Mechani-	879-886A	Environmental Fatigue of an Al—Li—Ću Alloy. I. Intrinsic Crack Propagation Kinetics in Hydrogenous Environments.	2415-2428A
cally Alloyed IN-9052. Intergranular Stress Corrosion Cracking of Alloy 600 and X-750 in High-Temperature Deaerated Water/Steam.	938-941A	Crack propagation, Environmental effects Delayed Hydride Cracking Behavior for Zircaloy-2 Tubing.	2049-2060A
Morphology and Aging of the Martensite Induced by Cathodic		Effect of High-Pressure Hydrogen on Crack Growth in Car- bon Steel.	2703-2707A
Hydrogen Charging of High-Carbon Austenitic Steels. A Critical Evaluation of the Stress-Corrosion Cracking Mech-	1979-1991A	Crack propagation, Impurity effects	
anism in High-Strength Aluminum Alloys. Corrosion potential	2407-2414A	Internal Hydrogen-Induced Subcritical Crack Growth in Austenitic Stainless Steels.	2605-2618A
Pitting Corrosion Behavior of Powder Metallurgy Mechani- cally Alloyed IN-9052.	938-941A	Crack propagation, Microstructural effects Fatigue Crack Propagation and Cryogenic Fracture Tough- ness Behavior in Powder Metallurgy Aluminum—Lithium	
Corrosion prevention See Passivation		Alloys. Microstructural Effects on Ambient and Elevated Tempera-	191-202A
Corrosion rate Modeling of the Corrosion Behavior and Its Interrelation With	1	ture Fatigue Crack Growth in Titanium Aluminide Intermet- allics.	817-828A
the Deformation Behavior and Microstructure in a Newly Developed 7.5Mn—5Cr—1.5Cu Alloy White Iron.	2319-2325A	Micromechanics of Shear Ligament Toughening. Fracture Toughness and Crack Growth Rate of Ferritic and	2021-2029A
Corrosion resistance, Deformation effects Mechanisms of Deformation-Induced Grain Boundary Chro-		Pearlitic Compacted Graphite Cast Irons at 25 and 150°C. Crack propagation, Pressure effects	2645-2653A
mium Depletion (Sensitization) Development in Type 316 Stainless Steels.	2917-2934A	Effect of High-Pressure Hydrogen on Crack Growth in Car- bon Steel.	2703-2707A
Corrosion resistance, Microstructural effects		Crack propagation, Stress effects	
Effects of Transformation on Texture and Iodine Stress Corrosion Cracking Resistance of Zircaloy Sheet. Corrosion resistant steels	2247-2256A	The Effect of Particulate SiC on Fatigue Crack Growth in a Cast-Extruded Aluminum Alloy Composite. Crack propagation, Temperature effects	97-112A
See Stainless steels Crack closure		Low-Temperature Fatigue of 316L and 316LN Austenitic Stainless Steels.	2385-2392A
The Growth of Short Fatigue Cracks Under Compressive and/or Tensile Cyclic Loading.	1079-1082A	Crack resistance See Crack propagation	

Cracking (fracturing) See also Crack closure Crack initiation Crack propagation		Modeling of Crystal Growth During Rapid Solidification. Solidification of Highly Undercooled Fe—P Alloys. Measurements of Rapid Solidification Rate in Highly Under-	2475-2485A 2761-2768A 2825-2828A
Stress corrosion cracking Dynamic Compaction of Titanium Aluminides by Explosively Generated Shock Waves: Experimental and Materials Sys-		cooled Melts With a Video System. Solute Distribution During Steady-State Cellular Growth. Crystal growth, Alloying effects	3035-3039A
tems. A Phase Diagram Approach to Study Liquation Cracking in	685-695A	Thermodynamic Consideration of Grain Refinement of Aluminum Alloys by Titanium and Carbon.	3071-3075A
Alloy 718. Cracking (fracturing), Environmental effects Environmental and Hold Time Effects on Fatigue of Low-Tin	887-902A	Crystal lattices See Hexagonal lattice Superlattices	
Lead-Based Solder. Cracks	357-366A	Crystal orientation See Crystal structure	
Effects of Material Rate Sensitivity and Void Nucleation on Fracture Initiation in a Circumferentially Cracked Bar.	161-170A	Crystal structure See also Widmanstatten structure	
Cratering (welding) See Weld defects		Crystallographic Characterization of Some Intermetallic Compounds in the Al—Cr System. The Effects of Interface Kinetics Anisotropy on the Growth	5-10A
Creep (materials) See also Creep rate		Direction of Cellular Microstructures. The AI—Al ₈ Mo ₃ Section of the Binary System Aluminum— Molybdenum.	585-593A 1729-1736A
Creep rupture strength Crack Initiation and Propagation During High-Temperature Fatigue of Oxide Dispersion-Strengthened Superalloys.	837-851A	The Effect of Continuous Heating on the Phase Transforma- tions in Zinc—Iron Electrodeposited Coatings.	1737-1743A
Instantaneous and Residual Stresses Developed in Hot Iso- static Pressing of Metals and Ceramics.	1071-1078A	A New Phase in a Rapidly Solidified and Consolidated NbAl ₃ —1TiB ₂ Alloy. Development of Structure and Porosity in Cast Al ₅ CuZr ₂ and	1901-1909A
The Deformation of an Aluminum—Silicon Eutectic Alloy Under Thermal Cycling Conditions. Transformation of Retained Austenite in Carburized 4320	1113-1115A	Al ₈₆ Mn ₉ Zr ₂₅ Intermetallic Compounds. An Investigation of FeNi Order in a Steel.	2545-2552A 2807-2809A
Steel. Creep (materials), Heating effects	1491-1500A	Crystallinity See Crystal structure	
Microstructural Evolution of Modified 9Cr—1Mo Steel.	1049-1058A	Crystallization See Recrystallization	
Creep (materials), Microstructural effects Creep Deformation of TiB ₂ -Reinforced Near-γ Titanium Aluminides.	447-454A	Crystallography The Crystallography and Atomic Structure of Line Defects in	
Surface Void Nucleation Under the Power-Law Creep Condi- tion in an AI—3 at % Mg Solid Solution Alloy. Development of a Necklace Microstructure During Isothermal Deformation and its Properties Relative to Uniform Micro-	935-937A	Twin Boundaries in Hexagonal-Close-Packed Metals. Crystals See Polycrystals	1185-1196A
structures.	1999-2008A	Single crystals CTT curves	
See Creep (materials)		See TTT curves Cubic lattice	
See Creep (materials)		See Body centered cubic lattice	
Creep rate Creep of Die Cast AZ91 Magnesium at Room Temperature	070 0774	See Deep drawing	
and Low Stress. Processing and Creep Characterization of a Model Metal Matrix Composite: Lead Reinforced With Nickel Fibers.	873-877A 1029-1036A	Current efficiency Loss of Current Efficiency in Aluminum Electrolysis Cells.	177-182B
Creep rupture strength, Microstructural effects Development of a Necklace Microstructure During Isothermal Deformation and its Properties Relative to Uniform Micro-	4000 0000	Current voltage characteristics Cathodic Copper Deposition at 65°C in the Absence and Presence of Bi ³ and Sb ³ Additives in Acidified CuSO ₄ Aqueous Solutions.	575-581B
STRUCTURES. Creep rupture strength, Temperature effects	1999-2008A	New Observations on the Anodic Oxidation of Copper in Hot Acidified Copper Sulfate Solutions.	623-630B
High-Temperature Rupture of Microstructurally Unstable 304 Stainless Steel Under Uniaxial and Triaxial Stress States. Creeping	2629-2635A	See Stress strain curves	
Sec Creep (materials) Crevices		CVD See Chemical vapor deposition	
See Cracks Cross slip		Cycles See Thermal cycling	
A Model for the Strain-Rate Dependence of Yielding in Ni ₃ Al Alloys.	125-128A	Cyclic loads The Growth of Short Fatigue Cracks Under Compressive	
Cross tension test See Tension tests		and/or Tensile Cyclic Loading. The Shape Memory Effect and Superelasticity in Two-Phase Polycrystalline a/B Brasses.	1079-1082A 1479-1490A
Crushing strength See Compressive strength		Influence of Cyclic Deformation on Surface Microstructure and Hardness of Ion-Implanted Nickel.	1633-1646A
Cryolite The Wettability of Carbon/TiB2 Composite Materials by Alu-		Cyclical heating See Thermal cycling	
minum in Cryolite Melts. A Degenerate Electron Gas Model for Solutions of Aluminum in Cryolite Melts.	617-621B 669-672B	Damage See Radiation damage	
Crystal defects	0310-000	Damping High-Damping Metals and Alloys.	607-616A
See also Dislocations Displacements (lattice) Stacking faults		Characterization of the Damping Properties of Die-Cast Zinc—Aluminum Alloys.	617-622A
The Geometry and Properties of Ledges in Interfaces. The Crystallography and Atomic Structure of Line Defects in Twin Boundaries in Hexagonal-Close-Packed Metals.	1177-1183A 1185-1196A	Development of Vibration-Damping Resins for Room- Temperature Application. Chlorosulfonated Polyethylene: a Versatile Polymer for	
Crystal growth See also Epitaxial growth	1100-1130A	Damping Acoustic Waves. On the Influence of Ply-Angle on Damping and Modulus of	633-640A
See also Epitaxial growth Diffusion-Controlled Kink Motion. Macroscopic Description of Interface Migration by Ledge and	1219-1224A	Elasticity of a Metal-Matrix Composite. Vibration Damping Characteristics of Laminated Steel Sheet.	641-651A 653-658A
Kink Motion Controlled by Volume Diffusion. Nonequilibrium Effects During the Ledgewise Growth of a	1225-1233A	See Phase decomposition	
Solid/Liquid Interface. Growth Kinetics of Solid/Liquid Gallium Interfaces. I. Experi- mental.	1259-1270A	Decomposition reactions, High temperature effects Discussion of "Evidence for the Existence of Potassium Bub- bles in AKS-Doped Tungsten Wire" and Reply.	2153-2156A
Growth Kinetics of Solid/Liquid Gallium Interfaces. II. Theo- retical. Observations of the Formation and Kinetics of Surface Steps	1271-1286A	Deep carburizing See Carburizing	
During Evaporation and Condensation. Ledgewise Vaporization.	1299-1304A 1305-1310A	Deep drawability	
Nonequilibrium Behavior in the Al—Ge Alloy Systems: Insights Into the Metastable Phase Diagram. Thermodynamical Study of Gas Transport in Thin Film	2141-2152A	See Drawability Deep drawing Earing in Cup Drawing Face-Centered Cubic Single Crystals	
Growth: Application to Bismuth Chalcogenides.	2401-2405A	and Polycrystals.	1525-1534A

Effect of Processing Variables on Texture and Texture Gradients in Tantalum.	2039-2048A	Creep of Die Cast AZ91 Magnesium at Room Temperature and Low Stress.	873-877A
See Hardening		Differential thermal analysis Solidification of Undercooled Sn—Sb Peritectic Alloys. II. Heterogeneous Nucleation.	765-773A
Defects See also Cracks		Diffusion	
Crystal defects Surface defects Weld defects		Determination of Liquid Diffusion Coefficients Along a Liquidus Phase Boundary. Grain Boundary Diffusion of Hydrogen in Nickel. On the Kinetics of Diffusion-Limited Layer Growth in Solid—	21-26B 351-355A
High-Damping Metals and Alloys. Influence of Microstructure on Centerburst Development in	607-616A	Solid Systems.	523-527B 715-721A
Steel Extrusions. Deflagration	807-815A	Reaction of Titanium and Ti—Al Alloys With Alumina. A Phase Diagram Approach to Study Liquation Cracking in Alloy 718.	887-902A
See Combustion Petermability		Correction to "Literature Survey on Diffusivities of Oxygen Aluminum, and Vanadium in Alpha Titanium, Beta Titanium,	4404 44054
See Formability		and in Rutile". Diffusion-Controlled Kink Motion.	1121-1125A 1219-1224A
Deformation See also Plastic deformation Prestraining		Macroscopic Description of Interface Migration by Ledge and Kink Motion Controlled by Volume Diffusion. Interface Dislocations and Ledges in Oxidation and Diffu-	1225-1233A
Deformation, Microstructural effects On the Influence of Microstructure on the Room-Temperature		sional Phase Transformations. Thickening of Grain-Boundary α Allotriomorphs in a Ti—Cr Alloy by Multiple Sets of Ledges.	1331-1339A 1341-1348A
Deformation Behavior of a Near- α Titanium Alloy.	1122-1125A	Intermetallic Phase Formation and Breakdown of Molybde- num Diffusion Barriers in NiMoCu Layers. Discussion of "A Mechanism for the Formation of Lower Bai-	1501-1510A
See Deformation		nite" and Authors' Heply.	1674-1678A
Delaminating The Mechanical Behavior of a Hybrid Metal Matrix Composite	2107-2117A	An Experimental and Theoretical Study of Cementite Dissolution in an Fe—Cr—C Alloy.	1745-1752A
ite. Dendrite	2107-2117A	See Diffusion	
See Dendritic structure Dendritic structure		See Diffusion	
The Effects of Interface Attachment Kinetics on Solidification Interface Morphologies.	235-249A	Diffusivity Thermochemistry and Diffusion of Nitrogen in Solid Molybde-	
A Volume-Averaged Two-Phase Model for Transport Phe- nomena During Solidification. On the Rate of Dendrite Arm Coarsening.	349-361B 569-574A	NUM. Diffusivity, Microstructural effects	219-224B
The Effects of Interface Kinetics Anisotropy on the Growth Direction of Cellular Microstructures.	585-593A	Effect of Retained Austenite on the Hydrogen Content and Effective Diffusivity of Martensitic Structure.	2579-2586A
Simultion of Freckles During Vertical Solidification of Binary Alloys.	847-859B	Diffusivity, Temperature effects Determination of Equilibrium Solid-Phase Transition Temper-	
The Energy and Solute Conservation Equations for Dendritic Solidification.	889-900B	atures Using DTA.	1993-1998A
Aging Characteristics of Electron Beam and Gas Tungsten Arc Fusion Zones of Al—Cu—Li Alloy 2090.	903-913A	See Particle size Thickness	
Correction to On the Rate of Dendrite Arm Coarsening". Growth-Speed Dependence of Primary Arm Spacings in Di- rectionally Solidified Pb—10 wt.% Sn.	1466A 2467-2473A	Dioxides See Sulfur dioxide	
Eutectic Spacing Selection in Lead-Based Alloy Systems. Measurements of Rapid Solidification Rate in Highly Under-	2523-2533A	Direct reduction Slag Foaming in Bath Smelting.	481-489B
cooled Melts With a Video System. Density	2825-2828A	Directional solidification	
A New Experimental Method for Determining Liquid Density and Surface Tension.	27-31B	Solidification Microporosity in Directionally Solidified Multi- component Nickel Aluminide. The Effects of Interface Attachment Kinetics on Solidification	225-234A
Synthesis of Iron Aluminides From Elemental Powders: Reaction Mechanisms and Densification Behavior.	277-286A	Interface Morphologies. Composite Growth in Hypermonotectic Alloys.	235-249A 339-348B
See Deoxidizing		In Situ Observation of Interactions Between Gaseous Inclusions and an Advancing Solid/Liquid Interface.	385-388B
Deoxidizing Desulfurization and Deoxidation of Cu—S—O Alloy in Induc-		Analysis of Crack Tip Sliding Displacement in Anisotropic Elastic Media and Its Application to Stage I Fatigue Crack Growth.	479-487A
tion Melting and Solidification Under Argon and Their Rates of Elimination in Vacuum Induction Melting. Deoxidation Rate of Copper Droplet Levitated in Ar—H ₂ Gas	405-416B	The Effects of Interface Kinetics Anisotropy on the Growth Direction of Cellular Microstructures.	585-593A
Stream.	631-639B	Simultion of Freckles During Vertical Solidification of Binary Alloys. In Situ Observation of Faceted Cellular Array Growth.	847-859B 941-945A
Dephosphorizing		Correction to "In Situ Observation of Faceted Cellular Array	041 04071
A Thermodynamic Study of Dephosphorization Using BaO—	22 200		941-945A
BaF ₂ , CaO—CaF ₂ , and BaO—CaO—CaF ₂ Systems. The Effect of Na ₂ O on Dephosphorization by CaO-Based Steelmaking Stags.	33-38B 39-46B	Growth". Nonequilibrium Effects During the Ledgewise Growth of a Solid/Liquid Interface.	941-945A 1249-1258A
BaF ₂ , CaO—CaF ₂ , and BaO—CaO—CaF ₂ Systems. The Effect of Na ₂ O on Dephosphorization by CaO-Based Stellmaking Slags. Activities of Chromium in Molten Copper at Dilute Concentrations by Solid-State Electrochemical Cell.		Growth". Nonequilibrium Effects During the Ledgewise Growth of a Solid/Liquid Interface. Atomic Structure of the Crystalline/Amorphous Interface in a Directionally Crystallized Priession Allow.	
BaF ₂ , CaO—CaF ₂ , and BaO—CaO—CaF ₂ Systems. The Effect of Na ₂ O on Dephosphorization by CaO-Based Steelmaking Slags. Activities of Chromium in Molten Copper at Dilute Concentrations by Solid-State Electrochemical Cell. Thermodynamic Behavior of Phosphorus in CaO—CaF ₂ —SiO ₂ and CaO—Na ₂ O—SiO ₂ Systems.	39-46B	Growth". Nonequilibrium Effects During the Ledgewise Growth of a Solid/Liquid Interface. Atomic Structure of the Crystalline/Amorphous Interface in a Directionally Crystallized PdepSigo Alloy. Study on Formation of Channel-Type Segregation. Surface Energy Reduction in Fibrous Monotectic Structures. Growth-Speed Dependence of Primary Arm Spacings in Di-	1249-1258A
BaF ₂ , CaO—CaF ₂ , and BaO—CaO—CaF ₂ Systems. The Effect of Na ₂ O on Dephosphorization by CaO-Based Stellmaking Slags. Activities of Chromium in Molten Copper at Dilute Concentrations by Solid-State Electrochemical Cell. Thermodynamic Behavior of Phosphorus in CaO—CaF ₂ —SiO ₂ and CaO—Na ₂ O—SiO ₂ Systems. Deposition See Electrodeposition	39-46B 475-480B	Growth". Nonequilibrium Effects During the Ledgewise Growth of a Solid/Liquid Interface. Atomic Structure of the Crystalline/Amorphous Interface in a Directionally Crystallized PdgeSigo Alloy. Study on Formation of Channel-Type Segregation. Surface Energy Reduction in Fibrous Monotectic Structures. Growth-Speed Dependence of Primary Arm Spacings in Directionally Solidified Pb—10 wt.% Sn. Eutectic Spacing Selection in Lead-Based Alloy Systems.	1249-1258A 1287-1298A 1663-1672A 1881-1886A 2467-2473A 2523-2533A
BaF ₂ , CaO—CaF ₂ , and BaO—CaO—CaF ₂ Systems. The Effect of Na ₂ O on Dephosphorization by CaO-Based Stellmaking Slags. Activities of Chromium in Molten Copper at Dilute Concentrations by Solid-State Electrochemical Cell. Thermodynamic Behavior of Phosphorus in CaO—CaF ₂ —SiO ₂ and CaO—Na ₂ O—SiO ₂ Systems. Deposition See Electrodeposition Vapor deposition Design	39-46B 475-480B	Growth." Nonequilibrium Effects During the Ledgewise Growth of a Solid/Liquid Interface. Atomic Structure of the Crystalline/Amorphous Interface in a Directionally Crystallized PdepSizo Alloy. Study on Formation of Channel-Type Segregation. Surface Energy Reduction in Fibrous Monotectic Structures. Growth-Speed Dependence of Primary Arm Spacings in Directionally Solidified Pb—10 wt.% Sn. Eutectic Spacing Selection in Lead-Based Alloy Systems. Solute Distribution During Steady-State Cellular Growth.	1249-1258A 1287-1298A 1663-1672A 1881-1886A 2467-2473A 2523-2533A 3035-3039A
BaF ₂ , CaO—CaF ₂ , and BaO—CaO—CaF ₂ Systems. The Effect of Na ₂ O on Dephosphorization by CaO-Based Steelmaking Slags. Activities of Chromium in Molten Copper at Dilute Concentrations by Solid-State Electrochemical Cell. Thermodynamic Behavior of Phosphorus in CaO—CaF ₂ —SiO ₂ and CaO—Na ₂ O—SiO ₂ Systems. Deposition See Electrodeposition Vapor deposition Deaign See also Computer aided design Three-Dimensional Mathematical Model for Transport Phe-	39-46B 475-480B 499-502B	Growth." Nonequilibrium Effects During the Ledgewise Growth of a Solid/Liquid Interface. Atomic Structure of the Crystalline/Amorphous Interface in a Directionally Crystallized PdepSizo Alloy. Study on Formation of Channel-Type Segregation. Surface Energy Reduction in Fibrous Monotectic Structures. Growth-Speed Dependence of Primary Arm Spacings in Directionally Solidified Pb—10 vt./s Sn. Eutectic Spacing Selection in Lead-Based Alloy Systems. Solute Distribution During Steady-State Cellular Growth. Statistical Analysis of the Disorder of Two-Dimensional Cellular Arrays in Directional Solidification. Eutectic Growth Under Rapid Solidification Conditions.	1249-1258A 1287-1298A 1663-1672A 1881-1886A 2467-2473A 2523-2533A
BaF ₂ , CaO—CaF ₂ , and BaO—CaO—CaF ₂ Systems. The Effect of Na ₂ O on Dephosphorization by CaO-Based Steelmaking Slags. Activities of Chromium in Molten Copper at Dilute Concentrations by Solid-State Electrochemical Cell. Thermodynamic Behavior of Phosphorus in CaO—CaF ₂ —SiO ₂ and CaO—Na ₂ O—SiO ₂ Systems. Deposition See Electrodeposition Vapor deposition Deaign See also Computer aided design Three-Dimensional Mathematical Model for Transport Phenomena in Horizontal Chemical Vapor Deposition Reactors.	39-46B 475-480B 499-502B	Growth." Nonequilibrium Effects During the Ledgewise Growth of a Solid/Liquid Interface. Atomic Structure of the Crystalline/Amorphous Interface in a Directionally Crystallized PdegSigo Alloy. Study on Formation of Channel-Type Segregation. Surface Energy Reduction in Fibrous Monotectic Structures. Growth-Speed Dependence of Primary Arm Spacings in Directionally Solidified Pb—10 wt.% Sn. Eutectic Spacing Selection in Lead-Based Alloy Systems. Solute Distribution During Steady-State Cellular Growth. Statistical Analysis of the Discrete of Two-Dimensional Cellular Arrays in Directional Solidification. Eutectic Growth Under Rapid Solidification Conditions. Directionally solidified eutectics Eutectic Growth Under Rapid Solidification Conditions.	1249-1258A 1287-1298A 1663-1672A 1881-1886A 2467-2473A 2523-2533A 3035-3039A 3041-3050A
BaF ₂ , CaO—CaF ₂ , and BaO—CaO—CaF ₂ Systems. The Effect of Na ₂ O on Dephosphorization by CaO-Based Stellmaking Slags. Activities of Chromium in Molten Copper at Dilute Concentrations by Solid-State Electrochemical Cell. Thermodynamic Behavior of Phosphorus in CaO—CaF ₂ —SiO ₂ and CaO—Na ₂ O—SiO ₂ Systems. Deposition See Electrodeposition Vapor deposition Design See also Computer aided design Three-Dimensional Mathematical Model for Transport Phenomena in Horizontal Chemical Vapor Deposition Reac-	39-46B 475-480B 499-502B	Growth." Nonequilibrium Effects During the Ledgewise Growth of a Solid/Liquid Interface. Atomic Structure of the Crystalline/Amorphous Interface in a Directionally Crystallized PdgoStgo Alloy. Study on Formation of Channel-Type Segregation. Surface Energy Reduction in Fibrous Monotectic Structures. Growth-Speed Dependence of Primary Arm Spacings in Divectionally Solidified Pb—10 wt% Sn. Eutectic Spacing Selection in Lead-Based Alloy Systems. Solute Distribution During Steady-State Cellular Growth. Statistical Analysis of the Discrete of Two-Dimensional Cellular Arrays in Directional Solidification. Eutectic Growth Under Rapid Solidification Conditions.	1249-1258A 1287-1298A 1663-1672A 1881-1886A 2467-2473A 2523-2533A 3035-3039A 3041-3050A 3051-3057A
BaF ₂ , CaO—CaF ₂ , and BaO—CaO—CaF ₂ Systems. The Effect of Na ₂ O on Dephosphorization by CaO-Based Steelmaking Slags. Activities of Chromium in Molten Copper at Dilute Concentrations by Solid-State Electrochemical Cell. Thermodynamic Behavior of Phosphorus in CaO—CaF ₂ —SiO ₂ and CaO—Na ₂ O—SiO ₂ Systems. Deposition See Electrodeposition Vapor deposition Deaign See also Computer aided design Three-Dimensional Mathematical Model for Transport Phenomena in Horizontal Chemical Vapor Deposition Reactors. Desorption See Outgassing Desulfurizing Desulfurizing Desulfurizing Kinetics of Molten Copper by Gas Bubbling.	39-46B 475-480B 499-502B 811-822B	Growth." Nonequilibrium Effects During the Ledgewise Growth of a Solid/Liquid Interface. Atomic Structure of the Crystalline/Amorphous Interface in a Directionally Crystallized PdepSizo Alloy. Study on Formation of Channel-Type Segregation. Surface Energy Reduction in Fibrous Monotectic Structures. Growth-Speed Dependence of Primary Arm Spacings in Directionally Solidified Pb—10 vit./s Sn. Eutectic Spacing Selection in Lead-Based Alloy Systems. Solute Distribution During Steady-State Cellular Growth. Statistical Analysis of the Disorder of Two-Dimensional Cellular Arrays in Directional Solidification. Eutectic Growth Under Rapid Solidification Conditions. Directionally solidified eutectics Eutectic Growth Under Rapid Solidification Conditions. Discontinuous precipitates	1249-1258A 1287-1298A 1663-1672A 1881-1886A 2467-2473A 2523-2533A 3035-3039A 3041-3050A 3051-3057A
BaF ₂ , CaO—CaF ₂ , and BaO—CaO—CaF ₂ Systems. The Effect of Na ₂ O on Dephosphorization by CaO-Based Steelmaking Slags. Activities of Chromium in Molten Copper at Dilute Concentrations by Solid-State Electrochemical Cell. Thermodynamic Behavior of Phosphorus in CaO—CaF ₂ —SlO ₂ and CaO—Na ₂ O—SlO ₂ Systems. Deposition See Electrodeposition Vapor deposition Design See also Computer aided design Three-Dimensional Mathematical Model for Transport Phenomena in Horizontal Chemical Vapor Deposition Reactors. Desorption See Outgassing Desulfurization Kinetics of Molten Copper by Gas Bubbling. Desulfurization and Deoxidation of Cu—S—O Alloy in Induction Meliting and Solidification Under Argon and Their Rade.	39-46B 475-480B 499-502B 811-822B	Growth". Nonequilibrium Effects During the Ledgewise Growth of a Solid/Liquid Interface. Atomic Structure of the Crystalline/Amorphous Interface in a Directionally Crystallized PdgoSizo Alloy. Study on Formation of Channel-Type Segregation. Surface Energy Reduction in Fibrous Monotectic Structures. Growth-Speed Dependence of Primary Arm Spacings in Directionally Solidified Pb—10 vt./s Sn. Eutectic Spacing Selection in Lead-Based Alloy Systems. Solute Distribution During Steady-State Cellular Growth. Statistical Analysis of the Disorder of Two-Dimensional Cellular Arrays in Directional Solidification. Eutectic Growth Under Rapid Solidification Conditions. Directionally solidified eutectics Eutectic Growth Under Rapid Solidification Conditions. Discontinuous precipitates See Cellular precipitates See Disks Disks, Diffusion	1249-1258A 1287-1298A 1663-1672A 1881-1886A 2467-2473A 2523-2533A 3035-3039A 3041-3050A 3051-3057A
BaF ₂ , CaO—CaF ₂ , and BaO—CaO—CaF ₂ Systems. The Effect of Na ₂ O on Dephosphorization by CaO-Based Steelmaking Slags. Activities of Chromium in Molten Copper at Dilute Concentrations by Solid-State Electrochemical Cell. Thermodynamic Behavior of Phosphorus in CaO—CaF ₂ —SlO ₂ and CaO—Na ₂ O—SlO ₂ Systems. Deposition See Electrodeposition Vapor deposition Design See also Computer aided design Three-Dimensional Mathematical Model for Transport Phenomens in Horizontal Chemical Vapor Deposition Reactors. Desorption See Outgassing Desulfurization Kinetics of Molten Copper by Gas Bubbling, Desulfurization and Deoxidation of Cu—S—O Alloy in Induction Melting and Solidification Under Argon and Their Rates of Elimination in Vacuum Induction Melting.	39-46B 475-480B 499-502B 811-822B	Growth." Nonequilibrium Effects During the Ledgewise Growth of a Solid/Liquid Interface. Atomic Structure of the Crystalline/Amorphous Interface in a Directionally Crystallized PdeoSigo Alloy. Study on Formation of Channel-Type Segregation. Surface Energy Reduction in Fibrous Monotectic Structures. Growth-Speed Dependence of Primary Arm Spacings in Directionally Soliditied Pb—10 wt.% Sn. Eutectic Spacing Selection in Lead-Based Alloy Systems. Solute Distribution During Steady-State Cellular Growth. Statistical Analysis of the Disorder of Two-Dimensional Cellular Arrays in Directional Solidification. Eutectic Growth Under Rapid Solidification Conditions. Directionally solidified eutectics Eutectic Growth Under Rapid Solidification Conditions. Discontinuous precipitates See Cellular precipitates See Disks Disks Disks, Diffusion Intermetallic Phase Formation and Breakdown of Molybdenum Diffusion Barriers in Ni—Mo—Cu Layers.	1249-1258A 1287-1298A 1663-1672A 1881-1886A 2467-2473A 2523-2533A 3035-3039A 3041-3050A 3051-3057A
BaF ₂ , CaO—CaF ₂ , and BaO—CaO—CaF ₅ Systems. The Effect of Na ₂ O on Dephosphorization by CaO-Based Steelmaking Slags. Activities of Chromium in Molten Copper at Dilute Concentrations by Solid-State Electrochemical Cell. Thermodynamic Behavior of Phosphorus in CaO—CaF ₂ —SiO ₂ and CaO—Na ₂ O—SiO ₂ Systems. Deposition See Electrodeposition Vapor deposition Deaign See also Computer aided design Three-Dimensional Mathematical Model for Transport Phenomena in Horizontal Chemical Vapor Deposition Reactors. Desorption See Outgassing Desulfurization Kinetics of Molten Copper by Gas Bubbling. Desulfurization and Deoxidation of Cu—S—O Alloy in Induction Melting and Solidification Under Argon and Their Rates of Elimination in Vacuum Induction Melting. Diagrama See also Phase diagrams S N diagrams	39-46B 475-480B 499-502B 811-822B	Growth". Nonequilibrium Effects During the Ledgewise Growth of a Solid/Liquid Interface. Atomic Structure of the Crystalline/Amorphous Interface in a Directionally Crystallized PdepSize Alloy. Study on Formation of Channel-Type Segregation. Surface Energy Reduction in Fibrous Monotectic Structures. Growth-Speed Dependence of Primary Arm Spacings in Directionally Solidified Pb—10 wt/s Sn. Eutectic Spacing Selection in Lead-Based Alloy Systems. Solute Distribution During Steady-State Cellular Growth. Statistical Analysis of the Disorder of Two-Dimensional Cellular Arrays in Directional Solidification. Eutectic Growth Under Rapid Solidification Conditions. Directionally solidified eutectics Eutectic Growth Under Rapid Solidification Conditions. Discontinuous precipitates See Cellular precipitates See Disks Disks, Diffusion Intermetallic Phase Formation and Breakdown of Molybdenum Diffusion Barriers in Ni—Mo—Cu Layers. Dislocation climb See Dislocation mobility	1249-1258A 1287-1298A 1683-1672A 1881-1886A 2467-2473A 2523-2533A 3035-3039A 3041-3050A 3051-3057A
BaF ₂ , CaO—CaF ₂ , and BaO—CaO—CaF ₂ Systems. The Effect of Na ₂ O on Dephosphorization by CaO-Based Steelmaking Slags. Activities of Chromium in Molten Copper at Dilute Concentrations by Solid-State Electrochemical Cell. Thermodynamic Behavior of Phosphorus in CaO—CaF ₂ —SlO ₂ and CaO—Na ₂ O—SlO ₂ Systems. Deposition See Electrodeposition Vapor deposition Design See also Computer aided design Three-Dimensional Mathematical Model for Transport Phenomena in Horizontal Chemical Vapor Deposition Reactors. Desorption See Outgassing Desulfurization Kinetics of Molten Copper by Gas Bubbling. Desulfurization and Deoxidation of Cu—S—O Alloy in Induction Meliting and Solidification Under Argon and Their Rates of Elimination in Vacuum Induction Meliting. Diagrams See also Phase diagrams	39-46B 475-480B 499-502B 811-822B 5-11B 405-416B	Growth". Nonequilibrium Effects During the Ledgewise Growth of a Solid/Liquid Interface. Atomic Structure of the Crystalline/Amorphous Interface in a Directionally Crystallized PdgoSizo Alloy. Study on Formation of Channel-Type Segregation. Surface Energy Reduction in Fibrous Monotectic Structures. Growth-Speed Dependence of Primary Arm Spacings in Directionally Solidified Pb—10 wt.% Sin. Eutectic Spacing Selection in Lead-Based Alloy Systems. Solute Distribution During Steady-State Cellular Growth. Statistical Analysis of the Disorder of Two-Dimensional Cellular Arrays in Directional Solidification. Eutectic Growth Under Rapid Solidification Conditions. Directionally solidified eutectics Eutectic Growth Under Rapid Solidification Conditions. Discontinuous precipitates See Cellular precipitates Discs See Disks Disks, Diffusion Intermetallic Phase Formation and Breakdown of Molybdenum Diffusion Barriers in Ni—Mo—Cu Layers. Dislocation climb	1249-1258A 1287-1298A 1683-1672A 1881-1886A 2467-2473A 2523-2533A 3035-3039A 3041-3050A 3051-3057A

Unification floating and Lose Dissess. Due to Tritum and Helium in 21-69 Statistics State. Statistics State	Bl. 4 4 4 - 110			
Accessard Fracture Due to Tritum and Helium in 21-69 Statisties State Accessard Fracture Due to Tritum and Helium in 21-69 Statisties State Statistics Sta			Distribution (material) See Distribution	
Description of Technical Properties of Hospital Properties of Hospit	Accelerated Fracture Due to Tritium and Helium in 21-6-9			
Statistics State. 978-889. Statistics State. 978-889. Michanical Properties of MacCult (1) Nicitation and Growth. Michael Properties of Name Tells are Promoted and Company of Michael Properties of Name Tells are Promoted and Company of Name Tells and Properties of Name Tells and Promoted and Company of Name Tells and Properties of Name T	Dislocation pinning	879-886A	Drawability Effect of Processing Variables on Texture and Texture Gradi-	
Mechanism of ApCoLL (Tr) Nucleation and Growth Mechanism of ApCoLL (Tr) Nucleation and Growth Mechanism of Approximent of Number Peris at Norm Term The Great Company and Annone Student of Line District The Cytalloging plan of Allorest Student of Line District The Cytalloging from Objection and Derivative District The Effect of Transformation of District Approximent of Line Students and Congenie Terms Distriction Cell Students and Mechanical Properties of Distriction Cell Students and Mechanical Properties Distriction Terminal Properties of Distriction Cell Students and Mechanical Properties Distriction Terminal Properties of Distriction Cell Students and Terminal Properties of Distriction Cell Students and Terminal Properties of Distriction Cell Students and Terminal Properties Distriction Terminal Properties of Distriction Cell Students and Congenitation Cell Students and Congenita	Stainless Steel.	879-886A		2039-2048A
Description Entrangle Service Of Notice Companies on Passary Transformation Sensory or a News or Transformation Passary or Sensory or a News or Transformation Passary or Sensory or Sensor	Mechanism of Al ₂ CuLi (T ₁) Nucleation and Growth.		See Deep drawing	
On the influence of Microstructure on the Room-Temperature Dischardinaria Insertion of a Name Transmission of Interpretate Boundaries. 1129-1123- Transcription in Interpretate Boundaries. 1129-1123- Transcription in Interpretate Boundaries. 1129-1123- Transcription in Interpretate Boundaries. 1129-1123- Transcription of Place Paramicromations. 1129-1123- Transcription of Place Paramicromations. 1129-1123- Transcription of Interpretate Boundaries. 1129-1123- Transcription of Interpretate Boundaries. 1129-1123- 1239-1239- 1239-1239-1239-1239-1239-1239-1239-1239-	Low-Cycle Fatigue Behavior of Nimonic PE16 at Room Tem-		Drawing (heat treatment)	
Dries Boundaries. Discussion Linguist Properties of Longie in Interfaces. The Crystalography and Alorimo Structure of Line Defects in Tamb Boundaries in Headproach Longie in Interfaces. The Crystalography and Alorimo Structure of Line Defects in Tamb Boundaries in Headproach Longie in Interfaces. Transformations. Toward a Sound Understanding of Dislocation Plasticity. The Effect of Transform And Machanical Properties of Objects on Facility and Properties of Objects and Machanical Properties of Objects on Actual Compositions. Dislocations, Defended Behavior of Corrections for Dislocation of Plastic Defended in Properties of Objects on Actual Compositions. The Effect of Transformation and Machanical Properties of Objects on Actual Compositions on Actual City Developed Interfaces. The Effect of Dislocation of Bistructures and Machanical Properties of Objects on Actual City Developed Interfaces. The Effect of Dislocation of Bistructures and Machanical Properties of Objects on Actual City Developed Interfaces. The Effect of Dislocation of Bistructures and Machanical Properties of Objects on Actual City Developed Interfaces. The Effect of Dislocation of Bistructures and Machanical Properties of Objects on Actual City Developed Interfaces. The Effect of Dislocation of Bistructures and Machanical Properties of Objects on Actual City Developed Interfaces. The Effect of Dislocation of Bistructures and Machanical Properties of Objects on Actual City Developed Interfaces. The Effect of Tiese Defended Interfaces. The Tiese Defended Interfac	On the Influence of Microstructure on the Room-Temperature Deformation Behavior of a Near-a Titanium Alloy.		Drill steels	
The conversity and Artonic Structure of Use Delects in Transfera. The Cythalography and Artonic Structure of Use Delects in Internate Distocutions and Ladges in Octation and Drint. 1985-1984 (1985-1984). The Internate Distocutions and Ladges in Octation and Drint. 1985-1984 (1985-1984). The International Distocution Planting of Delection Planting Planting of Delection Planting Planting of Delection Planting Plant	phase Boundaries.			
Twin Boundaries in Nesagonal-Cose-Peckod Media. In Second Prose of Transformation. Toward a Sound Understanding of Dislocation Plasticity. Toward a Sound Understanding of Dislocation Plasticity. The Effect of Tungster on Dislocation Recovery and Precipitation Barbard of Low-Activation Martenizine Of Steels. Palipos and Fracture Barbardor of an Aluminum—Lithium Alay 9800-15 at Ambient and Cryogenic Temperature. Palicocations, Deformation of February States and Mechanical Properties of Disposation Programs of Mechanical Properties of Disposation Programs of Mechanical Properties of Disposation Programs of Mechanical Properties of Disposation Programs (Mechanical Properties of Disposation Programs of Mechanical Properties of Disposation Programs (Mechanical Properties of Disposation Programs of Mechanical Properties of Disposation Programs (Mechanical Properties of Disposation Programs of Mechanical Properties of Disposation Programs (Mechanical Properties of Disposation Programs of Mechanical Properties of Disposation Programs (Mechanical Properties of Disposation Programs (Mechanical Properties of Disposation Programs of Mechanical Properties of Disposation Programs (Mechanical Properties of Disposation Programs of Mechanical Properties of Disposation Programs (Mechanical Properties of Disposation Programs of Mechanical Properties of Disposation Programs (Mechanical Properties of Disposation Programs of Mechanical Properties of Disposation Programs (Mechanical Properties of Disposation Programs of Disposation Programs (Mechanical Properties of Disposation Programs of Disposation Programs (Mechanical Properties of Disposation Programs of Disposation Prog	The Geometry and Properties of Ledges in Interfaces.	1165-1175A 1177-1183A	_	
air Josepha Fransformations. Toward a Sound Understanding of Dislocation Plasticity. 1898-17084 189	Twin Boundaries in Hexagonal-Close-Packed Metals.	1185-1196A		729B
Tail Delications, Alloying effects The Effect of Traigstan on Biolocation Recovery and Precipitation Behavior of Low-Achication Managements GV Steeds. Dislocations, Cargamic effects Dislocation Cell Structures and Mechanical Properties of Oxygen-Free High-Conductivity Coper During With Draw-Correction to Tubicocation Cell Structures and Mechanical Properties of Oxygen-Free High-Conductivity Coper During With Draw-Correction to Tubicocation Cell Structures and Mechanical Properties of Oxygen-Free High-Conductivity Coper During With Draw-Correction to Tubicocation Cell Structures and Mechanical Properties of Description Properties of Oxygen-Free High-Conductivity Coper During With Draw-Correction to Tubicocation Cell Structures and Mechanical Properties of Plastic Deformation on Application	sional Phase Transformations.		See also Duplex stainless steels	
Internation Bahavior of Low-Activation Marenesis 9Cr Steels. 225-225A	Dislocations, Alloying effects	1693-1708A	Dual phase steels, Mechanical properties Strain Distribution Effects on the Low-Cycle Fatigue Behavior	
Paigue and Fracture Behavior of an Aluminum—Lithium Alipy 800-15 at Ambeint and Orgonair Comparature. Polascoations, Deformation effects Dislocation (16) Structures and Mechanical Properties of Dislocation (16) Structures and Mechanical Properties of Correction to Tollscoation Cell Structures and Mechanical Properties of Correction to Tollscoation Cell Structures and Mechanical Properties of Correction to Tollscoation Cell Structures and Mechanical Properties of Correction to Tollscoation Cell Structures and Mechanical Properties of Correction to Tollscoation Cell Structures and Mechanical Properties of Passic Deformation on Al ₂ Coult (17) Proporties to State American and Yemperature Depandence of Supertim-tion State American Passic Passic Properties of Telephone (17) Passic Deformation in the Single-Crystal Superality (17) Passic Deformation on Al ₂ Coult (17) Passic Deformation in the Single-Crystal Superality (17) Passic Deformation In the Sing	tation Behavior of Low-Activation Martensitic 9Cr Steels.	2225-2235A	Hydrostatic Stresses and Their Effect on the Macroflow Be-	
Dislocation of Structures and Mechanical Properties of Oxygen-Free High-Conductivity Copper During Wire Draws Correction to Prolisocation Cell Structures and Mechanical Properties of Oxygen-Free High-Conductivity Copper During Wire Draws Correction to Polisocation Cell Structures and Mechanical Properties of Oxygen-Free High-Conductivity Copper During Properties of Dislocations and Temperature Dependence of Superation Properties of Plastic Deformation in the Single-Crystal Superation Properties of Plastic Deformation of Modified SCr—1Mo Steel. Dispersion Hardening Alloys Scripture Properties of Plastic Deformation of Modified Scr—1Mo Steel Plastic Properties of Plastic Pro	Fatigue and Fracture Behavior of an Aluminum-Lithium	723-729A	Phase Transformation in an Fe-10.1AI-28.6Mn-0.46C	2265-2276A
Ovgen-Frea High-Conductivity Copper During Wire Draws- Correction to Tibilisation Cell Structures and Mechanical Proporties of Oxygen-Frea High-Conductivity Copper During Wire Draws- In Effect of Plastic Deformation on Algold (Tr) Procipita- The Mechanican and Temperature Dependence of Superiat- tics Stacking Fault Formation in the Single-Crystal Superia- tics Stacking Fault Fault Superial- tics S			Ductile fracture, Corrosion effects	
Proporties of Oxygen-Frea High-Conductivity Coper During With Correspond 1 Various Spender". 2009-2018. Micromorbanics of Shear Ligament Toughening. 2001-2029A. Micromorbanics 2001-2029A. M	Oxygen-Free High-Conductivity Copper During Wire Draw- ing at Various Speeds.	258-261A	Hydrogen-Assisted Ductile Fracture in Spheroidized 1520 Steel. II. Pure Bending.	1615-1626A
Ing Wer Drawing at Various Speador. 100 (1) Prosicite Deformation on AlgCulu (Tri) Precipits. 101 (1) Prosicite Deformation on AlgCulu (Tri) Precipits. 102 (1) Prosicite Deformation on AlgCulu (Tri) Precipits. 103 (1) Provided the Machaniams and Temperature Dependence of Superational Professional Pr	Properties of Oxygen-Free High-Conductivity Copper Dur-			2021-2029A
The Mechanisms and Temperature Dependence of Superiation 2009-2318A 2009-2318	ing Wire Drawing at Various Speeds".			
Dispersion hardening alloys, Corrosion Plating Corrosion Bahavior of Powder Metallurgy Mechanical Propersion Bandward or Dewder Metallurgy Mechanical Composities of a Rapidy Solidined All—Limitation and Propagation. Intell Gas Abmittable Propersion of Tanglity Fragmentature Applications. Intell Gas Abmittable Propersion of Tanglity Fragmentat	The Mechanisms and Temperature Dependence of Superlat-	299-306A	Ductility	
Dispersion hardening A New Phase in a Papidry Solidified and Consolidated Mody—IT Big Alloy. Dispersion hardening alloys, Corrosion Dispersion hardening alloys, Meat hateatment According Alloyer of Powder Metallurgy Mechanically Alloyer of Powder Metallurgy Mechanically Alloyer of Powder Metallurgy Mechanical Propersion of a Rapidry Solidited All—LI—Minimal Alloys of Powder Metallurgy Mechanical Properties of a Rapidry Solidited All—LI—Minimal Properties of Alloys of Powder Metallurgy Mechanical Properties of Alloys of Chromium Alloys Mechanical Properties of Alloys of Chromium Alloys. Dispersion hardening alloys, Meat treatment Properties of Alloys of Chromium Alloys of Chromium Alloys of Chromium Alloys of Chromium Alloys. Dispersion hardening alloys, Mechanical properties of Alloys of Chromium Alloys. Dispersion hardening alloys, Mechanical Properties of Alloys of Chromium Alloys of Chromium Alloys of Chromium Alloys. Dispersion hardening alloys, Mechanical Properties of Alloys of Chromium Alloys of Chromium Alloys of Chromium Alloys. Dispersion hardening alloys, Structural hardening of Displacement (lattice) Displacement		2309-2318A	2014 + 15 vol.% SiC Particulate Composite.	113-123A
Dispersion hardening alloys, Corrosion Effect of Plastic Deformation alloys. Dispersion hardening alloys, Carbon and Experimental Subject of Propersion Supersion Hardening alloys, Carbon and Supersion Hardening alloys, Heat treatment Microdivocuted and Thorna Stability of a 11—43A IAItoy Contains Dispersion hardening alloys, Mechanical properties Crack Initiation and Propagation During High-Temperature Applications I. Inert Gas Alomization Processing. Dispersion hardening alloys, Mechanical properties Crack Initiation and Propagation During High-Temperature Papellation of Control Dispersion-Strengthered Supersion	Dislocations, Heating effects Microstructural Evolution of Modified 9Cr—1Mo Steel.	1049-1058A		
Ribect of Phase Morphology on the Mechanical Behavior of Two Triannum Aluminide Composites. Dispersion hardening alloys, Corosion Behavior of Powder Metallurgy Mechanically Aspect in Pobles. Dispersion hardening alloys, Corosion Behavior of Powder Metallurgy Mechanically Aspect in Pobles. Dispersion hardening alloys, Heat treatment Microcortectural and Thermal Stability of a TI—43M Alloy Conjugating Dispersion Programs of the Poor Supersion of Cardinal Propersion Supersion Programs (Particular Aspectation of Color Dispersion Programs Supersions). Dispersion hardening alloys, Mechanical properties Crack Initiation and Propagation During High-Temperature Patigue of Oxide Dispersion-Strengthened Supersiolys. Biografion hardening alloys, Structural hardening Toward a Sound Understanding of Dislocation Plesticity. Dispersion See Emulsions Dispersion hardening alloys, Structural hardening Toward a Sound Understanding of Dislocation Plesticity. Dispersion hardening alloys, Structural hardening Toward a Sound Understanding of Dislocation Plesticity. Dispersion hardening alloys, Structural hardening Toward a Sound Understanding of Dislocation Plesticity. Dispersions See Emulsions Displacement Spless See Displacement gliets Dispersion hardening alloys, Structural Plesticity. Displacement gliets See Displacement gliets See Displacement gliets See Displacement gliets See Displacement gliets Dispersion hardening alloys and provided in the Two-Phase See See Stables of Mechanical Propersies of AISI 4390 Steel Triough High-Temperature Thermomechanical Treatment. Dispersion hardening alloys, Structural Selfects Dispersion hardening alloys and Propagation on Iron, Tita-Illium, Alloy 6090-To at Ambient and Cryogenic Temperature and National Propersies of AISI 4390 Steel Triough High-Temperature Thermomechanical Treatment (attains) Dispersion hardening alloys of Mechanical Behavior of Two-Titanical Propersies o	Dispersion hardening		Ductility and Dynamic Strain Aging in Rapidly Solidified Alu-	
Dispersion hardening alloys, Nechanical streament 2009-2019A	NDAI3-111B2 Alloy.	1901-1909A	Mechanical Behavior of Cast Particulate SiC/AL (A356) Metal	
Pitting Corrosion Bahavior of Powder Metallurgy Mechani- ally Alloyard 1902. Dispersion hardening alloys, Heat treatment Microstructural and Thermal Stability of a TIII - 4324 Alloy Con- maining Dispersoids of Trianium Original Planting Corrosion Bahavior of Powder Metallurgy Alloyard (Pringing Applications II. Spray Alloyard Large Applications II. Spray Alloyard Large Applications. II. Spray Alloyard Large Applications of Binary TIAl-Base Alloys. Dispersion hardening alloys, Mechanical properties Crack Institution and Propagation During High-Temperature Fatigue and Fracture Behavior of an Aluminum—Lithium Alloyard Large and Fracture Behavior of Alloyard Alloyard Large and Fracture Behavior of Alloyard Large and Fracture Behavior of Alloyard Alloyard Large and Fracture Large and Alloyard Large and Fracture Behavior of Alloyard Large and Fracture Large and Fracture Behavior of Alloyard Large and Fracture Behavior of Allo		2009-2019A	Structure and Properties of a Rapidly Solidified Al-LI-	1000-1000-1
Microstructural and Thermal Stability of a Tim-43A Alloy Containing Dispersoids of Timanium Di-Borde. Dispersion hardening alloys, Mechanical properties Crack initiation and Propagation During High-Temperature Fatigue of Oxide Dispersion-Strengthemed Superalioys. Dispersion hardening alloys, Structural hardening Toward a Sound Understanding of Dislocation Plasticity. Dispersions See Emulsions Displacement Material Effects in Fretting Wear: Application to Iron, Titanium, and Aluminum Alloys. Displacement spikes See Displacement (lattice) Displacement (lattice) Structural Ledges in Interphase Boundaries. Displacements (lattice) Displacements (lattice) Displacements (lattice) Displacements (lattice) Structural Ledges in Interphase Boundaries. Displacements (lattice) Displacements (lat	Dispersion hardening alloys, Corrosion Pitting Corrosion Behavior of Powder Metallurgy Mechanically Alloyed IN-9052.	938-941A	Gas Atomization Processing. Structure and Properties of a Rapidly Solidified Al—Li— Mn—Zr Alloy for High-Temperature Applications. II. Spray	
Dispersion hardening alloys, Mechanical properties Crack initiation and Propagation During Hip-Temperature Fatigue of Oxide Dispersion-Strengthened Superatioys. Dispersion hardening alloys, Structural hardening Toward a Sound Understanding of Dislocation Plasticity. Dispersions See Emulsions Displacement Material Effects in Fretting Wear: Application to Iron, Tita- nium, and Aluminum Alloys. Displacements gilkes See Displacements (lattice) Displacements (lattice) Displacements (lattice) Structural Ledges in Interphase Boundaries. Displacements (lattice) Displacements (lattice) Structural Ledges in Interphase Boundaries. Dissibilation Geramich/Metal Interfaces. Dissolution See also Acid dissolution See also Acid dissolution Modeling of Base Metal Dissolution Behavior During Tran- sient Liquid-Phase Brazing Dissolution of Machanical Properties of Alloys Unclined Properties of Alloys (Phase Tracing) Morphology of Cementite Decomposition in an Fe—Cr—C Alloy. The Evaluation of In-Service Materials Degradation of Low- Alloy Steels by the Electrochemical Method. Dissolution See Dissolution See Dissolution Solute Distribution Around a Coherent Precipitate in a Multi- component Alloy. 2689-85148 1693-1706A 1693-170	Microstructural and Thermal Stability of a Ti-43Al Alloy Con-			2515-2522A
Crack Initiation and Propagation During High-Temperature Fatigue of Oxide Dispersion-Strengthened Supersion-Strengthened Supersion-Streng		1/21-1/28A		2619-2626A
Dispersions See Emulsions Displacement Material Effects in Fretting Wear: Application to Iron, Titanium, and Aluminum Alloys. Displacement spikes See Displacements (lattice) Displacements (lattice) Structural Ledges in Interphase Boundaries. Displacements (lattice) Displacements (lattice) Structural Ledges in Interphase Boundaries. Dissolution Effect of Plastic Deformation on Residual Stresses in Ceramic/Metal Interfaces. Dissolution See Brazing Dissolution See also Acid dissolution Modeling of Base Metal Dissolution Behavior During Transient Liquid-Phase Brazing. Dissolution Equilibrium of Magnesium Vapor in Liquid from. An Experimental and Theoretical Study of Cementite Dissolution in an Fe—Cr—C Alloy, Morphology of Cementite Decomposition in an Fe—Cr—C Alloy. Alloy Steels by the Electrochemical Method. Dissolution of In-Service Materials Degradation of Low-Alloys. The Evaluation of In-Service Materials Degradation of Low-Alloys. Dissolution of Malachite in Aqueous Ethylenediaminetetraceacetate Solution. Dissolution Distribution See Dissolution Distribution Solute Distribution Solute Distribution Solute Distribution See Dissolution Around a Coherent Precipitate in a Multi-component Alloy. 1693-1708A 1693-1708A 1693-1708A 1693-1708A 1693-1708A 1693-1708A 1693-1708A 1693-1708A 1693-1708A 1693-1708A 1693-1708A 1813-1804 Steel Through High-Temperature Thermome-chanical Treatment. 1093-1102A 1093-1102	Crack Initiation and Propagation During High-Temperature Fatigue of Oxide Dispersion-Strengthened Superalloys.	837-851A		3067-3071A
See Emulsions Displacement Material Effects in Fretting Wear: Application to Iron, Titanium, and Aluminum Alloys. Displacements glitice See Displacements (lattice) Displace	Dispersion hardening alloys, Structural hardening Toward a Sound Understanding of Dislocation Plasticity.	1693-1708A	Fatigue and Fracture Behavior of an Aluminum-Lithium	700 700 1
Displacement Material Effects in Fretting Wear: Application to Iron, Titanium, and Aluminum Alloys. Displacement spikes See Displacements (lattice) Structural Ledges in Interphase Boundaries. Displacements (lattice) Structural Ledges in Interphase Boundaries. Dissimilar materials, Johning Effect of Plastic Deformation on Residual Stresses in Ceramic/Metal Interfaces. Dissolution See also Acid dissolution Modeling of Base Metal Dissolution Behavior During Transient Liquid-Phase Brazing. Dissolution an Fe—Cr—C Alloy. Morphology of Cementite Decomposition in an Fe—Cr—C Alloy. The Evaluation of In-Service Materials Degradation of Lov-Alloy. The Evaluation of In-Service Materials Degradation of Lov-Alloy. Dissolution of Malachite in Aqueous Ethylenediaminetetraceta Solution. Dissolution Distribution Solute Distribution Solute Distribution Around a Coherent Precipitate in a Multicomponent Alloy. Distribution Solute Distribution Around a Coherent Precipitate in a Multicomponent Alloy. Distribution Solute Distribution Around a Coherent Precipitate in a Multicomponent Alloy. Distribution Solute Distribution Around a Coherent Precipitate in a Multicomponent Alloy. Distribution Solute Distribution Around a Coherent Precipitate in a Multicomponent Alloy. Distribution Solute Distribution Around a Coherent Precipitate in a Multicomponent Alloy. Distribution Solute Distribution Around a Coherent Precipitate in a Multicomponent Alloy. Distribution Solute Distribution Around a Coherent Precipitate in a Multicomponent Alloy. Distribution Solute Distribution Around a Coherent Precipitate in a Multicomponent Alloy. Distribution Solute Distribution Around a Coherent Precipitate in a Multicomponent Alloy. Distribution Solute Distribution Around a Coherent Precipitate in a Multicomponent Alloy. Distribution Solute Distribution Around a Coherent Precipitate in a Multicomponent Alloy. Distribution Solute Distribution Around a Coherent Precipitate in a Multicomponent Alloy. Distribution Solute Distribution Around a Co				723-729A
Displacements (lattice) Displacements (lattice) Structural Ledges in Interphase Boundaries. Dissimilar materials, Joining Effect of Plastic Deformation on Residual Stresses in Ceramic/Metal Interfaces. Dissociated ammonis brazing See Brazing Dissolution See also Acid dissolution Modeling of Base Metal Dissolution Behavior During Transient Liquid-Phase Brazing. Dissolution Equilibrium of Magnesium Vapor in Liquid from. An Experimental and Theoretical Study of Cementite Dissolution in an Fe—Cr—C Alloy. Morphology of Cementite Decomposition in an Fe—Cr—C Alloy. Morphology of Cementite Decomposition in an Fe—Cr—C Alloy. Morphology of Cementite Decomposition in an Fe—Cr—C Alloy. Alloy Steels by the Electrochemical Method. Dissolution of Malachite in Aqueous Ethylenediaminetetracetae Solution. Dissolution See Brazing Dissolution of Malachite in Aqueous Ethylenediaminetetracetae Solution. Dissolution of Malachite in Aqueous Ethylenediaminetetracetae S	Material Effects in Fretting Wear: Application to Iron, Tita-		Low-Temperature Improvement of Mechanical Properties of AISI 4340 Steel Through High-Temperature Thermome-	1093-1102A
Displacements (lattice) Structural Ledges in Interphase Boundaries. Dissimilar materials, Joining Effect of Plastic Deformation on Residual Stresses in Ceramic/Metal Interfaces. Dissociated ammonia brazing See Brazing Dissolution See also Acid dissolution Modeling of Base Metal Dissolution Behavior During Transient Liquid-Phase Brazing. Dissolution Equilibrium of Magnesium Vapor in Liquid Iron. An Experimental and Theoretical Study of Cementite Dissolution in an Fe—Cr—C Alloy. Morphology of Cementite Decomposition in an Fe—Cr—C Alloy. The Evaluation of In-Service Materials Degradation of Low-Alloy Steels by the Electrochemical Method. Dissolution Dissolution Soluto Dissolution Dissolution Dissolution Dissolution Dissolution Dissolution Dissolution Dissolution Distribution Solute Distribution Around a Coherent Precipitate in a Multicomponent Alloy. 1165-1175A 1161-1820A Ductility, Microstructural effects Ductility Mic		1535-1544A	Ductility, Heating effects	
Structural Ledges in Interphase Boundaries. Dissimilar materials, Joining Effect of Plastic Deformation on Residual Stresses in Ceramic/Metal Interfaces. Dissociated ammonia brazing See Brazing Dissolution See also Acid dissolution Modeling of Base Metal Dissolution Behavior During Transient Liquid-Phase Brazing. Dissolution Equilibrium of Magnesium Vapor in Liquid Iron. An Experimental and Theoretical Study of Cementite Dissolution in an Fe—Cr—C Alloy. Morphology of Cementite Decomposition in an Fe—Cr—C Alloy. The Evaluation of In-Service Materials Degradation of Low-Alloy Steels by the Electrochemical Method. Dissolution Soluto Dissolution And Achie in Aqueous Ethylenediaminetetracetase Solution. Dissolution Dissolution Solute Distribution Solute Distribution Around a Coherent Precipitate in a Multicomponent Alloy. 1165-1175A 1682-2825A 2822-2825A Ductility, Microstructural effects Ductility, Microstructural effects Ductility Enhancement in NIAI (B2)-Base Alloys by Method Composites. 1811-1820A 1811-1820A 1841-445A 2009-2019A 1841-445A 1855-55A Dissolution of Malachite in Aqueous Ethylenediaminetetracetase Solution. 2009-2019A 2009-2019A 2009-2019A 2009-2019A 2009-2019A 2009-2019A 2019ex stainless steels, Metal working High Strain Rate Superplasticity of a 25 wt.% Cr—7 wt.% Ni—3 wt.% Mo—0.14 wt.% N Duplex Stainless Steel. 2009-2019A 2009-2019A 2009-2019A 2019ex stainless steels, Phases (state of matter) The Effect of Temperature and Nitrogen Content on the Partition of Malachite in Aqueous Ethylenediaminetetracetase Solution. 2019-2106A 2029-2106A 2037-2106A 2037-2106A 2038-250-250 2041-445-45A 2045-55A 2049-250-250 2049-250-250 2049-250-250 2049-250-250 2049-250-250 2049-250-250 2049-250-250 2049-250-250 2049-250-250 2049-250-250 2049-250-250 2040-250-250 2040-250-250 2040-250-250 2040-250-250 2040-250-250 2040-250-250 2040-250-250 2040-250-250 2040-250-250 2040-250-250 2040-250-250 2040-250-250 2040-250-250 2040-250-250 2040-250-250 2040-250-250			Nb/Nb ₅ Si ₃ Alloys.	1573-1583A
Effect of Plastic Deformation on Residual Stresses in Ceramic/Metal Interfaces. 2822-2825A Dissolution Dissolution See Brazing Dissolution See also Acid dissolution Behavior During Transient Liquid-Phase Brazing. Dissolution Equilibrium of Magnesium Vapor in Liquid Iron. An Experimental and Theoretical Study of Cementite Dissolution in an Fe—Cr—C Alloy. Morphology of Cementite Decomposition in an Fe—Cr—C Alloy. Morphology of Cementite Decomposition in an Fe—Cr—C Alloy. The Evaluation of In-Service Materials Degradation of Low Alloy Steels by the Electrochemical Method. Dissolution py effects Dissolution of Malachite in Aqueous Ethylenediaminetetracetate Solution. Dissolution of Malachite in Aqueous Ethylenediaminetetracetate Solution Distribution Solute Distribution Around a Coherent Precipitate in a Multicomponent Alloy. 2822-2825A 2822-2825A 2822-2825A 2822-2825A Ductility, Microstructural effects Ductility, Microstructural effects Ductility, Microstructural Control. Effect of Phase Morphology on the Mechanical Behavior of Two Titanium Aluminide Composites. 2009-2019A	Structural Ledges in Interphase Boundaries.	1165-1175A	Effect of Long-Term Service Exposure on Microstructure and	
Dissolution See also Acid dissolution Modeling of Base Metal Dissolution Behavior During Transient Liquid-Phase Brazing Dissolution Equilibrium of Magnesium Vapor in Liquid Iron. An Experimental and Theoretical Study of Cementite Dissolution in an Fe—Cr—C Alloy. Morphology of Cementite Decomposition in an Fe—Cr—C Alloy. The Evaluation of In-Service Materials Degradation of Low-Alloy Steels by the Electrochemical Method. Dissolution, pH effects Dissolution Dissolution Dissolution Solute Distribution Solute Distribution Around a Coherent Precipitate in a Multicomponent Alloy. Dispolution	Effect of Plastic Deformation on Residual Stresses in Ceramic/Metal Interfaces.	2822-2825A	Steel.	1811-1820A
Dissolution See also Acid dissolution Modeling of Base Metal Dissolution Behavior During Transient Liquid-Phase Brazing. Dissolution Equilibrium of Magnesium Vapor in Liquid Iron. An Experimental and Theoretical Study of Cementite Dissolution in an Fe—Cr—C Alloy. Morphology of Cementite Decomposition in an Fe—Cr—C Alloy. The Evaluation of In-Service Materials Degradation of Low-Alloy Steels by the Electrochemical Method. Dissolution, pH effects Dissolution of Malachite in Aqueous Ethylenediaminetetraceactate Solution. Dissolving See Dissolution Distribution Solute Distribution Around a Coherent Precipitate in a Multicomponent Alloy. Effect of Phase Morphology on the Mechanical Behavior of Two Titanium Aluminide Composities 543-555A 918-9218 1745-1752A 1745-1752A 1763-1759A 2097-2106A 2097-2106A Effect of Phase Morphology on the Mechanical Behavior of Two Titanium Aluminide Composities 1083-1091A			Ductility Enhancement in NiAl (B2)-Base Alloys by	441-446A
Modeling of Base Metal Dissolution Behavior During Transient Liquid-Phase Brazing. Dissolution Equilibrium of Magnesium Vapor in Liquid Iron. An Experimental and Theoretical Study of Cementite Dissolution in an Fe—Cr—C Alloy. The Evaluation of In-Service Materials Degradation of Low- Alloy Steels by the Electrochemical Method. Dissolution, pH effects Dissolution. Dissolution Dissolution Distribution Solute Distribution Solute Distribution Around a Coherent Precipitate in a Multicomponent Alloy. Distribution Solute Distribution Around a Coherent Precipitate in a Multicomponent Alloy. Modeling of Base Metal working 543-555 943-555 943-555 943-555 943-555 943-555 943-555 943-555 1745-1752 1745-1752 1745-1752 1745-1752 1745-1752 1745-1752 1745-1752 1745-1752 1745-1752 1745-1752 1745-1752 1745-1752 1745-1752 1745-1752 1745-1752 1745-1752 1745-1752 1745-1752 1745-1754 1745-1752 1745-1752 1745-1752 1745-1752 1745-1752 1745-1752 1745-1752 1745-1752 1745-1752 1745-1752 1745-1752 1745-1752 1745-1752 1745-1752 1745-1752 1745-1752 1745-1752 1745-1752 1745-1754 1745-1752 1745-1752 1745-1752 1745-1752 1745-1752 1745-1752 1745-1752 1745-1752 1745-1752	Dissolution		Effect of Phase Morphology on the Mechanical Behavior of Two Titanium Aluminide Composites.	2009-2019A
An Experimental and Theoretical Study of Cementite Dissolution in an Fe—Cr—C Alloy. Morphology of Cementite Decomposition in an Fe—Cr—C Alloy. The Evaluation of In-Service Materials Degradation of Low-Alloy Steels by the Electrochemical Method. Dissolution, pH effects Dissolution of Malachite in Aqueous Ethylenediaminetetracetate Solution. Dissolving See Dissolution Distribution Solute Distribution Around a Coherent Precipitate in a Multicomponent Alloy. 1745-1752A 1745-175	Modeling of Base Metal Dissolution Behavior During Tran- sient Liquid-Phase Brazing.		Duplex stainless steels, Metal working High Strain Rate Superplasticity of a 25 wt % Cr—7 wt %	1083-1091A
Alloy. The Evaluation of In-Service Materials Degradation of Low-Alloy Steels by the Electrochemical Method. Dissolution, pH effects Dissolution of Malachite in Aqueous Ethylenediaminetetracetate Solution. Dissolving See Dissolution Distribution Solute Distribution Around a Coherent Precipitate in a Multicomponent Alloy. Dissolution Tris3-1759A 2097-2106A	An Experimental and Theoretical Study of Cementite Dissolu- tion in an Fe—Cr—C Alloy.		Duplex stainless steels, Phases (state of matter) The Effect of Temperature and Nitrogen Content on the Parti-	
Alloy Steels by the Electrochemical Method. Dissolution, pH effects Dissolution of Malachite in Aqueous Ethylenediaminetetracetate Solution. Dissolution Dissolution Dissolution Distribution Solute Distribution Around a Coherent Precipitate in a Multicomponent Alloy. 2097-2106A Carbide Precipitation in Welds of Two-Phase Austeniticomponent in Welds of Two-Phase Austeniticomponent Alloy. 2889-2902A Dynamic Fracture Behavior of SiC Whisker-Reinforced Aluminum Alloys. Dynamic Fatigue Experiments on Optical Fibers. 2889-2902A Dynamic Fracture Behavior of SiC Whisker-Reinforced Aluminum Alloys. Dynamic Fatigue Experiments on Optical Fibers. Dynamics See Richardics Dynamics Dynamics Supplied Fracture Behavior of SiC Whisker-Reinforced Aluminum Alloys. Dynamic Fatigue Experiments on Optical Fibers. Dynamics Supplied Fracture Behavior of SiC Whisker-Reinforced Aluminum Alloys. Dynamic Fatigue Experiments on Optical Fibers. Dynamics Supplied Fracture Behavior of SiC Whisker-Reinforced Aluminum Alloys. Dynamic Fatigue Experiments on Optical Fibers. Dynamics Supplied Fracture Behavior of SiC Whisker-Reinforced Aluminum Alloys. Dynamic Fracture Behavior of SiC Whisker-Reinforced Alumin	Alloy.	1753-1759A		2173-2179A
aacetate Solution. Dissolving See Dissolution Distribution Solute Distribution Around a Coherent Precipitate in a Multi- component Alloy. Distribution Solute Distribution Around a Coherent Precipitate in a Multi- component Alloy. See Dissolution Dynamic Fracture Behavior of SiC Whisker-Reinforced Aluminum Alloys. Dynamic Fracture Behavior of SiC Whisker-Rein	Alloy Steels by the Electrochemical Method. Dissolution, pH effects	2097-2106A	Carbide Precipitation in Welds of Two-Phase Austenitic— Ferritic Stainless Steel.	2889-2902A
See Dissolution Distribution Solute Distribution Around a Coherent Precipitate in a Multi- component Alloy. Distribution Solute Distribution Around a Coherent Precipitate in a Multi- component Alloy. Dynamics See Kinetics Dynapak extrusion Dynapak extrusion		569-574B	Dynamic Fracture Behavior of SiC Whisker-Reinforced Alu-	367, 2754
Solute Distribution Solute Distribution Around a Coherent Precipitate in a Multi- component Alloy. See Kinetics See Kinetics Dynapak extrusion			Dynamic Fatigue Experiments on Optical Fibers.	
component Alloy. 2199-2210A Dynapak extrusion	Distribution Solute Distribution Around a Coherent Pracinitate in a Multi-			
	component Alloy.			

Dynapak forging See Forging		Electrohydrodynamics See Magnetohydrodynamics	
Dynapak process See Extrusion Forging		Electrolytic cells High-Temperature Thermodynamic Properties of the Vanadium Carbides V ₂ C and VC _{0.73} Determined Using a Galvanic Cell Technique.	661-668B
Earing in Cup Drawing Face-Centered Cubic Single Crystals and Polycrystals.	1525-1534A	Electrolytic cells, Design Loss of Current Efficiency in Aluminum Electrolysis Cells.	177-182B
Efficiency See also Current efficiency		Electrolytic deposition See Electrodeposition	
Optimization and Continuous Casting. I. Problem Formulation and Solution Strategy.	641-648B	Electrolytic dissolution See Anodic dissolution	
Optimization and Continuous Casting. II. Application to Industrial Casters.	649-659B	Electromagnetic fields	
Elastic anisotropy Analysis of Crack Tip Sliding Displacement in Anisotropic Elastic Media and Its Application to Stage I Fatigue Crack Growth.	479-487A	Magnetohydrodynamic Flows in a Channel-Induction Fur- nace. Evolution of Boride Morphologies in TIAI—B Alloys. Lorentz Force Infiltration of Fibrous Preforms.	193-209B 1647-1662A 2903-2915A
The Relationship Between Plastic Anisotropy of Steel Sheet and Temper Rolling Strain. The Anisotropic Mechanical Properties of a Titanium Matrix	2156-2160A	Electromagnetic stirring An Improved Mathematical Model for Electromagnetic Casters and Testing by a Physical Model.	121-134B
Elastic constants	2975-2984A	Electromelting See Electric arc melting	
See also Elastic anisotropy Modulus of elasticity Poissons ratio		Electrometallurgy New Observiors on the Anodic Oxidation of Copper in Hot	623-630B
Mechanical Behavior of Cast Particulate SiC/AL (A356) Metal Matrix Composites.	1585-1593A	Acidified Copper Sulfate Solutions. Electron beam welding	023-030D
See Modulus of elasticity		Aging Characteristics of Electron Beam and Gas Tungsten Arc Fusion Zones of Al—Cu—Li Alloy 2090.	903-913A
Elastic properties See Elastic constants		Solidification Modeling and Solid-State Transformations in High-Energy Density Stainless Steel Welds.	915-926A
Electric arc melting See also Electroslag melting Development of Structure and Porosity in Cast Al ₅ CuZr ₂ and Al ₈₆ Mn ₉ Zr ₂₅ Intermetallic Compounds.	2545-2552A	Electron microscopy See also Transmission electron microscopy X-Ray Microanalysis of Phosphorus Segregation in Type 304L Stainless Steels.	253-255A
Electric arc welding		See Electronic structure	
See Arc welding Electric assemblies		Electronic assemblies See Electronic devices	
See Electronic devices Electric components		Electronic components See Electronic devices	
See Electronic devices Electric conductors (materials)		Electronic devices See also Computers	
See Semiconductors Electric devices		Electronic devices, Fabrication	
See Electronic devices		Modeling Chemical Vapor Deposition of Silicon With Local Equilibrium Consideration at the Substrate.	309-321B
Electric equipment See Electrodes Electronic devices		Electronic devices, Materials selection Thermodynamic Stability of Palladium Alloys. I. The Palladium—Niobium System.	1937-1943A
Electric furnaces, Design Correlation of Geometric Factor for Slag Resistance Electric Furnaces.	183-192B	Electronic equipment See Electronic devices	
Electric generators See Thermionic generators	100 1025	See also Fermi surface A Degenerate Electron Gas Model for Solutions of Aluminum	000 0700
Electric lamps See Incandescent lamps		in Cryolite Melts. Electrorefining	669-672B
Electric power generation Fracture Toughness Behavior of Ex-Service 2.25Cr—1Mo	455 4504	New Observations on the Anodic Oxidation of Copper in Hot Acidified Copper Sulfate Solutions.	623-630B
Steels From a 22-Year-Old Fossil Power Plant. Electric power plants See Electric power generation	455-468A	Electrorefining, Impurity effects Cathodic Copper Deposition at 65°C in the Absence and Presence of Bi ³ * and Sb ³ * Additives in Acidified CuSO ₄ Aqueous Solutions.	575-581B
Electric power stations See Electric power generation		Electroslag melting Magnetohydrodynamic and Thermal Behavior of Electroslag	
Electric welding See Arc welding		Remelting Slags. Electrowinning	111-120B
Electrical properties See Current voltage characteristics Lorenz number		See Hall Heroult process Elongation	
Electroceramics See Ceramics		Aging Characteristics of Electron Beam and Gas Tungsten Arc Fusion Zones of Al—Cu—Li Alloy 2090. Elongation. Corrosion effects	903-913A
Electrochemistry		Microstructure Property Relationships and Hydrogen Effects in a Particulate-Reinforced Aluminum Composite.	2445-2450A
Modeling of Corrosion Fatigue Crack Initiation Under Passive Electrochemical Conditions. The Electrochemical Behavior of a Semiconducting Nautral Pyrite in the Presence of Bacteria.	521-529A 765-774B	Elongation, Cryogenic effects The Effect of Through-Thickness Anisotropy on the Cryogenic Mechanical Properties of an Al—Cu—Li—Zr Alloy	
Electrocoatings, Phase transformations Activation Energy of δ-Γ ₁ Transformation in a Zn—Fe Electrodeposited Coating.	1887-1888A	(Vintage III 2090-T81). Elongation, High temperature effects	1789-1799A
Electrode potentials See Corrosion potential	10007	On the Embrittlement of a Rapidly Solidified Al—Fe—V—S Alloy After High-Temperature Exposure. Elongation, Microstructural effects	853-858A
Electrodeposition The Effect of Continuous Heating on the Phase Transformations in Zinc—Iron Electrodeposited Coatings.	1707 17401	Mechanical Properties and Retained Austenite in Intercriti- cally Heat-Treated Bainite-Transformed Steel and Their Variation With Silicon and Manganese Additions.	
Electrodeposition, Impurity effects	1737-1743A	The Role of the γ/γ Eutectic and Porosity on the Tensile Behavior of a Single-Crystal Nickel-Base Superalloy.	
Cathodic Copper Deposition at 65°C in the Absence and Presence of Bi ³⁺ and Sb ³⁺ Additives in Acidified CuSO ₄ Aqueous Solutions.	575-581B	Embrittlement See also Hydrogen embrittlement Liquid metal embrittlement	
See also Welding electrodes Correlation of Geometric Factor for Slag Resistance Electric Furnaces) 183_192B	Comparison of Secondary Hardening Embrittlement in Tung sten and Molybdenum Steels. In Situ Fracture Observations on Tempered Martensite Em brittlement in an AISI 4340 Steel	1119-1122A

The Reduction of the Interfacial Segregation of Phosphorus and its Embrittlement Effect by Lanthanum Addition in a		Equilibrium, Stress effects Coherent Phase Equilibrium in Alloys With Congruent Points.	1001_100EA
W—Ni—Fe Heavy Alloy. Embrittlement, High temperature effects	2969-2974A	Equilibrium constants See Chemical equilibrium	1921-1933A
On the Embrittlement of a Rapidly Solidified Al—Fe—V—Si Alloy After High-Temperature Exposure.	853-858A	Equilibrium diagrams See Phase diagrams	
Grain Boundary Pest of Boron-Doped Ni ₃ Al at 1200°C. Emission	1801-1809A	Esso Little process See Fluidized bed reduction	
See Acoustic emission Thermionic emission		Eutectic reactions	
Emulsions Preparation of Monosized Ultrafine Particles of Precious Metals Utilizing an Emulsion-Type Liquid Membrane Tech-		Morphology of Cementite Decomposition in an Fe—Cr—C Alloy.	1753-1759A
nique.	397-404B	Eutectic reactions, Alloying effects On the Nature of Eutectic Carbides in Cr—Ni White Cast Irons.	1709-1720A
Emulsoids See Emulsions Endurance (hosting)		Eutectics See also Directionally solidified eutectics	
Endurance (testing) See Fatigue tests		Eutectics, Cooling effects Nonequilibrium Austenite/←Phase Eutectic Revealed in Rap-	
Endurance limit See Fatigue limit		idly Solidified High-Carbon Iron Alloy. Eutectics, Directional solidification	791-792A
Energy See Free energy Surface energy		Eutectic Spacing Selection in Lead-Based Alloy Systems.	2523-2533A
Energy of activation See Activation energy		Eutectics, Mechanical properties The Deformation of an Aluminum—Silicon Eutectic Alloy Under Thermal Cycling Conditions.	1113-1115A
Energy of dissociation See Free energy		Eutectics, Welding Heat-Flow Simulation of Laser Remelting With Experimental	
Heat of formation		Validation. Eutectoid decomposition	101-109B
Energy of formation See Free energy Heat of formation		Thermodynamic Equilibrium in the Low-Solute Regions of Plutonium-Group IIIA Metal Binary Systems.	2237-2246A
Energy of fracture See Toughness		Eutectoid reactions See Eutectoid decomposition	
Energy of solution See Free energy Heat of solution		Evaluation A Theoretical Sensitivity Analysis for Full-Dome Formability Tests: Parameter Study for \mathbf{n} , \mathbf{m} , \mathbf{r} , and μ .	1775-1788A
Engine components See Turbine blades		Evaporation Effect of Evaporation and Temperature-Dependent Material	
Turbine disks Engines		Properties on Weld Pool Development. Observations of the Formation and Kinetics of Surface Steps	233-241B
See Aerospace engines Gas turbine engines		During Evaporation and Condensation. Ledgewise Vaporization.	1299-1304A 1305-1310A
Enthalpy Thermochemistry of Binary Alloys of Transition Metals: the Me—Sc, Me—Y, and Me—La (Me = Silver, Gold) Systems	1103-1111A	Exothermic reactions Synthesis of Iron Aluminides From Elemental Powders: Reaction Mechanisms and Densification Behavior. The Mass Transfer Kinetics of Niobium Solution Into Liquid Steel.	277-286A 417-427B
Enthalpies of Formation of Refractory Borides by High- Temperature Direct Synthesis Calorimetry: RuB _{1.1} and RhB _{1.1} .	1680-1683A	Expansion See Thermal expansion	
Surface Composition of Ternary Cu—Ag—Au Alloys. I. Ex- perimental Results. Surface Composition of Ternary Cu—Ag—Au Alloys. II. A Comparison of Experiment With Theoretical Models.	1833-1840A	Explosive compacting Dynamic Compaction of Titanium Aluminides by Explosively Generated Shock Waves: Experimental and Materials Sys-	
Entropy Surface Composition of Ternary Cu—Ag—Au Alioys. I. Ex-	1041-10401	tems. Shock Densification/Hot Isostatic Pressing of Titanium Aluminide.	685-695A 2667-2676A
perimental Results. Surface Composition of Ternary Cu—Ag—Au Alloys. II. A Comparison of Experiment With Theoretical Models.	1833-1840A 1841-1848A	Extraction Continuous Precipitation of Uranium Peroxide From High- Vanadium Mill Solutions.	135-136B
Entropy of activation See Entropy		Extractive metallurgy	130-1300
Entropy of formation See Entropy		See also Electrometallurgy Hydrometallurgy Pyrometallurgy	
Heat of formation Entropy of reaction		Pyrometallurgy The Kinetics of S ³⁵ Exchange Between SO ₂ /CO/CO ₂ Gas Mixtures and Copper Sulfide Meits at 1523K.	211-217B
See Entropy Entropy of solution		The Coming-of-Age of Process Engineering in Extractive Metallurgy.	737-754B
See Entropy Heat of solution		Extrusion Influence of Microstructure on Centerburst Development in Steel Extrusions.	807-815A
Entropy of transformation See Entropy		Development of a Necklace Microstructure During Isothermal Deformation and Its Properties Relative to Uniform Micro-	
Environment See Corrosion environments		structures. Extrusion casting	1999-2008A
Marine environments Space environment		See Pressure casting Extrusion pressing	
Epitaxial growth The Role of Ledges in Vapor/Solid Phase Transformation:	s	See Extrusion Extrusions, Mechanical properties	
Observed by Low-Energy Electron Microscopy and Photo emission Electron Microscopy. Equations	1311-1315A	Fatigue Crack Propagation and Cryogenic Fracture Tough- ness Behavior in Powder Metallurgy Aluminum—Lithium Alloys.	191-202A
The Energy and Solute Conservation Equations for Dendritic Solidification.	889-900B	On the Embrittlement of a Rapidly Solidified Al—Fe—V—S Alloy After High-Temperature Exposure.	853-858A
Fracture Toughness and Crack Growth Rate of Ferritic and Pearlitic Compacted Graphite Cast Irons at 25 and 150°C. Solidification of Highly Undercooled Fe—P Alloys.		Extrusions, Structural hardening A Calorimetric Study of Precipitation in an Al—Cu Alloy With Silicon Particles.	665-674A
Equiaxed structure Synthesis of Iron Aluminides From Elemental Powders: Reaction Mechanisms and Densification Behavior.	- 277-286A	Face centered cubic metals See FCC metals	
A Volume-Averaged Two-Phase Model for Transport Phenomena During Solidification.	349-361B	Facing (surfacing) See Surfacing	
Micromechanics of Shear Ligament Toughening. Equilibrium	2021-2029A	See also Delaminating	
See also Chemical equilibrium		Fatigue failure	

Failure, High temperature effects Lifetimes and Failure Mechanisms of W/Re Hairpin Fila-		Ferric compounds See Iron compounds	
	2077-2084A	Ferrite Strain Distribution Effects on the Low-Cycle Fatigue Behavior	
Failure analysis See also Fractography Lifetimes and Failure Mechanisms of W/Re Hairpin Filaments.	2077-2084A	of Fe—C—Mo Steels. The Role of Ledges in the Proeutectoid Ferrite and Proeutectoid Cementite Reactions in Steel.	675-683A 1367-1380A
False Brinelling See Fretting		Ferrite, Alloying effects The Effect of Temperature and Nitrogen Content on the Parti-	
Fasteners See Bolts		tioning of Alloy Elements in Duplex Stainless Steels. Ferroalloys	2173-2179A
Fatigue (materials) See Corrosion fatigue Fatigue life Fatigue limit		See Ferrochromium Ferrochromium Kinetics of the Reduction of Bushveld Complex Chromite Ore at 1416°C.	801-810B
Fatigue strength Low cycle fatigue Thermal fatigue		Ferrous alloys See also Cast iron Steels	
Fatigue failure The Initiation and Growth of Fatigue Cracks in a Titanium Al- uminide Alloy.	377-391A	Ferrous alloys, Corrosion Fatigue Behavior in the Potentiostatic Passive Corrosion Regime of the Iron-Base Superalloy A-286.	513-519A
Faceted Fatigue Fracture and Its Relation to the Crystallo- graphic Slip Systems in Cu—16 at.% Al Single Crystals. Analysis of Crack Tip Sliding Displacement in Anisotropic	415-425A	Modeling of Corrosion Fatigue Crack Initiation Under Passive Electrochemical Conditions.	521-529A
Elastic Media and Its Application to Stage I Fatigue Crack Growth. Thermomechanical Fatigue of Particulate-Reinforced Alumi-	479-487A	Ferrous alloys, Crystal growth Solidification of Highly Undercooled Fe—P Alloys. Measurements of Rapid Solidification Rate in Highly Under-	2761-2768A
num 2xxx-T4.	697-707A	cooled Melts With a Video System.	2825-2828A
Crack Initiation and Propagation During High-Temperature Fatigue of Oxide Dispersion-Strengthened Superalloys. Dynamic Fatigue Experiments on Optical Fibers. Fatigue Behavior of a 2xxx Series Aluminum Alloy Reinforced	837-851A 867-871A	Ferrous alloys, Heat treatment Structures and Tempering Behavior of Rapidly Solidified High-Carbon Iron Alloys.	775-782A
With 15 vol.% SiC _p . Thermomechanical Fatigue of a Lead Alloy.	1007-1019A 1059-1070A	Effect of Oxide Scale on Carbon Deposition on Fe—Ni Alloys in Carburizing Gas. Ferrous alloys, Mechanical properties	2393-2399A
The Growth of Short Fatigue Cracks Under Compressive and/or Tensile Cyclic Loading. On the Mechanism of Fatigue Crack Growth in Silicon Nitride. Material Effects in Fretting Wear: Application to Iron, Tita-	1079-1082A 1425-1434A	High-Damping Metals and Alloys. A Simple, Versatile Miniaturized Disk-Bend Test Apparatus for Quantitative Yield-Stress Measurements.	607-616A 2061-2068A
nium, and Aluminum Alloys. Fatigue failure, Environmental effects Environmental and Hold Time Effects on Fatigue of Low-Tin	1535-1544A	Ferrous alloys, Microstructure Nonequilibrium Austenite/c-Phase Eutectic Revealed in Rapidly Solidified High-Carbon Iron Alloy.	791-792A
Lead-Based Solder. Fatigue failure, Microstructural effects Fatigue Crack Propagation and Cryogenic Fracture Tough-	357-366A	Structural Ledges in Interphase Boundaries. Computer Simulation of Morphological Changes of Grain Boundary Precipitates Growing by the Ledge Mechanism. Interfacial Steps and Growth Mechanism in Ferrous Pearlites.	1165-1175A 1235-1245A 1349-1365A
ness Behavior in Powder Metallurgy Aluminum—Lithium Alloys. Microstructural Effects on Ambient and Elevated Tempera-	191-202A	Ferrous alloys, Phase transformations Phase Transformation in an Fe—9.0Al—29.5Mn—1.2Si Alloy.	1407-1415A
ture Fatigue Crack Growth in Titanium Aluminide Intermet- allics.	817-828A	An Experimental and Theoretical Study of Cementite Dissolution in an Fe—Cr—C Alloy.	1745-1752A
Fatigue failure, Stress effects The Effect of Particulate SiC on Fatigue Crack Growth in a Cast-Extruded Aluminum Alloy Composite.	97-112A	Morphology of Cementite Decomposition in an Fe—Cr—C Alloy.	1753-1759A
The Influence of Applied Stress, Crack Length, and Stress Intensity Factor on Crack Closure.	1559-1571A	Thermodynamics of the Iron Martensitic Transformation and the M _B Temperature of Iron. The Tempering of FeNiN Martensite. Lattice Changes of Iron—Carbon Martensite on Aging at	1761-1765A 1945-1956A
Fatigue failure, Temperature effects Low-Temperature Fatigue of 316L and 316LN Austenitic Stainless Steels.	2385-2392A	Room Temperature. Morphology and Aging of the Martensite Induced by Cathodic Hydrogen Charging of High-Carbon Austenitic Steels.	1957-1967A 1979-1991A
Fatigue fracture See Fatigue failure		Ferrous alloys, Phases (state of matter) A13-Type Phase Revealed in Rapidly Solidified High-Carbon	13/3-1331A
Fatigue life Fatigue Behavior in the Potentiostatic Passive Corrosion Re-		Iron Alloy. A New Phase in an Fe—9.0Al—29.5Mn—1.2Si Alloy.	251-253A 1417-1423A
gime of the Iron-Base Superalloy A-286. Modeling of Corrosion Fatigue Crack Initiation Under Passive Electrochemical Conditions.	513-519A 521-529A	Ferrous alloys, Surface properties Effect of Temperature and Composition on Surface Tension in Fe—Ni—Cr Alloys Containing Sulfur.	557-560B
Thermomechanical Fatigue of Particulate-Reinforced Alumi- num 2xxx-T4. Crack Initiation and Propagation During High-Temperature	697-707A	Ferrous compounds	337-300D
Fatigue of Oxide Dispersion-Strengthened Superalloys. Fatigue Behavior of a 2xxx Series Aluminum Alloy Reinforced	837-851A	See Iron compounds Ferrous metals	
With 15 vol.% SiC _p .	1007-1019A	See Ferrous alloys	
Fatigue life, Heating effects Influence of Cyclic Deformation on Surface Microstructure and Hardness of Ion-Implanted Nickel.	1633-1646A	Interface Structure in Infiltrated Composites of Aluminum Re- inforced With Alumina—Silica Fiber Preforms. Chemical Stability of Zirconia-Stabilized Alumina Fibers Dur-	1126-1128A
Fatigue limit Finite Element Prediction of the Fatigue Limit of Steel. Toward a Sound Understanding of Dislocation Plasticity.	1678-1680A 1693-1708A	ing Pressure Infiltration by Aluminum. Pressure Casting of a Zirconia-Toughened Alumian Fiber- Reinforced NiAl Composite.	2855-2862A 3059-3064A
Fatigue strength, Cryogenic effects Fatigue and Fracture Behavior of an Aluminum—Lithium Alloy 8090-T6 at Ambient and Cryogenic Temperature.	723-729A	Fiber composites, Crystal growth In Situ Observation of Nonfaceted Cellular Growth in a Narrow Channel.	1683-1687A
Fatigue tests Dynamic Fatigue Experiments on Optical Fihers. Behavior of Acoustic Emission for Low-Strength Structural	867-871A	Fiber composites, Directional solidification Composite Growth in Hypermonotectic Alloys.	339-348B
Steel During Fatigue and Corrosion Fatigue. FCC metals, Rolling	2677-2680A	Fiber composites, Fabrication Lorentz Force Infiltration of Fibrous Preforms.	2903-2915A
A Simple Theory for the Development of Inhomogeneous Rolling Textures.	2637-2643A	Fiber composites, Mechanical properties On the Influence of Ply-Angle on Damping and Modulus of Elasticity of a Metal-Matrix Composite.	641-651A
FCC metals, Structural hardening Toward a Sound Understanding of Dislocation Plasticity.	1693-1708A	Processing and Creep Characterization of a Model Metal Ma- trix Composite: Lead Reinforced With Nickel Fibers. Stress Concentration at a Notch Tip in Unidirectional Meta	1029-1036A
Fermi energy See Fermi surface		Matrix Composites. The Mechanical Behavior of a Hybrid Metal Matrix Compos-	2085-2095A
Fermi level See Fermi surface		ite. The Anisotropic Mechanical Properties of a Titanium Matrix	2107-2117A
Fermi surface A Degenerate Electron Gas Model for Solutions of Aluminum	000 000	Composite Reinforced With SiC Fibers. Fiber composites, Reactions (chemical)	2975-2984A
in Cryolite Melts.	669-672B	Reaction of Titanium and Ti-Al Alloys With Alumina.	715-721A

T- // 7.5 W. W D			
The K ₂ ZrF ₆ Wetting Process: Effect of Surface Chemistry on the Ability of a SiC-Fiber Preform To Be Impregnated by Aluminum. Chemical Stability of Zirconia-Stabilized Alumina Fibers Dur-	2133-2139A	Fluxing A Thermodynamic Study of Dephosphorization Using BaO— BaF ₂ , CaO—CaF ₂ , and BaO—CaO—CaF ₂ Systems. Monitoring of Slag Composition Changes by Density Mea-	33-38B
ing Pressure Infiltration by Aluminum. Fiber metal brazing	2855-2862A	surements. Focussons	305-307B
See Brazing Fiber reinforcement		See Displacements (lattice) Foil brazing	
See Filaments		See Brazing	
Fibers See Metal fibers Optical fibers		Forging See also Hot forging Upsetting	
Fibrous structure Surface Energy Reduction in Fibrous Monotectic Structures.	1881-1886A	Influence of Microstructure on Centerburst Development in Steel Extrusions.	807-815A
Fields (physics) See Electromagnetic fields		Forgings, Corrosion Accelerated Fracture Due to Tritium and Helium in 21-6-9 Stainless Steel.	879-886A
Filaments, Service life Lifetimes and Failure Mechanisms of W/Re Hairpin Fila-	0077 00044	Formability See also Drawability	
ments. Filler metal	2077-2084A	Stretchability A Theoretical Sensitivity Analysis for Full-Dome Formability	
See also Brazing alloys Solders		Tests: Parameter Study for n, m, r, and μ . The Relationship Between Plastic Anisotropy of Steel Sheet	1775-1788A
Weld metal Microstructural Development in Transient Liquid-Phase		and Temper Rolling Strain. Finite Element Modeling Simulation of In-Plane Forming Limit Diagrams of Sheets Containing Finite Defects.	2156-2160A 2655-2665A
Bonding.	2451-2457A	Formability, Microstructural effects	2005-2005A
See Thin films		Simulation of the Effect of Texture on Limit Strain in Biaxially Stretched Steel Sheet.	2069-2076A
Fines See Ultrafines		Forming See Extrusion	
Finite element method		Flanging	
Strain Distribution Effects on the Low-Cycle Fatigue Behavior of Fe—C—Mo Steels.	675-683A	Forging Hot forming	
Finite Element Prediction of the Fatigue Limit of Steel. Finite Element Modeling Simulation of In-Plane Forming Limit	1678-1680A	Stretching Forming limit	
Diagrams of Sheets Containing Finite Defects. Nonisothermal Punch Stretching: Measurements and Finite	2655-2665A	See Formability	
Element Modeling Simulations. Finsider process	3003-3011A	Forms (molds) See Molds	
See Direct reduction Fissures		Formulas Establishment of a General Formula for Fractional Softening.	2160-2162A
See Cracks		Fractography Faceted Fatigue Fracture and Its Relation to the Crystallo-	
Flame reduction process See Direct reduction		graphic Slip Systems in Cu—16 at.% Al Single Crystals. Cleavage Crystallography of Liquid Metal Embrittled Alumi-	415-425A
Flanging Earing in Cup Drawing Face-Centered Cubic Single Crystals		num Alloys. Fracture of Single Crystals of the Nickel-Base Superalloy	1849-1855A
and Polycrystals.	1525-1534A	PWA 1480E in Hydrogen at 22°C. The Mechanical Behavior of a Hybrid Metal Matrix Composite.	2031-2038A 2107-2117A
Flash smelting The Coming-of-Age of Process Engineering in Extractive Metallurgy.	737-754B	Effects of Intercritical Treatment and Tempering on Fracture Behavior in a Medium-Carbon 2Si—3Ni Steel.	2587-2596A
Mathematical Modeling of Sulfide Flash Smelting Process. III. Volatilization of Minor Elements.		Hydrogen Effects on Low-Cycle Fatigue of the Single-Crystal Nickel-Base Superalloy CMSX-2.	2597-2603A
Flaws See Defects		Internal Hydrogen-Induced Subcritical Crack Growth in Aus- tenitic Stainless Steels. Fracture Toughness and Crack Growth Rate of Ferritic and	2605-2618A
Flow		Pearlitic Compacted Graphite Cast Irons at 25 and 150°C. Shock Densification/Hot Isostatic Pressing of Titanium Alumi-	2645-2653A
See Fluid flow Plastic flow		nide.	2667-2676A
Flow stress See Yield strength		Fracture mechanics See also Crack opening displacement Applicate Crack Tin Stiding Displacement in Applications	
Fluid bed reduction		Analysis of Crack Tip Sliding Displacement in Anisotropic Elastic Media and Its Application to Stage I Fatigue Crack Grouth	470.4974
See Fluidized bed reduction Fluid flow		Growth. Processing and Creep Characterization of a Model Metal Ma-	479-487A 1029-1036A
See also Gas flow Fluid Flow Through Lances With Constant and Variable Pitch		trix Composite: Lead Reinforced With Nickel Fibers. In Situ Fracture Observations on Tempered Martensite Em- brittlement in an AISI 4340 Steel.	1029-1036A 1889-1892A
Swirled Inserts. Magnetohydrodynamic and Thermal Behavior of Electroslag	13-20B	Micromechanics of Shear Ligament Toughening.	2021-2029A
Remelting Slags. Magnetohydrodynamic Flows in a Channel-Induction Fur-	111-120B	Fracture strength Synthesis of Iron Aluminides From Elemental Powders: Reaction Mechanisms and Densification Behavior.	277-286A
nace: Computational Modeling of Stationary Gas-Tungsten-Arc Weld Pools and Comparison to Stainless Steel 304 Experi-		Fracture strength, Cryogenic effects	211-200A
mental Results. Role of Near-Wall Node Location on the Prediction of Melt	243-257B	Fatigue and Fracture Behavior of an Aluminum—Lithium Alloy 8090-T6 at Ambient and Cryogenic Temperature.	723-729A
Flow and Residence Time Distribution in Tundishes by Mathematical Modeling.		Fracture strength, Heating effects Effects of Intercritical Treatment and Tempering on Fracture Behavior in a Medium-Carbon 2Si—3Ni Steel.	2587-2596A
Fluid form deep drawing See Deep drawing		Fracture strength, Impurity effects	
Fluidity See Viscosity		Internal Hydrogen-Induced Subcritical Crack Growth in Austenitic Stainless Steels.	2605-2618A
Fluidized bed reduction The Coming-of-Age of Process Engineering in Extractive Metallurgy.	737-754B	Fracture strength, Microstructural effects Effect of Hydrogen as a Temporary β Stabilizer on Micro- structure and Brittle Fracture Behavior in a Titanium Alumi- nide Alloy.	71-81A
Flutter See Vibration		Fracture strength, Stress effects Hydrostatic Stresses and Their Effect on the Macroflow Be-	
Fluxes		havior and Microfracture Mechanism of Two-Phase Alloys.	2695-2702A
See also Mold fluxes Welding fluxes	000 000	Fracture toughness Tensile Deformation and Fracture Toughness of 2014 + 15 vol.% SiC Particulate Composite.	440 400
The Thermodynamic Behavior of Sulfur in BaO—BaF ₂ Slags The Redox Equilibria of Copper Ions in the Molten Silicate	Ð	Effects of Material Rate Sensitivity and Void Nucleation or	
Fluxes as a Measure of Basicity. A Thermodynamic Study of the System		Fracture Initiation in a Circumferentially Cracked Bar. Dynamic Fracture Behavior of SiC Whisker-Reinforced Alu-	161-170
Fe _x O + Al ₂ O ₃ + SiO ₂ at 1673K.	839-845B	minum Alloys.	367-375A

Fracture Toughness Behavior of Ex-Service 2.25Cr—1Mo Steels From a 22-Year-Old Fossil Power Plant.	455-468A	Fused sait electrolysis See Hall Herouit process	
In Situ Fracture Observations on Tempered Martensite Em- brittlement in an AISI 4340 Steel.	1889-1892A	Fused salts, Solubility A Degenerate Electron Gas Model for Solutions of Aluminum	000 0700
Fracture toughness, Alloying effects The Effect of Copper, Chromium, and Zirconium on the Microstructure and Mechanical Properties of Al—Zn—Mg—	0000 00404	in Cryolite Melts. Fusion (melting) See Melting	669-672B
Cu Alloys. Fracture toughness, Coating effects	2809-2818A	Fusion welding	
Delayed Failure of PH13-8Mo Steel Plated With Aluminum- IVD.	2935-2945A	See Arc welding Electron beam welding Laser beam welding	
Fracture toughness, Cryogenic effects Fatigue Crack Propagation and Cryogenic Fracture Toughness Behavior in Powder Metallurgy Aluminum—Lithium		Gallium, Binary systems Thermodynamics of Binary Systems Using Interaction Pa-	
Alloys. The Effect of Through-Thickness Anisotropy or the Cryogenic Mechanical Properties of an Al—Cu—Li—Zr Alloy	191-202A	rameters. Thermodynamic Equilibrium in the Low-Solute Regions of Plutonium-Group IIIA Metal Binary Systems.	593-605B 2237-2246A
(Vintage III 2090-T81).	1789-1799A	Gallium, Crystal growth	
Fracture toughness, Environmental effects Fracture of Single Crystals of the Nickel-Base Superalloy PWA 1480E in Hydrogen at 22°C.	2031-2038A	Growth Kinetics of Solid/Liquid Gallium Interfaces. I. Experi- mental. Growth Kinetics of Solid/Liquid Gallium Interfaces. II. Theo-	1259-1270A
Fracture toughness, Heating effects Effects of Intercritical Treatment and Tempering on Fracture		retical. Gallium, Environment Cleavage Crystallography of Liquid Metal Embrittled Alumi-	1271-1286A
Behavior in a Medium-Carbon 2Si—3Ni Steel. Fracture toughness, Microstructural effects	2587-2596A	num Alloys.	1849-1855A
Effect of Hydrogen as a Temporary β Stabilizer on Micro- structure and Brittle Fracture Behavior in a Titanium Alumi-		Galvanic cells See Electrolytic cells	
nide Alloy. Micromechanics of Shear Ligament Toughening. Fracture Toughness and Crack Growth Rate of Ferritic and	71-81A 2021-2029A	Galvannealing See Annealing	
Pearlitic Compacted Graphite Cast Irons at 25 and 150°C. Fractures, Microstructural effects	2645-2653A	Gas carburizing Effect of Oxide Scale on Carbon Deposition on Fe—Ni Alloys in Carburizing Gas.	2393-2399A
A Comparison of the Fracture Behavior of Two Commercially Produced Heats of HY180 Steel Differing in Sulfide Type.	2277-2285A	Gas evolution See Outgassing	
Fracturing		Gas fired furnaces	
See also Brittle fracture Cracking (fracturing) Ductile fracture		Modeling and Parametric Studies of Heat Transfer in a Direct- Fired Continuous Reheating Furnace.	513-521B
Intergranular fracture Transgranular fracture		Gas flow Desulfurization Kinetics of Molten Copper by Gas Bubbling.	5-11B
Comparison of Secondary Hardening Embrittlement in Tung- sten and Molybdenum Steels. Further Study on the Scattering of the Local Fracture Stress	1119-1122A	Mixing Characteristics of a Submerged Jet Measured Using an Isokinetic Sampling Probe.	439-445B
and Allied Toughness Value.	2287-2296A	Gas tungsten arc welding	
Fracturing, Corrosion effects Cleavage Crystallography of Liquid Metal Embrittled Aluminum Alloys.	1849-1855A	Effect of Evaporation and Temperature-Dependent Material Properties on Weld Pool Development. Computational Modeling of Stationary Gas-Tungsten-Arc Weld Pools and Comparison to Stainless Steel 304 Experi-	233-241B
Fracturing, Microstructural effects		mental Results.	243-257B
Fracture of Single Crystals of the Nickel-Base Superalloy PWA 1480E in Helium at 22°C.	731-738A	Correction to "A New Technique for Three-Dimensional Tran- sient Heat Transfer Computations of Autogenous Arc	
Free energy	10110011	Welding". Aging Characteristics of Electron Beam and Gas Tungsten	3898
See also Activation energy Thermochemistry and Diffusion of Nitrogen in Solid Molybde-		Arc Fusion Zones of Al—Cu—Li Alloy 2090. Solidification Modeling and Solid-State Transformations in	903-913A
num. Determination of Equilibrium Solid-Phase Transition Temper-	219-224B	High-Energy Density Stainless Steel Welds. The Chemistry and Structure of Wear-Resistant, Iron-Base	915-926A
atures Using DTA.	1993-1998A	Hardfacing Álloys.	983-991A
Free energy, Composition effects Thermodynamic Stability of Palladium Alloys. I. The Palladium—Niobium System.	1937-1943A	Gas turbine engines Development of a Necklace Microstructure During Isothermal Deformation and Its Properties Relative to Uniform Micro-	
Free energy of activation See Activation energy		Structures.	1999-2008A
Free energy of dissociation		Gas turbine engines, Materials selection The Initiation and Growth of Fatigue Cracks in a Titanium Al-	077 004 4
See Free energy Heat of formation		uminide Alloy. Dynamic Compaction of Titanium Aluminides by Explosively	377-391A
Free energy of formation		Generated Shock Waves: Experimental and Materials Systems.	685-695A
See Free energy Heat of formation		Crack Initiation and Propagation During High-Temperature Fatigue of Oxide Dispersion-Strengthened Superalloys.	837-851A
Free energy of reaction See Free energy		Gas turbines See Gas turbine engines	
Free energy of solution See Free energy		Geometry The Geometry and Properties of Ledges in Interfaces.	1177-1183A
Heat of solution Free energy of transformation		Germanium, Binary systems Nonequilibrium Behavior in the AI—Ge Alloy Systems: In-	
See Free energy		sights Into the Metastable Phase Diagram.	2141-2152A
Frequencies Characterization of the Damping Properties of Die-Cas Zinc—Aluminum Alloys.	617-622A	Germanium base alloys, Phases (state of matter) Nonequilibrium Behavior in the Al—Ge Alloy Systems: Insights Into the Metastable Phase Diagram.	2141-2152A
Fretting Material Effects in Fretting Wear: Application to Iron, Tita nium, and Aluminum Alloys.	1535-1544A	Germanium compounds, Physical properties Note on the Enthalpies of Formation of Cu ₃ Si and Cu ₃ Ge.	2162-2165A
Friction		Gibbs free energy See Free energy	
See also Internal friction The Thermal and Metallurgical State of Steel Strip During Ho	ot	Glass	
Rolling. II. Factors Influencing Rolling Loads. Tribological Behavior and Surface Analysis of Tribodeforme	321-333A	See also Metallic glasses Glass, Mechanical properties	
Al Alloy—50% Graphite Particle Composites.	1435-1441A	Dynamic Fatigue Experiments on Optical Fibers.	867-871A
Frictional wear Material Effects in Fretting Wear: Application to Iron, Tita nium, and Aluminum Alloys.	1535-1544A	Gold, Extraction The Electrochemical Behavior of a Semiconducting Nautral Pyrite in the Presence of Bacteria.	765-774B
Furnaces See Blast furnaces		Gold, Powder technology Preparation of Monosized Ultrafine Particles of Precious	
Electric furnaces Gas fired furnaces		Metals Utilizing an Emulsion-Type Liquid Membrane Tech-	397-404B
		nique.	357-404B

Gold, Recovering The Dissolution Behavior of Metals From Ag/Cu and Ag/Au Alloys in Aldic and Cyanide Solutions.	755-764B	Effect of Processing Variables on Texture and Texture Gradients in Tantalum.	2039-2048A
Gold base alloys, Reactions (chemical) Thermochemistry of Binary Alloys of Transition Metals: the	755-7648	Dynamic Recrystallization During Hot Deformation of Alumi- num: a Study Using Processing Maps. Grain structure	2339-2348A
	1103-1111A	See also Acicular structure Banded structure	
GP zone See Guinier Preston zone		Dendritic structure Equiaxed structure Behavior of Metal Alloys in the Semisolid State.	269-294B
Gradients See Temperature gradient		Plastic Deformation and Fracture of Binary TiAl-Base Alloys. Behavior of Metal Alloys in the Semisolid State.	427-439A 957-981A
Grading (classifying)		In Situ Observation of Nonfaceted Cellular Growth in a Nar- row Channel.	1683-1687A
See Evaluation Grain boundaries		Grain structure, Deformation effects	
Plastic Deformation and Fracture of Binary TiAl-Base Alloys. Analysis of Crack Tip Sliding Displacement in Anisotropic Elastic Media and its Application to Stage I Fatigue Crack	427-439A	Development of a Necklace Microstructure During Isothermal Deformation and its Properties Relative to Uniform Micro- structures.	1999-2008A
Growth. Comparison of Fracture Behavior in Intercritically Treated Medium-Carbon Nickel and Silicon Steels.	479-487A 1115-1119A	Granular materials, Mechanical properties Expressions for Predicting the Elasticity Modulus of Materials Reinforced by Second-Phase Grains.	507-511A
The Use of Transmission Electron Microscopy for the As- sessment of Interphase Boundaries. The Geometry and Properties of Ledges in Interfaces.	1139-1144A 1177-1183A	Granules See Granular materials	
Thickening of Grain-Boundary α Allotriomorphs in a Ti—Cr Alloy by Multiple Sets of Ledges.	1341-1348A	Graphic methods See Diagrams	
Effect of Grain Boundaries on Isothermal Solidification Dur- ing Transient Liquid Phase Brazing.	1627-1631A	Graphite, Composite materials On the Influence of Ply-Angle on Damping and Modulus of	
Surface Energy Reduction in Fibrous Monotectic Structures. Grain boundaries, Diffusion	1881-1886A	Elasticity of a Metal-Matrix Composite. Tribological Behavior and Surface Analysis of Tribodeformed	641-651A
Grain Boundary Diffusion of Hydrogen in Nickel.	351-355A	Al Alloy—50% Graphite Particle Composites.	1435-1441A
Grain boundaries, High temperature effects Grain Boundary Pest of Boron-Doped Ni ₂ Al at 1200°C. Grain boundaries, X ray analysis	1801-1809A	Graphitic structure See also Nodular graphitic structure On Thermal Shock Resistance of Austenitic Cast Irons.	1821-1831A
X-Ray Microanalysis of Phosphorus Segregation in Type 304L Stainless Steels.	253-255A	Gray cast iron See Gray iron	
Grain boundary migration Surface Void Nucleation Under the Power-Law Creep Condi-		Gray iron See also Nodular iron	
tion in an Al—3 at.% Mg Solid Solution Alloy. Grain boundary sliding	935-937A	Gray iron, Mechanical properties High-Damping Metals and Alloys.	607-616A
High-Temperature Rupture of Microstructurally Unstable 304 Stainless Steel Under Uniaxial and Triaxial Stress States.	2629-2635A	Characterization of the Damping Properties of Die-Cast Zinc—Aluminum Alloys.	
Grain growth Growth Path Envelope Analysis of Ostwald Ripening.	19-23A	Fracture Toughness and Crack Growth Rate of Ferritic and Pearlitic Compacted Graphite Cast Irons at 25 and 150°C.	2645-2653A
Correction to "Growth Path Envelope Analysis of Ostwald Ri- pening".	19-23A	Greasing See Lubrication	
In Situ Observation of Faceted Cellular Array Growth. Correction to "In Situ Observation of Faceted Cellular Array	941-945A	Grey iron See Gray iron	
Growth". A Mathematical Method for the Calculation of Ledge Growth	941-945A	Grinding (comminution)	
Kinetics. Interfacial Steps and Growth Mechanism in Ferrous Pearlites. Kinetic Equations for Concurrent Size and Shape Coarsening	1211-1218A 1349-1365A	See Ball milling Growth	
by the Ledge Mechanism. In Situ Observation of Nonfaceted Cellular Growth in a Nar-	1381-1390A	See Crystal growth Grain growth	
row Channe!. Simulation of Subgrain Growth by Subgrain Rotation: a One-	1683-1687A	Growth rate On the Rate of Dendrite Arm Coarsening.	569-574A
Dimensional Model. Grain growth, Deformation effects	2257-2263A	Thickening of Grain-Boundary α Allotriomorphs in a Ti—Ci Alloy by Multiple Sets of Ledges.	
The Thermal and Metallurgical State of Steel Strip During Hot Rolling. III. Microstructural Evolution.	335-349A	Correction to On the Rate of Dendrite Arm Coarsening*. Growth-Speed Dependence of Primary Arm Spacings in Di-	1466A
High Strain Rate Superplasticity of a 25 wt.% Cr—7 wt.% Ni—3 wt.% Mo—0.14 wt.% N Duplex Stainless Steel.	1083-1091A	rectionally Solidified Pb—10 wt.% Sn. Guinier Preston zone	2467-2473A
Grain growth, Welding effects Effect of Killing Time on the Microstructure and Toughness of		A Calorimetric Study of Precipitation in an Al—Cu Alloy With Silicon Particles.	665-674A
the Heat-Affected Zone in Titanium-Killed Steels. Grain refinement, Alloying effects	2818-2822A	Computer Simulation of the Effect of Coherency Strain on Cluster Growth Kinetics.	1197-1209A
Thermodynamic Consideration of Grain Refinement of Aluminum Alloys by Titanium and Carbon.	3071-3075A	Effect of Reinforcement on the Aging Response of Cast 6061 AI—Al ₂ O ₃ Particulate Composites.	2553-2563A
Grain refinement, Deformation effects		Halides See Chlorides	
High Strain Rate Superplasticity of a 25 wt.% Cr—7 wt.% Ni—3 wt.% Mo—0.14 wt.% N Duplex Stainless Steel.	1083-1091A	Hall Heroult process	477 400D
Recrystallization Controlled Rolling and Accelerated Cooling for High Strength and Toughness in V—Ti—N Steels. Effect of Interpass Time on Austenite Grain Refinement by	2681-2694A	Loss of Current Efficiency in Aluminum Electrolysis Cells. The Wettability of Carbon/TiB ₂ Composite Materials by Aluminum in Carbolito Modes.	177-182B 617-621B
Means of Dynamic Recrystallization of Austenite.	2947-2957A	minum in Cryolite Melts. A Degenerate Electron Gas Model for Solutions of Aluminum in Cryolite Melts.	669-672B
Grain refinement, Welding effects Effect of Killing Time on the Microstructure and Toughness of the Heat-Affected Zone in Titanium-Killed Steels.	2818-2822A	A Thermodynamic and Experimental Study of the Electro chemically Induced Cooling of the Anode in Hall—Héroul Cells.	
Grain size Quantitative Assessment of the Implications of Strain-		Hard coating See Hard surfacing	
Induced Microstructural Changes in Superplasticity. Plastic Deformation and Fracture of Binary TiAl-Base Alloys. Creep Deformation of TiB ₂ -Reinforced Near-y Titanium Al-	83-96A 427-439A	Hard facing See Hard surfacing	
uminides. Effect of Grain Boundaries on Isothermal Solidification Dur- ing Transient Liquid Phase Brazing.	447-454A 1627-1631A	Hard soldering	
Simulation of Subgrain Growth by Subgrain Rotation: a One- Dimensional Model.	2257-2263A	Hard surfacing	
Effect of Grain Size on High Strain Rate Deformation of Cop- per.	2349-2357A	Hardfacing Alloys.	983-991A
Grain size, Deformation effects The Thermal and Metallurgical State of Steel Strip During Hot		Hardenability, Cryogenic effects The Effect of Through-Thickness Anisotropy on the Cryo	
Rolling. III. Microstructural Evolution. Recrystallization and Superplasticity at 300°C in an	335-349A	(Village III 2000-101).	1789-1799A
Aluminum—Magnesium Alloy. Development of a Necklace Microstructure During Isothermal	1037-1047A	Effects of Vanadium and Processing Parameters on the	
Deformation and Its Properties Relative to Uniform Micro- structures.	1999-2008A	Structures and Properties of a Direct-Quenched Low Carbon Mo—B Steel.	2359-2374A

Hardening See also Surface hardening		Heat resistant alloys See Superalloys	
Low-Cycle Fatigue Behavior of Nimonic PE16 at Room Tem- perature.	499-506A	Heat resistant iron	
Strain Distribution Effects on the Low-Cycle Fatigue Behavior of Fe—C—Mo Steels.	675-683A	See Alloy cast iron Heat transfer	
Hardness	075-000A	Heat-Flow Simulation of Laser Remelting With Experimental	101-109B
See also Microhardness Mechanical, Elastic, and Structural Properties of Alloys of		Validation. Magnetohydrodynamic and Thermal Behavior of Electroslag	111-120B
Ru—Ta High-Temperature Intermetallic Compounds. A Calorimetric Study of Precipitation in an Al—Cu Alloy With	129-137A	Remelting Slags. A Mathematical Model of the Nickel Converter. I. Model De-	
Silicon Particles.	665-674A	velopment and Verification. Heat-Transfer Phenomena in Water-Cooled Zinc-Fuming	153-161B
Powder Metallurgy T15 Tool Steel. II. Microstructure and Properties After Heat Treatment.	2747-2759A	Furnace Jackets. Effect of Evaporation and Temperature-Dependent Material	163-175B
Hardness, Heating effects Structures and Tempering Behavior of Rapidly Solidified		Properties on Weld Pool Development. Computational Modeling of Stationary Gas-Tungsten-Arc	233-241B
High-Carbon Iron Alloys. Influence of Cyclic Deformation on Surface Microstructure	775-782A	Weld Pools and Comparison to Stainless Steel 304 Experi- mental Results.	243-257B
and Hardness of Ion-Implanted Nickel.	1633-1646A	The Thermal and Metallurgical State of Steel Strip During Hot Rolling. III. Microstructural Evolution.	335-349A
Hardness, Microstructural effects On Thermal Shock Resistance of Austenitic Cast Irons.	1821-1831A	A Volume-Averaged Two-Phase Model for Transport Phe-	349-361B
Effect of Phase Morphology on the Mechanical Behavior of Two Titanium Aluminide Composites.	2009-2019A	nomena During Solidification. Correction to "A New Technique for Three-Dimensional Transient Heat Transfer Computations of Autogenous Arc.	
HAZ	2003-2013A	Welding". Modeling and Parametric Studies of Heat Transfer in a Direct-	389B
See Heat affected zone		Fired Continuous Reheating Furnace. Thermal and Mechanical Considerations in Using Shape	513-521B
Hazelett process See Continuous casting		Memory Alloys to Control Vibrations in Flexible Structures. Optimization and Continuous Casting. I. Problem Formulation	623-627A
HCP metals, Microstructure		and Solution Strategy.	641-648B
The Crystallography and Atomic Structure of Line Defects in Twin Boundaries in Hexagonal-Close-Packed Metals.	1185-1196A	Optimization and Continuous Casting. II. Application to Industrial Casters.	649-659B
Heat affected zone Effect of Killing Time on the Microstructure and Toughness of		Heat Flux Transients at the Casting/Chill Interface During So- lidification of Aluminum Base Alloys.	717-727B
the Heat-Affected Zone in Titanium-Killed Steels.	2818-2822A	Contribution to the Metal/Mold Interfacial Heat Transfer. Modeling of Crystal Growth During Rapid Solidification.	729B 2475-2485A
Heat affected zone, Chemical analysis Secondary Ion Mass Spectrometry Method for Distinguishing		Microstructural Engineering Applied to the Controlled Cooling of Steel Wire Rod. I. Experimental Design and Heat	
the State of Carbon in Steels Using Negative Molecular lons.	1969-1978A	Transfer.	2769-2778A
Heat affected zone, Heat treatment	1303-13707	The Thermal and Metallurgical State of Steel Strip During Hot	007 0404
Aging Characteristics of Electron Beam and Gas Tungsten Arc Fusion Zones of Al—Cu—Li Alloy 2090.	903-913A	Rolling. I. Characterization of Heat Transfer. Heat transmission	307-319A
Heat affected zone, Mechanical properties		The Effects of Interface Kinetics Anisotropy on the Growth Direction of Cellular Microstructures.	585-593A
Microstructure and Local Brittle Zone Phenomena in High- Strength Low-Alloy Steel Welds.	139-149A	Heat Flux Transients at the Casting/Chill Interface During So-	717-727B
Fracture Toughness Behavior of Ex-Service 2.25Cr—1Mo Steels From a 22-Year-Old Fossil Power Plant.	455-468A	lidification of Aluminum Base Alloys. Processing Map for Hot Working of Alpha-Zirconium. Muld Republication of Management Indiana.	829-836A
The Relationship Between Carbon Content, Microstructure, and Intergranular Liquation Cracking in Cast Nickel Alloy		Mold Behavior and Its Influence on Quality in the Continuous Casting of Steel Slabs. I. Industrial Trials, Mold Tempera-	004 0740
718.	557-567A	ture Measurements, and Mathematical Modeling. Mold Behavior and Its Influence on Quality in the Continuous	861-874B
718. A Phase Diagram Approach to Study Liquation Cracking in Alloy 718.	557-567A 887-902A	Mold Behavior and its Influence on Quality in the Continuous Casting of Steel Slabs. II. Mold Heat Transfer, Mold Flux Behavior, Formation of Oscillation Marks, Longitudinal Off-	
718. A Phase Diagram Approach to Study Liquation Cracking in		Mold Behavior and Its Influence on Quality in the Continuous Casting of Steel Slabs. II. Mold Heat Transfer, Mold Flux Behavior, Formation of Oscillation Marks, Longitudinal Off- Corner Depressions, and Subsurface Cracks.	875-888B
718. A Phase Diagram Approach to Study Liquation Cracking in Alloy 718. Heat checking See Thermal fatigue Heat conductivity		Mold Behavior and Its Influence on Quality in the Continuous Casting of Steel Slabs. II. Mold Heat Transfer, Mold Flux Behavior, Formation of Oscillation Marks, Longitudinal Off-Corner Depressions, and Subsurface Cracks. Heat treatment See Annealing	
718. A Phase Diagram Approach to Study Liquation Cracking in Alloy 718. Heat checking See Thermal fatigue		Mold Behavior and its Influence on Quality in the Continuous Casting of Steel Slabs. II. Mold Heat Transfer, Mold Flux Behavior, Formation of Oscillation Marks, Longitudinal Off-Corner Depressions, and Subsurface Cracks. Heat treatment See Annealing Austenitizing Isothermal treatment	
718. A Phase Diagram Approach to Study Liquation Cracking in Alloy 718. Heat checking See Thermal fatigue Heat conductivity See Thermal conductivity Heat flow See Heat transmission		Mold Behavior and its Influence on Quality in the Continuous Casting of Steel Slabs. II. Mold Heat Transfer, Mold Flux Behavior, Formation of Oscillation Marks, Longitudinal Off-Corner Depressions, and Subsurface Cracks. Heat treatment See Annealing Austentitizing Isothermal treatment Quenching (cooling) Solution heat treatment	
718. A Phase Diagram Approach to Study Liquation Cracking in Alloy 718. Heat checking See Thermal fatigue Heat conductivity See Thermal conductivity Heat flow		Mold Behavior and its Influence on Quality in the Continuous Casting of Steel Slabs. II. Mold Heat Transfer, Mold Flux Behavior, Formation of Oscillation Marks, Longitudinal Off-Corner Depressions, and Subsurface Cracks. Heat treatment See Annealing Austenitizing Isothermal treatment Quenching (cooling) Solution heat treatment Tempering	
718. A Phase Diagram Approach to Study Liquation Cracking in Alloy 718. Heat checking See Thermal fatigue Heat conductivity See Thermal conductivity Heat flow See Heat transmission Heat flux See Heat transmission Heat measurement		Mold Behavior and its Influence on Quality in the Continuous Casting of Steel Slabs. II. Mold Heat Transfer, Mold Flux Behavior, Formation of Oscillation Marks, Longitudinal Off-Corner Depressions, and Subsurface Cracks. Heat treatment See Annealing Austenitizing Isothermal treatment Quenching (cooling) Solution heat treatment Tempering Heating See Superheating	
718. A Phase Diagram Approach to Study Liquation Cracking in Alloy 718. Heat checking See Thermal fatigue Heat conductivity See Thermal conductivity Heat flux See Heat transmission Heat flux See Heat transmission Heat measurement See Calorimetry		Mold Behavior and its Influence on Quality in the Continuous Casting of Steel Slabs. II. Mold Heat Transfer, Mold Flux Behavior, Formation of Oscillation Marks, Longitudinal Off-Corner Depressions, and Subsurface Cracks. Heat treatment See Annealing Austenitizing Isothermal treatment Quenching (cooling) Solution heat treatment Tempering Heating	
718. A Phase Diagram Approach to Study Liquation Cracking in Alloy 718. Heat checking See Thermal fatigue Heat conductivity See Thermal conductivity Heat flow See Heat transmission Heat flux See Heat transmission Heat measurement See Calorimetry Heat of activation See Activation energy		Mold Behavior and its Influence on Quality in the Continuous Casting of Steel Slabs. II. Mold Heat Transfer, Mold Flux Behavior, Formation of Oscillation Marks, Longitudinal Off-Corner Depressions, and Subsurface Cracks. Heat treatment See Annealing Austenitizing Isothermal treatment Quenching (cooling) Solution heat treatment Tempering Heating See Superheating Heating rate Synthesis of Iron Aluminides From Elemental Powders: Reaction Mechanisms and Densification Behavior.	
718. A Phase Diagram Approach to Study Liquation Cracking in Alloy 718. Heat checking See Thermal fatigue Heat conductivity See Thermal conductivity Heat flow See Heat transmission Heat flux See Heat transmission Heat measurement See Calorimetry Heat of activation		Mold Behavior and its Influence on Quality in the Continuous Casting of Steel Slabs. II. Mold Heat Transfer, Mold Flux Behavior, Formation of Oscillation Marks, Longitudinal Off-Corner Depressions, and Subsurface Cracks. Heat treatment See Annealing Austenitizing Isothermal treatment Quenching (cooling) Solution heat treatment Tempering Heating See Superheating Heating rate Synthesis of Iron Aluminides From Elemental Powders: Reaction Mechanisms and Densification Behavior. Heats (energies) See Heat of formation	875-888B
718. A Phase Diagram Approach to Study Liquation Cracking in Alloy 718. Heat checking See Thermal fatigue Heat conductivity See Thermal conductivity Heat flow See Heat transmission Heat flux See Heat transmission Heat measurement See Calorimetry Heat of activation See Activation energy Heat of decomposition See Heat of formation Heat of dissociation		Mold Behavior and its Influence on Quality in the Continuous Casting of Steel Slabs. II. Mold Heat Transfer, Mold Flux Behavior, Formation of Oscillation Marks, Longitudinal Off-Corner Depressions, and Subsurface Cracks. Heat treatment See Annealing Austenitizing Isothermal treatment Quenching (cooling) Solution heat treatment Tempering Heating See Superheating Heating rate Synthesis of Iron Aluminides From Elemental Powders: Reaction Mechanisms and Densification Behavior. Heats (energies)	875-888B
718. A Phase Diagram Approach to Study Liquation Cracking in Alloy 718. Heat checking See Thermal fatigue Heat conductivity See Thermal conductivity Heat flux See Heat transmission Heat flux See Heat transmission Heat measurement See Calorimetry Heat of activation See Activation energy Heat of decomposition See Heat of formation		Mold Behavior and its Influence on Quality in the Continuous Casting of Steel Slabs. II. Mold Heat Transfer, Mold Flux Behavior, Formation of Oscillation Marks, Longitudinal Off-Corner Depressions, and Subsurface Cracks. Heat treatment See Annealing Austenitizing Isothermal treatment Quenching (cooling) Solution heat treatment Tempering Heating See Superheating Heating rate Synthesis of Iron Aluminides From Elemental Powders: Reaction Mechanisms and Densification Behavior. Heats (energies) See Heat of formation Heat of mixing Heat of solution Heavy metal alloys	875-888B
718. A Phase Diagram Approach to Study Liquation Cracking in Alloy 718. Heat checking See Thermal fatigue Heat conductivity See Thermal conductivity Heat flow See Heat transmission Heat flux See Heat transmission Heat measurement See Calorimetry Heat of activation See Activation energy Heat of dissociation See Heat of formation Heat of dissociation See Heat of formation Heat of dissolution See Heat of solution See Heat of solution		Mold Behavior and its Influence on Quality in the Continuous Casting of Steel Slabs. II. Mold Heat Transfer, Mold Flux Behavior, Formation of Oscillation Marks, Longitudinal Off-Corner Depressions, and Subsurface Cracks. Heat treatment See Annealing Austenitizing Isothermal treatment Quenching (cooling) Solution heat treatment Tempering Heating See Superheating Heating rate Synthesis of Iron Aluminides From Elemental Powders: Reaction Mechanisms and Densification Behavior. Heats (energies) See Heat of formation Heat of mixing Heat of solution	875-888B
718. A Phase Diagram Approach to Study Liquation Cracking in Alloy 718. Heat checking See Thermal fatigue Heat conductivity See Thermal conductivity Heat flow See Heat transmission Heat flux See Heat transmission Heat measurement See Calorimetry Heat of activation See Activation energy Heat of decomposition See Heat of formation Heat of dissociation See Heat of Soution See Heat of Soution Heat of dissociation See Heat of Formation Heat of dissociation See Heat of formation Heat of dissociation See Heat of Formation Heat of dissociation Activities of Boron in the Binary Ni—B and the Ternary Co— Activities of Boron in the Binary Ni—B and the Ternary Co—	887-902A	Mold Behavior and its Influence on Quality in the Continuous Casting of Steel Slabs. II. Mold Heat Transfer, Mold Flux Behavior, Formation of Oscillation Marks, Longitudinal Off-Corner Depressions, and Subsurface Cracks. Heat treatment See Annealing Austenitizing Isothermal treatment Quenching (cooling) Solution heat treatment Tempering Heating See Superheating Heating rate Synthesis of Iron Aluminides From Elemental Powders: Reaction Mechanisms and Densification Behavior. Heats (energies) See Heat of formation Heat of mixing Heat of solution Heavy metal alloys See Lead base alloys Tin base alloys Tin base alloys Heavy metals	875-888B
718. A Phase Diagram Approach to Study Liquation Cracking in Alloy 718. Heat checking See Thermal fatigue Heat conductivity See Thermal conductivity Heat flow See Heat transmission Heat flux See Heat transmission Heat measurement See Calorimetry Heat of activation See Activation energy Heat of decomposition See Heat of formation Heat of dissociation See Heat of solution See Heat of Formation Heat of dissociation See Heat of Formation Heat of measurement Heat of dissociation See Heat of Formation Heat of dissociation Activities of Boron in the Binary Ni—B and the Ternary Co— Fe—B Melts. High-Temperature Thermodynamic Properties of the Vana-		Mold Behavior and its Influence on Quality in the Continuous Casting of Steel Slabs. II. Mold Heat Transfer, Mold Flux Behavior, Formation of Oscillation Marks, Longitudinal Off-Corner Depressions, and Subsurface Cracks. Heat treatment See Annealing Austenitizing Isothermal treatment Quenching (cooling) Solution heat treatment Tempering Heating See Superheating Heating rate Synthesis of Iron Aluminides From Elemental Powders: Reaction Mechanisms and Densification Behavior. Heats (energiea) See Heat of formation Heat of mixing Heat of solution Heavy metal alloys See Lead base alloys Tin base alloys Tin base alloys Tin base alloys Bismuth	875-888B
718. A Phase Diagram Approach to Study Liquation Cracking in Alloy 718. Heat checking See Thermal fatigue Heat conductivity See Thermal conductivity Heat flux See Heat transmission Heat flux See Heat transmission Heat of activation See Activation energy Heat of decomposition See Heat of formation Heat of dissociation See Heat of solution See Heat of Formation Heat of dissociation See Heat of solution See Heat of Solution See Heat of Solution See Heat of Solution Activities of Boron in the Binary Ni—B and the Ternary Co— Fe—B Melts. High-Temperature Thermodynamic Properties of the Vanadium Carbides V ₂ C and VC _{0.73} Determined Using a Galvanic Cell Technique.	887-902A	Mold Behavior and its Influence on Quality in the Continuous Casting of Steel Slabs. II. Mold Heat Transfer, Mold Flux Behavior, Formation of Oscillation Marks, Longitudinal Off-Corner Depressions, and Subsurface Cracks. Heat treatment See Annealing Austentitizing Isothermal treatment Quenching (cooling) Solution heat treatment Tempering Heating See Superheating Heating rate Synthesis of Iron Aluminides From Elemental Powders: Reaction Mechanisms and Densification Behavior. Heats (energies) See Heat of formation Heat of mixing Heat of solution Heavy metal alloys See Lead base alloys Tin base alloys Heavy metals See Antimony Bismuth Lead (metal) Tin	875-888B
718. A Phase Diagram Approach to Study Liquation Cracking in Alloy 718. Heat checking See Thermal fatigue Heat conductivity Heat flow See Heat transmission Heat flux See Heat transmission Heat at transmission Heat of activation See Calorimetry Heat of activation See Heat of formation Heat of dissociation See Heat of formation Heat of dissociation See Heat of formation Heat of dissociation See Heat of formation Carbides V ₂ C and V _{0,73} Determined Using a Galvanic Cell Technique. Gibbs Energy of Formation of Nickel Chromite. Gibbs Energy of Formation of Refractory Borides by High-	887-902A	Mold Behavior and its Influence on Quality in the Continuous Casting of Steel Slabs. II. Mold Heat Transfer, Mold Flux Behavior, Formation of Oscillation Marks, Longitudinal Off-Corner Depressions, and Subsurface Cracks. Heat treatment See Annealing Austentitizing Isothermal treatment Quenching (cooling) Solution heat treatment Tempering Heating See Superheating Heating rate Synthesis of Iron Aluminides From Elemental Powders: Reaction Mechanisms and Densification Behavior. Heats (energies) See Heat of formation Heat of mixing Heat of solution Heavy metal alloys See Lead base alloys Tin base alloys Tin base alloys Heavy metals See Antimony Bismuth Lead (metal)	875-888B
718. A Phase Diagram Approach to Study Liquation Cracking in Alloy 718. Heat checking See Thermal fatigue Heat conductivity See Thermal conductivity Heat flow See Heat transmission Heat flux See Heat transmission Heat measurement See Calorimetry Heat of activation See Activation energy Heat of decomposition See Heat of formation Heat of dissociation See Heat of formation Heat of dissociation See Heat of See The See Heat of See Activation Heat of Gissolution See Heat of Formation Heat of Insulation Heat of Formation Heat of Formation Heat of Formation Activities of Boron in the Binary Ni—B and the Ternary Co—Fe—B Melts. High-Temperature Thermodynamic Properties of the Vanadium Carbides V ₂ C and VC _{0.73} Determined Using a Galvanic Cell Technique. Gibbs Energy of Formation of Nickel Chromite. Enthalpies of Formation of Nickel Chromite. Enthalpies of Formation of Refractory Borides by High-Temperature Direct Synthesis Calorimetry: RuB _{1.1} and RhB _{1.1} .	47-52B 661-668B 673-675B	Mold Behavior and its Influence on Quality in the Continuous Casting of Steel Slabs. II. Mold Heat Transfer, Mold Flux Behavior, Formation of Oscillation Marks, Longitudinal Off-Corner Depressions, and Subsurface Cracks. Heat treatment See Annealing Austentitizing Isothermal treatment Quenching (cooling) Solution heat treatment Tempering Heating See Superheating Heating rate Synthesis of Iron Aluminides From Elemental Powders: Reaction Mechanisms and Densification Behavior. Heats (energies) See Heat of formation Heat of mixing Heat of solution Heavy metal alloys See Lead base alloys Tin base alloys Heavy metals See Antimony Bismuth Lead (metal) Tin Hellarc welding See Gas tungsten arc welding Helmholtz free energy	875-888B
718. A Phase Diagram Approach to Study Liquation Cracking in Alloy 718. Heat checking See Thermal fatigue Heat conductivity See Thermal conductivity Heat flow See Heat transmission Heat flux See Heat transmission Heat measurement See Calorimetry Heat of activation See Activation energy Heat of decomposition See Heat of formation Heat of dissociation See Heat of formation Heat of dissociation See Heat of Tormation Heat of Idissociation See Heat of Formation Heat of Gissociation See Heat of Formation Activities of Boron in the Binary Ni—B and the Ternary Co—Fe—B Melts. High-Temperature Thermodynamic Properties of the Vanadium Carbides V ₂ C and VC _{0.73} Determined Using a Galvanic Cell Technique. Gibbs Energy of Formation of Refractory Borides by High-Temperature Direct Synthesis Calorimetry: RuB _{1.1} and RhB _{1.1} .	47-52B 661-668B 673-675B 1680-1683A	Mold Behavior and its Influence on Quality in the Continuous Casting of Steel Slabs. II. Mold Heat Transfer, Mold Flux Behavior, Formation of Oscillation Marks, Longitudinal Off-Corner Depressions, and Subsurface Cracks. Heat treatment See Annealing Austenitizing Isothermal treatment Quenching (cooling) Solution heat treatment Tempering Heating See Superheating Heating rate Synthesis of Iron Aluminides From Elemental Powders: Reaction Mechanisms and Densification Behavior. Heats (energies) See Heat of formation Heat of mixing Heat of solution Heavy metal alloys See Lead base alloys Tin base alloys Tin base alloys Heavy metals See Antimony Bismuth Lead (metal) Tin Heliarc welding See Gas tungsten arc welding Helmholtz free energy See Free energy	875-888B
718. A Phase Diagram Approach to Study Liquation Cracking in Alloy 718. Heat checking See Thermal fatigue Heat conductivity See Thermal conductivity Heat flow See Heat transmission Heat flow See Heat transmission Heat measurement See Calorimetry Heat of activation See Activation energy Heat of decomposition See Heat of formation Heat of dissociation See Heat of formation Heat of dissociation See Heat of solution Heat of dissociation See Heat of Formation Activities of Boron in the Binary Ni—B and the Ternary Co— Fe—B Melts. High-Temperature Thermodynamic Properties of the Vanadium Carbides V ₂ C and VC _{0.73} Determined Using a Galvanic Cell Technique. Gibbs Energy of Formation of Nickel Chromite. Enthalpies of Formation of Refractory Borides by High-Temperature Direct Synthesis Calorimetry: RuB-1,1 and RnB-1,1 Heats of Formation of Aluminum—Cerium Intermetallic Compounds. Note on the Enthalpies of Formation of Cu ₃ Si and Cu ₃ Se.	47-52B 661-668B 673-675B	Mold Behavior and its Influence on Quality in the Continuous Casting of Steel Slabs. II. Mold Heat Transfer, Mold Flux Behavior, Formation of Oscillation Marks, Longitudinal Off-Corner Depressions, and Subsurface Cracks. Heat treatment See Annealing Austenitizing Isothermal treatment Quenching (cooling) Solution heat treatment Tempering Heating See Superheating Heating rate Synthesis of Iron Aluminides From Elemental Powders: Reaction Mechanisms and Densification Behavior. Heats (energies) See Heat of formation Heat of mixing Heat of solution Heavy metal alloys See Lead base alloys Tin base alloys Tin base alloys Heavy metals See Antimony Bismuth Lead (metal) Tin Hellarc welding See Gas tungsten arc welding Helmholtz free energy See Free energy Hematite, Reduction (chemical) The Influence of Specific Impurities on the Nucleation and	875-888B
718. A Phase Diagram Approach to Study Liquation Cracking in Alloy 718. Heat checking See Thermal fatigue Heat conductivity See Thermal conductivity Heat flow See Heat transmission Heat flux See Heat transmission Heat measurement See Calorimetry Heat of activation See Activation energy Heat of decomposition See Heat of formation Heat of dissociation See Heat of formation Heat of dissociation See Heat of solution Heat of dissociation See Heat of Formation Activities of Boron in the Binary Ni—B and the Ternary Co— Fe—B Melts. High-Temperature Thermodynamic Properties of the Vanadium Carbides V ₂ C and VC _{0.73} Determined Using a Galvanic Cell Technique. Gibbs Energy of Formation of Nickel Chromite. Enthalpies of Formation of Refractory Borides by High-Temperature Direct Synthesis Calorimetry: RuB-1,1 and RnB-1,1 Heats of Formation of Aluminum—Cerium Intermetallic Compounds. Note on the Enthalpies of Formation of Cu ₃ Si and Cu ₃ Ge. A Thermodynamic Assessment of the Fe—Cr—Ni—C System.	47-52B 661-668B 673-675B 1680-1683A 2119-2123A	Mold Behavior and its Influence on Quality in the Continuous Casting of Steel Slabs. II. Mold Heat Transfer, Mold Flux Behavior, Formation of Oscillation Marks, Longitudinal Off-Corner Depressions, and Subsurface Cracks. Heat treatment See Annealing Austentizing Isothermal treatment Quenching (cooling) Solution heat treatment Tempering Heating See Superheating Heating rate Synthesis of Iron Aluminides From Elemental Powders: Reaction Mechanisms and Densification Behavior. Heats (energies) See Heat of formation Heat of mixing Heat of solution Heavy metal siloys See Lead base alloys Tin base alloys Tin base alloys Heavy metals See Antimony Bismuth Lead (metal) Tin Heilarc welding See Gas tungsten arc welding Helmoltz free energy See Free energy Hematite, Reduction (chemical) The Influence of Specific Impurities on the Nucleation and Growth of Magnetite During Reduction of Artificially Prepared Hematite.	875-888B
718. A Phase Diagram Approach to Study Liquation Cracking in Alloy 718. Heat checking See Thermal fatigue Heat conductivity See Thermal conductivity Heat flow See Heat transmission Heat flux See Heat transmission Heat measurement See Calorimetry Heat of activation See Activation energy Heat of decomposition See Heat of formation Heat of dissolution See Heat of formation Heat of dissolution See Heat of Formation Heat of formation Activities of Boron in the Binary Ni—B and the Ternary Co— Fe—B Melts. High-Temperature Thermodynamic Properties of the Vanadium Carbides V ₂ C and VC _{0.73} Determined Using a Galvanic Cell Technique. Gibbs Energy of Formation of Nickel Chromite. Enthalpies of Formation of Refractory Borides by High-Temperature Direct Synthesis Calorimetry: RuB _{1.1} and RiB _{1.1} . Heats of Formation of Aluminum—Cerium Intermetallic Compounds. Note on the Enthalpies of Formation of Cu ₃ Si and Cu ₃ Se. A Thermodynamic Assessment of the Fe—Cr—Ni—C System. Chemical Potential Diagram of Al—Ti—C System: Al ₂ C ₃ Formation on TiC Formed in Al—Ti Liquids Containing Carbon.	47-52B 661-668B 673-675B 1680-1683A 2119-2123A 2162-2165A	Mold Behavior and its Influence on Quality in the Continuous Casting of Steel Slabs. II. Mold Heat Transfer, Mold Flux Behavior, Formation of Oscillation Marks, Longitudinal Off-Corner Depressions, and Subsurface Cracks. Heat treatment See Annealing Austenitizing Isothermal treatment Quenching (cooling) Solution heat treatment Tempering Heating See Superheating Heating rate Synthesis of Iron Aluminides From Elemental Powders: Reaction Mechanisms and Densification Behavior. Heats (energies) See Heat of formation Heat of mixing Heat of solution Heavy metal alloys See Lead base alloys Tin base alloys Heavy metals See Antimony Bismuth Lead (metal) Tin Heliarc welding See Gas tungsten arc welding Helmholtz free energy See Free energy Hematite, Reduction (chemical) The Influence of Specific Impurities on the Nucleation and Growth of Magnetic During Reduction of Artificially Prepared Hematite.	875-888B 277-286A 503-511B
718. A Phase Diagram Approach to Study Liquation Cracking in Alloy 718. Heat checking See Thermal fatigue Heat conductivity See Thermal conductivity Heat flow See Heat transmission Heat flux See Heat transmission Heat measurement See Calorimetry Heat of activation See Activation energy Heat of decomposition See Heat of formation Heat of dissolution See Heat of formation Heat of dissolution See Heat of Soution Activities of Boron in the Binary Ni—B and the Ternary Co—Fe—B Melts. High-Temperature Thermodynamic Properties of the Vanadium Carbides V ₂ C and VC _{0.73} Determined Using a Galvanic Cell Technique. Gibbs Energy of Formation of Nickel Chromite. Enthalpies of Formation of Refractory Borides by High-Temperature Direct Synthesis Calorimetry: RuB _{1.1} and RiB _{1.2} . Heats of Formation of Aluminum—Cerium Intermetallic Compounds. Note on the Enthalpies of Formation of Cu ₃ Si and Cu ₃ Ge. A Thermodynamic Assessment of the Fe—Cr—Ni—C System. Chemical Potential Diagram of Al—Ti—C System: Al ₄ C ₃ Formation on I'C Formed in Al—Ti Liquids Containing Carbon.	47-52B 661-668B 673-675B 1680-1683A 2119-2123A 2162-2165A 2187-2198A	Mold Behavior and its Influence on Quality in the Continuous Casting of Steel Slabs. II. Mold Heat Transfer, Mold Flux Behavior, Formation of Oscillation Marks, Longitudinal Off-Corner Depressions, and Subsurface Cracks. Heat treatment See Annealing Austentizing Isothermal treatment Quenching (cooling) Solution heat treatment Tempering Heating See Superheating Heating rate Synthesis of Iron Aluminides From Elemental Powders: Reaction Mechanisms and Densification Behavior. Heats (energies) See Heat of formation Heat of mixing Heat of solution Heavy metal slloys See Lead base alloys Tin base alloys Tin base alloys Tin base alloys Heavy metals See Antimony Bismuth Lead (metal) Tin Heliarc welding See Gas tungsten arc welding Helmholtz free energy See Free energy Hematite, Reduction (chemical) The Influence of Specific Impurities on the Nucleation and Growth of Magnetite During Reduction of Artificially Prepared Hematite. Heterogeneous structure, Cooling effects Solidification of Undercooled Sn—Sb Peritectic Alloys. II.	875-888B 277-286A
718. A Phase Diagram Approach to Study Liquation Cracking in Alloy 718. Heat checking See Thermal fatigue Heat conductivity See Thermal conductivity Heat flow See Heat transmission Heat flux See Heat transmission Heat measurement See Calorimetry Heat of activation See Activation energy Heat of decomposition See Heat of formation Heat of dissociation See Heat of formation Heat of dissociation See Heat of Solution Activities of Boron in the Binary Ni—B and the Ternary Co—Fe—B Melts. High-Temperature Thermodynamic Properties of the Vanadium Carbides V ₂ C and VC _{0.73} Determined Using a Galvanic Cell Technique. Gibbs Energy of Formation of Nickel Chromite. Enthalpies of Formation of Refractory Borides by High-Temperature Direct Synthesis Calorimetry: RuB _{1.1} and RB _{1.2} . Heats of Formation of Aluminum—Cerium Intermetallic Compounds. Note on the Enthalpies of Formation of Cu ₃ Si and Cu ₃ Ge. A Thermodynamic Assessment of the Fe—Cr—Ni—C System. Chemical Potential Diagram of Al—Ti—C System: Al ₄ C ₃ Formation on TiC Formed in Al—Ti Liquids Containing Carbon. Heat of mixing Thermodynamics of Aluminum—Barium Alloys. The Energy and Solute Conservation Equations for Dendritic Solidification.	47-52B 661-668B 673-675B 1680-1683A 2119-2123A 2162-2165A 2187-2198A 3075-3076A	Mold Behavior and its Influence on Quality in the Continuous Casting of Steel Slabs. II. Mold Heat Transfer, Mold Flux Behavior, Formation of Oscillation Marks, Longitudinal Off-Corner Depressions, and Subsurface Cracks. Heat treatment See Annealing Austenitizing Isothermal treatment Quenching (cooling) Solution heat treatment Tempering Heating See Superheating Heating rate Synthesis of Iron Aluminides From Elemental Powders: Reaction Mechanisms and Densification Behavior. Heats (energies) See Heat of formation Heat of mixing Heat of solution Heavy metal alloys See Lead base alloys Tin base alloys Heavy metals See Antimony Bismuth Lead (metal) Tin Heliarc welding See Gas tungsten arc welding Helmholtz free energy See Free energy Hematite, Reduction (chemical) The Influence of Specific Impurities on the Nucleation and Growth of Magnetic During Reduction of Artificially Prepared Hematite.	875-888B 277-286A 503-511B
718. A Phase Diagram Approach to Study Liquation Cracking in Alloy 718. Heat checking See Thermal fatigue Heat conductivity See Thermal conductivity Heat flow See Heat transmission Heat measurement See Calorimetry Heat of activation See Heat of formation Heat of dissociation See Heat of formation Heat of dissociation See Heat of formation Heat of dissociation See Heat of Sountion Heat of Heat of See Heat of Sounties High-Temperature Thermodynamic Properties of the Vanadium Carbides V ₂ C and VC _{0.73} Determined Using a Galvanic Cell Technique. Gibbs Energy of Formation of Nickel Chromite. Enthalples of Formation of Refractory Borides by High-Temperature Direct Synthesis Calorimetry: RuB _{1.1} and RhB _{1.1} . Heats of Formation of Aluminum—Cerium Intermetallic Compounds. Note on the Enthalples of Formation of Cu ₃ Si and Cu ₃ Ge. A Thermodynamic Assessment of the Fe—Cr—Ni—C System. Chemical Potential Diagram of Al—Ti—C System: Al ₄ C ₃ Formation on TiC Formed in Al—Ti Liquids Containing Carbon. Heat of mixing Thermodynamics of Aluminum—Barium Alloys. The Energy and Solute Conservation Equations for Dendritic Solidification. Thermochemistry of Binary Alloys of Transition Metals: the Me—Sc. Me—Y, and Me—La (Me = Silver, Gold) Sys-	47-52B 661-668B 673-675B 1680-1683A 2119-2123A 2162-2165A 2187-2198A 3075-3076A 607-616B	Mold Behavior and its Influence on Quality in the Continuous Casting of Steel Slabs. II. Mold Heat Transfer, Mold Flux Behavior, Formation of Oscillation Marks, Longitudinal Off-Corner Depressions, and Subsurface Cracks. Heat treatment See Annealing Austenitizing Isothermal treatment Quenching (cooling) Solution heat treatment Tempering Heating See Superheating Heating rate Synthesis of Iron Aluminides From Elemental Powders: Reaction Mechanisms and Densification Behavior. Heats (energies) See Heat of formation Heat of mixing Heat of solution Heavy metal alloys See Lead base alloys Tin base alloys Heavy metals See Antimony Bismuth Lead (metal) Tin Heliarc welding See Gas tungsten arc welding Helmholtz free energy See Free energy Hematite, Reduction (chemical) The Influence of Specific Impurities on the Nucleation and Growth of Magnetite During Reduction of Artificially Prepared Hematite. Heterogeneous structure, Cooling effects Solidification of Undercooled Sn—Sb Peritectic Alloys. II. Heterogeneous Nucleation.	875-888B 277-286A 503-511B
718. A Phase Diagram Approach to Study Liquation Cracking in Alloy 718. Heat checking See Thermal fatigue Heat conductivity Heat flow See Heat transmission Heat flux See Heat transmission Heat of activation See Activation energy Heat of activation See Heat of formation Heat of dissociation See Heat of Solution See Heat of Solution See Heat of Solution See Heat of Formation Heat of Missociation Activities of Boron in the Binary Ni—B and the Ternary Co— Fe—B Melts. High-Temperature Thermodynamic Properties of the Vanadium Carbides V ₂ C and VC _{0.73} Determined Using a Galvanic Cell Technique. Gibbs Energy of Formation of Nickel Chromite. Enthalpies of Formation of Refractory Borides by High-Temperature Direct Synthesis Calorimetry: RuB _{1.1} and RhB _{1.2} . Heats of Formation of Aluminum—Cerium Intermetallic Compounds. Note on the Enthalpies of Formation of Cu ₃ Si and Cu ₃ Ge. A Thermodynamic Assessment of the Fe—C/r—Ni—C System. Chemical Potential Diagram of Al—Ti—C System: Al ₄ C ₃ Formation on TiC Formed in Al—Ti Liquids Containing Carbon. Heat of mixing Thermodynamics of Aluminum—Barium Alloys. The Energy and Solute Conservation Equations for Dendritic Solidification.	47-52B 661-668B 673-675B 1680-1683A 2119-2123A 2162-2165A 2187-2198A 3075-3076A 607-616B	Mold Behavior and its Influence on Quality in the Continuous Casting of Steel Slabs. II. Mold Heat Transfer, Mold Flux Behavior, Formation of Oscillation Marks, Longitudinal Off-Corner Depressions, and Subsurface Cracks. Heat treatment See Annealing Austentizing Isothermal treatment Quenching (cooling) Solution heat treatment Tempering Heating See Superheating Heating rate Synthesis of Iron Aluminides From Elemental Powders: Reaction Mechanisms and Densification Behavior. Heats (energies) See Heat of formation Heat of mixing Heat of solution Heavy metal siloys See Lead base alloys Tin base alloys Tin base alloys Tin base alloys Heavy metals See Antimony Bismuth Lead (metal) Tin Heliarc welding See Gas tungsten arc welding Helmholtz free energy See Free energy Hematite, Reduction (chemical) The Influence of Specific Impurities on the Nucleation and Growth of Magnetite During Reduction of Artificially Prepared Hematite. Heterogeneous structure, Cooling effects Solidification of Undercooled Sn—Sb Peritectic Alloys. II. Hexagonal close packed lattice See Hexagonal lattice	875-888B 277-286A 503-511B

HI smelt process		Chrysture and Proportion of a Danidh, Catalified \$1, 11	
See Direct reduction		Structure and Properties of a Rapidly Solidified Al—Li— Mn—Zr Alloy for High-Temperature Applications. I. Inert	
High alloy steels See also Stainless steels		Gas Atomization Processing. Shock Densification/Hot Isostatic Pressing of Titanium Alumi- nide.	2503-2514A 2667-2676A
High alloy steels, Corrosion Hydrogen Compatibility of Femnal Alloys.	215-224A	Powder Metallurgy T15 Tool Steel. I. Characterization of Powder and Hot Isostatically Pressed Material.	2733-2745A
High alloy steels, Phase transformations		Hot pressing	
Phase Transformation in an Fe—10.1AI—28.6Mn—0.46C Alloy.	2265-2276A	See also Hot isostatic pressing Synthesis of Iron Aluminides From Elemental Powders: Reac- tion Mechanisms and Densification Behavior.	277-286A
High carbon steels, Chemical analysis Secondary Ion Mass Spectrometry Method for Distinguishing		Hot reduction	211 20011
the State of Carbon in Steels Using Negative Molecular lons.	1000 10704	See Hot working	
High carbon steels, Heat treatment	1969-1978A	Hot rolling Recrystallization of Austenite After Deformation at High Tem-	
Electron Microscopy Study of the Aging and First Stage of	707 0004	peratures and Strain Rates—Analysis and Modeling.	151-160A
Tempering of High-Carbon Fe—C Martensite. Microstructural Engineering Applied to the Controlled Cool-	797-806A	The Thermal and Metallurgical State of Steel Strip During Hot Rolling. I. Characterization of Heat Transfer.	307-319A
ing of Steel Wire Rod. I. Experimental Design and Heat Transfer.	2769-2778A	The Thermal and Metallurgical State of Steel Strip During Hot Rolling. II. Factors Influencing Rolling Loads.	321-333A
Microstructural Engineering Applied to the Controlled Cooling of Steel Wire Rod. II. Microstructural Evolution and Me-		The Thermal and Metallurgical State of Steel Strip During Hot	335-349A
chanical Properties Correlations.	2779-2790A	Rolling. III. Microstructural Evolution. Prediction of Steel Flow Stresses at High Temperatures and	
Microstructural Engineering Applied to the Controlled Cooling of Steel Wire Rod. III. Mathematical Model—		Strain Rates. Thermal Behavior of Steel Rolling With Nonconventional	1545-1558A
Formulation and Predictions.	2791-2805A	Rolls. Establishment of a General Formula for Fractional Softening.	1767-1774A 2160-2162A
High energy milling See Mechanical alloying		Recrystallization Controlled Rolling and Accelerated Cooling for High Strength and Toughness in V—Ti—N Steels.	2681-2694A
High pressure		Hot roughing	2001-2054A
Solid Solubilities of Manganese and Titanium in Aluminum at 0.1 MPa and 2.1 GPa.	783-786A	See Hot rolling	
High speed tool steels, Phases (state of matter)		Hot strength See Tensile strength	
An Experimental Study of Carbide/Austenite Equilibria in the High-Speed Steel Alloy System.	1391-1405A	Hot tensile strength	
High strength low alloy steels, Alloy development		See Tensile strength	
The Mass Transfer Kinetics of Niobium Solution Into Liquid Steel.	417-427B	Hot workability Torsional Hot Workability in 0.47C—0.86Mn—0.5Cr—B	
High strength low alloy steels, Chemical analysis		Steel From 650-870°C.	469-477A
Secondary Ion Mass Spectrometry Method for Distinguishing the State of Carbon in Steels Using Negative Molecular		Hot workability, Microstructural effects	
lons.	1969-1978A	Ductility Enhancement in NiAl (B2)-Base Alloys by Microstructural Control.	441-446A
High strength low alloy steels, Phases (state of matter) Thermodynamic Properties of the Fe—Mn—V—C System.	1911-1920A	Hot working	
High strength low alloy steels, Rolling	1911-1920A	See also Hot forming Hot rolling	
Recrystallization Controlled Rolling and Accelerated Cooling	2681-2694A	Processing Map for Hot Working of Alpha-Zirconium. Dynamic Recrystallization During Hot Deformation of Alumi-	829-836A
for High Strength and Toughness in V—TI—N Steels. Effect of Interpass Time on Austenite Grain Refinement by		num: a Study Using Processing Maps. Characterization of Hot Deformation Behavior of Brasses	2339-2348A
Means of Dynamic Recrystallization of Austenite.	2947-2957A	Using Processing Maps. I. α Brass.	2985-2992A
High strength low alloy steels, Welding Microstructure and Local Brittle Zone Phenomena in High-		Characterization of Hot Deformation Behavior of Brasses Using Processing Maps. II. β Brass and α — β Brass.	2993-3001A
Strength Low-Alloy Steel Welds.	139-149A	Hydrides	0040 00004
High strength steels See also High strength low alloy steels		Delayed Hydride Cracking Behavior for Zircaloy-2 Tubing. Fracture Initiation at Hydrides in Zirconium.	2049-2060A 2327-2337A
High strength steels, Mechanical properties		Hydrodynamics	
A Comparison of the Fracture Behavior of Two Commercially Produced Heats of HY180 Steel Differing in Sulfide Type.	2277-2285A	See Magnetohydrodynamics	
High temperature tests		Hydrogen, Diffusion Grain Boundary Diffusion of Hydrogen in Nickel.	351-355A
High-Temperature Rupture of Microstructurally Unstable 304 Stainless Steel Under Uniaxial and Triaxial Stress States.	2629-2635A	Modeling Surface Effects on Hydrogen Permeation in Metals. Effect of Retained Austenite on the Hydrogen Content and Ef-	1001-1006A
HIP		fective Diffusivity of Martensitic Structure.	2579-2586A
See Hot isostatic pressing		Hydrogen, Environment Morphology and Aging of the Martensite Induced by Cathodic	
Homogenizing Development of Structure and Porosity in Cast Al ₅ CuZr ₂ and		Hydrogen Charging of High-Carbon Austenitic Steels. Fracture of Single Crystals of the Nickel-Base Superalloy	1979-1991A
Al ₈₆ Mn ₉ Zr ₂₅ Intermetallic Compounds.	2545-2552A	PWA 1480E in Hydrogen at 22°C.	2031-2038A
Hot compression See Hot pressing		Delayed Hydride Cracking Behavior for Zircaloy-2 Tubing. Hydrogen Effects on Low-Cycle Fatigue of the Single-Crystal	2049-2060A
Hot cracking		Nickel-Base Superalloy CMSX-2. Effect of High-Pressure Hydrogen on Crack Growth in Car-	2597-2603A
See Cracking (fracturing) Hot cracking (welds)		bon Steel.	2703-2707A
See Weld defects		Hydrogen, Impurities Internal Hydrogen-Induced Subcritical Crack Growth in Aus-	
Hot deformation See Deformation		tenitic Stainless Steels.	2605-2618A
Hot ductility		Hydrogen compounds See Ammonia	
See Ductility		Hydrides	
Hot extraction See Extraction		Hydrogen embrittlement The Kinetics and Micromechanics of Hydrogen-Assisted	
Hot forging		Cracking in Fe—3% Si Single Crystals. Hydrogen Compatibility of Femnal Alloys.	59-70A 215-224A
Low-Temperature Improvement of Mechanical Properties of AISI 4340 Steel Through High-Temperature Thermome-		Room-Temperature Aging of Hydrogen in α-Iron After Ca-	
chanical Treatment.	1093-1102A	thodic Charging. Grain Boundary Diffusion of Hydrogen in Nickel.	261-264A 351-355A
Establishment of a General Formula for Fractional Softening. Hot forming	2160-2162A	Brittle Fracture of an Au/Ag Alloy Induced by a Surface Film. Accelerated Fracture Due to Tritium and Helium in 21-6-9	531-541A
See also Hot forging		Stainless Steel. Hydrogen-Assisted Ductile Fracture in Spheroidized 1520	879-886A
Development of Deformation Instability in Hot Tensile Test Specimens.	2297-2302A	Steel, II. Pure Bending. Morphology and Aging of the Martensite Induced by Cathodic	1615-1626A
Hot fractures		Hydrogen Charging of High-Carbon Austenitic Steels.	1979-1991A
See Fractures Hot hardness		Fracture of Single Crystals of the Nickel-Base Superalloy PWA 1480E in Hydrogen at 22°C.	2031-2038A
See Hardness		Delayed Hydride Cracking Behavior for Zircaloy-2 Tubing. A Critical Evaluation of the Stress-Corrosion Cracking Mech-	2049-2060A
Hot isostatic pressing Instantaneous and Residual Stresses Developed in Hot Iso-		anism in High-Strength Aluminum Alloys. Microstructure Property Relationships and Hydrogen Effects	2407-2414A
static Pressing of Metals and Ceramics.	1071-1078A	in a Particulate-Reinforced Aluminum Composite.	2445-2450A

		Industry molling	
Hydrogen Effects on Low-Cycle Fatigue of the Single-Crystal Nickel-Base Superalloy CMSX-2. Internal Hydrogen-Induced Subcritical Crack Growth in Austenitic Stainless Steels.	2597-2603A 2605-2618A	Induction melting See also Levitation melting Magnetohydrodynamic Flows in a Channel-Induction Furnace.	193-209B
Effect of High-Pressure Hydrogen on Crack Growth in Car- bon Steel.	2703-2707A	Desulfurization and Deoxidation of Cu—S—O Alloy in Induc- tion Meiting and Solidification Under Argon and Their Rates of Elimination in Vacuum Induction Meiting.	405-416B
Hydrogen embrittlement, Alloying effects The Influence of Palladium on the Hydrogen-Assisted Crack-	2429-2443A	In Situ Formation of Three-Dimensional TiC Reinforcements in Ti-TiC Composites.	859-865A
ing Resistance of PH 13-8 Mo Stainless Steel. Hydrogen ion concentration	2423-2443A	Development of Structure and Porosity in Cast Al ₅ CuZr ₂ and Al ₆₈ Mn ₉ Zr ₂₅ Intermetallic Compounds.	2545-2552A
See pH Hydrolytic resistance		Inductovac process See Induction melting	
See Corrosion resistance Hydromagnetic stability		Industrial wastes, Recovering Leaching of Nickel From Supported Nickel Waste Catalyst	
See Magnetohydrodynamics		Using Aqueous Sulfur Dioxide Solution.	775-781B
Hydromagnetics See Magnetohydrodynamics		Inert atmospheres Fracture of Single Crystals of the Nickel-Base Superalloy	721 728A
Hydrometallurgy Representation of the Solubility of Lead Chloride in Various		PWA 1480E in Helium at 22°C. Intermetallic Phase Formation and Breakdown of Molybde-	731-738A 1501-1510A
Chloride Solutions With Pitzer's Model. Dissolution of Malachite in Aqueous Ethylenediaminetetr-	491-498B	num Diffusion Barriers in Ni—Mo—Cu Layers. Infiltration	1301-1310A
aacetate Solution.	569-574B	Interface Structure in Infiltrated Composites of Aluminum Re- inforced With Alumina—Silica Fiber Preforms.	1126-1128A
Cathodic Copper Deposition at 65°C in the Absence and Presence of Bl ³ * and Sb ³ * Additives in Acidified CuSO ₄ Aqueous Solutions.	575-581B	Tribological Behavior and Surface Analysis of Tribodeformed Al Alloy—50% Graphite Particle Composites.	1435-1441A
The Coming-of-Age of Process Engineering in Extractive Metallurgy.	737-754B	Ingots	
The Dissolution Behavior of Metals From Ag/Cu and Ag/Au Alloys in Aidic and Cyanide Solutions.	755-764B	See Rolling ingots Initiation	
The Electrochemical Behavior of a Semiconducting Nautral Pyrite in the Presence of Bacteria.	765-774B	See Crack initiation	
Hydrostatic pressure Hydrostatic Stresses and Their Effect on the Macroflow Be-		Injection Fluid Flow Through Lances With Constant and Variable Pitch	10.000
havior and Microfracture Mechanism of Two-Phase Alloys.	2695-2702A	Swirled Inserts. Injections in the Iron Blast Furnace: a Graphics Study by	13-20B
Hydrostatic tests Hydrostatic Stresses and Their Effect on the Macroflow Be-		Means of the Rist Operating Diagram. Mixing Characteristics of a Submerged Jet Measured Using	363-383B
havior and Microfracture Mechanism of Two-Phase Alloys.	2695-2702A	an Isokinetic Sampling Probe. Inorganic compounds	439-445B
Hysteresis, Heating effects Effects of Thermal Cycling on the Martensitic Transformation in Two-Phase α/β Brasses.	1473-1478A	See Ceramics	
I V characteristics	1475-1470A	Inorganic salts See Fused salts	
See Current voltage characteristics Ilmenite, Reduction (chemical)		Inspection The Evaluation of In-Service Materials Degradation of Low-	
Phase Transformations During Heating of Ilmenite Concentrates.	711-716B	Alloy Steels by the Electrochemical Method. Instability	2097-2106A
Impact strength Mechanical, Elastic, and Structural Properties of Alloys of		See Stability	
Ru—Ta High-Temperature Intermetallic Compounds. Powder Metallurgy T15 Tool Steel. II. Microstructure and Properties After Heat Treatment.	129-137A	Intensity See Stress intensity	
Properties After Heat Treatment. Impact strength, Alloying effects	2747-2759A	Interface reactions The Mass Transfer Kinetics of Niobium Solution Into Liquid	
The Reduction of the Interfacial Segregation of Phosphorus and its Embrittlement Effect by Lanthanum Addition in a W—Ni—Fe Heavy Alloy.	2969-2974A	Steel. Reaction of Titanium and Ti—Al Alloys With Alumina. Interface Structure in Infiltrated Composites of Aluminum Re-	417-427B 715-721A
Impact strength, Deformation effects		inforced With Alumina—Silica Fiber Preforms. The K ₂ ZrF ₆ Wetting Process: Effect of Surface Chemistry on	1126-1128A
Low-Temperature Improvement of Mechanical Properties of AISI 4340 Steel Through High-Temperature Thermome-		the Ability of a SiC-Fiber Preform To Be Impregnated by Aluminum.	2133-2139A
chanical Treatment. Impact strength, Heating effects	1093-1102A	Microstructural Development in Transient Liquid-Phase Bonding.	2451-2457A
Effects of Intercritical Treatment and Tempering on Fracture Behavior in a Medium-Carbon 2Si—3Ni Steel.	2587-2596A	Preliminary Studies on NiAl/Nb ₂ Be ₁₇ Reaction and Effective- ness of BeO as an Interfacial Reaction Barrier. Chemical Stability of Zirconia-Stabilized Alumina Fibers Dur-	2535-2538A
Impact strength, Impurity effects The Reduction of the Interfacial Segregation of Phosphorus and its Embrittlement Effect by Lanthanum Addition in a		ing Pressure Infiltration by Aluminum. Interfaces in XD Processed TiB ₂ /NiAl Composites.	2855-2862A 3013-3018A
W-Ni-Fe Heavy Alloy.	2969-2974A	Interface reactions, Heating effects Intermetallic Phase Formation and Breakdown of Molybde-	4504 45404
Impact strength, Microstructural effects Microstructurally Toughened Particulate-Reinforced Aluminum Matrix Composition	171-182A	num Diffusion Barriers in Ni—Mo—Cu Layers. Microstructural and Thermal Stability of a Ti—43Al Alloy Containing Dispersoids of Titanium Di-Boride.	1501-1510A 1721-1728A
num Matrix Composites. NiAl-Based Microstructurally Toughened Composites.	171-182A 183-189A	taining Dispersoids of Titanium Di-Boride. Interface reactions, Impurity effects	
Impact toughness See Impact strength		Effect of Sulfur Removal on Al ₂ O ₃ Scale Adhesion.	739-752A
Imperfections See Defects		Interfaces Microstructurally Toughened Particulate-Reinforced Alumi-	171 1924
Impregnation		num Matrix Composites. The Effects of Interface Attachment Kinetics on Solidification Interface Morphologies.	171-182A 235-249A
The K ₂ ZrF ₆ Wetting Process: Effect of Surface Chemistry on the Ability of a SiC-Fiber Preform To Be Impregnated by		In Situ Observation of Interactions Between Gaseous Inclusions and an Advancing Solid/Liquid Interface.	385-388B
Aluminum. Incandescent lamps	2133-2139A	An Ultrasonic Method for Reconstructing the Two- Dimensional Liquid/Solid Interface in Solidifying Bodies.	467-473B
Discussion of "Evidence for the Existence of Potassium Bub- bles in AKS-Doped Tungsten Wire" and Reply.	2153-2156A	Modeling of Base Metal Dissolution Behavior During Tran- sient Liquid-Phase Brazing.	543-555A
Incineration	2133-2156A	The Effects of Interface Kinetics Anisotropy on the Growth Direction of Cellular Microstructures.	585-593A
See Combustion Inclusions		Thermal and Mechanical Considerations in Using Shape Memory Alloys to Control Vibrations in Flexible Structures.	623-627A
See Nonmetallic inclusions		The Use of Transmission Electron Microscopy for the Assessment of Interphase Boundaries.	1139-1144A
Inconel See Nickel base alloys		Electron Microscopy of Transformation Dislocations at Inter- phase Boundaries.	1145-1158A
Superalloys Indentation		On the Role of Elastic Interactions in the Nucleation and Growth of Ledges.	1159-1164A
On the Constraint Factor Associated With the Indentation of Work-Hardening Materials With a Spherical Ball.	2375-2384A	A Mathematical Method for the Calculation of Ledge Growth Kinetics.	1211-1218A
Indium, Binary systems Thermodynamics of Binary Systems Using Interaction Pa-		Computer Simulation of Morphological Changes of Grain Boundary Precipitates Growing by the Ledge Mechanism. Nonequilibrium Effects During the Ledgewise Growth of a	1235-1245A
rameters.	593-605B	Solid/Liquid Interface.	1249-1258A

Growth Kinetics of Solid/Liquid Gallium Interfaces. I. Experi- mental. Growth Kinetics of Solid/Liquid Gallium Interfaces. II. Theo.	1259-1270A	Intermetallic compounds See Intermetallics	
Growth Kinetics of Solid/Liquid Gallium Interfaces. II. Theo- retical. The Role of Ledges in Vapor/Solid Phase Transformations Observed by Low-Energy Electron Microscopy and Photo-	1271-1286A	Intermetallic phases Thermodynamics of Aluminum—Barium Alloys. Microstructural Effects on Ambient and Elevated Tempera-	607-616B
emission Electron Microscopy. The Role of Ledges in Stress Tensor-Mediated Surface Pro-	1311-1315A	ture Fatigue Crack Growth in Titanium Aluminide Intermet- allics.	817-828A
cesses for Silicon and GaAs. Interface Dislocations and Ledges in Oxidation and Diffu-	1317-1322A	Microstructural Evolution in Rapidly Solidified Al—Fe Alloys: an Alternative Explanation.	927-934A
sional Phase Transformations. Thickening of Grain-Boundary α Allotriomorphs in a Ti—Cr	1331-1339A	The AI—AI ₈ Mo ₃ Section of the Binary System Aluminum— Molybdenum.	1729-1736A
Alloy by Multiple Sets of Ledges. Interfacial Steps and Growth Mechanism in Ferrous Pearlites.	1341-1348A 1349-1365A	Effect of Phase Morphology on the Mechanical Behavior of Two Titanium Aluminide Composites. Structure and Properties of a Rapidly Solidified Al—Li—	2009-2019A
The Role of Ledges in the Proeutectoid Ferrite and Proeutectoid Cementite Reactions in Steel.	1367-1380A	Mn—Zr Alloy for High-Temperature Applications. I. Inert Gas Atomization Processing.	2503-2514A
Kinetic Equations for Concurrent Size and Shape Coarsening by the Ledge Mechanism.	1381-1390A	Structure and Properties of a Rapidly Solidified AI—Li— Mn—Zr Alloy for High-Temperature Applications. II. Spray	2000 201471
Effect of Grain Boundaries on Isothermal Solidification Dur- ing Transient Liquid Phase Brazing.	1627-1631A	Atomization and Deposition Processing. Containerless Processing and Rapid Solidification of Nb—Si	2515-2522A
In Situ Observation of Nonfaceted Cellular Growth in a Nar- row Channel.	1683-1687A	Alloys in the Niobium-Rich Eutectic Range. Containerless Processing and Rapid Solidification of Nb—Si	2713-2721A
Effect of Plastic Deformation on Residual Stresses in Ceramic/Metal Interfaces. Interfaces, Atomic properties	2822-2825A	Alloys of Hypereutectic Composition. Chemical Stability of Zirconia-Stabilized Alumina Fibers Dur- ing Pressure Infiltration by Aluminum.	2723-2732A 2855-2862A
Atomic Structure of the Crystalline/Amorphous Interface in a Directionally Crystallized Pd ₈₀ Si ₂₀ Alloy.	1287-1298A	Intermetallic phases, Cooling effects Experimental Determination of the Phase Equilibria of	
Interfaces, Corrosion effects Microstructure Property Relationships and Hydrogen Effects	0445 04504	Aluminum-Rich Al—Li—Cu Alloys. Solidification of Undercooled Sn—Sb Peritectic Alloys. I.	203-213A
in a Particulate-Reinforced Aluminum Composite. Interfaces, Crystal growth	2445-2450A	Microstructural Evolution. Solidification of Undercooled Sn—Sb Peritectic Alloys. II.	753-764A
Diffusion-Controlled Kink Motion. Macroscopic Description of Interface Migration by Ledge and	1219-1224A	Heterogeneous Nucleation. Intermetallic phases, Heating effects	765-773A
Kink Motion Controlled by Volume Diffusion.	1225-1233A	Intermetallic Phase Formation and Breakdown of Molybde- num Diffusion Barriers in Ni—Mo—Cu Layers.	1501-1510A
Interfaces, Mechanical properties The Mechanical Behavior of a Hybrid Metal Matrix Composite. Interfaces, Microstructure	2107-2117A	Intermetallic phases, Microstructure Crystallographic Characterization of Some Intermetallic Compounds in the AI—Cr System.	5-10A
Structural Ledges in Interphase Boundaries. The Geometry and Properties of Ledges in Interfaces. The Crystallography and Atomic Structure of Line Defects in	1165-1175A 1177-1183A	Intermetallics, Alloying elements A New Phase in a Rapidly Solidified and Consolidated NbAl ₃ —1TiB ₂ Alloy.	1901-1909A
Twin Boundaries in Hexagonal-Close-Packed Metals.	1185-1196A	Intermetallics, Casting	
Interfacial energy See Surface energy		Evolution of Boride Morphologies in TiAl—B Alloys. Intermetallics, Composite materials	1647-1662A
Interfacial surface tension See Surface tension		NiAl-Based Microstructurally Toughened Composites. Creep Deformation of TiB ₂ -Reinforced Near-y Titanium Al-	183-189A
Intergranular corrosion Intergranular Stress Corrosion Cracking of Alloy 600 and X-		uminides. Reaction of Titanium and Ti—Al Alloys With Alumina. Preliminary Studies on NiAl/Nb ₂ Be ₁₇ Reaction and Effective-	447-454A 715-721A
750 in High-Temperature Deaerated Water/Steam. The Evaluation of in-Service Materials Degradation of Low- Alloy Steels by the Electrochemical Method.	1857-1864A 2097-2106A	ness of BeO as an Interfacial Reaction Barrier. Interfaces in XD Processed TiB ₂ /NiAl Composites. Pressure Casting of a Zirconia-Toughened Alumian Fiber-	2535-2538A 3013-3018A
Intergranular corrosion, Alloying effects The Influence of Palladium on the Hydrogen-Assisted Cracking Resistance of PH 13-8 Mo Stainless Steel.	2429-2443A	Pressure Casting of a Zirconia-Toughened Alumian Fiber- Reinforced NiAl Composite. Intermetallics, Directional solidification Solidification Microporosity in Directionally Solidified Multi-	3059-3064A
Intergranular fracture Fracture Toughness Behavior of Ex-Service 2.25Cr—1Mo Steels From a 22-Year-Old Fossil Power Plant.	455-468A	component Nickel Aluminide. Intermetallics, Heat treatment Microstructural and Thermal Stability of a Ti—43Al Alloy Con-	225-234A
Comparison of Fracture Behavior in Intercritically Treated Medium-Carbon Nickel and Silicon Steels.	1115-1119A	taining Dispersoids of Titanium Di-Boride.	1721-1728A
Intergranular fracture, Environmental effects Environmental and Hold Time Effects on Fatigue of Low-Tin Lead-Based Solder.	357-366A	Intermetallics, Mechanical properties Effect of Hydrogen as a Temporary β Stabilizer on Microstructure and Brittle Fracture Behavior in a Titanium Aluministed Allers	71-81A
Intergranular fracture, Heating effects	337-300A	nide Alloy. A Model for the Strain-Rate Dependence of Yielding in Ni ₃ Al Alloys.	125-128A
Effects of Intercritical Treatment and Tempering on Fracture Behavior in a Medium-Carbon 2Si—3Ni Steel. Intergranular fracture, Microstructural effects	2587-2596A	Mechanical, Elastic, and Structural Properties of Alloys of Ru—Ta High-Temperature Intermetallic Compounds. The Initiation and Growth of Fatigue Cracks in a Titanium Al-	129-137A
The Relationship Between Carbon Content, Microstructure, and Intergranular Liquation Cracking in Cast Nickel Alloy	557 507A	uminide Alloy. Mechanical Properties of High Temperature Alloys of AlRu. Plastic Deformation and Fracture of Binary TIAl-Base Alloys.	377-391A 403-414A 427-439A
718. Surface Void Nucleation Under the Power-Law Creep Condition in an AL—3 at % Mg Solid Solution Alloy	557-567A 935-937A	Ductility Enhancement in NiAl (B2)-Base Alloys by Microstructural Control.	441-446A
tion in an Al—3 at.% Mg Solid Solution Alloy. High-Temperature Rupture of Microstructurally Unstable 304 Stainless Steel Under Uniaxial and Triaxial Stress States.	935-937A 2629-2635A	Microstructural Effects on Ambient and Elevated Tempera- ture Fatigue Crack Growth in Titanium Aluminide Intermet-	
Intergranular precipitation On the Stress Corrosion Cracking of Al—Li Alloys: the Role		allics. 1000 to 1200K Time-Dependent Compressive Deformation of	817-828A
of Grain Boundary Precipitates. The Relationship Between Carbon Content, Microstructure, and Intergranular Liquation Cracking in Cast Nickel Alloy	264-267A	Single-Crystalline and Polycrystalline B2 Ni—40Al. Grain Boundary Pest of Boron-Doped Ni ₉ Al at 1200°C. A Simple, Versatile Miniaturized Disk-Bend Test Apparatus for Quantitative Viold Stress Massurgments.	1595-1607A 1801-1809A
718. Aging Characteristics of Electron Beam and Gas Tungsten	557-567A	for Quantitative Yield-Stress Measurements. The Effects of Chromium Additions to Binary TiAl-Base Alloys	2061-2068A 2619-2626A
Aging Characteristics of Electron Beam and das Tungsten Arc Fusion Zones of Al—Cu—Li Alloy 2090. Computer Simulation of Morphological Changes of Grain	903-913A	loys. Ductilization of Ni—Ni ₄ Mo Alloys by Boron Additions.	3067-3071A
Boundary Precipitates Growing by the Ledge Mechanism. Phase Transformation in an Fe—10.1AI—28.6Mn—0.46C Alloy.	1235-1245A 2265-2276A	Intermetallics, Metal working Strength and Ductile-Phase Toughening in the Two-Phase Nb/Nb ₅ Si ₃ Alloys.	1573-1583A
Intergranular precipitation, Deformation effects Mechanisms of Deformation-Induced Grain Boundary Chromium Depletion (Sensitization) Development in Type 316		Intermetallics, Metallography Electron Microscopy of Transformation Dislocations at Interphase Boundaries.	1145-1158A
Stainless Steels. Intergranular precipitation, High temperature effects	2917-2934A	Intermetallics, Microstructure Development of Structure and Porosity in Cast Al ₅ CuZr ₂ and Al ₆₆ Mn ₉ Zr ₂₅ Intermetallic Compounds.	2545-2552A
Effect of Long-Term Service Exposure on Microstructure and Mechanical Properties of a CrMoV Steam Turbine Rotor Steel.	1811-1820A	Intermetallics, Phases (state of matter) A New Phase in a Rapidly Solidified and Consolidated	
Intermediates On the Kinetics of Diffusion-Limited Layer Growth in Solid—		NbAl ₃ —1TiB ₂ Alloy. An Investigation of Fe—Ni Order in a Steel.	1901-1909A 2807-2809A
Solid Systems. A Calorimetric Study of Precipitation in an Al—Cu Alloy With Silicon Particles.	523-527B 665-674A	Intermetallics, Physical properties Heats of Formation of Aluminum—Cerium Intermetallic Compounds.	2119-2123A

Note on the Enthalpies of Formation of Cu ₃ Si and Cu ₃ Ge.	2162-2165A	Irradiation damage See Radiation damage	
Intermetallics, Powder technology Synthesis of Iron Aluminides From Elemental Powders: Reac-		Isostatic pressing	
tion Mechanisms and Densification Behavior. Dynamic Compaction of Titanium Aluminides by Explosively	277-286A	See Hot isostatic pressing Isothermal treatment	
Generated Shock Waves: Experimental and Materials Sys- tems. Shock Densification/Hot Isostatic Pressing of Titanium Alumi-	685-695A	Interrupted and Isothermal Solidification Studies of Low and Medium Carbon Steels.	1871-1880A
nide.	2667-2676A	IV characteristics See Current voltage characteristics	
Intermetallics, Reactions (chemical) Thermodynamics of Aluminum—Barium Alloys.	607-616B	Jet engines	
Internal combustion engines See Gas turbine engines		See Gas turbine engines Joining	
Internal friction High-Damping Metals and Alloys.	607-616A	See Bonding Brazing	
Internal stress		Joints See Brazed joints	
See Residual stress fon implantation		Soldered joints Welded joints	
Influence of Cyclic Deformation on Surface Microstructure and Hardness of Ion-Implanted Nickel.	1633-1646A	Junghans Rossi casting See Continuous casting	
Iron, Alloying elements Ductility Enhancement in NiAl (B2)-Base Alloys by Microstructural Control.	441-446A	Killed steels See also Aluminum killed steels	
Iron, Binary systems Thermodynamics of Binary Systems Using Interaction Parameters.	593-605B	Killed steels, Welding Effect of Killing Time on the Microstructure and Toughness of the Heat-Affected Zone in Titanium-Killed Steels.	2818-2822A
Iron, Corrosion Room-Temperature Aging of Hydrogen in α -Iron After Ca-		Kinematography See Cinematography	
thodic Charging. Active and Passive Behavior of Sintered Iron in Ammoniacal	261-264A	Kinetics See also Reaction kinetics	
Ammonium Carbonate Solution. Iron, Joining	323-332B	The Kinetics and Micromechanics of Hydrogen-Assisted Cracking in Fe—3% Si Single Crystals.	59-70A
Effect of Plastic Deformation on Residual Stresses in Ceramic/Metal Interfaces.	2822-2825A	A Model for the Strain-Rate Dependence of Yielding in Ni ₃ Al Alloys.	125-128A
Iron, Mechanical properties The Growth of Short Fatigue Cracks Under Compressive		The Kinetics of S ³⁵ Exchange Between SO ₂ /CO/CO ₂ Gas Mixtures and Copper Sulfide Melts at 1523K.	211-217B
and/or Tensile Cyclic Loading.	1079-1082A	The Effects of Interface Attachment Kinetics on Solidification Interface Morphologies.	235-249A
The Effect of Reaction Condition on Composition and Proper-		Leaching Kinetics of Copper From Natural Chalcocite in Alka- line Na ₄ EDTA Solutions. Kinetics of Removal of Bismuth and Lead From Molten Cop-	295-303B
ties of Ultrafine Amorphous Powders in (Fe,Co,Ni)—B Systems Prepared by Chemical Reduction.	2125-2132A	per Alloys in Vacuum Induction Melting. Knowledge-Based Simulation and Identification of Various	447-465B
Thermodynamic Properties of the Fe—Mn—V—C System.	1911-1920A	Metallurgical Reactors. Chemical Vapor Deposition Kinetics of Tungsten From WCl ₆	541-555B
A Thermodynamic Assessment of the Fe—Cr—Ni—C System.	2187-2198A	Onto Nickel Plate at Elevated Temperatures. The Effects of Interface Kinetics Anisotropy on the Growth	560-563B
On the Constraint Factor Associated With the Indentation of		Direction of Cellular Microstructures. The Effect of the Thermal Path to Reach Isothermal Temper-	585-593A
Work-Hardening Materials With a Spherical Ball. Iron, Ternary systems	2375-2384A	ature on Transformation Kinetics. Computer Simulation of the Effect of Coherency Strain on Cluster Growth Kinetics.	993-999A 1197-1209A
Activities of Boron in the Binary Ni—B and the Ternary Co— Fe—B Melts.	47-52B	A Mathematical Method for the Calculation of Ledge Growth Kinetics.	1211-1218A
Representation of Excess Thermodynamic Properties of Ter- nary Systems Using Interaction Parameters. An Assessment of the Fe—C—SI System.	583-591B 2211-2223A	Diffusion-Controlled Kink Motion. Growth Kinetics of Solid/Liquid Gallium Interfaces. I. Experi-	1219-1224A
Iron and steel making	2211-22204	mental. Growth Kinetics of Solid/Liquid Gallium Interfaces. II. Theo-	1259-1270A
See also Ironmaking Steel making Mixing Characteristics of a Subpersed let Macaured Heise		retical. Observations of the Formation and Kinetics of Surface Steps	1271-1286A
Mixing Characteristics of a Submerged Jet Measured Using an Isokinetic Sampling Probe. The Redox Equilibria of Copper Ions in the Molten Silicate	439-445B	During Evaporation and Condensation. Kinetic Equations for Concurrent Size and Shape Coarsening by the Ledge Mechanism.	1299-1304A 1381-1390A
Fluxes as a Measure of Basicity. Dissolution Equilibrium of Magnesium Vapor in Liquid Iron.	823-829B 918-921B	Carbonitride Precipitate Growth in Titanium/Niobium Microal- loyed Steels.	1511-1524A
Iron base alloys See Ferrous alloys		Simulation of Subgrain Growth by Subgrain Rotation: a One- Dimensional Model.	2257-2263A
Iron carbides, Chemical analysis		Environmental Fatigue of an Al—Li—Cu Alloy. I. Intrinsic Crack Propagation Kinetics in Hydrogenous Environments.	2415-2428A
Secondary Ion Mass Spectrometry Method for Distinguishing the State of Carbon in Steels Using Negative Molecula Ions.		Krupp Renn process See Direct reduction	
Iron compounds	1909-1970A	Kryptol electric furnaces See Electric furnaces	
See also iron carbides Pyrite		Ladle degassing	
Iron compounds, Phases (state of matter) An Investigation of Fe—Ni Order in a Steel.	2807-2809A	Removal of Nitrogen From Steel Using Novel Fluxes. Ladle metallurgy	783-790B
Iron compounds, Powder technology Synthesis of Iron Aluminides From Elemental Powders: Reaction Mechanisms and Densification Behavior.	- 277-286A	Removal of Nitrogen From Steel Using Novel Fluxes. Lamellar structure	783-790B
Iron ores	211-200A	Micromechanics of Shear Ligament Toughening. Microstructural Engineering Applied to the Controlled Cool- ing of Steel Wire Rod. III. Mathematical Model—	2021-2029A
See also Hematite Pyrite		Formulation and Predictions.	2791-2805A
Iron ores, Reduction (chemical) The Reduction Mechanism of a Natural Chromite at 1416°C	53-63B	See Laminates	
Iron oxides See Hematite		Laminates, Mechanical properties On the Influence of Ply-Angle on Damping and Modulus of	
Iron powder See Iron		Elasticity of a Metal-Matrix Composite. Vibration Damping Characteristics of Laminated Steel Sheet	641-651A 653-656A
Ironmaking Injections in the Iron Blast Furnace: a Graphics Study b Means of the Rist Operating Diagram.	y 363-383B	Lances Fluid Flow Through Lances With Constant and Variable Pitch Swirled Inserts.	13-20B
Slag Foaming in Bath Smelting. The Influence of Specific Impurities on the Nucleation an	481-489B	Lanthanum, Alloying elements The Reduction of the Interfacial Segregation of Phosphorus	3
Growth of Magnetite During Reduction of Artificially Prepared Hematite.	503-511B	and its Embrittlement Effect by Lanthanum Addition in a W—Ni—Fe Heavy Alloy.	

Lanthanum hass allows Desettons (showless)		Lauden Base	
Lanthanum base alloys, Reactions (chemical) Thermochemistry of Binary Alloys of Transition Metals: the Me—Sc, Me—Y, and Me—La (Me = Silver, Gold) Sys-		Leuders lines See Luders lines Levitation	
tems	1103-1111A		1647-1662A
Laser beam hardening The Prediction of Case Depth in Laser Transformation Hard- ening.	2459-2466A		2713-2721A
Laser beam welding Heat-Flow Simulation of Laser Remelting With Experimental		Containerless Processing and Rapid Solidification of Nb—Si Alloys of Hypereutectic Composition.	2723-2732A
Validation. Solidification Modeling and Solid-State Transformations in	101-109B	Life	
High-Energy Density Stainless Steel Welds.	915-926A	See Fatigue life Service life	
Laser processing See also Laser beam hardening Laser beam welding		Light metal alloys See Aluminum base alloys Magnesium base alloys	
In Situ Technique for Measuring the Absorption During Laser Surface Remelting.	139-141B	Titanium base alloys	
Laser welding		Light metals See Aluminum	
See Laser beam welding		Magnesium Titanium	
Lattice constant See Lattice parameters		Line defects	
Lettice defects		See Dislocations	
See Crystal defects Lattice displacements		Liquefaction See Melting	
See Displacements (lattice)		Liquid cooling	
Lattice parameters Crystallographic Characterization of Some Intermetallic		See Water cooling	
Compounds in the Al—Cr System. An Experimental Study of Carbide/Austenite Equilibria in the High-Speed Steel Alloy System.	5-10A 1391-1405A	Liquid metal embrittlement Cleavage Crystallography of Liquid Metal Embrittled Alumi- num Alloys.	1849-1855A
A New Phase in an Fe-9.0Al-29.5Mn-1.2Si Alloy.	1417-1423A	Liquid metal forging	
A New Phase in a Rapidly Solidified and Consolidated NbAl ₃ —1TiB ₂ Alloy. Lattice Changes of Iron—Carbon Martensite on Aging at	1901-1909A	See Squeeze casting	
Lattice Changes of Iron—Carbon Martensite on Aging at Room Temperature.	1957-1967A	Liquid metals, Directional solidification Solute Distribution During Steady-State Cellular Growth.	3035-3039A
Lattice parameters, Composition effects Thermodynamic Stability of Palladium Alloys. I. The Palladium—Niobium System.	1937-1943A	Liquid metals, Environment Cleavage Crystallography of Liquid Metal Embrittled Aluminum Alloys.	1849-1855A
Lattice parameters, Heating effects The Tempering of FeNiN Martensite.	1945-1956A	Liquid metals, Physical properties A New Experimental Method for Determining Liquid Density and Surface Tension.	27-31B
Lattice sites Room-Temperature Aging of Hydrogen in α -Iron After Cathodic Charging.	261-264A	Liquid metals, Reactions (chemical) Activities of Chromium in Molten Copper at Dilute Concentra-	
Laves phase The Relationship Between Carbon Content, Microstructure,		tions by Solid-State Electrochemical Cell. Thermochemistry of Binary Alloys of Transition Metals: the Me—Sc, Me—Y, and Me—La (Me = Silver, Gold) Systems	475-480B
and Intergranular Liquation Cracking in Cast Nickel Alloy 718.	557-567A	tems Chemical Potential Diagram of Al—Ti—C System: Al ₄ C ₃ For-	
A Phase Diagram Approach to Study Liquation Cracking in Alloy 718. Layers	887-902A	mation on TiC Formed in Al—Ti Liquids Containing Carbon. Liquid phase diffusion See Diffusion	3075-3076A
See Multilayers		Liquid phase sintering	
Surface layer Leaching		Growth Path Envelope Analysis of Ostwald Ripening. Correction to "Growth Path Envelope Analysis of Ostwald Ri-	19-23A
See also Acid leaching		pening".	19-23A
Alkaline leaching Bacterial leaching		Liquid phase sintering, Field effects Gravitational Limit of Particle Volume Fraction in Liquid-	
Knowledge-Based Simulation and Identification of Various Metallurgical Reactors.	541-555B	Phase Sintering.	786-791A
Leaching of Nickel From Supported Nickel Waste Catalyst Using Aqueous Sulfur Dioxide Solution.		Liquid phases Determination of Liquid Diffusion Coefficients Along a	
Lead (metal), Binary systems	775-7010	Liquidus Phase Boundary.	21-26B
Thermodynamics of Binary Systems Using Interaction Pa- rameters.		Modeling of Base Metal Dissolution Behavior During Tran- sient Liquid-Phase Brazing.	543-555A
Lead (metal), Composite materials	593-605B	Microstructural Development in Transient Liquid-Phase Bonding.	2451-2457A
Processing and Creep Characterization of a Model Metal Ma-		Nucleation of Solidification in Liquid Droplets.	2487-2501A
trix Composite: Lead Reinforced With Nickel Fibers. Lead (metal), Extraction	1029-1036A	See Liquid metals	
Heat-Transfer Phenomena in Water-Cooled Zinc-Fuming Furnace Jackets.	163-175B	Liquidus Determination of Liquid Diffusion Coefficients Along a Liquidus Phase Boundary.	21-26B
Lead (metal), Impurities Kinetics of Removal of Bismuth and Lead From Molten Copper Alloys in Vacuum Induction Melting.	447-465B	Lithium, Ternary systems Calculation of Phase Diagrams and Solidification Paths of	
Lead (metal), Solubility Representation of the Solubility of Lead Chloride in Various Chloride Solutions With Pitzer's Model.	491-498B	Aluminum-Rich Al—Li—Cu Alloys. Live loads	2837-2848A
Lead base alloys, Casting	4014000	See Cyclic loads Lixiviation	
Numerical Simulation of a Solidifying Pb—Sn Alloy: the Ef- fects of Cooling Rate on Thermosolutal Convection and		See Leaching	
Macrosegregation.	529-540B	Loads (forces) See Roll load	
Lead base alloys, Crystal growth The Energy and Solute Conservation Equations for Dendrition Solidification.	889-900B	Long range order, Heating effects Electron Microscopy Study of the Aging and First Stage of	
Lead base alloys, Directional solidification Growth-Speed Dependence of Primary Arm Spacings in Di		Tempering of High-Carbon Fe—C Martensite. Loose powder sintering Synthesis of Iron Aluminides From Elemental Powders: Reac-	797-806A
rectionally Solidified Pb—10 wt.% Sn. Eutectic Spacing Selection in Lead-Based Alloy Systems. Statistical Analysis of the Disorder of Two-Dimensional Cellu		tion Mechanisms and Densification Behavior. Lorenz number	277-286A
lar Arrays in Directional Solidification.	3041-3050A	Lorentz Force Infiltration of Fibrous Preforms.	2903-2915A
Lead base alloys, Mechanical properties Environmental and Hold Time Effects on Fatigue of Low-Tir Lead-Based Solder.	357-366A	Low alloy steels See also High strength low alloy steels Silicon steels	
Thermomechanical Fatigue of a Lead Alloy.	1059-1070A	Low alloy steels, Structural hardening	
Lead base alloys, Oxidation Oxidation Kinetics of a Pb—30 at.% In Alloy.	1865-1869A	Carbonitride Precipitate Growth in Titanium/Niobium Microal- loyed Steels.	1511-1524A

A

Low carbon steels, Casting Interrupted and Isothermal Solidification Studies of Low and	1071 10004	Manganese, Solubility Solid Solubilities of Manganese and Titanium in Aluminum at 0.1 MPa and 2.1 GPa.	783-786A
Medium Carbon Steels. Low carbon steels, Chemical analysis	1871-1880A	Manganese base alloys, Mechanical properties	
Secondary Ion Mass Spectrometry Method for Distinguishing the State of Carbon in Steels Using Negative Molecular Ions.	1969-1978A	High-Damping Metals and Alloys. Manganese compounds, Microstructure Development of Structure and Porosity in Cast Al ₅ CuZr ₂ and	607-616A
Low carbon steels, Composite materials Vibration Damping Characteristics of Laminated Steel Sheet.	653-656A	Al ₆₆ Mn ₉ Zr ₂₅ Intermetallic Compounds. Marine atmospheres	2545-2552A
Low carbon steels, Corrosion Hydrogen-Assisted Ductile Fracture in Spheroidized 1520	404E 4000A	See Marine environments Marine environments	
Steel. II. Pure Bending. Low carbon steels, Heat treatment Microstructural Engineering Applied to the Controlled Cool-	1615-1626A	Modeling of the Corrosion Behavior and Its Interrelation With the Deformation Behavior and Microstructure in a Newly Developed 7.5Mn—5Cr—1.5Cu Alloy White Iron.	2319-2325A
ing of Steel Wire Rod. I. Experimental Design and Heat Transfer. Microstructural Engineering Applied to the Controlled Cool- ing of Steel Wire Rod. II. Microstructural Evolution and Me-	2769-2778A	Martensite Strain Distribution Effects on the Low-Cycle Fatigue Behavior of Fe—C—Mo Steels.	675-683A
chanical Properties Correlations. Microstructural Engineering Applied to the Controlled Cooling of Steel Wire Rod. III. Mathematical Model—	2779-2790A	Martensite, Diffusion Effect of Retained Austenite on the Hydrogen Content and Effective Diffusivity of Martensitic Structure.	2579-2586A
Formulation and Predictions. Low carbon steels, Mechanical properties	2791-2805A	Martensite, Phase transformations The Tempering of FeNiN Martensite. Lattice Changes of Iron—Carbon Martensite on Aging at	1945-1956A
Effects of Material Rate Sensitivity and Void Nucleation on Fracture Initiation in a Circumferentially Cracked Bar.	161-170A	Room Temperature. Morphology and Aging of the Martensite Induced by Cathodic	1957-1967A
Effect of High-Pressure Hydrogen on Crack Growth in Carbon Steel.	2703-2707A	Hydrogen Charging of High-Carbon Austenitic Steels. Martensitic transformations	1979-1991A
Low carbon steels, Rolling Recrystallization of Austenite After Deformation at High Temperatures and Strain Rates—Analysis and Modeling.	151-160A	Thermodynamics of the Iron Martensitic Transformation and the M _s Temperature of Iron.	1761-1765A
Prediction of Steel Flow Stresses at High Temperatures and Strain Rates.	1545-1558A	Lattice Changes of Iron—Carbon Martensite on Aging at Room Temperature. Thermodynamic Equilibrium in the Low-Solute Regions of	1957-1967A
Low carbon steels, Welding Slag—Metal Reactions During Welding. I. Evaluation and Re-		Plutonium-Group IIIA Metal Binary Systems. Martensitic transformations, Environmental effects	2237-2246A
assessment of Existing Theories. Further Study on the Scattering of the Local Fracture Stress and Allied Toughness Value.	65-71B 2287-2296A	Morphology and Aging of the Martensite Induced by Cathodic Hydrogen Charging of High-Carbon Austenitic Steels.	1979-1991A
Low cycle fatigue Low-Cycle Fatigue Behavior of Nimonic PE16 at Room Tem-		Martensitic transformations, Heating effects The Aging Effect on Cu—Zn—Al Shape Memory Alloys With	25-33A
perature. Strain Distribution Effects on the Low-Cycle Fatigue Behavior	499-506A	Low Contents of Aluminum. Effects of Thermal Cycling on the Martensitic Transformation in Two-Phase α/β Brasses.	1473-1478A
of Fe—C—Mo Steels. Crack Initiation and Propagation During High-Temperature Fatigue of Oxide Dispersion-Strengthened Superalloys.	675-683A 837-851A	The Tempering of FeNii Martensite. Martensitic transformations, Stress effects	1945-1956A
Low cycle fatigue, Environmental effects Hydrogen Effects on Low-Cycle Fatigue of the Single-Crystal	2597-2603A	The Shape Memory Effect and Superelasticity in Two-Phase Polycrystalline α/β Brasses.	1479-1490A
Nickel-Base Superalloy CMSX-2. Low cycle fatigue, Temperature effects	2097-2003A	Mass spectroscopy See Secondary ion mass spectroscopy	
Low-Temperature Fatigue of 316L and 316LN Austenitic Stainless Steels. Low pressure	2385-2392A	Mass transfer Slag—Metal Reactions During Welding, II. Theory. Slag—Metal Reactions During Welding, III. Verification of the	73-81B
The High-Temperature Work Function Behavior of Polycrystalline Osmium.	1609-1613A	Theory. A Mathematical Model of the Nickel Converter. I. Model De-	83-100B 153-161B
Lubrication See also Self lubrication		velopment and Verification. A Volume-Averaged Two-Phase Model for Transport Phenomena During Solidification.	349-361B
The Thermal and Metallurgical State of Steel Strip During Hot Rolling. I. Characterization of Heat Transfer.	307-319A	The Mass Transfer Kinetics of Niobium Solution Into Liquid Steel. Kinetics of Removal of Bismuth and Lead From Molten Cop-	417-427B
See Luders lines		per Alloys in Vacuum Induction Melting. Modeling Surface Effects on Hydrogen Permeation in Metals.	447-465B 1001-1006A
The Relationship Between Plastic Anisotropy of Steel Sheet and Temper Rolling Strain.	2156-2160A	Massive type transformation Solidification and Phase Equilibria in the Fe—C—Cr—NbC System.	2181-2186A
Characterization of Hot Deformation Behavior of Brasses Using Processing Maps. I. α Brass. Characterization of Hot Deformation Behavior of Brasses	2985-2992A	Massive type transformation, Welding effects Solidification Modeling and Solid-State Transformations in	
Using Processing Maps. II. β Brass and $\alpha-\beta$ Brass. Machinery and equipment	2993-3001A	High-Energy Density Stainless Steel Welds. Materials	915-926A
See Chemical processing equipment		See Ceramics Composite materials	
Macrofractography See Fractography		Construction materials Dissimilar materials	
Magnesium, Binary systems Thermodynamics of Binary Systems Using Interaction Parameters.	593-605B	Granular materials Polymers Refractories	
Magnesium, Reactions (chemical) Dissolution Equilibrium of Magnesium Vapor in Liquid Iron.		Materials testing See High temperature tests	
Magnesium base alloys, Mechanical properties	918-921B	Mechanical tests Nondestructive testing	
High-Damping Metals and Alloys. Creep of Die Cast AZ91 Magnesium at Room Temperature and Low Stress.	607-616A 873-877A	Mathematical analysis See also Numerical analysis	
Magnetic hysteresis See Hysteresis		Statistical analysis A New Experimental Method for Determining Liquid Density and Surface Tension.	27-31B
Magnetohydrodynamic waves See Magnetohydrodynamics		Analysis of an Aluminum Single Crystal With Unstable Initia Orientation (001)[110] in Channel Die Compression.	
Magnetohydrodynamics		Quantitative Assessment of the Implications of Strain- Induced Microstructural Changes in Superplasticity.	83-96A
Magnetohydrodynamic and Thermal Behavior of Electrosia; Remetting Slags.	111-120B	Slag—Metal Reactions During Welding. III. Verification of the Theory.	83-100B
Magnetohydrodynamic Flows in a Channel-Induction Fundame.	193-209B	A Mathematical Model of the Nickel Converter. I. Model De velopment and Verification.	153-161B
Manganese, Extraction Reductive Ammonia Leaching of Manganese Nodules b		Correlation of Geometric Factor for Slag Resistance Electric Furnaces.	183-192B
Thiosulfate. Manganese, Quaternary systems	259-261B	Representation of the Solubility of Lead Chloride in Various Chloride Solutions With Pitzer's Model. Expressions for Predicting the Elasticity Modulus of Materials	491-498B
Thermodynamic Properties of the Fe—Mn—V—C System.	1911-1920A	Reinforced by Second-Phase Grains.	507-511A

	On the Rate of Dendrite Arm Coarsening. Creep of Die Cast AZ91 Magnesium at Room Temperature and Low Stress.	569-574A 873-877A	Simulation of the Effect of Texture on Limit Strain in Biaxially Stretched Steel Sheet.	2069-2076A
	The Effect of the Thermal Path to Reach Isothermal Temperature on Transformation Kinetics.	993-999A	A Simple Theory for the Development of Inhomogeneous Rolling Textures.	2637-2643A
	Modeling Surface Effects on Hydrogen Permeation in Metals. Instantaneous and Residual Stresses Developed in Hot Iso-	1001-1006A	Microstructural Engineering Applied to the Controlled Cool- ing of Steel Wire Rod. I. Experimental Design and Heat Transfer.	2769-2778A
	static Pressing of Metals and Ceramics. On the Role of Elastic Interactions in the Nucleation and	1071-1078A	Microstructural Engineering Applied to the Controlled Cooling of Steel Wire Rod. III. Mathematical Model—	2.00 2.101
	Growth of Ledges. Structural Ledges in Interphase Boundaries.	1159-1164A 1165-1175A	Formulation and Predictions. Coarsening Resistance of M ₂ C Carbides in Secondary Hard-	2791-2805A
	Growth Kinetics of Solid/Liquid Gallium Interfaces. I. Experi- mental. Growth Kinetics of Solid/Liquid Gallium Interfaces. II. Theo-	1259-1270A	ening Steels. I. Theoretical Model for Multicomponent Coarsening Kinetics.	2863-2868A
	retical. The Role of Ledges in Stress Tensor-Mediated Surface Pro-	1271-1286A	The Anisotropic Mechanical Properties of a Titanium Matrix Composite Reinforced With SiC Fibers.	2975-2984A
	cesses for Silicon and GaAs. Correction to On the Rate of Dendrite Arm Coarsening". Earing in Cup Drawing Face-Centered Cubic Single Crystals	1317-1322A 1466A	Solute Distribution During Steady-State Cellular Growth. Third-Order Bounds on the Elastic Moduli of Metal-Matrix Composites.	3035-3039A 3065-3067A
	and Polycrystals. A Theoretical Sensitivity Analysis for Full-Dome Formability	1525-1534A	Mathematics See also Finite element method	
	Tests: Parameter Study for n , m , r , and μ . The Effect of Temperature and Nitrogen Content on the Parti-	1775-1788A	Geometry Mathematical analysis	
	tioning of Alloy Elements in Duplex Stainless Steels. Development of Deformation Instability in Hot Tensile Test	2173-2179A	Mathematical models Statistical methods	
	Specimens. Application of Analytical Techniques to Stress Relaxation Ex-	2297-2302A	Topology Report on Panel Discussion. II. Critical Problems in the Math-	
	periments in Commercial Zinc. On the Constraint Factor Associated With the Indentation of Work-Hardening Materials With a Spherical Ball.	2303-2307A 2375-2384A	ematics of Ledgewise Growth. Matrices (mathematical)	1247-1248A
	The Prediction of Case Depth in Laser Transformation Hard- ening.	2459-2466A	Stress Concentration at a Notch Tip in Unidirectional Metal Matrix Composites.	2085-2095A
N	athematical models		Mattes	
	Fluid Flow Through Lances With Constant and Variable Pitch Swirled Inserts. Heat-Flow Simulation of Laser Remelting With Experimental	13-20B	See also Copper mattes A Mathematical Model of the Nickel Converter. I. Model Development and Verification.	153-161B
	Validation. Magnetohydrodynamic and Thermal Behavior of Electroslag	101-109B	Measurement	155-1015
	Remelting Slags. An Improved Mathematical Model for Electromagnetic Cast-	111-120B	A New Experimental Method for Determining Liquid Density and Surface Tension.	27-31B
	ers and Testing by a Physical Model. A Model for the Strain-Rate Dependence of Yielding in Ni ₃ Al	121-134B	Measuring See Measurement	
	Alloys. Recrystallization of Austenite After Deformation at High Tem-	125-128A	Mechanical alloying	
	peratures and Strain Rates—Analysis and Modeling. Heat-Transfer Phenomena in Water-Cooled Zinc-Fuming Furnace Jackets.	151-160A	Fatigue Crack Propagation and Cryogenic Fracture Tough- ness Behavior in Powder Metallurgy Aluminum—Lithium Alloys.	191-202A
	Effect of Evaporation and Temperature-Dependent Material Properties on Weld Pool Development.	163-175B 233-241B	The Formation of Metastable Phases by Mechanical Alloying in the Aluminum and Copper System.	2849-2854A
	Computational Modeling of Stationary Gas-Tungsten-Arc Weld Pools and Comparison to Stainless Steel 304 Experi-		Anomalous Combustion Effects During Mechanical Alloying. Mechanical hysteresis	3019-3024A
	mental Results. Application of Thermodynamic Models to the Calculation of	243-257B	See Hysteresis	
	Solidification Paths of Aluminum-Rich Al—Li Alloys. The Thermal and Metallurgical State of Steel Strip During Hot Political Characterization of Leat Transfer.	267-271A	Mechanical joining See Bolting	
	Rolling, I. Characterization of Heat Transfer. Modeling Chemical Vapor Deposition of Silicon With Local Equilibrium Consideration at the Substrate.	307-319A 309-321B	Mechanical properties See Compressive properties	
	The Thermal and Metallurgical State of Steel Strip During Hot Rolling. II. Factors Influencing Rolling Loads.	321-333A	Creep (materials) Ductility	
	The Thermal and Metallurgical State of Steel Strip During Hot Rolling. III. Microstructural Evolution.	335-349A	Elastic constants Fracture strength Hardness	
	Correction to "A New Technique for Three-Dimensional Tran- sient Heat Transfer Computations of Autogenous Arc	2000	Impact strength Modulus of rupture	
	Welding". Role of Near-Wall Node Location on the Prediction of Melt	3898	Plasticity Proof stress	
	Flow and Residence Time Distribution in Tundishes by Mathematical Modeling. Modeling and Parametric Studies of Heat Transfer in a Direct-	429-437B	Shock resistance Strain	
	Fired Continuous Reheating Furnace. On the Kinetics of Diffusion-Limited Layer Growth in Solid—	513-521B	Tensile properties Thermoelastic properties	
	Solid Systems. Numerical Simulation of a Solidifying Pb—Sn Alloy: the Ef-	523-527B	Toughness Wear resistance	
	fects of Cooling Rate on Thermosolutal Convection and Macrosegregation.	529-540B	Mechanical tests See also Bend tests	
	Knowledge-Based Simulation and Identification of Various Metallurgical Reactors.	541-555B	Dynamic tests Fatigue tests	
	Modeling of Base Metal Dissolution Behavior During Tran- sient Liquid-Phase Brazing. Representation of Excess Thermodynamic Properties of Ter-	543-555A	Hydrostatic tests Tension tests	
	nary Systems Using Interaction Parameters. Thermodynamics of Binary Systems Using Interaction Pa-	583-591B	A Theoretical Sensitivity Analysis for Full-Dome Formability Tests: Parameter Study for n, m, r, and μ .	1775-1788A
	rameters. Optimization and Continuous Casting, I. Problem Formulation	593-605B	Mechanics See Fracture mechanics	
	and Solution Strategy. Optimization and Continuous Casting. II. Application to In-		Mechanisms See Corrosion mechanisms	
	dustrial Casters. A Degenerate Electron Gas Model for Solutions of Aluminum	649-659B	Medium carbon steels, Casting Interrupted and Isothermal Solidification Studies of Low and	
	in Cryolite Melts. Contribution to the Metal/Mold Interfacial Heat Transfer. Mathematical Modeling of Sulfide Flash Smelting Process. III.	669-672B 729B	Medium Carbon Steels. Medium carbon steels, Chemical analysis	1871-1880A
	Volatilization of Minor Elements. Three-Dimensional Mathematical Model for Transport Phenomena in Horizontal Chemical Vapor Deposition Reactions.		Secondary Ion Mass Spectrometry Method for Distinguishing the State of Carbon in Steels Using Negative Molecular Ions.	1969-1978A
	tors. Simultion of Freckles During Vertical Solidification of Binary	811-822B	Medium carbon steels, Heat treatment	
	Alloys. Mathematical Modeling of the Isothermal Impingement of Liq		The Prediction of Case Depth in Laser Transformation Hard- ening.	2459-2466A
	uid Droplets in Spraying Processes. A Mathematical Method for the Calculation of Ledge Growth Kinetics.	901-914B 1211-1218A	Microstructural Engineering Applied to the Controlled Cool- ing of Steel Wire Rod. I. Experimental Design and Heat Transfer.	2769-2778A
	Carbonitride Precipitate Growth in Titanium/Niobium Microal loyed Steels.		Microstructural Engineering Applied to the Controlled Cooling of Steel Wire Rod. II. Microstructural Evolution and Me	
	Surface Composition of Ternary Cu—Ag—Au Alloys. II. / Comparison of Experiment With Theoretical Models.	1841-1848A	chanical Properties Correlations. Microstructural Engineering Applied to the Controlled Cool	2779-2790A
	Determination of Equilibrium Solid-Phase Transition Temper atures Using DTA.	1993-1998A	ing of Steel Wire Rod. III. Mathematical Model— Formulation and Predictions.	2791-2805A

Medium carbon steels, Mechanical properties Effects of Intercritical Treatment and Tempering on Fracture		Metastable phases, Cooling effects A13-Type Phase Revealed in Rapidly Solidified High-Carbon	
Behavior in a Medium-Carbon 2Si—3Ni Steel.	2587-2596A	Iron Alloy. Solidification of Undercooled Sn—Sb Peritectic Alloys. I.	251-253A
See also Electric arc meiting		Microstructural Evolution.	753-764A
Induction melting Heat-Flow Simulation of Laser Remelting With Experimental Validation.	101-109B	Metastable phases, Heating effects Elastic Moduli and Tensile and Physical Properties of Heat- Treated and Quenched Powder Metallurgical Ti—6Al—4V	709-714A
Memory (shape)		Alloy. Structures and Tempering Behavior of Rapidly Solidified	775-782A
See Shape memory Matal carbides		High-Carbon Iron Alloys. Correction to "Elastic Moduli and Tensile and Physical Prop-	113-102A
See also Iron carbides Titanium carbide		erties of Heat-Treated and Quenched Powder Metallurgical Ti—6AI—4V Alloy".	1129A
Vanadium carbide Chemical Potential Diagram of Al—Ti—C System: Al ₄ C ₃ Formation on TiC Formed in Al—Ti Liquids Containing Carbon.	3075-3076A	Metastable phases, Stress effects Coherent Phase Equilibrium in Alloys With Congruent Points.	1921-1935A
Metal fibers, Composite materials Processing and Creep Characterization of a Model Metal Ma-	0013-0010A	Metathesis See Decomposition reactions	
trix Composite: Lead Reinforced With Nickel Fibers.	1029-1036A	Metering (measurement) See Measurement	
Metal filements See Metal fibers		MHD See Magnetohydrodynamics	
Metal powders See also Carbonyl powders		Microalloyed steels	
Metal powders, Microstructure		See High strength low alloy steels Microalloying	
Powder Metallurgy T15 Tool Steel. I. Characterization of Powder and Hot Isostatically Pressed Material.	2733-2745A	Recrystallization Controlled Rolling and Accelerated Cooling for High Strength and Toughness in V—Ti—N Steels.	2681-2694A
Metal powders, Phases (state of matter) The Formation of Metastable Phases by Mechanical Alloying in the Aluminum and Copper System.	2849-2854A	Microanalysis X-Ray Microanalysis of Phosphorus Segregation in Type 304L Stainless Steels.	253-255A
Metal powders, Reactions (chemical) The Effect of Reaction Condition on Composition and Proper-		Microbial leaching	
ties of Ultrafine Amorphous Powders in (Fe,Co,Ni)—B Systems Prepared by Chemical Reduction.	2125-2132A	See Bacterial leaching Microcracking	
Metal powders, Surface properties		See Crack initiation	
Ultrasound Treatment of Centrifugally Atomized 316 Stain- less Steel Powders.	3025-3033A	Microfractography See Fractography	
Metal scrap See also Steel scrap		Microhardness Shock Densification/Hot Isostatic Pressing of Titanium Alumi-	
Metal scrap, Recovering		nide.	2667-2676A
The Dissolution Behavior of Metals From Ag/Cu and Ag/Au Alloys in Aidic and Cyanide Solutions. Metal working	755-764B	Microhardness, Heating effects Effect of Reinforcement on the Aging Response of Cast 6061 AI—Al ₂ O ₃ Particulate Composites.	2553-2563A
See Cold working Hot working		Microporosity, Cooling effects Solidification Microporosity in Directionally Solidified Multi-	
Thermomechanical treatment		component Nickel Aluminide.	225-234A
Metallic compounds See Intermetallics		Microscopy See also Electron microscopy Use of Differential Interference Contrast Microscopy to De-	
Metallic glasses, Atomic properties Atomic Structure of the Crystalline/Amorphous Interface in a Directionally Crystallized Pd ₈₀ Si ₂₀ Alloy.	1287-1298A	tect Duplex Carbides in Alloy White Cast Irons. Microstructure Control Carbon Structure	1673-1674A
Metallographic structures See Microstructure		See also Crystal structure Dislocation density Fibrous structure	
Metallography See Crystallography		Grain size Grain structure	
Specimen preparation		Graphitic structure Heterogeneous structure	
Metalloid alloys See Germanium base alloys		Lamellar structure Orientation	
Metalloid compounds See Boron compounds		Texture Interrupted and Isothermal Solidification Studies of Low and Medium Carbon Steels.	1871-1880A
Germanium compounds Silicon compounds		Microstructure, Alloying effects	
Metalloids See Arsenic		The Effects of Chromium Additions to Binary TiAl-Base Alloys.	2619-2626A
Boron Carbon		The Effect of Copper, Chromium, and Zirconium on the Mi- crostructive and Mechanical Properties of Al—Zn—Mg—	2809-2818A
Germanium Silicon		Cu Alloys. Microstructure, Cooling effects	2009-2018A
Metallurgical enalysis See Microanalysis		Microstructural Engineering Applied to the Controlled Cooling of Steel Wire Rod. I. Experimental Design and Heat Transfer.	2769-2778A
Phase ratio Metallurgical constituents		Microstructural Engineering Applied to the Controlled Cool- ing of Steel Wire Rod. II. Microstructural Evolution and Me- chanical Properties Correlations.	2779-2790A
See Laves phase Metallurgy		Microstructural Engineering Applied to the Controlled Cooling of Steel Wire Rod. III. Mathematical Model	
See Physical metallurgy Powder metallurgy		Formulation and Predictions. Microstructure, Welding effects	2791-2805A
Metals See FCC metals		Effect of Killing Time on the Microstructure and Toughness of the Heat-Affected Zone in Titanium-Killed Steels.	2818-2822A
Filler metal HCP metals Liquid metals		Carbide Precipitation in Welds of Two-Phase Austenitic— Ferritic Stainless Steel.	2889-2902A
Metastable phases		Migration See Diffusion	
Microstructural Evolution in Rapidly Solidified Al—Fe Alloys an Alternative Explanation.	927-934A	Motion	
Nonequilibrium Behavior in the Al—Ge Alloy Systems: in sights Into the Metastable Phase Diagram.	2141-2152A	Mild carbon steels See Low carbon steels	
The Formation of Metastable Phases by Mechanical Alloying in the Aluminum and Copper System.	2849-2854A	Mild steels See Carbon steels	
Metastable phases, Alloying effects Effect of Phosphorus on Carbon Activity, Carbide Precipita		Mixing	
tion, and Coarsening in Ferritic Fe—C—P Alloys. Ductility Enhancement in NiAl (B2)-Base Alloys b	35-43A	See Mechanical alloying Mobility	
Microstructural Control.	441-446A	See Dislocation mobility	

1

Modulus of elasticity Mechanical, Elastic, and Structural Properties of Alloys of	100 1074	Motor vehicle engines See Automotive engines	
Ru—Ta High-Temperature Intermetallic Compounds. Expressions for Predicting the Elasticity Modulus of Materials Reinforced by Second-Phase Grains.	129-137A 507-511A	Moulds See Molds	
On the Influence of Ply-Angle on Damping and Modulus of Elasticity of a Metal-Matrix Composite.	641-651A	Movement See Motion	
Stress Concentration at a Notch Tip in Unidirectional Metal	2085-2095A	See Motion Moving	
On the Constraint Factor Associated With the Indentation of Work-Hardening Materials With a Spherical Ball.	2375-2384A	See Motion Multilavers	
Structure and Properties of a Rapidly Solidified Al—Li— Mn—Zr Alloy for High-Temperature Applications. I. Inert Gas Atomization Processing.	2503-2514A	Effect of Plastic Deformation on Residual Stresses in Ceramic/Metal Interfaces.	2822-2825A
Modulus of elasticity, Heating effects Elastic Moduli and Tensile and Physical Properties of Heat- Treated and Quenched Powder Metallurgical Ti—6AI—4V Alloy.	700 7444	Multilayers, Diffusion Intermetallic Phase Formation and Breakdown of Molybde- num Diffusion Barriers in Ni—Mo—Cu Layers.	1501-1510A
Correction to "Elastic Moduli and Tensile and Physical Prop- erties of Heat-Treated and Quenched Powder Metallurgical	709-714A	Natural aging See Aging (natural) Necking	
Ti—6AI—4V Alloy". Modulus of rigidity See Shear modulus	1129A	Development of Deformation Instability in Hot Tensile Test Specimens.	2297-2302A
Modulus of rupture On the Influence of Ply-Angle on Damping and Modulus of		Necking, Microstructural effects Simulation of the Effect of Texture on Limit Strain in Biaxially Stretched Steel Sheet.	2069-2076A
Elasticity of a Metal-Matrix Composite. Modulus of shear See Shear modulus	641-651A	Neutral atmospheres See Inert atmospheres	
Modulus of torsion		Nickel, Binary systems Activities of Boron in the Binary Ni—B and the Ternary Co—	
See Shear modulus Moistening		Fe—B Melts. Thermodynamics of Binary Systems Using Interaction Pa-	47-52B
See Wetting Mold fluxes		rameters. Coherent Phase Equilibrium in Alloys With Congruent Points.	593-605B 1921-1935A
Monitoring of Slag Composition Changes by Density Measurements. Moids	305-307B	Nickel, Bonding Microstructural Development in Transient Liquid-Phase Bonding.	2451-2457A
Mold Behavior and Its Influence on Quality in the Continuous Casting of Steel Slabs. I. Industrial Trials, Mold Tempera-		Nickel, Brazing Modeling of Base Metal Dissolution Behavior During Tran-	
ture Measurements, and Mathematical Modeling. Mold Behavior and its Influence on Quality in the Continuous Casting of Steel Slabs. II. Mold Heat Transfer, Mold Flux	861-874B	sient Liquid-Phase Brazing. Effect of Grain Boundaries on Isothermal Solidification During Transient Liquid Phase Brazing.	543-555A 1627-1631A
Behavior, Formation of Oscillation Marks, Longitudinal Off- Corner Depressions, and Subsurface Cracks. Molten metals	875-888B	Nickel, Coating Chemical Vapor Deposition Kinetics of Tungsten From WCl ₆ Onto Nickel Plate at Elevated Temperatures.	560-563B
See Liquid metals Molten salts		Nickel, Composite materials	
See Fused salts		Processing and Creep Characterization of a Model Metal Ma- trix Composite: Lead Reinforced With Nickel Fibers.	1029-1036A
Molybdenum, Alloying elements Solidification Microporosity in Directionally Solidified Multi- component Nickel Aluminide.	225-234A	Nickel, Diffusion Intermetallic Phase Formation and Breakdown of Molybde- num Diffusion Barriers in Ni—Mo—Cu Layers.	1501-1510A
Molybdenum, Binary systems The Al—Al ₈ Mo ₃ Section of the Binary System Aluminum— Molybdenum.	1729-1736A	Nickel, Extraction A Mathematical Model of the Nickel Converter. I. Model Development and Verification.	153-161B
Molybdenum, Diffusion Intermetallic Phase Formation and Breakdown of Molybdenum Diffusion Barriers in Ni—Mo—Cu Layers.	1501-1510A	Nickel, Heat treatment Influence of Cyclic Deformation on Surface Microstructure and Hardness of Ion-Implanted Nickel.	1633-1646A
Molybdenum, Joining Effect of Plastic Deformation on Residual Stresses in Ceramic/Metal Interfaces.	2822-2825A	Nickel, Mechanical properties Analysis of Crack Tip Sliding Displacement in Anisotropic Elastic Media and Its Application to Stage I Fatigue Crack	
Molybdenum, Solubility Thermochemistry and Diffusion of Nitrogen in Solid Molybde- num.	219-224B	Growth. Nickel, Oxidation Interface Dislocations and Ledges in Oxidation and Diffu-	479-487A
Molybdenum chromium nickel steels See Nickel chromium molybdenum steels		sional Phase Transformations. Nickel, Powder technology	1331-1339A
Molybdenum chromium steels See Chromium molybdenum steels		The Effect of Reaction Condition on Composition and Properties of Ultrafine Amorphous Powders in (Fe,Co,Ni)—B Systems Prepared by Chemical Reduction.	2125-2132A
Molybdenum compounds, Mechanical properties Ductilization of Ni—Ni ₄ Mo Alloys by Boron Additions.	3067-3071A	Nickel, Quaternary systems A Thermodynamic Assessment of the Fe—Cr—Ni—C Sys-	
Molybdenum nickel chromium steels See Nickel chromium molybdenum steels		tem. Nickel, Recovering	2187-2198A
Molybdenum steels See also Chromium molybdenum steels		Leaching of Nickel From Supported Nickel Waste Catalyst Using Aqueous Sulfur Dioxide Solution.	775-781B
Molybdenum steels, Metal working Effects of Vanadium and Processing Parameters on the Structures and Properties of a Direct-Quenched Low- Carbon Mo—B Steel.	2359-2374A	Nickel, Ternary systems Representation of Excess Thermodynamic Properties of Ternary Systems Using Interaction Parameters.	583-591B
Molybdenum steels, Structural hardening Comparison of Secondary Hardening Embrittlement in Tungsten and Molybdenum Steels.	1119-1122A	Nickel base alloys, Corrosion Grain Boundary Diffusion of Hydrogen in Nickel. Intergranular Stress Corrosion Cracking of Alloy 600 and X- 750 in High-Temperature Deaerated Water/Steam.	351-355A 1857-1864A
Monel See Nickel base alloys		Nickel base alloys, Crystal growth Measurements of Rapid Solidification Rate in Highly Under-	
Monitoring Monitoring of Slag Composition Changes by Density Mea-		cooled Melts With a Video System. Nickel base alloys, Mechanical properties	2020-2020A
surements. Transformation of Retained Austenite in Carburized 4320 Steel. Fracture Initiation at Hydrides in Zirconium.	305-307B 1491-1500A 2327-2337A	Quantitative Assessment of the Implications of Strain- Induced Microstructural Changes in Superplasticity. Analysis of Crack Tip Silding Displacement in Anisotropic Elastic Media and Its Application to Stage I Fatigue Crack	83-96A
Monocrystals	2021-2031A	Growth. Low-Cycle Fatigue Behavior of Nimonic PE16 at Room Tem-	479-487A
See Śingle crystals		perature.	499-506A
Motion		Fracture of Single Crystals of the Nickel-Base Superalloy	

A

The Role of the γ/γ' Eutectic and Porosity on the Tensile Behavior of a Single-Crystal Nickel-Base Superalloy. Development of a Necklace Microstructure During Isothermal Deformation and its Properties Relative to Uniform Micro-	1443-1451A	Coarsening Resistance of M ₂ C Carbides in Secondary Hard- ening Steels. III. Comparison of Theory and Experiment. Niobium, Alloying elements	2877-2888A
structures. Fracture of Single Crystals of the Nickel-Base Superalloy	1999-2008A	Effect of Hydrogen as a Temporary β Stabilizer on Micro- structure and Brittle Fracture Behavior in a Titanium Alumi-	74.044
PWA 1480E in Hydrogen at 22°C. Hydrogen Effects on Low-Cycle Fatigue of the Single-Crystal	2031-2038A	nide Alloy. The Initiation and Growth of Fatigue Cracks in a Titanium Al-	71-81A
Nickel-Base Superalloy CMSX-2. Ductilization of Ni—Ni ₄ Mo Alloys by Boron Additions.	2597-2603A 3067-3071A	uminide Alloy. The Mass Transfer Kinetics of Niobium Solution Into Liquid Steel.	377-391A 417-427B
Nickel base alloys, Melting Magnetohydrodynamic and Thermal Behavior of Electroslag Remelting Slags.	111-120B	Dynamic Compaction of Titanium Aluminides by Explosively Generated Shock Waves: Experimental and Materials Systems.	685-695A
Nickel base alloys, Microstructure The Mechanisms and Temperature Dependence of Superlat- tice Stacking Fault Formation in the Single-Crystal Superal-		Microstructural Effects on Ambient and Elevated Tempera- ture Fatigue Crack Growth in Titanium Aluminide Intermet- allics.	817-828A
loy PWA 1480. Nickel base alloys, Oxidation On the Role of Yttrium During High-Temperature Oxidation of	2309-2318A	Microstructural Evolution of Modified 9Cr—1Mo Steel. Carbonitride Precipitate Growth in Titanium/Niobium Microal- loyed Steels. Solidification and Phase Equilibria in the Fe—C—Cr—NbC	1049-1058A 1511-1524A
an Ni—Cr—Al—Fe—Y Alloy. Nickel base alloys, Surface properties	1463-1465A	System.	2181-2186A
Effect of Sulfur Removal on Al ₂ O ₃ Scale Adhesion. Nickel base alloys, Welding	739-752A	Niobium, Binary systems Thermodynamic Stability of Palladium Alloys. I. The Palladium—Niobium System.	1937-1943A
The Relationship Between Carbon Content, Microstructure, and Intergranular Liquation Cracking in Cast Nickel Alloy 718.	557-567A	Niobium, Solubility Correction to "Nitrogen Solubility in Solid Niobium".	142B
A Phase Diagram Approach to Study Liquation Cracking in Alloy 718.	887-902A	Niobium base alloys, Phases (state of matter) Containerless Processing and Rapid Solidification of Nb—Si	
Nickel chromium molybdenum steels, Mechanical properties		Alloys in the Niobium-Rich Eutectic Range. Containerless Processing and Rapid Solidification of Nb—Si	2713-2721A
Material Effects in Fretting Wear: Application to Iron, Tita- nium, and Aluminum Alloys.	1535-1544A	Alloys of Hypereutectic Composition. Niobium compounds, Composite materials	2723-2732A
In Situ Fracture Observations on Tempered Martensite Em- brittlement in an AISI 4340 Steel.	1889-1892A	Preliminary Studies on NiAl/Nb ₂ Be ₁₇ Reaction and Effectiveness of BeO as an Interfacial Reaction Barrier.	2535-2538A
Nickel chromium molybdenum steels, Metal working Low-Temperature Improvement of Mechanical Properties of AISI 4340 Steel Through High-Temperature Thermome- chanical Treatment.	1093-1102A	Niobium compounds, Metal working Strength and Ductile-Phase Toughening in the Two-Phase Nb/Nb ₆ Si ₃ Alloys.	1573-1583A
Nickel chromium molybdenum steels, Phase transformations		Niobium compounds, Metallography Electron Microscopy of Transformation Dislocations at Inter-	114E 11E0A
Transformation of Retained Austenite in Carburized 4320 Steel.	1491-1500A	phase Boundaries. Niobium compounds, Phases (state of matter)	1145-1158A
Nickel chromium molybdenum steels, Structural hardening On the Constraint Factor Associated With the Indentation of		A New Phase in a Rapidly Solidified and Consolidated NbAl ₃ —1TiB ₂ Alloy.	1901-1909A
Work-Hardening Materials With a Spherical Ball. Nickel chromium steels	2375-2384A	Nitrides See Silicon nitride	
See also Nickel chromium molybdenum steels		Nitrogen, Alloying additive Recrystallization Controlled Rolling and Accelerated Cooling for High Strength and Toughness in V—Ti—N Steels.	2681-2694A
Nickel chromium steels, Steel making Gibbs Energy of Formation of Nickel Chromite.	673-675B	Nitrogen, Solubility	
Nickel chromium steels, Welding Slag—Metal Reactions During Welding. I. Evaluation and Re- assessment of Existing Theories.	65-71B	Correction to "Nitrogen Solubility in Solid Niobium". Thermochemistry and Diffusion of Nitrogen in Solid Molybdenum.	142B 219-224B
Nickel compounds, Composite materials NiAl-Based Microstructurally Toughened Composites.	183-189A	Nitrogen compounds See Ammonia	
Preliminary Studies on NiAI/Nb ₂ Be ₁₇ Reaction and Effective- ness of BeO as an Interfacial Reaction Barrier. Interfaces in XD Processed TiB ₂ /NiAI Composites.	2535-2538A 3013-3018A	Nodular graphitic structure Fracture Toughness and Crack Growth Rate of Ferritic and	0045 00504
Pressure Casting of a Zirconia-Toughened Alumian Fiber- Reinforced NiAl Composite.	3059-3064A	Pearlitic Compacted Graphite Cast Irons at 25 and 150°C. Nodular iron, Mechanical properties	2645-2653A
Nickel compounds, Directional solidification Solidification Microporosity in Directionally Solidified Multi- component Nickel Aluminide.	225-234A	Fracture Toughness and Crack Growth Rate of Ferritic and Pearlitic Compacted Graphite Cast Irons at 25 and 150°C.	2645-2653A
Nickel compounds, Mechanical properties A Model for the Strain-Rate Dependence of Yielding in Ni ₃ Al	ELO LOVA	Nodules (graphite) See Nodular graphitic structure	
Alloys. Ductility Enhancement in NiAl (B2)-Base Alloys by	125-128A	Noise control Thermal and Mechanical Considerations in Using Shape Memory Alloys to Control Vibrations in Flexible Structures.	623-627A
Microstructural Control. 1000 to 1200K Time-Dependent Compressive Deformation of	441-446A	Development of Vibration-Damping Resins for Room- Temperature Application.	629-631A
Single-Crystalline and Polycrystalline B2 Ni—40Al. Grain Boundary Pest of Boron-Doped Ni ₉ Al at 1200°C. A Simple, Versatile Miniaturized Disk-Bend Test Apparatus	1595-1607A 1801-1809A	Chlorosulfonated Polyethylene: a Versatile Polymer for Damping Acoustic Waves.	633-640A
for Quantitative Yield-Stress Measurements. Ductilization of Ni—Ni ₄ Mo Alloys by Boron Additions.	2061-2068A 3067-3071A	Vibration Damping Characteristics of Laminated Steel Sheet. Nondestructive testing	653-656A
Nickel compounds, Metallography Electron Microscopy of Transformation Dislocations at Interphase Boundaries.	1145-1158A	See also Acoustic emission testing The Evaluation of In-Service Materials Degradation of Low- Alloy Steels by the Electrochemical Method.	2097-2106A
Nickel compounds, Phases (state of matter) An Investigation of Fe—Ni Order in a Steel.	2807-2809A	Nonferrous alloys See Cobalt base alloys	
Nickel molybdenum chromium steels See Nickel chromium molybdenum steels	2007-2009A	Manganese base alloys Nickel base alloys Scandium base alloys	
Nickel molybdenum steels		Yttrium base alloys Zinc base alloys	
See Nickel chromium molybdenum steels Nickel steels		Zirconium base alloys Nonferrous metals	
See also Nickel chromium steels Nickel steels, Mechanical properties		See Cobalt Copper	
Comparison of Fracture Behavior in Intercritically Treated Medium-Carbon Nickel and Silicon Steels.	1115-1119A	Gallium Indium	
Nickel steels, Structural hardening Coarsening Resistance of M ₂ C Carbides in Secondary Hard-		Manganese Nickel Yttrium	
ening Steels. I. Theoretical Model for Multicomponent Coarsening Kinetics.	2863-2868A	Zinc	
Coarsening Resistance of M ₂ C Carbides in Secondary Hard- ening Steels. II. Alloy Design Aided by a Thermochemical	and a count	Zirconium Nonferrous smelting	
Database.	2869-2876A	See Smelting	

In Stut Observation of Interactions Between Cascous Inclusions and shark-accept Selection between Cascous Inclusions and shark-accept Selection between Cascous Inclusions and Carterians and Cascous Included Properties of Two Commercials (2017) and Accept Selection (2017) and Accept	Namedalla inclusione		Acchaig of an Aluminum Cinate Constal With Heatable Indial	
Sign Estuations. Sign Estuations. Sign Estuations. Sign Estuations. Proclased betase of HY180 Seat Deliron in active hyper. Proclased betase of HY180 Seat Deliron in Estuation (2017) Proclased betase of HY180 Seat Deliron in Estuation (2017) Proclased Seat on HY180 Seat Deliron in Acquiring in Seat Seat Seat Seat Seat Seat Seat Seat	sions and an Advancing Solid/Liquid Interface.	385-388B	Fracture of Single Crystals of the Nickel-Base Superalloy	
Produced Heats of HYTMS Seed Differing in Suitified Type. The Fig. 19 Produced Heats of HYTMS Seed Differing in Suitified Type. The Fig. 19 Produced Heats of HYTMS Seed Differing in Suitified Type. Effect of Suiting Films on the Meconstruction and Cognitions of Mechanical Education Construction and Cognitions. See Hythogone Mechanical Education Committee Seed Seed Not American Constitution of Hythogone Administration of Hythogone Administrati	Steel Extrusions.	807-815A	Earing in Cup Drawing Face-Centered Cubic Single Crystals	
The Crigin of Transformation Technics in Steal Week Metals Effect of King from on the Microstructura and Toughness of See Hydrogen and Transmiss Medie Steals. See Hydrogen S	Produced Heats of HY180 Steel Differing in Sulfide Type.	2277-2285A		1020-1034A
Nomestais See Hydrogen Mich Austility Notch See Notch Austility Notch See Notch Austility Notch See Notch Austility Notch Basel Related With Aluminum- Base See Toron of Phil 5-Mox Seel Plated With Aluminum- Base See Toron of Phil 5-Mox Seel Plated With Aluminum- Base See Toron of Phil 5-Mox Seel Plated With Aluminum- Base See Toron of Phil 5-Mox Seel Plated With Aluminum- Base See Toron of Phil 5-Mox Seel Plated With Aluminum- Base See Toron of Phil 5-Mox Seel Plated With Aluminum- Base See Toron of Phil 5-Mox Seel Plated With Aluminum- Base See Toron of Phil 5-Mox Seel Plated With Aluminum- Base See Toron of Phil 5-Mox Seel Plated With Aluminum- Base See Toron of Phil 5-Mox Seel Plated With Aluminum- Base See Toron of Phil 5-Mox Seel Plated With Aluminum- Base See Toron of Phil 5-Mox Seel Plated With Aluminum- Base Seel Toron of Phil 5-Mox Seel Plated With Aluminum- Base See Toron of Phil 5-Mox Seel Plated With Aluminum- Base See Toron of Phil 5-Mox Seel Plated With Aluminum- Base See Toron of Phil 5-Mox Seel Plated With Aluminum- Base See Toron of Phil 5-Mox Seel Plated With Aluminum- Base See Toron of Phil 5-Mox Seel Plated With Aluminum- Base See Toron of Phil 5-Mox Seel Plated With Aluminum- Base See Toron of Phil 5-Mox Seel Plated With Aluminum- Base See Toron of Phil 5-Mox Seel Plated With Aluminum- Base See Toron of Phil 5-Mox Seel Plated With Aluminum- Base See Toron of Phil 5-Mox Seel Plated With Aluminum- Base See Toron of Phil 5-Mox Seel Plated With Aluminum- Base See Toron of Phil 5-Mox Seel Plated With Aluminum- Base See Toron of Phil 5-Mox Seel Plated With Aluminum- Base See Toron of Phil 5-Mox Seel Plated With Aluminum- Base See Toron of Phil 5-Mox Seel Plated With Aluminum- Base Seel Toron of Phil 5-Mox Seel Plated With Aluminum- Base See Toro	for High Strength and Toughness in V—Ti—N Steels.	2681-2694A	The Origin of Transformation Textures in Steel Weld Metals	657-663A
Notes described by See Ductinity See Ductinity See Ductinity Notch effect See Notch sensitivity Notch area strength Notch area strength Notch area strength Notch area strength Notch analysis	the Heat-Affected Zone in Titanium-Killed Steels.	2818-2822A	Nonequilibrium Austenite/e-Phase Eutectic Revealed in Rap-	
Notch effect de Notch Academy (1997) The Mechanical Behavior of a Hybrid Metal Matrix Composition (1997) The Mechanical Behavior of a Hybrid Metal Matrix Composition (1997) The Mechanical Behavior of a Hybrid Metal Matrix Composition (1997) The Mechanical Behavior of a Hybrid Metal Matrix Composition (1997) The Mechanical Behavior of a Hybrid Metal Matrix Composition (1997) The Mechanical Behavior of a Hybrid Metal Matrix Composition (1997) The Mechanical Behavior of Philademy (1997) The Mechanical Behavior of Hybrid Metal Matrix Composition (1997) The Mechanical Behavior of Hybrid Metal Matrix Composition (1997) The Mechanical Behavior of Hybrid Metal Matrix Composition (1997) The Mechanical Behavior of Philademy (1997) The Mechanical Behavior of Physical Metal Matrix Composition (1997) The Mechanical Behavior of Physical Metal Matrix Composition (1997) The Mechanical Physical Metal Matrix Composition (1997) The Mechanical Physical Metal Matrix Composition (1997) The Mechanical Metal Matrix Composition (1997) The Mechanical Physical Metal Matrix Composition (1997) The State of Longition of Physical Metal Matrix Composition (1997) The State of Longition (1997) The Mechanical Metal Matrix Composition (1997) The State of Longition (1997) The Mechanical Metal Matrix Composition (1997) The Mechanical Metal Metal Metal Matrix (1997) The Mechanical Metal M			Effect of Processing Variables on Texture and Texture Gradi-	
Note Note harmorphisms of a hybrid Matal Marix Composed Planethracial Bahavior of a hybrid Matal Marix Composed The Mechanical Bahavior of a hybrid Matal Marix Composed The Mechanical Bahavior of a hybrid Matal Marix Composed The Mechanical Bahavior of a hybrid Matal Marix Composed The Mechanical Bahavior of a hybrid Matal Marix Composed The Mechanical Bahavior of a hybrid Matal Marix Composed The Mechanical Bahavior of a hybrid Matal Marix Composed The Mechanical Properties of a Direct-Gusended Lovaction Mechanical Properties of a Direct-Gusended Lovaction Mechanical Properties of a Direct-Gusended Lovaction Mechanical Properties of Mech	Notch ductility		Effects of Transformation on Texture and Iodine Stress Cor-	
Notch ingact strength See injoined strength Notch insugation Behavior of a Hybrid Metal Matrix Composition Institutional Behavior of a Hybrid Metal Matrix Composition Institutional Behavior of a Hybrid Metal Matrix Composition Institutional Behavior of a Hybrid Metal Matrix Composition Institution and Processing Parameters on the Structures and Proparties of a Direct-Quenched Low Structures and Proparties of a Direct-Quenched Low Notich toughness, Coaling effects Effects of Vanadium and Processing Parameters on the Structures and Proparties of a Direct-Quenched Low Notiched bard tests See Tension lests Notiched bard tests See Tension lests Notiched Caroling Selevior of zor-Activation Marteratics Sor's Resident Stream Nuclear reactors, Materials satection Nuclear reactors components, Mechanical proparties for Quentities Yield-Stream Aground Nuclear reactor components, Mechanical proparties for Quentities Yield-Stream Aground Nuclear reactors See Nicides Institute Yield-Stream Aground Nuclear reactors Nuclearies Nucleari	•		Influence of Initial Ingot Breakdown on the Microstructural	
See impact stereging Notch searchists Notch searchists Notch suppress, Coating effects Delayed Failure of PH15-8Mo Steel Plated With Aluminum- IVD. Notch toughness, Coating effects Delayed Failure of PH15-8Mo Steel Plated With Aluminum- IVD. Notch toughness, Coating effects Delayed Failure of PH15-8Mo Steel Plated With Aluminum- IVD. Notch toughness, Coating effects Structures and Proporties of a Direct-Quenched Low- Carbon Mo—B Steel. Notched bar tensile leaf See Fernion tests Notched are tensile isets Note Fernion tests Notched are tensile isets See Rocking Function of Coatine Season of Season (Logge in Coatine) and 1895-1896 Note are sector components, Mechanical properties A simple, versale Minimitarized Dela-Searof Test Apparatus for Cuantitative Yield-Stress Measurements. Note Rocking Function of Coatine Season (Logge in Coatine) Note Rocking Function of Coatine Season (Logge in Coatine) Note Rocking Function of Coatine Season (Logge in Coatine) Note Rocking Function of Coatine Season (Logge in Coatine) Note Rocking Function of Coatine Season (Logge in Coatine) Note Rocking Function of Coatine Season (Logge in Coatine) Note Rocking Function of Coatine Season (Logge in Coatine) Note Rocking Function of Coatine Season (Logge in Coatine) Note Rocking Function of Coatine Season (Logge in Coatine) Note Rocking Function of Coatine Season (Logge in Coatine) Note Rocking Function of Coatine Season (Logge in Coatine) Note Rocking Function of Coatine Season (Logge in Coatine) Note Rocking Function of Coatine Season (Logge in Coatine) Note Rocking Function of Coatine Season (Logge in Coatine) Note Rocking Function of Coatine Season (Logge in Coatine) Note Rocking Function of Coatine Season (Logge in Coatine) Note Rocking Function of Coatine Season (Logge in Coatine) Note Rocking Function of Coatine Season	See Notch sensitivity		Interfaces in XD Processed TiB ₂ /NiAl Composites.	
Notch toughness, Costing effects Delayor Fallward or PH15-8No Steel Plated With Aluminum- British toughness, Costing effects Delayor Fallward or PH15-8No Steel Plated With Aluminum- British toughness, Delayoration effects Effects of Vendation and Properties of a Direct-Quenched Low- Curbon Mc-Bissel. Notch Bughness, Delayoration of the Size of Steel Steel Plate of Steel Stee			The High-Temperature Work Function Behavior of Polycrys-	
In the Mich toughness, Coating effects Deligned Failure of PHIS-8MO Steel Plated With Aluminum Noth toughness, Deformation effects Effects of Vanadium and Processing Parameters on the Structures and Properties of a Direct-Quenched Low Noth toughness, Deformation effects Effects of Vanadium and Processing Parameters on the Structures and Properties of a Direct-Quenched Low Nothod bar tenalie tests Nothad band test See B	Notch sensitivity The Mechanical Behavior of a Hybrid Metal Matrix Compos-		Outgassing	1609-1613A
Notch toughness, Deformation effects Effects of Variadium and Processing Parameters on the Structures and Struc	ite.	2107-2117A	Discussion of "Evidence for the Existence of Potassium Bub-	2153-2156A
Notche Date Transition reactors. Materials selection The Effect of Original France of Dischards and Diffusion Residence of Transition Residence of Tra	Delayed Failure of PH13-8Mo Steel Plated With Aluminum-	0005 00454	Oxidation	
Effects of Vanadium and Processing Parameters on the Structures and Properties of a Direct-Guenched Love 2559-2374A Notched bart tensile test 580 Tanison netsts 580		2935-2945A	Pyrite in the Presence of Bacteria.	765-774B
Carbon Mo—B Steel. Notchade bare tensale test See Tension tests Note and tensale test See Bend tests See See Alministic Seed on Carbon Depotition on Femal Effect of Salidar Bend on Alpha Seed Seed Seed Seed Seed Seed Seed See	Effects of Vanadium and Processing Parameters on the		sional Phase Transformations.	
Notched bart dead Notched bend text Notched bend	Carbon Mo—B Steel.	2359-2374A		1003-1003A
Notched bend test See Bend test See Bend test See Bend test rests. Nuclear reactor fungsten on Dislocation Recovery and Precipitation Behavior of Low-Activation Materians SC Steels. Nuclear reactor components, Oxorabin Delisyed Pydriad Cracing behavior in Zorabiny-Zubing. Nuclear reactor components, Mechanical properties for Quantitative Yield-Stress Measurements. Nuclear reactors See Nuclear reactors See Nuclear fusion reactors Nucleation of Elastic Interactions in the Nucleation and On the Ries of Elastic Interactions in the Nucleation and On the Ries of Elastic Interactions in the Nucleation and On the Ries of Elastic Interactions in the Nucleation and On the Ries of Elastic Interactions in the Nucleation and On the Ries of Elastic Interactions in the Nucleation. Modeling of Cystall Coverh During Rapid Solidification. Nucleation, Cooling effects Solidification of Undersocold Sn—Sb Pertitectic Alloys. II. Heterogeneous Nucleation. See Nuclearino In Undersocold Sn—Sb Pertitectic Alloys. II. Heterogeneous Nucleation. See Nucleation Colling of Mecta The Effect of Plastic Deformation of Fallow. Nucleation of Undersocold Sn—Sb Pertitectic Alloys. II. Pathogeneous Nucleation. See Nucleation. See Nucleation. Delivation-Controlled Kink Moling of Plastic Biometria of See Oxide Solidification of Undersocold Sn—Sb Pertitectic Alloys. II. See Nucleation. Delivation-Controlled Kink Moling of Plastic Biometria of See Oxide Solidification of Undersocold Sn—Sb Pertitectic Alloys. II. 19-23A Nucleation. Delivation of Control Reliability of Palladium Alloys II. 19-23A Nucleation. Delivation of Control Reliability of Palladium Alloys II. 19-23A Nucleation. Delivation of Solidification in Liquid Oropetes. 10 quenching See Oxide Good Solidification in Liquid Oropetes. 2867-2804. Nucleation. Delivation of Solidification in Liquid Oropetes. 287-2804. Nucleation of Solidification in Liquid Oropetes. 287-2804. Nucleation of Solidification in Liquid Oropetes. 288-2804. See Solidification in Liquid Oropetes. 287-2804. Nucleation			On the Role of Yttrium During High-Temperature Oxidation of	1463-1465A
Nuclear fuelor meactors. Materials selection The Effect of Tungsten on Disocation Recovery and Precipitation Behavior of Low-Activation Materials by States. Nuclear reactors As Imple, Vertails Ministurized Disk-Bend Test Apparatus for Quantitative Yield-Stress Measurements. Nuclear reactors See Nuclear reactors See Nuclear reactors Nucleation of Al ₂ Cut. (Tr.) Nucleation and Growth. Mechanical properties of States in the Nucleation and Growth of Ladges. The Robo of Ladges in Stress Pensor-Mediated Surface Processes for Stilicon and GaAs. The Robo of Ladges in Stress Tensor-Mediated Surface Processes for Stilicon and GaAs. Nucleation of Solidification in Liquid Droplets. Nucleation of Solidification in Liquid Droplets. Nucleation, Octoring effects Thermodynamic Consideration of Grain Refinement of Alumnum Alloys by Titanium and Carbon. Nucleation, Colling effects Thermodynamic Consideration of Grain Refinement of Alumnum Alloys by Titanium and Carbon. Nucleation of Please Deformation of Al ₂ Cut. (Tr.) Precipitation of the Nucleation of Colling effects Thermodynamic Stability of Palladium Alloys. I. The Platidium, Platinium and Carbon. Nucleation of Scowth Path Envelope Analysis of Ostwald Ripening. Correction to Growth Path Envelope Analysis of Ostwald Ripening. Correction to Growth Path Envelope Analysis of Ostwald Ripening. Correction to Growth Path Envelope Analysis of Ostwald Ripening. Correction to Growth Path Envelope Analysis of Ostwald Ripening. Correction to Growth Path Envelope Analysis of Ostwald Ripening. Correction to Growth Path Envelope Analysis of Ostwald Ripening. Correction to Growth Path Envelope Analysis of Ostwald Ripening. Correction to Growth Path Envelope Analysis of Ostwald Ripening. Correction to Growth Path Envelope Analysis of Ostwald Ripening. Correction to Growth Path Envelope Analysis of Ostwald Ripening. Correction to Growth Path Envelope Analysis of Ostwald Ripening. Correction to Growth Path Envelope Analysis of Ostwald Ripening. Correction to Growth Path Envelope Analysis			Oxide coatings	
Nuclear reactors See Nuclear reactors See Nuclear reactors See Nuclear reactors Nucleating Himself Project Pro			in Carburizing Gas.	2393-2399A
Delayed Hydride Cracking Behavior for Zircaloy-2 Tubing, 2049-2660A Nuclear reactor components, Mechanical properties A Simple, Versatile Ministurized Disk-Bend Test Apparatus for Quantitative Yield-Stress Measurements. Nuclear reactors See Nucleat rusion reactors Nucleation Mechanism of Al ₂ Cul. (T ₁) Nucleation and Growth. On the Role of Elastic Interactions in the Nucleation and Growth Of Ledges. The Pole of Ledges are Tensor-Mediated Surface Properties Thermodynamic Consideration of Solidification in Liquid Droplets. Nucleation, Alloying effects Thermodynamic Consideration of Grain Refinement of Aluminum Alloys py Titanium and Carbon. Nucleation, Cooling effects Solidification of Undercooled Sm.—Sb Peritectic Alloys. II. Evilution of Borids Morphologies in TAI—B Alloys. Nucleation, Deformation of Morphologies in TAI—B Alloys. Nucleation, Deformation effects Thermodynamic Consideration of Solidification of Morphologies in TAI—B Alloys. Nucleation, Deformation of Electrophysics of Alloys and Solidification in Liquid Droplets. Nucleation, Deformation of Morphologies in TAI—B Alloys. Nucleation, Deformation of Morphologies in Tai—B Alloys. Nucleation, Deformation of Solidification in Liquid Droplets. Nucleation, Deformation of Solidification in Liquid Droplets. Oil quanching and Envirophysiolation of Solidification in Liquid Droplets. Dispance of Solidification in Liquid Droplets. Oil quanching in Envirophysiolation of Solidification in Liquid Droplets. Dispance of Solidification in Liquid Droplets. Oil quanching in Envirophysiolation of Solidification in Liquid Droplets. Dispance of Solidification in Liquid Droplets. Oil quanching in Envirophysiolation of Solidification in Liquid Droplets. Dispance of Properties of President Properties Of President Properties Of President Properties Of President Propertie	The Effect of Tungsten on Dislocation Recovery and Precipi-	2225-2235A		2535-2538A
Nuclear reactor Components, Mechanical properties A Simple, Versatile Ministurized Disk-Band Tost Apparatus See Qualismine Valed-Stress Measurements. Nucleation Ministurized Disk-Band Tost Apparatus See Nucleation Assemble Ministurized Disk-Band Tost Apparatus See Nucleation Ministurized Disk-Band Tost Apparatus See Nucleation Ministurized Disk-Band Tost Apparatus See Nucleation Assemble Ministurized Disk-Band Tost Apparatus On the Rigid of Elastic Interactions in the Nucleation and Growth of Ladges in Stress Tensor-Mediated Surface Pro- cesses for Silicon and GaAs. The Role of Ladges in Stress Tensor-Mediated Surface Pro- cesses for Silicon and GaAs. Nucleation Alloying effects The Internation See Nucleation of Grain Relinement of Alumi- num Alloys by Titanium and Carbon. Evolution of Borde Morphologies in Tital—B Alloys. Nucleation Cooling effects The Effect of Plastic Deformation on Alg-CuLI (T ₁) Precipita- tion. Nucleation Deformation effects The Effect of Plastic Deformation on Alg-CuLI (T ₁) Precipita- tion. Nucleation Deformation effects The Effect of Plastic Deformation on Alg-CuLI (T ₁) Precipita- tion. Nucleation Cortrolled Kink Motion. Nucleation Cortrolled Kink Motion. Numerical analysis Growth Path Envelope Analysis of Ostwald Ripening. Correction to Growth Path Envelope Analysis of Ostwald Ripening. Low-Temperature Improvement of Mechanical Properties of Alst 34do Steel Through High-Temperature Thermome- chanical Treatment. 1923-1943A 1923-1		2040 20004	Oxide coatings, Surface properties Effect of Sulfur Removal on Al ₂ O ₃ Scale Adhesion.	739-752A
A Simple, Versatisi Ministurized Disk-Bend Test Apparatus for Quantitative Yeld-Stress Measurements. Nucleation Nucleation Al-Culti (T ₁) Nucleation and Growth. On the Role of Elastic Interactions in the Nucleation and The Role of Ledges in Stress Tensor-Medicined Surface Processes for Silicon and GaAs. Modeling of Orystal Growth During Rapid Solidification. Nucleation of Solidification in Liquid Droplets. Nucleation Algloing effects Thermodynamic Consideration of Grain Refinement of Aluminum Alloys by Trianium and Garbon. Nucleation of Boride Morphologies in TIAI—B Alloys. Nucleation Deformation effects The Effect of Plastic Deformation on AlgCulti (T ₁) Precipitation. Nucleation of Solidification in Liquid Droplets. Nucleation Plant Envelope Analysis of Ostwald Ripening. Correction to 'Growth Path Envelope Analysis of Ostwald Ripening. Correction to 'Growth Path Envelope Analysis of Ostwald Ripening. Correction to 'Growth Path Envelope Analysis of Ostwald Ripening. Correction to 'Growth Path Envelope Analysis of Ostwald Ripening. Correction to 'Growth Path Envelope Analysis of Ostwald Ripening. Correction to 'Growth Path Envelope Analysis of Ostwald Ripening. Correction to 'Growth Path Envelope Analysis of Ostwald Ripening. Correction to 'Growth Path Envelope Analysis of Ostwald Ripening. Correction to 'Growth Path Envelope Analysis of Ostwald Ripening. Correction to 'Growth Path Envelope Analysis of Ostwald Ripening. Correction to 'Growth Path Envelope Analysis of Ostwald Ripening. Correction to 'Growth Path Envelope Analysis of Ostwald Ripening. Correction to 'Growth Path Envelope Analysis of Ostwald Ripening. Correction to 'Growth Path Envelope Analysis of Ostwald Ripening. Correction to 'Growth Path Envelope Analysis of Ostwald Ripening. Correction to 'Growth Path Envelope Analysis of Ostwald Ripening. Correction to 'Growth Path Envelope Analysis		2049-2000A	Oxide films	
Nucleation Mechanism of Al ₂ CuL ₂ (T ₁) Nucleation and Growth. On the Role of Elastic Interactions in the Nucleation and Growth Ot Ledges. The Role of Ledges in Stress Tensor-Mediated Surface Processes for Silicon and GaAs. The Role of Ledges in Stress Tensor-Mediated Surface Processes for Silicon and GaAs. Modeling of Crystal Growth During Rapid Solidification. 287-287A Modeling of Crystal Growth During Rapid Solidification. 287-288A Modeling of Crystal Growth During Rapid Solidification. 288-288A Modeling of Crystal Growth During Rapid Solidification. 288-288A Modeling of Crystal Growth During Rapid Solidification. 289-306A Nucleation, Robing effects The Effect of Plastic Deformation on AlgCuLl (T ₁) Precipitation. 289-306A Nucleation of Borded Morphologies in TIAI—B Alkys. Nuclei (transformation) See Nucleation Numerical analysis Growth Path Envelope Analysis of Ostwald Ripening. Correction to 'Growth Path Envelope Analysis of Ostwald Ripening. Correction to 'Growth Path Envelope Analysis of Ostwald Ripening. Correction to 'Growth Path Envelope Analysis of Ostwald Ripening. Correction to 'Growth Path Envelope Analysis of Ostwald Ripening. 299-306A 299-30	A Simple, Versatile Miniaturized Disk-Bend Test Apparatus	2061-2068A		
Nucleation of ApCuLi (T ₁) Nucleation and Growth. On the Role of Elastic Interactions in the Nucleation and Growth of Ledges. The Role of Ledges in Stress Tensor-Mediated Surface Processes for Silicon and GaAs. The Role of Ledges in Stress Tensor-Mediated Surface Processes for Silicon and GaAs. The Role of Ledges in Stress Tensor-Mediated Surface Processes for Silicon and GaAs. Nucleation of Solidification in Liquid Droplets. Nucleation of Solidification in Liquid Droplets. Nucleation, Rooling effects Solidification of Undercooled Sh—Sb Peritectic Alloys. II. Heterogeneous Nucleation. Evolution of Boride Morphologies in Tal—B Alloys. The Effect of Plastic Deformation on Alg-CuLi (T ₁) Precipitation. Nucleation, Deformation effects The Effect of Plastic Deformation on Alg-CuLi (T ₁) Precipitation. Nucleation, Deformation effects The Effect of Plastic Deformation on Alg-CuLi (T ₁) Precipitation. Nucleation of Solidification in Liquid Droplets. Nucleation of Solidification in Liquid Droplets. Nucleation of Solidification in Liquid Droplets. Oil quenching Low-Temperature Thermomen of Algorithms of Solidification in Liquid Droplets. Oil quenching Low-Temperature Thermomen of Algorithms of Solidification in Liquid Droplets. Oil quenching Low-Temperature Thermomen of Algorithms of Solidification in Liquid Droplets. Oil quenching Low-Temperature Thermomen of Algorithms of Solidification in Liquid Droplets. Order disorder	Nuclear reactors		See Aluminum oxide	
Mechanism of Al ₂ CuLi (T ₁) Nucleation and Growth. On the Role of Elastic Interactions in the Nucleation and Growth of Ledges. The Role of Ledges in Stress Tensor-Mediated Surface Prosport of Ledges in Care Interaction of Solidification in Liquid Droplets. Nucleation of Solidification in Liquid Droplets. Nucleation, Cooling effects Solidification of Undercooled Sn—Sb Peritectic Alloys. II. Heterogeneous Nucleation. Evolution of Boride Morphologies in TiAl—B Alloys. Nucleation, Deformation effects The Effect of Plastic Deformation on Al ₂ CuLi (T ₁) Precipitation. Nucleation, Deformation effects The Effect of Plastic Deformation on Al ₂ CuLi (T ₁) Precipitation. Nucleation of Solidification in Liquid Droplets. Nucleation of Solidification in Liquid Droplets. Nucleation of Solidification in Liquid Droplets. 299-308A Nucleation of Solidification in Liquid Droplets. Nucleation of Solidification in Liquid Droplets. 299-308A Nucleation of Solidification in Liquid Droplets. Nucleation of Solidification in Liquid Droplets. 299-308A 19-23A 19-23			Oxidizing See Oxidation	
Growth of Ledges in Stress Tensor-Mediated Surface Processes for Silicon and GaAs. The Role of Ledges in Stress Tensor-Mediated Surface Processes for Silicon and GaAs. Modeling of Crystal Growth During Rapid Solidification. Nucleation of Solidification in Liquid Droplets. Nucleation, Alloying effects Thermodynamic Consideration of Grain Refinement of Aluminum Alloys by Titanium and Carbon. Nucleation, Cooling effects Solidification of Undercooled Sn—Sb Peritectic Alloys. II. Heterogeneous Nucleation. Solidification of Undercooled Sn—Sb Peritectic Alloys. II. Heterogeneous Nucleation. Nucleation, Deformation effects The Effect of Plastic Deformation on Al ₂ CuLi (T ₁) Precipitation. Soe Nucleation, Deformation effects The Effect of Plastic Deformation on Al ₂ CuLi (T ₁) Precipitation. Soe Nucleation Solidification in Liquid Droplets. Soe Nucleation of Solidification in Liquid Droplets. Soe Nucleation of Solidification in Liquid Droplets. 299-308A Nucleation, Deformation effects The Effect of Plastic Deformation on Al ₂ CuLi (T ₁) Precipitation. Soe Nucleation of Solidification in Liquid Droplets. 299-308A Nucleation, Deformation effects The Effect of Plastic Deformation on Al ₂ CuLi (T ₁) Precipitation. Soe Nucleation of Solidification in Liquid Droplets. 299-308A Nucleation of Solidification in Liquid Droplets. 299-308A 19-23A Nucleation of Solidification in Liquid Droplets. 299-308A 299-	Mechanism of Al ₂ CuLi (T ₁) Nucleation and Growth.	287-297A		
cesses for Silicion and GaAs. Modeling of Crystal Growth During Rapid Solidification. Nucleation of Solidification in Liquid Droplets. Nucleation, Alloying effects Thermodynamic Consideration of Grain Refinement of Aluminum Alloys by Titanium and Carbon. Nucleation, Cooling effects Solidification of Undercooled Sm.—Sb Peritectic Alloys. II. Heterogeneous Nucleation. Evolution of Boride Morphologies in TiAl—B Alloys. Nucleation, Deformation effects The Effect of Plastic Deformation on Al ₂ CuLi (T ₁) Precipitation. Nucleal (transformation) See Nucleation See Nucleation Numerical analysis Growth Path Envelope Analysis of Ostwald Ripening. Diffusion-Controlled Kink Motion. Nucleation of Solidification in Liquid Droplets. 299-306A Nucleation (Solidification) Signification of Solidification in Liquid Droplets. 299-306A Nucleation of Solidification in Liquid Droplets. 299-306A Nucleation (Solidification) Signification of Solidification in Liquid Droplets. 299-306A Nucleation (Solidification) Signification of Solidification in Liquid Droplets. 299-306A Nucleation (Solidification) Signification of Solidification in Liquid Droplets. 299-306A Nucleation (Solidification) Signification of Solidification in Liquid Droplets. 299-306A Nucleation (Solidification) Signification of Solidification in Liquid Droplets. 299-306A Nucleation (Solidification) Signification of Solidification in Liquid Droplets. 299-306A Nucleation (Solidification) Signification of Solidification in Liquid Droplets. 299-306A Nucleation of Solidification in Liquid Droplets. 299-306A Nucleation (Solidification) Signification of Solidification in Liquid Droplets. 299-306A Nucleation (Solidification) Signification of Solidification in Liquid Droplets. 299-306A Nucleation of Solidification in Liquid Droplets. 299-306A Nucleation (Solidification) Signification of Solidification in Liquid Droplets. 299-306A Nucleation of Solidification in Liquid Droplets. 299-306A Nucleation (Solidification) Signification of Solidification of Solidificatio	Growth of Ledges.	1159-1164A	Aluminum, and Vanadium in Alpha Titanium, Beta Titanium,	1121-1125A
Nucleation of Solidification in Liquid Droplets. Nucleation, Alloying effects Thermodynamic Consideration of Grain Refinement of Aluminum Alloys by Triantium and Carbon. Nucleation, Cooling effects Solidification of Undercooled Sn—Sb Peritectic Alloys. II. Heterogeneous Nucleation. Evolution of Borde Morphologies in TIAI—B Alloys. Nucleation, Deformation effects The Effect of Plastic Deformation on Al ₂ CuLi (T ₁) Precipitation. Nucleation, Deformation effects The Effect of Plastic Deformation on Al ₂ CuLi (T ₁) Precipitation. See Nucleation Numerical analysis Growth Path Envelope Analysis of Ostwald Ripening. Correction to 'Growth Path Envelope Analysis of Ostwald Ripening'. Diffusion-Controlled Kink Motion. Nucleation of Solidification in Liquid Droplets. Oil quenching Low-Temporature Improvement of Mechanical Properties of AlSI 4340 Steel Through High-Temperature Thermomechanical Treatment. Oiling (lubrication) See Lubrication Optical Hibers, Mechanical properties Optical Hibers, Mechanical P	cesses for Silicon and GaAs.		Oxygen compounds	1121-11200
Thermodynamic Consideration of Grain Refinement of Aluminum and Carbon. Nucleation, Cooling effects Solidification of Undertocoled Sn—Sb Peritectic Alloys. II. Heterogeneous Nucleation. Evolution of Boride Morphologies in TIAI—B Alloys. Nucleation, Deformation effects The Effect of Plastic Deformation on Al ₂ CuLi (T ₁) Precipitation. See Nucleation See Nucleation See Nucleation Nucleation of Undertogeneous Analysis of Ostwald Ripening. Correction to "Growth Path Envelope Analysis of Ostwald Ripening." Diffusion-Controlled Kink Motion. Nucleation of Solidification in Liquid Droplets. Oil quenching Low-Temperature Improvement of Mechanical Properties of AISI 4340 Steel Through High-Temperature Thermomechanical Treatment. Optical Fibers, Mechanical properties Dynamic Fatigue Experiments on Optical Fibers. Order disorder See also Long range order An Investigation of Fe—Mi Order in a Steel. Statistical Analysis of the Disorder of Two-Dimensional Cellular Arrays in Directional Solidification Ordered alloys See Intermetallics Ordering See Order disorder See Chromistion of Solidification Ores See Chromistructure 765-773A 647-1682A 765-773A 647-1682A 765-773A 647-1682A 765-773A 764-7682A 765-773A 764-7682A 765-773A 764-7682A 765-773A 765-77	Nucleation of Solidification in Liquid Droplets.			
Nucleation, Cooling effects Solidification of Undercooled Sn—Sb Peritectic Alloys. II. Heterogeneous Nucleation. Evolution of Boride Morphologies in TIAI—B Alloys. Nucleation, Deformation effects The Effect of Plastic Deformation on Al ₂ CuLi (T ₁) Precipitation. Nuclei (transformation) See Nucleation Numerical analysis Growth Path Envelope Analysis of Ostwald Ripening. Correction to "Growth Path Envelope Analysis of Ostwald Ripening." Correction to "Growth Path Envelope Analysis of Ostwald Ripening." Correction to "Growth Path Envelope Analysis of Ostwald Ripening. Correction to "Growth Path Envelope Analysis of Ostwald Ripening." Correction to "Growth Path Envelope Analysis of Ostwald Ripening. Correction to "Growth Path Envelope Analysis of Ostwald Ripening. Correction to "Growth Path Envelope Analysis of Ostwald Ripening. Correction to "Growth Path Envelope Analysis of Ostwald Ripening. Correction to "Growth Path Envelope Analysis of Ostwald Ripening. Correction to "Growth Path Envelope Analysis of Ostwald Ripening. Correction to "Growth Path Envelope Analysis of Ostwald Ripening. Correction to "Growth Path Envelope Analysis of Ostwald Ripening. Correction to "Growth Path Envelope Analysis of Ostwald Ripening. Correction to "Growth Path Envelope Analysis of Ostwald Ripening. Correction to "Growth Path Envelope Analysis of Ostwald Ripening. Correction to "Growth Path Envelope Analysis of Ostwald Ripening. Correction to "Growth Path Envelope Analysis of Ostwald Ripening. Correction to "Growth Path Envelope Analysis of Develope Analysis of The State Correction to "Growth Path Envelope Analysis of The State Correction to "Growth Path Envelope Analysis of The State Correction to "Growth Path Envelope Analysis of The State Correction to "Growth Path Envelope Analysis of The State Correction to "Growth Path Envelope Analysis of The State Correction to "Growth Path Envelope Analysis of The State Correction to "Growth Path Envelope Analysis of The State Correction to "Growth Path Envelope Analysis of The State Co	Thermodynamic Consideration of Grain Refinement of Alumi-			
Solidification of Undercooled Sn—Sb Peritectic Alloys. II. Heterogeneous Nucleation. Evolution of Borride Morphologies in TIAI—B Alloys. Nucleation, Deformation of fects The Effect of Plastic Deformation on Al ₂ CuLi (T ₁) Precipitation. Nucleid (transformation) See Nucleation Numerical analysis Growth Path Envelope Analysis of Ostwald Ripening. Correction to "Growth Path Envelope Analysis of Ostwald Ripening". Diffusion-Controlled Kink Motion. Nucleation of Solidification in Liquid Droplets. Oil quenching Lw-Temperature Improvement of Mechanical Properties of AISI 4340 Steel Through High-Temperature Thermomechanical Treatment. Oiling (lubrication) See also Long range order An Investigation of Fe—Ni Order in a Steel. Statistical Analysis of the Disorder of Two-Dimensional Cellular Array in Directional Solidification. Ordered alloys See Intermetallics Ordering See Order disorder Ores See Chromium ores Copper ores Iron ores Orientation Orientation Final Competition of Ects and Shape Coarsening by the Ledge Mechanism. Palladium, Judying elements The Influence of Palladium on the Hydrogen-Assisted Cracking Resistance of PH 13-8 Mo Stainless Steel. 2429-2443A 2487-2501A Palladium, Binary systems Thermodynamic Stability of Palladium Alloys. I. The Palladium, Properties of Atomics Structure Thermodynamic Stability of Palladium Alloys. I. The Palladium, Properties of Atomics Structure and Properties of Atomics Structure and Properties and Properties of Architecture of Properties of Atomics Structure and Properties of Architecture of Palladium Properties and Properties of Procious Metals Ultilizing an Emulsion-Type Liquid Membrane Technique. Palladium, Binary systems Thermodynamic Stability of Palladium Alloys. I. The Palladium-Properties Atomics Structure of Homoscied Properties and Properties Atomics Structure of the Crystallized Pdg-Sig Alloy. Palladium, Binary systems Thermodynamic Stability of Palladium Alloys. I. The Palladium Properties Atomics Structure of the Crystallized Pdg-Sig Alloy. Palladi		3071-3075A	Packing (liquid structure)	
Evolution of Boride Morphologies in TIAI—B Alloys. Nucleation, Deformation effects The Effect of Plastic Deformation on Al ₂ CuLi (T ₁) Precipitation. Nuclei (transformation) See Nucleation Numerical analysis Growth Path Envelope Analysis of Ostwald Ripening. Correction to 'Growth Path Envelope Analysis of Ostwald Ripening. Diffusion-Controlled Kink Motion. Nucleation of Solidification in Liquid Droplets. Diffusion-Controlled Fine Through High-Temperature Thermomechanical Treatment. Oli quenching Low-Temperature Improvement of Mechanical Properties of AISI 4340 Steel Through High-Temperature Thermomechanical Treatment. Oliling (lubrication) See Lubrication Optical fibers, Mechanical properties Dynamic Fatigue Experiments on Optical Fibers. Order disorder See also Long range order An Investigation of Fe-Ni Order in a Steel. Statistical Analysis of the Disorder of Two-Dimensional Cellular Arrays in Directional Solidification. Ordered alloys See Intermetallics Ordering See Order disorder Ores See Chromium ores Copper ores Lino nores Orientation The Influence of Paliadium on the Hydrogen-Assisted Cracking Resistance of PH 13-8 Mo Stainless Steel. 2429-2443A The Influence of Paliadium Alloys. I. The Paliadium—Nicibium System. 1937-1943A 1948-1948 1937-1948 1937-1948 1937-1948 1937-1948 194	Solidification of Undercooled Sn-Sb Peritectic Alloys. II.	765-773A		
The Effect of Plastic Deformation on Al _Z CuLi (T ₁) Precipitation. Nuclei (transformation) See Nucleation Numerical analysis Growth Path Envelope Analysis of Ostwald Ripening. Correction to 'Growth Path Envelope Analysis of Ostwald Ripening'. Diffusion-Controlled Kink Motion. Nucleation of Solidification in Liquid Droplets. Diffusion-Controlled Kink Motion. Alist 4340 Steel Through High-Temperature Thermomechanical Treatment. Diling (lubrication) See Lubrication Optical fibers, Mechanical properties Dynamic Fatigue Experiments on Optical Fibers. Drader disorder See also Long range order An Investigation of Fe—Ni Order in a Steel. Statistical Analysis of the Disorder of Two-Dimensional Cellular Arrays in Directional Solidification. Ordered alloys See Intermetallics Ordering See Order disorder Ores See Chromium ores Copper ores Iron ores Orientation 299-306A Palladium, Binary systems. Thermodynamic Stability of Palladium Alloys. I. The Palladium—Niobium System. 1927-1943A 1927-1943A Palladium base alloys, Atomic properties Atomic Structure of the Crystalline/Amorphous Interface in a Directional Composition of the Crystalline/Amorphous Interface in a Directional Composition of the Crystalline/Amorphous Interface in a Directional Composition of the Crystalline/Amorphous Interface in a Directional Structure of the Crystalline/Amorphous Interface on Directional Structure of the Crystalline/Amorphous Interface on Directional Structure of the Crystalline/Amorphous Interface on a Directional Structure of the Crystalline/Amorphous Interface on Directio	Evolution of Boride Morphologies in TiAl—B Alloys.		The Influence of Palladium on the Hydrogen-Assisted Crack-	2420.24424
tion. Nuclei (transformation) See Nucleation Numerical analysis Growth Path Envelope Analysis of Ostwald Ripening. Correction to "Growth Path Envelope Analysis of Ostwald Ripening". Diffusion-Controlled Kink Motion. Diffusion-Controlled Kink				2923-2993A
Numerical analysis Growth Path Envelope Analysis of Ostwald Ripening. Correction to 'Growth Path Envelope Analysis of Ostwald Ripening'. Diffusion-Controlled Kink Motion. Nucleation of Solidification in Liquid Droplets. Oil quenching Low-Temperature Improvement of Mechanical Properties of AISI 4340 Steel Through High-Temperature Thermome-chanical Treatment. Oiling (lubrication) See Lubrication Optical fibers, Mechanical properties Dynamic Fatigue Experiments on Optical Fibers. Order disorder See also Long range order An Investigation of Fe—Ni Order in a Steel. Statistical Analysis of the Disorder of Two-Dimensional Cellular Arrays in Directional Solidification. Ordered alloys See Intermetallics Ordered alloys See Order disorder Ordering See Order disorder Ores See Chromium ores Copper ores Iron ores Orientation Palladium, Powder technology Preparation of Monosized Ultrafine Particles of Precious Metals Utilizing an Emulsion-Type Liquid Membrane Technique. 19-23A Atomic Structure of the Crystalline/Amorphous Interface in a Directional Cytystallized Pology, Phases (state of matter) Thermodynamic Stability of Palladium Alloys. I. The Palladium—Niobium System. Parameters See Lattice parameters See Lattice parameters See Lattice parameters See Lattice parameters Particle size Low-Cycle Fatigue Behavior of Nimonic PE16 at Room Temperature. Crystallization of a Faceted Primary Phase in a Stirred Slurry. The Effect of Reaction Condition on Composition and Properties of Ultrafine Annorphous Powders in (Fe,Co,Ni)—B Systems Preparation. 8397-404B 397-404B 40 Steel Through Indication in Cliquid Membrane Technique. Indication of Crystallized Oligos, State of matter) Thermodynamic Stability of Palladium Alloys. I. The Palladium—Niobium System. Parameters See Lattice parameters See Lattice parameters Particle size Low-Cycle Fatigue Behavior of Nimonic PE16 at Room Temperature. Crystallization of a		299-306A	Thermodynamic Stability of Palladium Alloys. I. The	1937-1943A
Growth Path Envelope Analysis of Ostwald Ripening. Correction to 'Growth Path Envelope Analysis of Ostwald Ripening'. Diffusion-Controlled Kink Motion. 1219-1224A Nucleation of Solidification in Liquid Dropiets. Oil quenching Low-Temperature Improvement of Mechanical Properties of AISI 4340 Steel Through High-Temperature Thermomechanical Treatment. Oiling (lubrication) See Lubrication Optical fibers, Mechanical properties Dynamic Fatigue Experiments on Optical Fibers. Order disorder See also Long range order An Investigation of Fe—Ni Order in a Steel. Statistical Analysis of the Disorder of Two-Dimensional Cellular Arrays in Directional Solidification. Ordered alloys See Intermetallics Ordering See Order disorder Ores See Chromium ores Copper ores Iron ores Orientation Metals Utilizing an Emulsion-Type Liquid Membrane Technique. 19-23A 1219-1224A 2487-2501A Metals Utilizing an Emulsion-Type Liquid Membrane Technique. 19-23A 1219-1224A 2487-2501A Directionally Crystallized Pd ₀₀ Si ₂₀ Alloy. Palladium base alloys, Atomic properties Atomic Structure of the Crystallized Pd ₀₀ Si ₂₀ Alloy. Directionally Crystallized Pd ₀₀ Si ₂₀ Alloy. 19-23A Atomic Structure of the Crystallized Pd ₀₀ Si ₂₀ Alloy. 19-23A Atomic Structure of the Crystallized Pd ₀₀ Si ₂₀ Alloy. 19-23A Atomic Structure of the Crystallized Pd ₀₀ Si ₂₀ Alloy. 19-23A Atomic Structure of the Crystallized Pd ₀₀ Si ₂₀ Alloy. 19-23A Atomic Structure of the Crystallized Pd ₀₀ Si ₂₀ Alloy. 19-23A Directionally Crystallized Pd ₀₀ Si ₂₀ Alloy. 19-23A Atomic Structure of the Crystallized Pd ₀₀ Si ₂₀ Alloy. 19-23A Directionally Crystallized Pd ₀₀ Si ₂₀ Al	See Nucleation		Palladium, Powder technology	
Correction to Grown Path Envelope Analysis of Ostwald Rippening*. Diffusion-Controlled Kink Motion. 1219-1224A Nucleation of Solidification in Liquid Droplets. 2487-2501A Di quenching Low-Temperature Improvement of Mechanical Properties of AISI 4340 Steel Through High-Temperature Thermomechanical Treatment. Diling (lubrication) See Lubrication Optical fibers, Mechanical properties Dynamic Fatigue Experiments on Optical Fibers. Drider disorder See also Long range order An Investigation of Fe—Ni Order in a Steel. Statistical Analysis of the Disorder of Two-Dimensional Cellular Arrays in Directional Solidification. Ordered alloys See Intermetallics Ordering See Order disorder Ores See Chromium ores Copper ores Iron ores Palladium base alloys, Atomic properties Atomic Structure of the Crystallized Pd ₆₀ Si ₂₀ Alloy. Palladium base alloys, Atomic properties Atomic Structure of the Crystallized Pd ₆₀ Si ₂₀ Alloy. Palladium base alloys, Atomic properties Atomic Structure of the Crystallized Pd ₆₀ Si ₂₀ Alloy. Palladium base alloys, Atomic properties Atomic Structure of the Crystallized Pd ₆₀ Si ₂₀ Alloy. Palladium base alloys, Atomic properties Atomic Structure of the Crystallized Pd ₆₀ Si ₂₀ Alloy. Palladium base alloys, Atomic properties Atomic properties of the Crystallized Pd ₆₀ Si ₂₀ Alloy. Palladium base alloys, Atomic properties Atomic Strability Of Palladium Alloys. I. The Palladium—Niobium System. Parameters See Lattice parameters Particle size Low-Cycle Fatigue Behavior of Nimonic PE16 at Room Temperature. Crystallization of a Facsted Primary Phase in a Stirred Slurry. Crystallization of a Facsted Primary Phase in a Stirred Slurry. Crystallization of a Facsted Primary Phase in a Stirred Slurry. Crystallization of a Facsted Primary Phase in a Stirred Slurry. Crystallization of a Facsted Primary Phase in a Stirred Slurry. Crystallization of a Facsted Primary Phase in a Stirred Slurry. Crystallization of a Facsted Primary Phase in a Stirred Slurry. Crystallization of a Facsted Primary	Numerical analysis Growth Path Envelope Analysis of Ostwald Ripening.	19-23A	Metals Utilizing an Emulsion-Type Liquid Membrane Tech-	207 404B
Diffusion-Controlled Kink Motion. Nucleation of Solidification in Liquid Dropiets. 2487-2501A Oil quenching Low-Temperature Improvement of Mechanical Properties of AISI 4340 Steel Through High-Temperature Thermomechanical Treatment. Oiling (lubrication) See Lubrication Optical fibers, Mechanical properties Dynamic Fatigue Experiments on Optical Fibers. Order disorder See also Long range order An Investigation of Fe—Ni Order in a Steel. Statistical Analysis of the Disorder of Two-Dimensional Cellular Arrays in Directional Solidification. Ordered alloys See Intermetallics Ordering See Order disorder See Chromium ores Copper ores Iron ores Orientation 1287-1298A Atomic Structure of the Crystallized Pd ₆₀ Si ₂₀ Alloy. Directionally Crystallized Pd ₆₀ Si ₂₀ Alloy. Allow-Crystallized Pd ₆₀ Si ₂₀ Alloy. Directionally Crystallized Pd ₆₀ Si ₂₀ Alloy. Directionally Crystallized Pd ₆₀ Si ₂₀ Alloy. Directionally Crystallized Pd ₆₀ Si ₂₀ Alloy. 1287-1298A Atomic Structure of the Crystallized Pd ₆₀ Si ₂₀ Alloy. Directionally Crystallized Pd ₆₀ Si ₂₀ Alloy. 1287-1298A Atomic Structure of the Crystallized Pd ₆₀ Si ₂₀ Alloy. Thermodynamic Stability of Palladium Alloys. I. The Palladium—Niobium System. 1937-1943A See Lattice parameters Particle size Lave Crystallized Pd ₆₀ Si ₂₀ Alloy. 1937-1943A 2807-2809A See Lattice parameters Particle size Lave Crystallized Pd ₆₀ Si ₂₀ Alloy. 1937-1943A 2807-2809A See Lattice parameters Particle size Lave Crystallized Pd ₆₀ Si ₂₀ Alloy. 1937-1943A 2807-2809A See Lattice parameters Particle size Lave Crystallized Pd ₆₀ Si ₂₀ Alloy. 1937-1943A 2807-2809A 1937-1943A 2807-2809A 2807-2809A 381-1390A 2807-2809A 3041-3050A 381-1390A 2907-2809A 3041-3050A Atomic Structure of the Crystallized Pd ₆₀ Si ₂₀ Alloy. 1937-1943A 1937-1943A 1937-1943A 1937-1943A 1947-1945A 1947-1945A 1947-1945A 1947-1945A 1948-1949-1949 1949-506A 1949-50	pening".			397-4048
Oil quenching Low-Temperature Improvement of Mechanical Properties of AISI 4340 Steel Through High-Temperature Thermome-chanical Treatment. 1093-1102A Oiling (lubrication) See Lubrication Optical fibers, Mechanical properties Dynamic Fatigue Experiments on Optical Fibers. Order disorder See also Long range order An Investigation of Fe—Ni Order in a Steel. Statistical Analysis of the Disorder of Two-Dimensional Cellular Arrays in Directional Solidification. Ordered alloys See Intermetallics Ordering See Order disorder See Chromium ores Copper ores Iron ores Orientation Palladium base alloys, Phases (state of matter) Thermodynamic Stability of Palladium Alloys. I. The Palladium—Niobium System. 1937-1943A Particle size distribution of Concurrent Size and Shape Coarsening by the Ledge Mechanism. 1093-1102A Parameters See Lattice parameters See Lattice parameters See Lattice parameters See Lattice parameters See Lattice parameters See Lattice parameters See Lattice parameters See Lattice parameters See Lattice parameters See Lattice parameters See Lattice parameters See Lattice parameters See Lattice parameters See Lattice parameters See Lattice parameters Particle size discribution of Particle size and Shape Coarsening by the Edge Mechanism. 1093-1102A 1093-1102A 1093-1102A Particle size discribution of Figure Parameters See Lattice parameters See Lattice parameters See Lattice parameters Particle size and Shape Coarsening by the Ledge Mechanism. 1093-1102A 109	Diffusion-Controlled Kink Motion.	1219-1224A	Atomic Structure of the Crystalline/Amorphous Interface in a	1287-1298A
AISI 4340 Steel Through High-Temperature Thermome- chanical Treatment. 1093-1102A Oiling (lubrication) See Lubrication Optical fibers, Mechanical properties Dynamic Fatigue Experiments on Optical Fibers. Order disorder See also Long range order An Investigation of Fe—Ni Order in a Steel. Statistical Analysis of the Disorder of Two-Dimensional Cellular Arrays in Directional Solidification. Ordered alloys See Intermetallics Ordering See Order disorder Ores See Chromium ores Copper ores Iron ores Orientation 1093-1102A 867-871A Palladium—Niobium System. Palladium—Niobium System. Palladium—Niobium System. 1937-1943A Parameters See Lattice parameters Particle shape Kinetic Equations for Concurrent Size and Shape Coarsening by the Ledge Mechanism. Particle size Low-Cycle Fatigue Behavior of Nimonic PE16 at Room Temperature. Crystallization of a Faceted Primary Phase in a Stirred Surry. Crystallization of a Faceted Primary Phase in a Stirred Surry. Crystallization of a Faceted Primary Phase in a Stirred Surry. Crystallization of Fee.Co,Ni)—B System. 499-506A 575-584A Particle size Low-Cycle Fatigue Behavior of Nimonic PE16 at Room Temperature. Crystallization of a Faceted Primary Phase in a Stirred Surry. Crystallization of a Faceted Primary Phase in a Stirred Surry. Crystallization of Effect of Reaction Condition on Composition and Properties of Ultrafine Amorphous Powders in (Fe,Co,Ni)—B System. 499-506A 575-584A Particle size Low-Cycle Fatigue Behavior of Nimonic PE16 at Room Temperature. Crystallization of a Faceted Primary Phase in a Stirred Surry. Crystallization of a Faceted Primary Phase in a Stirred Surry. Crystallization of a Faceted Primary Phase in a Stirred Surry. Crystallization of a Faceted Primary Phase in a Stirred Surry. Crystallization of a Faceted Primary Phase in a Stirred Surry. Crystallization of a Faceted Primary Phase in a Stirred Surry. Crystallization of a Faceted Primary Phase in a Stirred Surry. Crystallization of a Faceted Primary Phase in a Stirred Surry. Crystalliza	Oil quenching		Palladium base alloys, Phases (state of matter)	
Olling (lubrication) See Lubrication Optical fibers, Mechanical properties Dynamic Fatigue Experiments on Optical Fibers. Order disorder See also Long range order An Investigation of Fe—Ni Order in a Steel. Statistical Analysis of the Disorder of Two-Dimensional Cellular Arrays in Directional Solidification. Ordered alloys See Intermetallics Ordering Green order disorder Ores See Chromium ores Copper ores Iron ores Orientation Optical fibers, Mechanical properties Berarders See Lattice parameters Particle shape Kinetic Equations for Concurrent Size and Shape Coarsening by the Ledge Mechanism. 1381-1390A 1381-1390A Particle size Low-Cycle Fatigue Behavior of Nimonic PE16 at Room Temperature. Crystallization of a Faceted Primary Phase in a Stirred Surry. Crystallization of a Faceted Primary Phase in a Stirred Surry. Crystallization of a Faceted Primary Phase in a Stirred Surry. Crystallization of Fee-Niconal Reduction. Particle size Low-Cycle Fatigue Behavior of Nimonic PE16 at Room Temperature. Crystallization of a Faceted Primary Phase in a Stirred Surry. Crystallization of a Faceted Primary Phase in a Stirred Surry. Crystallization of Effect of Reaction Condition on Composition and Properties of Ultrafine Amorphous Powders in (Fe,Co,Ni)—B Systems Prepared by Chemical Reduction. Particle size Low-Cycle Fatigue Behavior of Nimonic PE16 at Room Temperature. Crystallization of a Faceted Primary Phase in a Stirred Surry. Crystallization of a Faceted Primary Phase in a Stirred Surry. Crystallization of Effect of Reaction Condition on Composition and Properties of Ultrafine Amorphous Powders in (Fe,Co,Ni)—B Systems Prepared by Chemical Reduction. Particle size Low-Cycle Fatigue Behavior of Nimonic PE16 at Room Temperature. Crystallization of a Faceted Primary Phase in a Stirred Surry. Crystallization of a Faceted Primary Phase in a Stirred Surry. Crystallization of a Faceted Primary Phase in a Stirred Surry. Crystallization of a Faceted Primary Phase in a Stirred Surry. Crystallization of a Faceted Prim	AISI 4340 Steel Through High-Temperature Thermome-		Palladium—Niobium System.	1937-1943A
See Lubrication Optical fibers, Mechanical properties Dynamic Fatigue Experiments on Optical Fibers. 867-871A Order disorder See also Long range order An Investigation of Fe—Ni Order in a Steel. Statistical Analysis of the Disorder of Two-Dimensional Cellular Arrays in Directional Solidification. Ordered alloys See Intermetallics Ordering See Order disorder Ores See Chromium ores Copper ores Iron ores Orientation Orientation Optical fibers, Mechanical properties B867-871A 867-871A 867-871A 867-871A 867-871A 867-871A 867-871A 867-871A Particle slape Kinetic Equations for Concurrent Size and Shape Coarsening by the Ledge Mechanism. 1381-1390A 499-506A 575-584A Terflect of Reaction Condition on Composition and Properties of Ultrafine Amorphous Powders in (Fe,Co,Ni)—B Systems Prepared by Chemical Reduction. Particle size Low-Cycle Fatigue Behavior of Nimonic PE16 at Room Temperature. Crystallization of a Faceted Primary Phase in a Stirred Slurry Crystallization of Composition and Properties of Ultrafine Amorphous Powders in (Fe,Co,Ni)—B Systems Prepared by Chemical Reduction. Particle size Low-Cycle Fatigue Behavior of Nimonic PE16 at Room Temperature. Crystallization of a Faceted Primary Phase in a Stirred Slurry Crystallization of a Faceted Primary Phase in a Stirred Slurry Crystallization of a Faceted Primary Phase in a Stirred Slurry Crystallization of a Faceted Primary Phase in a Stirred Slurry Crystallization of a Faceted Primary Phase in a Stirred Slurry Crystallization of a Faceted Primary Phase in a Stirred Slurry Crystallization of a Faceted Primary Phase in a Stirred Slurry Crystallization of a Faceted Primary Phase in a Stirred Slurry Crystallization of a Faceted Primary Phase in a Stirred Slurry Crystallization of a Faceted Primary Phase in a Stirred Slurry Crystallization of a Faceted Primary Phase in a Stirred Slurry Crystallization of a Faceted Primary Phase in a Stirred Slurry Crystallization of a Faceted Primary Phase in a Stirred Slurry Crystallization of a Faceted Primary		1093-1102A		
Dynamic Fatigue Experiments on Optical Fibers. 867-871A Order disorder See also Long range order An Investigation of Fe—Ni Order in a Steel. Statistical Analysis of the Disorder of Two-Dimensional Cellular Arrays in Directional Solidification. Ordered alloys See Intermetallics Ordering See Order disorder Ores See Chromium ores Copper ores Iron ores Orientation Orientation Orientation Dy the Ledge Mechanism. 2807-2809A 2807-2809A 2807-2809A 3041-3050A 3041-3050A 2807-2809A 3041-3050A 3041-3050A Departicle size Low-Cycle Fatigue Behavior of Nimonic PE16 at Room Temperature. Crystallization of a Faceted Primary Phase in a Stirred Slurry. The Effect of Reaction Condition on Composition and Properties of Ultrafine Amorphous Powders in (Fe,Co,Ni)—B Systems Prepared by Chemical Reduction. Particle size Low-Cycle Fatigue Behavior of Nimonic PE16 at Room Temperature. Crystallization of a Faceted Primary Phase in a Stirred Slurry. The Effect of Reaction Condition on Composition and Properties of Ultrafine Amorphous Powders in (Fe,Co,Ni)—B Systems Prepared by Chemical Reduction. Particle size Low-Cycle Fatigue Behavior of Nimonic PE16 at Room Temperature. Crystallization of a Faceted Primary Phase in a Stirred Slurry. The Effect of Reaction Condition on Composition and Properties of Ultrafine Amorphous Powders in (Fe,Co,Ni)—B Systems Prepared by Chemical Reduction. Particle size Low-Cycle Fatigue Behavior of Nimonic PE16 at Room Temperature. Crystallization of a Faceted Primary Phase in a Stirred Slurry. The Effect of Reaction Condition on Composition and Properties of Ultrafine Amorphous Powders in (Fe,Co,Ni)—B Systems Prepared by Chemical Reduction. Particle size Low-Cycle Fatigue Behavior of Nimonic PE16 at Room Temperature. Crystallization of a Faceted Primary Phase in a Stirred Slurry. Crystallization of a Faceted Primary Phase in a Stirred Slurry. Crystallization of a Faceted Primary Phase in a Stirred Slurry. Crystallization of a Faceted Primary Phase in a Stirred Slurry. Crystallization of	See Lubrication		Particle shape	
See also Long range order An Investigation of Fe—Ni Order in a Steel. Statistical Analysis of the Disorder of Two-Dimensional Cellular Arrays in Directional Solidification. Ordered alloys See Intermetallics Ordering See Order disorder Ores See Chromium ores Copper ores Iron ores Orientation Orientation See Orientation Orientation A99-506A 575-584A 499-506A 575-584A 575-58		867-871A		1381-1390A
An Investigation of Fe—Ni Order in a Steel. 2807-2809A Statistical Analysis of the Disorder of Two-Dimensional Cellular Arrays in Directional Solidification. 2807-2809A Statistical Analysis of the Disorder of Two-Dimensional Cellular Arrays in Directional Solidification. 3041-3050A 3041-3050A 3041-3050A 3041-3050A 3041-3050A Ordered alloys See Intermetallics Ordering See Order disorder Ores See Chromium ores Copper ores Iron ores Orientation Orientation 2807-2809A S041-3050A S0				
lar Arrays in Directional Solidification. Ordered alloys See Intermetallics Ordering See Order disorder Ores See Chromium ores Copper ores Iron ores Copper ores Iron ores Corientation Orientation Orderidation Orderidation Orderidation Orderidation See Order disorder Ores See Chromium ores Copper ores Iron ores Copper ores Iron ores Orientation	An Investigation of Fe—Ni Order in a Steel.	2807-2809A	perature.	
See Intermetallics Ordering See Order disorder Ores See Chromium ores Copper ores In ores Copper ores In ores Corientation Particle size distribution Quantitative Assessment of the Implications of Strain-Induced Microstructural Changes in Superplasticity. Kinetic Equations for Concurrent Size and Shape Coarsening by the Ledge Mechanism. Carbonitride Precipitate Growth in Titanium/Niobium Microal-Inon ores Orientation Particulate composites, Casting	lar Arrays in Directional Solidification.	3041-3050A	The Effect of Reaction Condition on Composition and Proper-	010-00411
See Order disorder Cres See Chromium ores See Chromium ores Copper ores Iron ores Cres Cres Cres Cres Cres Cres Cres C				2125-2132A
Ores Kinetic Equations for Concurrent Size and Shape Coarsening See Chromium ores Copper ores Iron ores Corper ores Iron ores Cribonitride Precipitate Growth in Titanium/Niobium Microal- Iron ores Particulate composites, Casting			Quantitative Assessment of the Implications of Strain-	20.01
See Chromium ores by the Ledge Mechanism. 1381-1390A Copper ores Carbonitride Precipitate Growth in Titanium/Niobium Microal- Iron ores loyed Steels. Orientation Particulate composites, Casting	Ores		Kinetic Equations for Concurrent Size and Shape Coarsening	
Orientation Particulate composites, Casting	Copper ores		Carbonitride Precipitate Growth in Titanium/Niobium Microal-	
See also Orientation relationships Behavior of Metal Alloys in the Semisolid State. 269-294B				1511-1524A
			Behavior of Metal Alloys in the Semisolid State.	269-294B

Δ

In Situ Formation of Three-Dimensional TiC Reinforcements in Ti-TiC Composites. Behavior of Metal Alloys in the Semisolid State.	859-865A 957-981A	Representation of Excess Thermodynamic Properties of Ter- nary Systems Using Interaction Parameters. Thermodynamics of Binary Systems Using Interaction Pa-	583-591B
Particulate composites, Corrosion Microstructure Property Relationships and Hydrogen Effects in a Particulate-Reinforced Aluminum Composite.	2445-2450A	rameters. Thermodynamics of Aluminum—Barium Alloys. Phase Relations and Thermodynamics of the System Fe— Cr—O in the Temperature Range of 1600-1825°C (1873-	593-605B 607-616B
Particulate composites, Directional solidification In Situ Observation of Interactions Between Gaseous Inclu-		2098K) Under Strongly Reducing Conditions. Oxygen Pressure Dependence of Cu ₂ O—CuO—Gd ₂ O ₃	689-703B
sions and an Advancing Solid/Liquid Interface. Particulate composites, Mechanical properties	385-388B	Phase Diagram. Thermodynamic Properties of the Fe—Mn—V—C System. Nonequilibrium Behavior in the Al—Ge Alloy Systems: In-	705-710B 1911-1920A
The Effect of Particulate SiC on Fatigue Crack Growth in a	97-112A	Nonequilibrium Behavior in the Al—Ge Alloy Systems: In- sights Into the Metastable Phase Diagram. Phase Equilibria in Alloys Displaying Diffusional and Displa-	2141-2152A
Cast-Extruded Aluminum Alloy Composite. Tensile Deformation and Fracture Toughness of 2014 + 15 vol.% SiC Particulate Composite.	113-123A	cive Characteristics.	2565-2578A
Creep Deformation of TiB ₂ -Reinforced Near-γ Titanium Al- uminides.	447-454A	Phase diagram reactions, Stress effects Coherent Phase Equilibrium in Alloys With Congruent Points.	1921-1935A
Thermomechanical Fatigue of Particulate-Reinforced Alumi- num 2xxx-T4. Fatigue Behavior of a 2xxx Series Aluminum Alloy Reinforced	697-707A	Phase diagrams The Decomposition of the Beta Phase in the Copper—Tin	
With 15 vol.% SiC _p . Tribological Behavior and Surface Analysis of Tribodeformed	1007-1019A	System. Determination of Liquid Diffusion Coefficients Along a	11-18A
Al Alloy—50% Graphite Particle Composites. Mechanical Behavior of Cast Particulate SiC/AL (A356) Metal	1435-1441A	Liquidus Phase Boundary. Activities of Boron in the Binary Ni—B and the Ternary Co— Fe—B Melts.	21-26B 47-52B
Matrix Composites. The Mechanical Behavior of a Hybrid Metal Matrix Composite.	1585-1593A 2107-2117A	Experimental Determination of the Phase Equilibria of Aluminum-Rich Al—Li—Cu Alloys.	203-213A
Third-Order Bounds on the Elastic Moduli of Metal-Matrix Composites.	3065-3067A	Equilibrium Phase Relations and Thermodynamics of the Cr—O System in the Temperature Range of 1500°C to	
Particulate composites, Reactions (chemical) Interfaces in XD Processed TiB ₂ /NiAl Composites.	3013-3018A	1825°C. Solidification Microporosity in Directionally Solidified Multi-	225-232B
Particulate composites, Structural hardening	3013-3016A	component Nickel Aluminide. Application of Thermodynamic Models to the Calculation of Solidification Paths of Aluminum-Rich Al—Li Alloys.	225-234A 267-271A
Microstructurally Toughened Particulate-Reinforced Alumi- num Matrix Composites. NiAl-Based Microstructurally Toughened Composites.	171-182A 183-189A	Behavior of Metal Alloys in the Semisolid State. Synthesis of Iron Aluminides From Elemental Powders: Reac-	269-294B
Effect of Reinforcement on the Aging Response of Cast 6061 Al—Al ₂ O ₃ Particulate Composites.	2553-2563A	tion Mechanisms and Densification Behavior. Plastic Deformation and Fracture of Binary TiAl-Base Alloys.	277-286A 427-439A
Passivation		Ductility Enhancement in NiAl (B2)-Base Alloys by Microstructural Control. Numerical Simulation of a Solidity of Bb. Sp. Alloys the Ef.	441-446A
Pitting Corrosion Behavior of Powder Metallurgy Mechani- cally Alloyed IN-9052. Environmental Fatigue of an Al—Li—Cu Alloy. I. Intrinsic	938-941A	Numerical Simulation of a Solidifying Pb—Sn Alloy: the Effects of Cooling Rate on Thermosolutal Convection and Macrosegregation.	529-540B
Crack Propagation Kinetics in Hydrogenous Environments.	2415-2428A	Representation of Excess Thermodynamic Properties of Ter- nary Systems Using Interaction Parameters.	583-591B
Pearlite Interfacial Steps and Growth Mechanism in Ferrous Pearlites.	1349-1365A	Thermodynamics of Binary Systems Using Interaction Parameters.	593-605B
Penetration Grain Boundary Diffusion of Hydrogen in Nickel.	351-355A	Thermodynamics of Aluminum—Barium Alloys. Oxygen Pressure Dependence of Cu ₂ O—CuO—Gd ₂ O ₃ Phase Diagram.	607-616B 705-710B
Modeling Surface Effects on Hydrogen Permeation in Metals. Permalloy	1001-1006A	Reaction of Titanium and Ti—Al Alloys With Alumina. Solidification of Undercooled Sn—Sb Peritectic Alloys. I.	715-721A
See Ferrous alloys Nickel base alloys		Microstructural Evolution. Solidification of Undercooled Sn—Sb Peritectic Alloys. II.	753-764A
Permanent mold castings See Die castings		Heterogeneous Nucleation. A Phase Diagram Approach to Study Liquation Cracking in	765-773A
Permeation See Penetration		Alloy 718. Solidification Modeling and Solid-State Transformations in High-Energy Density Stainless Steel Welds.	887-902A 915-926A
pH Reductive Ammonia Leaching of Manganese Nodules by		Intermetallic Phase Formation and Breakdown of Molybde-	957-981A
Thiosulfate. The Redox Equilibria of Copper Ions in the Molten Silicate Fluxes as a Measure of Basicity.	259-261B 823-829B	num Diffusion Barriers in Ni—Mo—Cu Layers. Evolution of Boride Morphologies in TiAl—B Alloys. On the Nature of Eutectic Carbides in Cr—Ni White Cast	1501-1510A 1647-1662A
pH factor See pH		Irons. The Al—Al ₈ Mo ₃ Section of the Binary System Aluminum— Molybdenum.	1709-1720A 1729-1736A
pH value See pH		Morphology of Cementite Decomposition in an Fe—Cr—C Alloy.	1753-1759A
Phase boundary Determination of Liquid Diffusion Coefficients Along a	21-26B	Thermodynamic Properties of the Fe—Mn—V—C System. Coherent Phase Equilibrium in Alloys With Congruent Points. Thermodynamic Stability of Palladium Alloys. 1. The	1911-1920A 1921-1935A
Liquidus Phase Boundary. Thermodynamic Equilibrium in the Low-Solute Regions of Plutonium-Group IIIA Metal Binary Systems.	2237-2246A	Palladium—Niobium System. Determination of Equilibrium Solid-Phase Transition Temperatures Using DTA.	1937-1943A 1993-1998A
Phase decomposition		Heats of Formation of Aluminum—Cerium Intermetallic Compounds.	2119-2123A
See also Eutectoid decomposition The Decomposition of the Beta Phase in the Copper—Tin System.	11-18A	Nonequilibrium Behavior in the Al—Ge Alloy Systems: Insights Into the Metastable Phase Diagram.	2141-2152A
Phase Transformations During Heating of Ilmenite Concentrates.	711-716B	Solidification and Phase Equilibria in the Fe—C—Cr—NbC System.	2181-2186A
An Experimental and Theoretical Study of Cemeritite Dissolu- tion in an Fe—Cr—C Alloy.	1745-1752A	A Thermodynamic Assessment of the Fe—Cr—Ni—C System. An Assessment of the Fe—C—Si System.	2187-2198A 2211-2223A
Morphology of Cementite Decomposition in an Fe—Cr—C Alloy. Phase Transformation in an Fe—10.1AI—28.6Mn—0.46C	1753-1759A	Thermodynamic Equilibrium in the Low-Solute Regions of Plutonium-Group IIIA Metal Binary Systems.	2237-2246A
Alloy. Containerless Processing and Rapid Solidification of Nb—Si	2265-2276A	Phase Equilibria in Alloys Displaying Diffusional and Displa- cive Characteristics.	2565-2578A
Alloys of Hypereutectic Composition. Phase decomposition, Cooling effects	2723-2732A	Calculation of Phase Diagrams and Solidification Paths of Aluminum-Rich Al—Li—Cu Alloys.	2837-2848A
Microstructural Engineering Applied to the Controlled Cooling of Steel Wire Rod. I. Experimental Design and Heat		Phase ratio Hydrogen Compatibility of Femnal Alloys.	215-224A
Transfer. Microstructural Engineering Applied to the Controlled Cooling of Steel Wire Rod. II. Microstructural Evolution and Me-	2769-2778A	Use of Differential Interference Contrast Microscopy to De- tect Duplex Carbides in Alloy White Cast Irons. Secondary Ion Mass Spectrometry Method for Distinguishing	1673-1674A
chanical Properties Correlations. Microstructural Engineering Applied to the Controlled Cool- ing of Steel Wire Rod. III. Mathematical Model—	2779-2790A	the State of Carbon in Steels Using Negative Molecular lons. Effect of Phase Morphology on the Mechanical Behavior of	1969-1978A
Formulation and Predictions.	2791-2805A	Effect of Phase Morphology on the Mechanical Behavior of Two Titanium Aluminide Composites. Development of Structure and Porosity in Cast Al ₅ CuZr ₂ and	2009-2019A
Phase decomposition, Heating effects Structures and Tempering Behavior of Rapidly Solidified High-Carbon Iron Alloys.	775-782A	Al ₈₆ Mn ₉ Zr ₂₅ Intermetallic Compounds. Phase ratio, Composition effects	2545-2552A
Phase diagram reactions See also Eutectic reactions		Effect of Reinforcement on the Aging Response of Cast 6061 AI—Al ₂ O ₃ Particulate Composites.	2553-2563A
Martensitic transformations Phase decomposition		Phase ratio, Heating effects The Tempering of FeNiN Martensite.	1945-1956A

Phase stability Thermodynamic Stability of Palladium Alloys. I. The Palladium—Niobium System.	1937-1943A	Pitting potential See Corrosion potential Pitting (corrosion)	
Nonequilibrium Behavior in the Al—Ge Alloy Systems: Insights Into the Metastable Phase Diagram.	2141-2152A	Plasma arc casting See Casting	
Phase stability, Stress effects Coherent Phase Equilibrium in Alloys With Congruent Points.	1921-1935A	Plasma arc plating See Plasma spraying	
Phase structure See Solid phases		Plasma arc spraying	
Phase transformations See also Martensitic transformations		See Plasma spraying Plasma arc welding	
Massive type transformation The Effect of the Thermal Path to Reach Isothermal Temper- ature on Transformation Kinetics. Real-Time Atomic-Level Observations of In Situ Chemical Re-	993-999A	The Chemistry and Structure of Wear-Resistant, Iron-Base Hardfacing Alloys. Plasma jet spraying	983-991A
actions and Transformations Utilizing High-Resolution Electron Microscopy.	1323-1329A	See Plasma spraying Plasma processing	
Interface Dislocations and Ledges in Oxidation and Diffusional Phase Transformations. Phase Transformation in an Fe—9.0AI—29.5Mn—1.2Si	1331-1339A	See Plasma arc welding Plasma spraying	
Alloy. The Effect of Continuous Heating on the Phase Transformations in Zinc—Iron Electrodeposited Coatings.	1407-1415A 1737-1743A	Plasma spraying Mathematical Modeling of the Isothermal Impingement of Liq- uid Droplets in Spraying Processes.	901-914B
Interrupted and Isothermal Solidification Studies of Low and Medium Carbon Steels.	1871-1880A	Plastic deformation The Effect of Plastic Deformation on Al ₂ CuLi (T ₁) Precipita-	301-31-45
Activation Energy of δ-Γ ₁ Transformation in a Zn—Fe Electro- deposited Coating.	1887-1888A	tion. Development of Deformation Instability in Hot Tensile Test	299-306A
Determination of Equilibrium Solid-Phase Transition Temper- atures Using DTA. Effects of Transformation on Texture and Iodine Stress Cor-	1993-1998A	Specimens.	2297-2302A
rosion Cracking Resistance of Zircaloy Sheet. Phase Equilibria in Alloys Displaying Diffusional and Displa-	2247-2256A	Plastic deformation, Stress effects Hydrostatic Stresses and Their Effect on the Macroflow Be-	
cive Characteristics.	2565-2578A	havior and Microfracture Mechanism of Two-Phase Alloys. Plastic flow, Deformation effects	2695-2702A
Phase transformations, Anisotropy Transformation of Retained Austenite in Carburized 4320 Steel.	1491-1500A	Recrystallization of Austenite After Deformation at High Tem- peratures and Strain Rates—Analysis and Modeling. Prediction of Steel Flow Stresses at High Temperatures and	151-160A
Phase transformations, Environmental effects Morphology and Aging of the Martensite Induced by Cathodic Hydrogen Charging of High-Carbon Austentitic Steels.	1979-1991A	Strain Rates. Plastic strain	1545-1558A
Phases (state of matter)	1070-1001A	See Plastic deformation Plasticity	
See also Intermetallic phases Liquid phases		See also Superplasticity Toward a Sound Understanding of Dislocation Plasticity.	1693-1708A
Metastable phases Solid phases A New Phase in an Fe—9.0Al—29.5Mn—1.2Si Alloy.	1417-1423A	Plasticity, Alloying effects The Effects of Chromium Additions to Binary TiAl-Base Al-	1000 17001
A New Phase in a Rapidly Solidified and Consolidated NbAl ₃ —1TiB ₂ Alloy.	1901-1909A	loys.	2619-2626A
Phosphorus, Alloying elements Effect of Phosphorus on Carbon Activity, Carbide Precipita-		Plastics See Polymers	
tion, and Coarsening in Ferritic Fe—C—P Alloys. Phosphorus, Impurities	35-43A	Plate metal, Forming Effect of Processing Variables on Texture and Texture Gradi- ents in Tantalum.	2039-2048A
X-Ray Microanalysis of Phosphorus Segregation in Type 304L Stainless Steels. The Reduction of the Interfacial Segregation of Phosphorus and Its Embrittlement Effect by Lanthanum Addition in a W—Ni—Fe Heavy Alloy.	253-255A 2969-2974A	Plate metal, Microstructure Influence of Initial Ingot Breakdown on the Microstructural and Textural Development of High-Purity Tantalum.	2959-2968A
Photo oxidation	2505-2514A	Plating See Alloy plating	
See Oxidation Photodecomposition		Platinum, Powder technology Preparation of Monosized Ultrafine Particles of Precious	
See Decomposition reactions Photography		Metals Utilizing an Emulsion-Type Liquid Membrane Technique.	397-404B
See Cinematography		Platinum metal alloys	
Physical chemistry High-Temperature Thermodynamic Properties of the Vana- dium Carbides V ₂ C and VC _{0.73} Determined Using a Gal-		See Palladium base alloys Platinum metal compounds See Ruthenium compounds	
vanic Cell Technique. A Degenerate Electron Gas Model for Solutions of Aluminum		Platinum metals	
in Cryolite Melts. Gibbs Energy of Formation of Nickel Chromite. Thermochemical Nature of Minor Elements in Copper Smelt-	669-672B 673-675B	See Osmium Palladium Platinum	
ing Mattes. The Redox Equilibria of Copper lons in the Molten Silicate	677-688B	Plutonium, Binary systems Thermodynamic Equilibrium in the Low-Solute Regions of	
Fluxes as a Measure of Basicity. A Thermodynamic and Experimental Study of the Electro- chemically Induced Cooling of the Anode in Hall—Heroult	823-829B	Plutonium-Group IIIA Metal Binary Systems. Poissons ratio, Heating effects	2237-2246A
Cells. A Thermodynamic Study of the System		Elastic Moduli and Tensile and Physical Properties of Heat- Treated and Quenched Powder Metallurgical Ti—8AI—4V	
A Thermodynamic Study of the System $Fe_\chi O + Al_2O_3 + SiO_2$ at 1673K. Dissolution Equilibrium of Magnesium Vapor in Liquid Iron.	839-845B 918-921B	Alloy. Correction to "Elastic Moduli and Tensile and Physical Properties of Heat-Treated and Quenched Powder Metallurgical	709-714A
Physical metallurgy Equilibrium Phase Relations and Thermodynamics of the Cr—O System in the Temperature Range of 1500°C to		Ti—6Al—4V Alloy". Poissons ratio, Microstructural effects	1129A
1825°C. Physical properties	225-232B	On Thermal Shock Resistance of Austenitic Cast Irons. Polarization (electrodes)	1821-1831A
See Adhesion Anisotropy		See Anodic polarization	
Density Diffusivity		Pole figures Analysis of an Aluminum Single Crystal With Unstable Initial	45-58A
Porosity Solubility		Orientation (001)[110] in Channel Die Compression. Delayed Hydride Cracking Behavior for Zircaloy-2 Tubing. A Simple Theory for the Development of Inhomogeneous	2049-2060A
Surface tension Wettability		A Simple Theory for the Development of Inhomogeneous Rolling Textures.	2637-2643A
Pinning See Dislocation pinning		Poling See Deoxidizing	
Pinning (dislocation) See Dislocation pinning		Pollutants See Industrial wastes	
Pitting (corrosion)		Polycrystals, Forming	
Pitting Corrosion Behavior of Powder Metallurgy Mechani-	000 0444	Earing in Cup Drawing Face-Centered Cubic Single Crystals	1505 15344

Polycrystals, Heat treatment Influence of Cyclic Deformation on Surface Microstructure and Hardness of Ion-Implanted Nickel.	1633-1646A	Precipitates See also Cellular precipitates Solute Distribution Around a Coherent Precipitate in a Multi-	
Polycrystals, Mechanical properties 1000 to 1200K Time-Dependent Compressive Deformation of		component Alloy. Precipitates, Crystal growth	2199-2210A
Single-Crystalline and Polycrystalline B2 Ni—40Al. Polycrystals, Transport properties	1595-1607A	Mechanism of Al ₂ CuLi. (T ₁) Nucleation and Growth. Report on Panel Discussion. II. Critical Problems in the Math- ematics of Ledgewise Growth.	287-297A 1247-1248A
The High-Temperature Work Function Behavior of Polycrys- talline Osmium.	1609-1613A	Coarsening Resistance of M ₂ C Carbides in Secondary Hard- ening Steels. I. Theoretical Model for Multicomponent	
Polymers, Mechanical properties Development of Vibration-Damping Resins for Room- Temperature Application.	629-631A	Coarsening Resistance of M ₂ C Carbides in Secondary Hard- ening Steels. II. Alloy Design Aided by a Thermochemical	2863-2868A
Polymers, Physical properties Chlorosulfonated Polyethylene: a Versatile Polymer for Damping Acoustic Waves.	633-640A	Database. Coarsening Resistance of M ₂ C Carbides in Secondary Hardening Steels. III. Comparison of Theory and Experiment.	2869-2876A 2877-2888A
Pores See Porosity	000 01011	Precipitation See also Intergranular precipitation	
Porosity		Continuous Precipitation of Uranium Peroxide From High- Vanadium Mill Solutions.	135-136B
See also Microporosity The Role of the γ/γ' Eutectic and Porosity on the Tensile Behavior of a Single-Crystal Nickel-Base Superalloy.	1443-1451A	Coarsening Resistance of M ₂ C Carbides in Secondary Hard- ening Steels. II. Alloy Design Aided by a Thermochemical Database.	2869-2876A
Porosity, Heating effects		Precipitation, Alloying effects	
Development of Structure and Porosity in Cast Al ₅ CuZr ₂ and Al ₈₆ Mn ₉ Zr ₂₅ Intermetallic Compounds.	2545-2552A	Effect of Phosphorus on Carbon Activity, Carbide Precipita- tion, and Coarsening in Ferritic Fe—C—P Alloys. The Effect of Tungsten on Dislocation Recovery and Precipi-	35-43A
Potassium, Sorption Discussion of "Evidence for the Existence of Potassium Bubbles in AKS-Doped Tungsten Wire" and Reply.	2153-2156A	tation Behavior of Low-Activation Martensitic 9Cr Steels. Precipitation, Deformation effects Little Classic Details Control of a 2E at 8 Cr. 7 at 8	2225-2235A
Pots (electrolytic) See Electrolytic cells		High Strain Rate Superplasticity of a 25 wt.% Cr—7 wt.% Ni—3 wt.% Mo—0.14 wt.% N Duplex Stainless Steel.	1083-1091A
Powder compacts		Precipitation, Heating effects Microstructural Evolution of Modified 9Cr—1Mo Steel.	1049-1058A
See also Sintered compacts Powder Metallurgy T15 Tool Steel. I. Characterization of Powder and Hot Isostatically Pressed Material.	2733-2745A	Precipitation, Welding effects Carbide Precipitation in Welds of Two-Phase Austenitic— Ferritic Stainless Steel.	2889-2902A
Powder compacts, Composite materials Fatigue Behavior of a 2xxx Series Aluminum Alloy Reinforced		Precipitation hardening	
With 15 vol.% SiCp.	1007-1019A	Mechanism of Al ₂ CuLi (T ₁) Nucleation and Growth. The Effect of Plastic Deformation on Al ₂ CuLi (T ₁) Precipita-	287-297A
Powder compacts, Mechanical properties 1000 to 1200K Time-Dependent Compressive Deformation of		tion. A Calorimetric Study of Precipitation in an Al—Cu Alloy With	299-306A
Single-Crystalline and Polycrystalline B2 Ni—40Al. Structure and Properties of a Rapidly Solidified Al—Li—	1595-1607A	Silicon Particles. On the Role of Elastic Interactions in the Nucleation and	665-674A
Mn—Zr Alloy for High-Temperature Applications. I. Inert Gas Atomization Processing.	2503-2514A	Growth of Ledges. Computer Simulation of the Effect of Coherency Strain on	1159-1164A
Structure and Properties of a Rapidly Solidified Al—Li— Mn—Zr Alloy for High-Temperature Applications. II. Spray		Cluster Growth Kinetics. Kinetic Equations for Concurrent Size and Shape Coarsening	1197-1209A
Atomization and Deposition Processing.	2515-2522A	by the Ledge Mechanism. Carbonitride Precipitate Growth in Titanium/Niobium Microal-	1381-1390A
Powder metallurgy Development of a Necklace Microstructure During Isothermal Deformation and Its Properties Relative to Uniform Micro- structures.	1999-2008A	loyed Steels. The Effect of Copper, Chromium, and Zirconium on the Mi- crostructure and Mechanical Properties of Al—Zn—Mg—	1511-1524A
Powder metallurgy parts, Corrosion Pitting Corrosion Behavior of Powder Metallurgy Mechani-		Cu Alloys. Precipitation hardening, Composition effects	2809-2818A
Pitting Corrosion Behavior of Powder Metallurgy Mechani- cally Alloyed IN-9052. Microstructure Property Relationships and Hydrogen Effects	938-941A	Effect of Reinforcement on the Aging Response of Cast 6061 AI—AI ₂ O ₃ Particulate Composites.	2553-2563A
in a Particulate-Reinforced Aluminum Composite.	2445-2450A	Precipitation hardening alloys See also Precipitation hardening steels	
Powder metallurgy parts, Heat treatment Elastic Moduli and Tensile and Physical Properties of Heat- Treated and Quenched Powder Metallurgical Ti—6AI—4V		Precipitation hardening alloys, Corrosion On the Stress Corrosion Cracking of Al—Li Alloys: the Role	
Alloy. Correction to "Elastic Moduli and Tensile and Physical Prop-	709-714A	of Grain Boundary Precipitates. Environmental Fatigue of an Al—Li—Cu Alloy. I. Intrinsic	264-267A
erties of Heat-Treated and Quenched Powder Metallurgica Ti—6AI—4V Alloy".	1129A	Crack Propagation Kinetics in Hydrogenous Environments.	2415-2428A
Powder metallurgy parts, Mechanical properties Fatigue Crack Propagation and Cryogenic Fracture Tough		Precipitation hardening steels, Corrosion The Influence of Palladium on the Hydrogen-Assisted Crack- ing Resistance of PH 13-8 Mo Stainless Steel.	2429-2443A
ness Behavior in Powder Metallurgy Aluminum—Lithium Alloys.	191-202A	Precipitation hardening steels, Phases (state of matter) Solute Distribution Around a Coherent Precipitate in a Multi-	
Crack Initiation and Propagation During High-Temperature Fatigue of Oxide Dispersion-Strengthened Superalloys.	837-851A	component Alloy.	2199-2210A
Powder Metallurgy T15 Tool Steel. II. Microstructure and Properties After Heat Treatment. Powder technology	2747-2759A	Precipitation hardening steels, Structural hardening Coarsening Resistance of M ₂ C Carbides in Secondary Hard- ening Steels. III. Comparison of Theory and Experiment.	2877-2888A
See Atomizing Powder metallurgy		Preferential attack (corrosion) See Intergranular corrosion	
Preparation of Monosized Ultrafine Particles of Precious		Pressing See Hot pressing	
Metals Utilizing an Emulsion-Type Liquid Membrane Tech nique.	397-404B	Pressure	
Powders See also Metal pourders		See High pressure Low pressure	
See also Metal powders Powders, Reactions (chemical)		Pressure casting Pressure Casting of a Zirconia-Toughened Alumian Fiber-	
Anomalous Combustion Effects During Mechanical Alloying Power generation	. 3019-3024A	Reinforced NiAl Composite. Pressure sintering	3059-3064A
See Electric power generation Power plants		See Hot pressing	
See Electric power generation		Pressure vessel components, Corrosion Delayed Hydride Cracking Behavior for Zircaloy-2 Tubing.	2049-2060A
Powerhouses See Electric power generation Practicus metal allows		Pressure vessels, Nondestructive testing The Evaluation of In-Service Materials Degradation of Low Alloy Steels by the Electrochemical Method.	2097-2106A
Precious metal alloys See Gold base alloys Silver base alloys		Pressureless sintering See Loose powder sintering	
Precious metals See Gold		Prestraining Yielding Behavior of Prestrained Interstitial-Free Steel and	1
Cibros		70/00 Page 1	202 404 4

Primary displacements See Displacements (lattice)		Quenching stresses See Residual stress	
Process control		Radar	
Magnetohydrodynamic Flows in a Channel-Induction Fur- nace.	193-209B	Microstructure of Ultrafine Carbonyl Iron Powder.	2709-2711A
Modeling Chemical Vapor Deposition of Silicon With Local Equilibrium Consideration at the Substrate. An Ultrasonic Method for Reconstructing the Two-	309-321B	Radiation damage A Simple, Versatile Miniaturized Disk-Bend Test Apparatus for Quantitative Yield-Stress Measurements.	2061-2068A
Dimensional Liquid/Solid Interface in Solidifying Bodies. Optimization and Continuous Casting, I. Problem Formulation	467-473B	Radiocrystallography See Crystallography	
and Solution Strategy. Optimization and Continuous Casting. II. Application to Industrial Casters.	641-648B 649-659B	Rapid solidification Fatigue Crack Propagation and Cryogenic Fracture Tough-	
The Coming-of-Age of Process Engineering in Extractive Metallurgy.	737-754B	ness Behavior in Powder Metallurgy Aluminum—Lithium Alloys.	191-202A
Prediction of Steel Flow Stresses at High Temperatures and	1545-1558A	A13-Type Phase Revealed in Rapidly Solidified High-Carbon Iron Alloy.	251-253A
Process metallurgy See Extractive metallurgy Refining		Plastic Deformation and Fracture of Binary TiAl-Base Alloys. Dynamic Compaction of Titanium Aluminides by Explosively Generated Shock Waves: Experimental and Materials Sys- tems.	427-439A 685-695A
Proof stress		Heat Flux Transients at the Casting/Chill Interface During So-	
Ductility and Dynamic Strain Aging in Rapidly Solidified Aluminum Alloys.	1021-1028A	lidification of Aluminum Base Alloys. Solidification of Undercooled Sn—Sb Peritectic Alloys. I. Microstructural Evolution.	717-727B 753-764A
Propagation See Crack propagation		Solidification of Undercooled Sn—Sb Peritectic Alloys. II. Heterogeneous Nucleation.	765-773A
Fropelier shafts See Shafts (power)		Structures and Tempering Behavior of Rapidly Solidified High-Carbon Iron Alloys.	775-782A
Properties (attributes)		Nonequilibrium Austenite/c-Phase Eutectic Revealed in Rap- idly Solidified High-Carbon Iron Alloy.	791-792A
See Surface properties Properzi process		On the Embrittlement of a Rapidly Solidified Al—Fe—V—Si Alloy After High-Temperature Exposure.	853-858A
See Continuous casting		Mathematical Modeling of the Isothermal Impingement of Liq- uid Droplets in Spraying Processes.	901-914B
Protective coatings Chemical Vapor Deposition Kinetics of Tungsten From WCl ₆		Microstructural Evolution in Rapidly Solidified Al—Fe Alloys: an Alternative Explanation.	927-934A
Onto Nickel Plate at Elevated Temperatures. Protective coatings, Phase transformations	560-563B	Ductility and Dynamic Strain Aging in Rapidly Solidified Aluminum Alloys.	1021-1028A
The Effect of Continuous Heating on the Phase Transformations in Zinc—Iron Electrodeposited Coatings.	1737-1743A	A New Phase in a Rapidly Solidified and Consolidated NbAl ₃ —1TiB ₂ Alloy.	1901-1909A
Puddling	1737-17438	Nonequilibrium Behavior in the Al—Ge Alloy Systems: Insights Into the Metastable Phase Diagram.	2141-2152A
See Ironmaking Purification		Modeling of Crystal Growth During Rapid Solidification. Structure and Properties of a Rapidly Solidified Al—Li—	2475-2485A
Desulfurization and Deoxidation of Cu—S—O Alloy in Induction Melting and Solidification Under Argon and Their Rates		Mn—Zr Alloy for High-Temperature Applications. I. Inert Gas Atomization Processing.	2503-2514A
of Elimination in Vacuum Induction Meiting.	405-416B	Structure and Properties of a Rapidly Solidified Al—Li— Mn—Zr Alloy for High-Temperature Applications. II. Spray Atomization and Deposition Processing.	2515-2522A
Pyrite, Oxidation The Electrochemical Behavior of a Semiconducting Nautral		Containerless Processing and Rapid Solidification of Nb—Si Alloys in the Niobium-Rich Eutectic Range.	
Pyrite in the Presence of Bacteria. Pyrite, Reduction (chemical)	765-774B	Containerless Processing and Rapid Solidification of Nb—Si Alloys of Hypereutectic Composition.	
The Electrochemical Behavior of a Semiconducting Nautral Pyrite in the Presence of Bacteria.	765-774B	Solidification of Highly Undercooled Fe—P Alloys. Measurements of Rapid Solidification Rate in Highly Undercooled Melts With a Video System.	2761-2768A
Pyroceram See Ceramics		Eutectic Growth Under Rapid Solidification Conditions.	3051-3057A
Pyrometallurgy Knowledge-Based Simulation and Identification of Various		Rare earth alloys See Lanthanum base alloys	
Metallurgical Reactors. Representation of Excess Thermodynamic Properties of Ter-	541-555B	Rare earth compounds See Cerium compounds	
nary Systems Using Interaction Parameters. Thermodynamics of Binary Systems Using Interaction Pa-	583-591B	Rare earth metals	
rameters.	593-605B	See Cerium Lanthanum	
Thermodynamics of Aluminum—Barium Alloys. The Wettability of Carbon/TiB ₂ Composite Materials by Alu-	607-616B	Rates	
minum in Cryolite Melts. The Coming-of-Age of Process Engineering in Extractive	617-621B	See Cooling rate Corrosion rate	
Metallurgy. Mathematical Modeling of Sulfide Flash Smelting Process. III.	737-754B	Growth rate Heating rate	
Volatilization of Minor Elements. Kinetics of the Reduction of Bushveld Complex Chromite Ore	791-799B	Strain rate	
at 1416°C.	801-810B	Wear rate Ratios	
A Reassesment of the Activity of Chromium in the Fe—Cr—O System at 1873K.	915-918B	See Phase ratio Poissons ratio	
Quaternary systems, Phases (state of matter) Thermodynamic Properties of the Fe—Mn—V—C System.	1911-1920A	Reaction kinetics	
A Thermodynamic Assessment of the Fe—Cr—Ni—C System.	2187-2198A	Slag—Metal Reactions During Welding, II. Theory. The Mass Transfer Kinetics of Niobium Solution Into Liquid	73-81B
Quench aging The Aging Effect on Cu—Zn—Al Shape Memory Alloys With		Steel. Deoxidation Rate of Copper Droplet Levitated in Ar—H ₂ Gas	417-427B 631-639B
Low Contents of Aluminum. Quench bend tests	25-33A	Stream. High-Temperature Thermodynamic Properties of the Vana dium Carbides V ₂ C and VC _{0,73} Determined Using a Gal	
See Bend tests		vanic Cell Technique. A Degenerate Electron Gas Model for Solutions of Aluminum	661-6688
Quenching (cooling) See also Oil guenching		in Cryolite Melts.	669-672B
Quenching and tempering		Gibbs Energy of Formation of Nickel Chromite. Phase Relations and Thermodynamics of the System Fe-	673-675B
The Aging Effect on Cu—Zn—Al Shape Memory Alloys With Low Contents of Aluminum.	25-33A	Cr_O in the Temperature Range of 1600-1825°C (1873	689-7038
Elastic Moduli and Tensile and Physical Properties of Heat- Treated and Quenched Powder Metallurgical Ti—6AI—4V		Oxygen Pressure Dependence of Cu ₂ O—CuO—Gd ₂ O	3
Alloy. Recrystallization and Superplasticity at 300°C in an	709-714A	The Conning-of-Age of Flocess Engineering in Extractive	705-710B
Aluminum—Magnesium Alloy. Correction to "Elastic Moduli and Tensile and Physical Prop-	1037-1047A	Leaching of Nickel From Supported Nickel Waste Catalys	
erties of Heat-Treated and Quenched Powder Metallurgica Ti—6AI—4V Alloy".	1129A	Using Aqueous Sulfur Dioxide Solution. Kinetics of the Reduction of Bushveld Complex Chromite Or	775-781B
Quenching and tempering		Intermetallic Phase Formation and Breakdown of Molybde	
The Effect of Tungsten on Dislocation Recovery and Precipi- tation Behavior of Low-Activation Martensitic 9Cr Steels. Effects of Vanadium and Processing Parameters on the	2225-2235A	num Diffusion Barriers in Ni—Mo—Cu Layers. Oxidation Kinetics of a Pb—30 at.% In Alloy. The Effect of Reaction Condition on Composition and Prope	1501-1510A 1865-1869A
Structures and Properties of a Direct-Quenched Low Carbon Mo—B Steel.	2359-2374A	ties of Ultrafine Amorphous Powders in (Fe,Co,Ni)—B Sys	3- 2125-2132A

The K ₂ ZrF ₆ Wetting Process: Effect of Surface Chemistry on the Ability of a SiC-Fiber Preform To Be Impregnated by Aluminum.	2133-2139A	Refractory alloys See Niobium base alloys Tungsten base alloys	
Anomalous Combustion Effects During Mechanical Alloying. Chemical Potential Diagram of Al—Ti—C System: Al ₄ C ₃ For-	3019-3024A	Refractory materials See Refractories	
mation on TiC Formed in Al—Ti Liquids Containing Carbon. Reaction kinetics, pH effects Dissolution of Malachite in Aqueous Ethylenediaminetetr- aacetate Solution.	3075-3076A 569-574B	Refractory metal compounds See Molybdenum compounds Niobium compounds	
Reactions (chemical) See also Combustion Decomposition reactions		Tantalum compounds Refractory metals See Chromium	
Deoxidizing Dephosphorizing Desulfurizing Dissolution Exothermic reactions		Molybdenum Niobium Tantalum Tungsten	
Interface reactions Oxidation		Vanadium Relaxation	
Slag—Metal Reactions During Welding. I. Evaluation and Re- assessment of Existing Theories.	65-71B 73-81B	See Stress relaxation Remelting	
Slag — Metal Reactions During Welding. II. Theory. Slag — Metal Reactions During Welding. III. Verification of the Theory. Real-Time Atomic-Level Observations of In Situ Chemical Re-	83-100B	See Melting Renn furnace See Direct reduction	
actions and Transformations Utilizing High-Resolution Electron Microscopy. Reactivity (chemical)	1323-1329A	Residual stress Instantaneous and Residual Stresses Developed in Hot Iso-	1071 10794
See Activity (chemical)		static Pressing of Metals and Ceramics. Residual stress, Deformation effects	1071-1078A
Reclamation See Recycling Recovering		Effect of Plastic Deformation on Residual Stresses in Ceramic/Metal Interfaces.	2822-2825A
The Dissolution Behavior of Metals From Ag/Cu and Ag/Au Alloys in Aidic and Cyanide Solutions. Leaching of Nickel From Supported Nickel Waste Catalyst	755-764B	Resins See Polymers Politage	
Using Aqueous Sulfur Dioxide Solution.	775-781B	See Corrosion resistance	
Processing Map for Hot Working of Alpha-Zirconium.	829-836A	Resistance welds See Welded joints	
Recrystallization See also Grain refinement Torsional Hot Workability in 0.47C—0.86Mn—0.5Cr—B		Resurfacing See Surfacing	
Steel From 650-870°C. Effect of Processing Variables on Texture and Texture Gradi-	469-477A	Retained austenite, Diffusion Effect of Retained Austenite on the Hydrogen Content and Ef-	
ents in Tantalum. Recrystallization Controlled Rolling and Accelerated Cooling	2039-2048A	fective Diffusivity of Martensitic Structure.	2579-2586A
for High Strength and Toughness in V—Ti—N Steels. Influence of Initial Ingot Breakdown on the Microstructural and Textural Development of High-Purity Tantalum.	2681-2694A 2959-2968A	Retained austenite, Heating effects Mechanical Properties and Retained Austenite in Intercriti- cally Heat-Treated Bainite-Transformed Steel and Their Variation With Silicon and Manganese Additions.	489-498A
Recrystallization, Deformation effects Recrystallization of Austenite After Deformation at High Temperatures and Strein Rates—Analysis and Modeling. Processing Map for Hot Working of Alpha-Zirconium. Recrystallization and Superplasticity at 300°C in an	151-160A 829-836A	Retained austenite, Phase transformations Transformation of Retained Austenite in Carburized 4320 Steel.	1491-1500A
Aluminum—Magnesium Alloy. High Strain Rate Superplasticity of a 25 wt.% Cr—7 wt.%	1037-1047A	Revaporization See Vaporizing	
Ni—3 wt.% Mo—0.14 wt.% N Duplex Stainless Steel. Development of a Necklace Microstructure During Isothermal	1083-1091A	Reviews Behavior of Metal Alloys in the Semisolid State.	269-294B
Deformation and Its Properties Relative to Uniform Micro- structures. Dynamic Recrystallization During Hot Deformation of Alumi-	1999-2008A	The Coming-of-Age of Process Engineering in Extractive Metallurgy.	737-754B
num: a Study Using Processing Maps. Effect of Interpass Time on Austenite Grain Refinement by Means of Dynamic Recrystallization of Austenite.	2339-2348A 2947-2957A	Behavior of Metal Alloys in the Semisolid State. Correction to "Literature Survey on Diffusivities of Oxygen Aluminum, and Vanadium in Alpha Titanium, Beta Titanium,	957-981A
Recrystallization, Temperature effects Establishment of a General Formula for Fractional Softening.	2160-2162A	and in Rutile". The Influence of Applied Stress, Crack Length, and Stress intensity Factor on Crack Closure.	1121-1125A 1559-1571A
Recycling A Thermodynamic Study of Dephosphorization Using BaO—BaF ₂ , CaO—CaF ₂ , and BaO—CaO—CaF ₂ Systems.	33-38B	Rheocasting Behavior of Metal Alloys in the Semisolid State. Rehavior of Metal Alloys in the Semisolid State.	269-294B
Red hardness See Hardness	00 002	Behavior of Metal Alloys in the Semisolid State. Rheological properties See Viscosity	957-981A
Reducing agents The Effect of Reaction Condition on Composition and Proper-		Rods	
ties of Ultrafine Amorphous Powders in (Fe,Co,Ni)—B Systems Prepared by Chemical Reduction.	2125-2132A	See Wire rod Roll force	
Reduction See Reduction (chemical)		See Roll load Roll load	
Reduction (chemical) See also Deoxidizing		The Thermal and Metallurgical State of Steel Strip During Hot Rolling. II. Factors Influencing Rolling Loads. Thermal Behavior of Steel Rolling With Nonconventional	321-333A
Direct reduction The Reduction Mechanism of a Natural Chromite at 1416°C. Preparation of Monosized Ultrafine Particles of Precious Metals Utilizing an Emulsion-Type Liquid Membrane Tech-		Rolls. Roll pressing See Rolling	1767-1774A
nique. Reduction (metal working) See Rolling	397-404B	Rolling See also Cold rolling	
Reduction of area, Microstructural effects The Role of the γ/γ Eutectic and Porosity on the Tensile Be		Controlled rolling Hot rolling Rolling direction	
havior of a Single-Crystal Nickel-Base Superalloy. Refining	1443-1451A	The Relationship Between Plastic Anisotropy of Steel Sheet and Temper Rolling Strain. A Simple Theory for the Development of Inhomogeneous	2156-2160A
See also Electrorefining Vacuum refining Desulfurization Kinetics of Molten Copper by Gas Bubbling.	5-11B	Rolling Textures. Effect of Interpass Time on Austenite Grain Refinement by	2637-2643A
Desulfurization Ninetics of Morten Copper by cas Bubbling. Desulfurization and Deoxidation of Cu—S—O Alloy in Induction Melting and Solidification Under Argon and Their Rate of Elimination in Vacuum Induction Melting.	>	Rolling direction	2947-2957A
Refractories, Synthesis		Orientation (001)[110] in Channel Die Compression.	45-58A
Enthalpies of Formation of Refractory Borides by High Temperature Direct Synthesis Calorimetry: RuB _{1.1} an		Rolling ingots, Microstructure Influence of Initial Ingot Breakdown on the Microstructural	2050 20684

Rolling mill rolls, Service life Thermal Behavior of Steel Rolling With Nonconventional		Growth Kinetics of Solid/Liquid Gallium Interfaces. II. Theoretical.	1271-1286A
Rolls. Rolling texture	1767-1774A	Seeding See Nucleation	
Analysis of an Aluminum Single Crystal With Unstable Initial Orientation (001)[110] in Channel Die Compression. A Simple Theory for the Development of Inhomogeneous	45-58A	Segregations Determination of Liquid Diffusion Coefficients Along a	04.000
Rolling Textures. Influence of Initial Ingot Breakdown on the Microstructural	2637-2643A	Liquidus Phase Boundary. Microstructurally Toughened Particulate-Reinforced Alumi- num Matrix Composites.	21-26B 171-182A
and Textural Development of High-Purity Tantalum. Rolling texture, Deformation effects	2959-2968A	X-Ray Microanalysis of Phosphorus Segregation in Type 304L Stainless Steels.	253-255A
Effect of Processing Variables on Texture and Texture Gradi- ents in Tantalum.	2039-2048A	Simultion of Freckles During Vertical Solidification of Binary Alloys.	847-859B
Rolls		Surface Composition of Ternary Cu—Ay—Au Alloys. I. Experimental Results.	1833-1840A
See Rolling mill rolls Rotating beam fatigue tests		Surface Composition of Ternary Cu—Ag—Au Alloys. II. A Comparison of Experiment With Theoretical Models.	1841-1848A
See Fatigue tests Rotors, Mechanical properties		Lattice Changes of Iron—Carbon Martensite on Aging at Room Temperature.	1957-1967A
Effect of Long-Term Service Exposure on Microstructure and Mechanical Properties of a CrMoV Steam Turbine Rotor Steel.	1811-1820A	Segregations, Alloying effects The Effect of Temperature and Nitrogen Content on the Partitioning of Alloy Elements in Duplex Stainless Steels.	2173-2179A
Roughing (rolling) See Hot rolling		The Reduction of the Interfacial Segregation of Phosphorus and its Embrittlement Effect by Lanthanum Addition in a	0000 00744
Roughness Micromechanics of Shear Ligament Toughening.	2021-2029A	W—Ni—Fe Heavy Alloy. Segregations, Cooling effects Numerical Simulation of a Solidifying Pb—Sn Alloy: the Ef-	2969-2974A
Rupture modulus See Modulus of rupture		fects of Cooling Rate on Thermosolutal Convection and Macrosegregation.	529-540B
Rupture strength		Study on Formation of Channel-Type Segregation.	1663-1672A
See Creep rupture strength Ruthenium compounds, Mechanical properties Mechanicai, Elastic, and Structural Properties of Alloys of		Segregations, Deformation effects Mechanisms of Deformation-Induced Grain Boundary Chro- mium Depletion (Sensitization) Development in Type 316 Stainless Steels.	2917-2934A
Ru—Ta High-Temperature Intermetallic Compounds. Mechanical Properties of High Temperature Alloys of AIRu.	129-137A 403-414A	Segregations, High temperature effects	
Rutile, Diffusion Correction to "Literature Survey on Diffusivities of Oxygen		Grain Boundary Pest of Boron-Doped Ni ₃ Al at 1200°C. Segregations, Impurity effects	1801-1809A
Aluminum, and Vanadium in Alpha Titanium, Beta Titanium, and in Rutile".	1121-1125A	Effect of Sulfur Removal on Al ₂ O ₃ Scale Adhesion. Segregations, Welding effects	739-752A
S N diagrams Finite Element Prediction of the Fatique Limit of Steel.	1678-1680A	Solidification Modeling and Solid-State Transformations in High-Energy Density Stainless Steel Welds.	915-926A
Saline water See Salt water		Carbide Precipitation in Welds of Two-Phase Austenitic— Ferritic Stainless Steel.	2889-2902A
Salt water, Environment		Self diffusion See Diffusion	
A Critical Evaluation of the Stress-Corrosion Cracking Mech- anism in High-Strength Aluminum Alloys. Environmental Fatigue of an Al—Li—Cu Alloy. I. Intrinsic Crack Propagation Kinetics in Hydrogenous Environments.	2407-2414A 2415-2428A	Self lubrication Tribological Behavior and Surface Analysis of Tribodeformed Al Alloy—50% Graphite Particle Composites.	1435-1441A
Sand casting See Dry sand casting	2410-24201	Semiconductors See also Germanium	
Sand castings Contribution to the Metal/Mold Interfacial Heat Transfer.	729B	Silicon Thermodynamical Study of Gas Transport in Thin Film Growth: Application to Bismuth Chalcogenides.	2401-2405A
Sandwich construction, Mechanical properties Vibration Damping Characteristics of Laminated Steel Sheet.	653-656A	Semicontinuous casting See Continuous casting	
Sap process See Dispersion hardening		Semikilling	
Scandium base alloys, Reactions (chemical)		See Deoxidizing Sensible heat	
Thermochemistry of Binary Alloys of Transition Metals: the Me—Sc, Me—Y, and Me—La (Me = Silver, Gold) Sys-	1103-1111A	See Enthalpy Sensitivity	
tems Schottky effect	1103-1111A	See Notch sensitivity	
See Work functions Scorification		Sensitizing, Deformation effects Mechanisms of Deformation-Induced Grain Boundary Chro-	
See Fluxing		mium Depletion (Sensitization) Development in Type 316 Stainless Steels.	2917-2934A
Scrap See Metal scrap		Separation See Extraction	
Scrap metal See Metal scrap		Slagging Service life	
Scrap steel		Fracture Toughness Behavior of Ex-Service 2.25Cr—1Mo Steels From a 22-Year-Old Fossil Power Plant.	455-468A
See Steel scrap Season cracking		Effect of Long-Term Service Exposure on Microstructure and Mechanical Properties of a CrMoV Steam Turbine Rotor	455-4007
See Stress corrosion cracking Secondary displacements		Steel.	1811-1820A
See Displacements (lattice)		Shafts (power), Forming Influence of Microstructure on Centerburst Development in	807-815A
Secondary hardening Comparison of Secondary Hardening Embrittlement in Tung- sten and Molybdenum Steels.	1119-1122A	Steel Extrusions. Shape See Particle shape	807-613A
The Effect of Tungsten on Dislocation Recovery and Precipi- tation Behavior of Low-Activation Martensitic 9Cr Steels.	2225-2235A	Shape memory, Heating effects	
Coarsening Resistance of M ₂ C Carbides in Secondary Hard- ening Steels. I. Theoretical Model for Multicomponent Coarsening Kinetics.	2863-2868A	Effects of Thermal Cycling on the Martensitic Transformation in Two-Phase α/β Brasses.	1473-1478A
Coarsening Resistance of M ₂ C Carbides in Secondary Hard- ening Steels. II. Alloy Design Aided by a Thermochemica Database.	i	Shape memory, Stress effects The Shape Memory Effect and Superelasticity in Two-Phase Polycrystalline α/β Brasses.	1479-1490A
Coarsening Resistance of M ₂ C Carbides in Secondary Hard- ening Steels. III. Comparison of Theory and Experiment.	2869-2876A 2877-2888A	Shape memory alloys, End uses Thermal and Mechanical Considerations in Using Shape Memory Alloys to Control Vibrations in Flexible Structures.	623-627A
Secondary ion mass spectroscopy Secondary Ion Mass Spectrometry Method for Distinguishing the State of Carbon in Steels Using Negative Molecula	9	Shape memory alloys, Heat treatment The Aging Effect on Cu—Zn—Al Shape Memory Alloys With	
lons.	1969-1978A	Low Contents of Aluminum.	25-33A
Seebeck effect Growth Kinetics of Solid/Liquid Gallium Interfaces. I. Experimental.	1259-1270A	Shear modulus Stress Concentration at a Notch Tip in Unidirectional Metal Matrix Composites.	2085-2095A

Shear modulus, Composition effects Third-Order Bounds on the Elastic Moduli of Metal-Matrix Composites.	3065-3067A	Silicon steels, Corrosion The Kinetics and Micromechanics of Hydrogen-Assisted Cracking in Fe—3% Si Single Crystals.	59-70A
Shear properties See Shear modulus		Silicon steels, Mechanical properties Comparison of Fracture Behavior in Intercritically Treated	1115-1119A
Shear strength Shear strength Stress Concentration at a Notch Tip in Unidirectional Metal		Silver, Crystal growth Observations of the Formation and Kinetics of Surface Steps	
Matrix Composites. The Anisotropic Mechanical Properties of a Titanium Matrix Composite Reinforced With SiC Fibers.	2085-2095A 2975-2984A	During Evaporation and Condensation. Silver, Extraction The Electrochemical Behavior of a Semiconducting Nautral	1299-1304A
Sheet metal, Coating The Effect of Continuous Heating on the Phase Transformations in Zinc—Iron Electrodeposited Coatings.	1737-1743A	Pyrite in the Presence of Bacteria. Silver, Recovering The Dissolution Behavior of Metals From Ag/Cu and Ag/Au	765-774B
Sheet metal, Composite materials Vibration Damping Characteristics of Laminated Steel Sheet.	653-656A	Alloys in Aidic and Cyanide Solutions. Silver base alloys, Corrosion	755-764B
Sheet metal, Forming A Theoretical Sensitivity Analysis for Full-Dome Formability		Brittle Fracture of an Au/Ag Alloy Induced by a Surface Film. Silver base alloys, Crystal growth	531-541A
Tests: Parameter Study for n, m, r, and μ . Effect of Processing Variables on Texture and Texture Gradients in Tantalum.	1775-1788A 2039-2048A	Modeling of Crystal Growth During Rapid Solidification. Silver base alloys, Reactions (chemical)	2475-2485A
Finite Element Modeling Simulation of In-Plane Forming Limit Diagrams of Sheets Containing Finite Defects.	2655-2665A	Thermochemistry of Binary Alloys of Transition Metals: the Me—Sc, Me—Y, and Me—La (Me = Silver, Gold) Systems	1103-1111A
Sheet metal, Mechanical properties Development of Vibration-Damping Resins for Room- Temperature Application.	629-631A	Simulation See also Computer simulation Heat-Flow Simulation of Laser Remelting With Experimental	
Sheet steel		Validation. An Improved Mathematical Model for Electromagnetic Cast-	101-109B
See Strip steel Sherritt Gordon process		ers and Testing by a Physical Model. Microstructure and Local Brittle Zone Phenomena in High-	121-134B
See Alkaline leaching Extraction		Strength Low-Alloy Steel Welds. Recrystallization of Austenite After Deformation at High Tem-	139-149A
Hydrometallurgy		peratures and Strain Rates—Analysis and Modeling. Effects of Material Rate Sensitivity and Void Nucleation on	151-160A
See Continuous coating		Fracture Initiation in a Circumferentially Cracked Bar. The Effects of Interface Attachment Kinetics on Solidification	161-170A
Shipbuilding Effect of Killing Time on the Microstructure and Toughness of the Heat-Affected Zone in Titanium-Killed Steels.	2818-2822A	Interface Morphologies. Composite Growth in Hypermonotectic Alloys. In Situ Observation of Interactions Between Gaseous Inclu-	235-249A 339-348B
Shock resistance, Microstructural effects		sions and an Advancing Solid/Liquid Interface. Mixing Characteristics of a Submerged Jet Measured Using	385-388B
On Thermal Shock Resistance of Austenitic Cast Irons. Shock waves	1821-1831A	an Isokinetic Sampling Probe. Knowledge-Based Simulation and Identification of Various	439-445B
Dynamic Compaction of Titanium Aluminides by Explosively Generated Shock Waves: Experimental and Materials Sys-		Metallurgical Reactors. The Effects of Interface Kinetics Anisotropy on the Growth	541-555B
tems. Silicon, Alloying elements	685-695A	Direction of Cellular Microstructures. Simultion of Freckles During Vertical Solidification of Binary Alloys.	585-593A 847-859B
Effects of Microalloying Elements and Heat Treatments on Tensile Properties in Cu—23Zn—3.4Al—1Ni—X Alloys.	256-258A	In Situ Observation of Faceted Cellular Array Growth. Correction to "In Situ Observation of Faceted Cellular Array	941-945A
On the Nature of Eutectic Carbides in Cr—Ni White Cast Irons.	1709-1720A	Growth". Nonequilibrium Effects During the Ledgewise Growth of a	941-945A 1249-1258A
Silicon, Crystal growth Observations of the Formation and Kinetics of Surface Steps		Solid/Liquid Interface. The Influence of Applied Stress, Crack Length, and Stress In-	
During Evaporation and Condensation.	1299-1304A	tensity Factor on Crack Closure. In Situ Observation of Nonfaceted Cellular Growth in a Nar-	1559-1571A 1683-1687A
Silicon, Oxidation Interface Dislocations and Ledges in Oxidation and Diffusional Phase Transformations.	1331-1339A	row Channel. Simulation of the Effect of Texture on Limit Strain in Biaxially Stretched Steel Sheet. Finite Element Modeling Simulation of In-Plane Forming Limit	2069-2076A
Silicon, Ternary systems An Assessment of the Fe—C—Si System.	2211-2223A	Diagrams of Sheets Containing Finite Defects.	2655-2665A
Silicon carbide, Composite materials The Effect of Particulate SiC on Fatigue Crack Growth in a		Single crystals, Composite materials In Situ Formation of Three-Dimensional TiC Reinforcements in Ti-TiC Composites.	859-865A
Cast-Extruded Aluminum Alloy Composite. Tensile Deformation and Fracture Toughness of	97-112A	Single crystals, Corrosion The Kinetics and Micromechanics of Hydrogen-Assisted	
2014 + 15 vol.% SiC Particulate Composite. Microstructurally Toughened Particulate-Reinforced Alumi-		Cracking in Fe—3% Si Single Crystals.	59-70A
num Matrix Composites. Dynamic Fracture Behavior of SiC Whisker-Reinforced Aluminum Alloys.	367-375A	Single crystals, Crystal growth Growth Kinetics of Solid/Liquid Gallium Interfaces. I. Experi- mental.	1259-1270A
Thermomechanical Fatigue of Particulate-Reinforced Aluminum 2xxx-T4.	697-707A	Growth Kinetics of Solid/Liquid Gallium Interfaces. II. Theoretical.	1271-1286A
Fatigue Behavior of a 2xxx Series Aluminum Alloy Reinforced With 15 vol.% SiCp.	1007-1019A	Ledgewise Vaporization. Single crystals, Forming	1305-1310A
Mechanical Behavior of Cast Particulate SiC/AL (A356) Meta Matrix Composites. The Mechanical Behavior of a Hybrid Metal Matrix Compos-	1585-1593A	Earing in Cup Drawing Face-Centered Cubic Single Crystals and Polycrystals.	1525-1534A
ite. Microstructure Property Relationships and Hydrogen Effects		Single crystals, Mechanical properties Faceted Fatigue Fracture and Its Relation to the Crystallo-	
in a Particulate-Reinforced Aluminum Composite. The Anisotropic Mechanical Properties of a Titanium Matrix	2445-2450A	graphic Slip Systems in Cu—16 at.% Al Single Crystals. Analysis of Crack Tip Sliding Displacement in Anisotropic	415-425A
Composite Reinforced With SiC Fibers. Third-Order Bounds on the Elastic Moduli of Metal-Matrix		Elastic Media and Its Application to Stage I Fatigue Crack Growth.	479-487A
Composites. Silicon carbide, Reactions (chemical)	3065-3067A	Fracture of Single Crystals of the Nickel-Base Superalloy PWA 1480E in Helium at 22°C.	731-738A
The K ₂ ZrF ₈ Wetting Process: Effect of Surface Chemistry or the Ability of a SiC-Fiber Preform To Be Impregnated by		The Role of the γ/γ Eutectic and Porosity on the Tensile Behavior of a Single-Crystal Nickel-Base Superalloy.	1443-1451A
Aluminum.	2133-2139A	1000 to 1200K Time-Dependent Compressive Deformation of Single-Crystalline and Polycrystalline B2 Ni—40Al.	1595-1607A
Silicon compounds See also Silicon carbide		Fracture of Single Crystals of the Nickel-Base Superalloy PWA 1480E in Hydrogen at 22°C. Hydrogen Effects on Low-Cycle Fatigue of the Single-Crystal	2031-2038A
Silicon nitride Silicon compounds, Metal working		Nickel-Base Superalloy CMSX-2.	2597-2603A
Strength and Ductile-Phase Toughening in the Two-Phase Nb/Nb ₅ Si ₃ Alloys. Silicon iron	1573-1583A	Single crystals, Microstructure The Mechanisms and Temperature Dependence of Superlat- tice Stacking Fault Formation in the Single-Crystal Superal-	
See Silicon steels		loy PWA 1480. Single crystals, Rolling	2309-2318A
Silicon nitride, Mechanical properties On the Mechanism of Fatigue Crack Growth in Silicon Nitride	. 1425-1434A	Analysis of an Aluminum Single Crystal With Unstable Initial Orientation (001)[110] in Channel Die Compression.	45-58A

Single crystals, Structural hardening Toward a Sound Understanding of Dislocation Plasticity.	1693-1708A	Slag Foaming in Bath Smelting. Smelting, Impurity effects	481-489B
Sintered compacts, Corrosion Active and Passive Behavior of Sintered Iron in Ammoniacal Ammonium Carbonate Solution.	222 2220	Thermochemical Nature of Minor Elements in Copper Smett- ing Mattes.	677-6888
Sintered compacts, Mechanical properties Shock Densification/Hot Isostatic Pressing of Titanium Alumi-	323-332B	SN diagrams See S N diagrams	
nide. Sintering (powder metallurgy)	2667-2676A	Sodium, Binary systems Thermodynamics of Binary Systems Using Interaction Parameters.	593-605B
See Liquid phase sintering Loose powder sintering		Sodium, Solubility A Degenerate Electron Gas Model for Solutions of Aluminum	
Sites See Lattice sites		in Cryolite Melts.	669-672B
Size distribution (particle) See Particle size distribution		See Cryolite	
Skull casting See Casting		Soft annealing See Annealing	
Siab casting Mold Behavior and Its Influence on Quality in the Continuous		Soft solders See Solders	
Casting of Steel Slabs. I. Industrial Trials, Mold Tempera- ture Measurements, and Mathematical Modeling. Mold Behavior and Its Influence on Quality in the Continuous Casting of Steel Slabs. II. Mold Heat Transfer, Mold Flux	861-874B	Softening See also Strain softening Low-Cycle Fatigue Behavior of Nimonic PE16 at Room Temperature.	499-506/
Behavior, Formation of Oscillation Marks, Longitudinal Off- Corner Depressions, and Subsurface Cracks.	875-888B	Strain Distribution Effects on the Low-Cycle Fatigue Behavior of Fe—C—Mo Steels.	675-683
Slabbing (rolling) See Rolling Slagging		Soldered joints, Mechanical properties Environmental and Hold Time Effects on Fatigue of Low-Tin Lead-Based Solder.	357-366/
The Effect of Na ₂ O on Dephosphorization by CaO-Based St- eelmaking Slags. Activities of Chromium in Molten Copper at Dilute Concentra-	39-46B	Solders, Mechanical properties Environmental and Hold Time Effects on Fatigue of Low-Tin	
tions by Solid-State Electrochemical Cell. Thermodynamic Behavior of Phosphorus in CaO—CaF ₂ —	475-480B	Lead-Based Solder. Solders, Oxidation	357-366/
SiO ₂ and CaO—Na ₂ O—SiO ₂ Systems. Siags See also Blast furnace slags	499-502B	Oxidation Kinetics of a Pb—30 at.% In Alloy. Solid phases An Ultrasonic Method for Reconstructing the Two-	1865-1869/
Fluid Flow Through Lances With Constant and Variable Pitch Swirled Inserts.	13-20B	Dimensional Liquid/Solid Interface in Solidifying Bodies.	467-473
A Mathematical Model of the Nickel Converter. I. Model De- velopment and Verification. Correlation of Geometric Factor for Slag Resistance Electric	153-161B	Solid solubility Thermodynamic Properties of the Fe—Mn—V—C System. The Formation of Metastable Phases by Mechanical Alloying	1911-1920
Furnaces. Equilibrium Phase Relations and Thermodynamics of the Cr—O System in the Temperature Range of 1500°C to	183-192B	in the Aluminum and Copper System. Solid solubility, Pressure effects	2849-2854
1825°C. Monitoring of Slag Composition Changes by Density Measurements.	225-232B 305-307B	Solid Solubilities of Manganese and Titanium in Aluminum at 0.1 MPa and 2.1 GPa. Solid solutions, Diffusion	783-786
The Thermodynamic Behavior of Sulfur in BaO—BaF ₂ Slags. Slag Foaming in Bath Smelting. The Redox Equilibria of Copper Ions in the Molten Silicate	333-338B 481-489B	On the Kinetics of Diffusion-Limited Layer Growth in Solid— Solid Systems.	523-527
Fluxes as a Measure of Basicity. Slags, Reactions (chemical)	823-829B	Solid solutions, Mechanical properties Surface Void Nucleation Under the Power-Law Creep Condi- tion in an AI—3 at.% Mg Solid Solution Alloy.	935-937
Slag—Metal Reactions During Welding. I. Evaluation and Re- assessment of Existing Theories. Slag—Metal Reactions During Welding. II. Theory.	65-71B 73-81B	Solidification See also Directional solidification	
Slag—Metal Reactions During Welding. III. Verification of the Theory.	83-100B	Rapid solidification Experimental Determination of the Phase Equilibria of	203-213
Removal of Nitrogen From Steel Using Novel Fluxes. A Thermodynamic Study of the System Fe _x O + Al ₂ O ₃ + SiO ₂ at 1673K.	783-790B 839-845B	Aluminum-Rich Al—Li—Cu Alloys. Application of Thermodynamic Models to the Calculation of Solidification Paths of Aluminum-Rich Al—Li Alloys.	267-27
Silp See also Cross slip	039-0435	Behavior of Metal Alloys in the Semisolid State. A Volume-Averaged Two-Phase Model for Transport Phe-	269-29- 349-36
Slip planes Mechanical Properties of High Temperature Alloys of AIRu.	403-414A	nomena During Solidification. Numerical Simulation of a Solidifying Pb—Sn Alloy: the Effects of Cooling Rate on Thermosolutal Convection and	
Faceted Fatigue Fracture and Its Relation to the Crystallo- graphic Slip Systems in Cu—16 at.% Al Single Crystals. Plastic Deformation and Fracture of Binary TIAl-Base Alloys.	415-425A 427-439A	Macrosegregation. Crystallization of a Faceted Primary Phase in a Stirred Slurry. Contribution to the Metal/Mold Interfacial Heat Transfer.	529-546 575-58- 729
Fatigue Behavior in the Potentiostatic Passive Corrosion Re- gime of the Iron-Base Superalloy A-286.	513-519A	The Energy and Solute Conservation Equations for Dendritic Solidification.	889-900
Fracture of Single Crystals of the Nickel-Base Superalloy PWA 1480E in Helium at 22°C. On the Influence of Microstructure on the Room-Temperature	731-738A	Solidification Modeling and Solid-State Transformations in High-Energy Density Stainless Steel Welds.	915-92 957-98
Deformation Behavior of a Near- α Titanium Alloy. The Role of the γ/γ' Eutectic and Porosity on the Tensile Be-	1122-1125A	Behavior of Metal Alloys in the Semisolid State. Evolution of Boride Morphologies in TiAl—B Alloys. Interrupted and Isothermal Solidification Studies of Low and	1647-166
havior of a Single-Crystal Nickel-Base Superalloy. Toward a Sound Understanding of Dislocation Plasticity.	1443-1451A 1693-1708A	Medium Carbon Steels. Solidification and Phase Equilibria in the Fe—C—Cr—NbC	1871-188
A Simple Theory for the Development of Inhomogeneous Rolling Textures.	2637-2643A	System. Nucleation of Solidification in Liquid Droplets.	2181-2180 2487-250
Slip, Corrosion effects Intergranular Stress Corrosion Cracking of Alloy 600 and X- 750 in High-Temperature Deaerated Water/Steam.	1857-1864A	Solidification, Microstructural effects Effect of Grain Boundaries on Isothermal Solidification During Transient Liquid Phase Brazing.	1627-1631
Slip, Cryogenic effects Fatigue and Fracture Behavior of an Aluminum—Lithium		Solubility See also Solid solubility	
	723-729A	Correction to "Nitrogen Solubility in Solid Niobium". Thermochemistry and Diffusion of Nitrogen in Solid Molybde- num.	219-22
Alloy 8090-T6 at Ambient and Cryogenic Temperature. Slip, Deformation effects		Representation of the Solubility of Lead Chloride in Various	
Alloy 8090-T6 at Ambient and Cryogenic Temperature. SIIP, Deformation effects Processing Map for Hot Working of Alpha-Zirconium. Silip planes	829-836A	Chloride Solutions With Pitzer's Model.	491-49
Alloy 8090-T6 at Ambient and Cryogenic Temperature. Silip, Deformation effects Processing Map for Hot Working of Alpha-Zirconium. Silip planes Effect of Phase Morphology on the Mechanical Behavior of Two Titanium Aluminide Composites.	2009-2019A	A Degenerate Electron Gas Model for Solutions of Aluminum in Cryolite Melts.	
Alfoy 8090-T6 at Ambient and Cryogenic Temperature. Slip, Deformation effects Processing Map for Hot Working of Alpha-Zirconium. Slip planes Effect of Phase Morphology on the Mechanical Behavior of	2009-2019A 2021-2029A	A Degenerate Electron Gas Model for Solutions of Aluminum	491-498 669-672 2199-2210
Alfoy 8090-T6 at Ambient and Cryogenic Temperature. Slip, Deformation effects Processing Map for Hot Working of Alpha-Zirconium. Slip planes Effect of Phase Morphology on the Mechanical Behavior of Two Titanium Aluminide Composites. Micromechanics of Shear Ligament Toughening. Fracture of Single Crystals of the Nickel-Base Superalloy	2009-2019A 2021-2029A 2031-2038A	A Degenerate Electron Gas Model for Solutions of Aluminum in Cryolite Melts. Solutes Solute Distribution Around a Coherent Precipitate in a Multi-	669-672

Solution heat treatment Elastic Moduli and Tensile and Physical Properties of Heat-		Squeeze casting Chemical Stability of Zirconia-Stabilized Alumina Fibers Dur-	2855-2862A
Treated and Quenched Powder Metallurgical Ti—6AI—4V Alloy.	709-714A	ing Pressure Infiltration by Aluminum. Stability	2000-2002A
High Strain Rate Superplasticity of a 25 wt.% Cr—7 wt.% Ni—3 wt.% Mo—0.14 wt.% N Duplex Stainless Steel. Correction to "Elastic Moduli and Tensile and Physical Properties of Heat-Treated and Quenched Powder Metallurgical	1083-1091A	See also Phase stability Thermal stability Kinetic Equations for Concurrent Size and Shape Coarsening	1381-1390A
Ti—6AI—4V Alloy". Solution potential	1129A	by the Ledge Mechanism. Stabilizers (agents) Effect of Hydrogen as a Temporary β Stabilizer on Micro-	1301-1390A
See Corrosion potential Solution strengthening, Alloying effects		structure and Brittle Fracture Behavior in a Titanium Alumi- nide Alloy.	71-81A
In Situ Formation of Three-Dimensional TiC Reinforcements in Ti-TiC Composites. Solutions	859-865A	Stacking faults, Deformation effects The Mechanism and Temperature Dependence of Superlattice Stackings and Temperature Dispersion of Superlation of the Single-Crystal Superalloy PWA 1480.	2309-2318A
See Solid solutions Solvus (metallurgical) See Solid solubility		Stainless steels See also Austenitic stainless steels	
Sonics		Duplex stainless steels Stainless steels, Casting	
See Ultrasonics Sorption See Absorption (energy) Adsorption		Optimization and Continuous Casting. I. Problem Formulation and Solution Strategy. Optimization and Continuous Casting. II. Application to In- dustrial Casters.	641-648B 649-659B
Sound waves See Shock waves		Stainless steels, Corrosion The Influence of Palladium on the Hydrogen-Assisted Cracking Resistance of PH 13-8 Mo Stainless Steel.	2429-2443A
Space environment Composite Growth in Hypermonotectic Alloys. Gravitational Limit of Particle Volume Fraction in Liquid-	339-348B	Stainless steels, Joining Effect of Plastic Deformation on Residual Stresses in Ceramic/Metal Interfaces.	2822-2825A
Phase Sintering. Space ships See Spacecraft	786-791A	Stainless steels, Steel making A Thermodynamic Study of Dephosphorization Using BaO—	
Space vehicles See Spacecraft		BaF ₂ , CaO—CaF ₂ , and BaO—CaO—CaF ₂ Systems. Static casting See Casting	33-38B
Spacecraft, Materials selection On the Influence of Ply-Angle on Damping and Modulus of		Static fatigue See Creep rupture strength	
Elasticity of a Metal-Matrix Composite. Spacing	641-651A	Static pressure	
On the Rate of Dendrite Arm Coarsening. In Situ Formation of Three-Dimensional TiC Reinforcements	569-574A	See Hydrostatic pressure Statistical analysis	
in Ti-TiC Composites. The Role of Ledges in the Proeutectoid Ferrite and Proeutec-	859-865A	Computer Simulation of the Effect of Coherency Strain on Cluster Growth Kinetics. Eutectic Spacing Selection in Lead-Based Alloy Systems.	1197-1209A 2523-2533A
toid Cementite Reactions in Steel. Correction to On the Rate of Dendrite Arm Coarsening". Eutectic Spacing Selection in Lead-Based Alloy Systems.	1367-1380A 1466A 2523-2533A	Statistical Analysis of the Disorder of Two-Dimensional Cellu- lar Arrays in Directional Solidification.	3041-3050A
Spalling, Impurity effects Effect of Sulfur Removal on Al ₂ O ₃ Scale Adhesion.	739-752A	Statistical methods Growth Path Envelope Analysis of Ostwald Ripening. Correction to "Growth Path Envelope Analysis of Ostwald Ri-	19-23A
Specific density See Density		pening". Steel alloys	19-23A
Specific gravity See Density		See Alloy steels Steel constituents	
Specific volume See Density		See Austenite Bainite	
Specific weight See Density		Cementite Ferrite Martensite	
Specimen preparation Use of Differential Interference Contrast Microscopy to Detect Duplex Carbides in Alloy White Cast Irons.	1673-1674A	Pearlite Steel making The Effect of Na ₂ O on Dephosphorization by CaO-Based St-	
Speiter See Zinc		eelmaking Slags. Gibbs Energy of Formation of Nickel Chromite.	39-46B 673-675B
Spheroidal graphite See Nodular graphitic structure		Phase Relations and Thermodynamics of the System Fe— Cr—O in the Temperature Range of 1600-1825°C (1873- 2098K) Under Strongly Reducing Conditions.	689-703B
Spheroidal iron See Nodular iron		Removal of Nitrogen From Steel Using Novel Fluxes. A Thermodynamic Study of the System Fe _x O + Al ₂ O ₃ + SiO ₂ at 1673K.	783-790B 839-845B
Spheroidal structure See Nodular graphitic structure		An Assessment of the Fe—C—Si System. Steel scrap, Recovering	2211-2223A
Spheroidizing Hydrogen-Assisted Ductile Fracture in Spheroidized 1520	1045 40004	A Thermodynamic Study of Dephosphorization Using BaO—BaF ₂ , CaO—CaF ₂ , and BaO—CaO—CaF ₂ Systems.	33-38B
Steel. II. Pure Bending. Splat cooling	1615-1626A	Steels See also Alloy steels Carbon steels	
Nonequilibrium Austenite/c-Phase Eutectic Revealed in Rap- idly Solidified High-Carbon Iron Alloy. Microstructural Evolution in Rapidly Solidified Al—Fe Alloys: an Alternative Explanation.	791-792A 927-934A	Dual phase steels Structural steels Tool steels	
Containerless Processing and Rapid Solidification of Nb—Si Alloys in the Niobium-Rich Eutectic Range. Containerless Processing and Rapid Solidification of Nb—Si Alloys of Hypereutectic Composition.	2713-2721A 2723-2732A	Steels, Casting Behavior of Metal Alloys in the Semisolid State. Contribution to the Metal/Mold Interfacial Heat Transfer. Behavior of Metal Alloys in the Semisolid State.	269-294B 729B 957-981A
Sponginess See Porosity		Steels, Coating The Effect of Continuous Heating on the Phase Transforma-	00,-201A
Spray forming Mathematical Modeling of the Isothermal Impingement of Lig-		tions in Zinc—Iron Electrodeposited Coatings. Activation Energy of δ-Γ ₁ Transformation in a Zn—Fe Electrodeposited Coating.	1737-1743A 1887-1888A
uid Droplets in Spraying Processes. Spraying	901-914B	Steels, End uses	1007-1000A
See also Spray forming Structure and Properties of a Rapidly Solidified AI—Li— Mn—Zr Alloy for High-Temperature Applications. II. Spray		Heat Flux Transients at the Casting/Chill Interface During So- lidification of Aluminum Base Alloys. Steels, Forging	717-727B
Atomization and Deposition Processing.	2515-2522A	Establishment of a General Formula for Fractional Softening.	2160-2162A
Spring alloys, Alloy development Effects of Microalloying Elements and Heat Treatments on		Steels, Forming A Theoretical Sensitivity Analysis for Full-Dome Formability	

Steels, Mechanical properties Yielding Behavior of Prestrained Interstitial-Free Steel and 70/30 Brass.	393-401A	Stress Concentration at a Notch Tip in Unidirectional Metal Matrix Composites. Hydrostatic Stresses and Their Effect on the Macroflow Be-	2085-2095A
Development of Vibration-Damping Resins for Room- Temperature Application.		havior and Microfracture Mechanism of Two-Phase Alloys.	2695-2702A
The Influence of Applied Stress, Crack Length, and Stress Intensity Factor on Crack Closure.	629-631A 1559-1571A	Stress concentration Effects of Material Rate Sensitivity and Void Nucleation on Fracture Initiation in a Circumferentially Cracked Bar.	161-170A
Steels, Microstructure The Role of Ledges in the Proeutectoid Ferrite and Proeutec-		Stress Concentration at a Notch Tip in Unidirectional Metal Matrix Composites.	2085-2095A
toid Cementite Reactions in Steel. Discussion of "A Mechanism for the Formation of Lower Bai-	1367-1380A	Stress corrosion See Corrosion fatique	
nite" and Authors' Reply.	1674-1678A	Stress corrosion cracking	
Steels, Phases (state of matter) Effect of Phosphorus on Carbon Activity, Carbide Precipitation, and Coarsening in Ferritic Fe—C—P Alloys.	35-43A	The Kinetics and Micromechanics of Hydrogen-Assisted Cracking in Fe—3% Si Single Crystals. Hydrogen Compatibility of Femnal Alloys.	59-70A 215-224A
Steels, Powder technology Instantaneous and Residual Stresses Developed in Hot Isostatic Pressing of Metals and Ceramics.	1071-1078A	On the Stress Corrosion Cracking of AI—Li Alloys: the Role of Grain Boundary Precipitates. Grain Boundary Diffusion of Hydrogen in Nickel. Brittle Fracture of an Au/Ag Alloy Induced by a Surface Film.	264-267A 351-355A 531-541A
Steels, Rolling Thermal Behavior of Steel Rolling With Nonconventional		Brittle Fracture of an Au/Ag Alloy Induced by a Surface Film. A Mechanistic Study of Transgranular Stress Corrosion Cracking of Type 304 Stainless Steel.	1453-1461A
Rolls. Establishment of a General Formula for Fractional Softening.	1767-1774A 2160-2162A	Intergranular Stress Corrosion Cracking of Alloy 600 and X-750 in High-Temperature Deserated Water/Steam.	1857-1864A
Steels, Welding	E TOO E TOEM	Delayed Hydride Cracking Behavior for Zircaloy-2 Tubing. A Critical Evaluation of the Stress-Corrosion Cracking Mech-	2049-2060A
Effect of Temperature and Composition on Surface Tension in Fe—Ni—Cr Alloys Containing Sulfur.	557-560B	anism in High-Strength Aluminum Alloys.	2407-2414A
The Origin of Transformation Textures in Steel Weld Metals Containing Acicular Ferrite.	657-663A	Stress corrosion cracking, Alloying effects The Influence of Palladium on the Hydrogen-Assisted Cracking Resistance of PH 13-8 Mo Stainless Steel.	2429-2443A
Sticking (adhesion) See Adhesion		Stress corrosion cracking, Microstructural effects Effects of Transformation on Texture and Iodine Stress Cor-	
Stirring See also Electromagnetic stirring		rosion Cracking Resistance of Zircaloy Sheet.	2247-2256A
Crystallization of a Faceted Primary Phase in a Stirred Slurry. In Situ Formation of Three-Dimensional TiC Reinforcements	575-584A	Stress corrosion resistance See Corrosion resistance	
in Ti-TiC Composites.	859-865A	Stress distribution See Stress concentration	
Strain Tensile Deformation and Fracture Toughness of		Stress intensity	
2014 + 15 vol.% SiC Particulate Composite. Strain Distribution Effects on the Low-Cycle Fatigue Behavior	113-123A	The Effect of Particulate SiC on Fatigue Crack Growth in a Cast-Extruded Aluminum Alloy Composite.	97-112A
of Fe—C—Mo Steels. The Relationship Between Plastic Anisotropy of Steel Sheet	675-683A	Dynamic Fracture Behavior of SiC Whisker-Reinforced Aluminum Alloys.	367-375A
and Temper Rolling Strain.	2156-2160A	The Initiation and Growth of Fatigue Cracks in a Titanium Al- uminide Alloy.	377-391A
Strain aging Ductility and Dynamic Strain Aging in Rapidly Solidified Alu-		The Influence of Applied Stress, Crack Length, and Stress In- tensity Factor on Crack Closure.	1559-1571A
minum Alloys. Strain hardening Mechanical Behavior of Cast Particulate SiC/AL (A356) Metal	1021-1028A	A Critical Evaluation of the Stress-Corrosion Cracking Mechanism in High-Strength Aluminum Alloys.	2407-2414A
Matrix Composites. 1000 to 1200K Time-Dependent Compressive Deformation of	1585-1593A	Application of Analytical Techniques to Stress Relaxation Ex-	0000 00074
Single-Crystalline and Polycrystalline B2 Ni—40Al. Toward a Sound Understanding of Dislocation Plasticity. Establishment of a General Formula for Fractional Softening.	1595-1607A 1693-1708A 2160-2162A	periments in Commercial Zinc. Stress rupture strength See Creep rupture strength	2303-2307A
On the Constraint Factor Associated With the Indentation of Work-Hardening Materials With a Spherical Ball.	2375-2384A	Stress strain curves Processing Map for Hot Working of Alpha-Zirconium.	829-836A
Finite Element Modeling Simulation of In-Plane Forming Limit Diagrams of Sheets Containing Finite Defects.	2655-2665A	The Shape Memory Effect and Superelasticity in Two-Phase Polycrystalline α/β Brasses.	1479-1490A
Hydrostatic Stresses and Their Effect on the Macroflow Be- havior and Microfracture Mechanism of Two-Phase Alloys.	2695-2702A	Prediction of Steel Flow Stresses at High Temperatures and Strain Rates.	1545-1558A
Ultrasound Treatment of Centrifugally Atomized 316 Stainless Steel Powders.	3025-3033A	Mechanical Behavior of Cast Particulate SiC/AL (A356) Metal Matrix Composites.	1585-1593A
Strain hardening, Microstructural effects	00E0-0000A	1000 to 1200K Time-Dependent Compressive Deformation of Single-Crystalline and Polycrystalline B2 Ni—40Al.	1595-1607A
Effect of Grain Size on High Strain Rate Deformation of Cop- per.	2349-2357A	A Simple, Versatile Miniaturized Disk-Bend Test Apparatus	
Strain rate		for Quantitative Yield-Stress Measurements. Stress Concentration at a Notch Tip in Unidirectional Metal	2061-2068A
A Model for the Strain-Rate Dependence of Yielding in Ni ₃ Al Alloys.	125-128A	Matrix Composites. The Mechanical Behavior of a Hybrid Metal Matrix Compos-	2085-2095A 2107-2117A
Recrystallization of Austenite After Deformation at High Tem- peratures and Strain Rates—Analysis and Modeling.	151-160A	ite. Establishment of a General Formula for Fractional Softening.	2160-2162A
Effects of Material Rate Sensitivity and Void Nucleation on Fracture Initiation in a Circumferentially Cracked Bar.	161-170A	Application of Analytical Techniques to Stress Relaxation Ex- periments in Commercial Zinc.	2303-2307A
Thermal and Mechanical Considerations in Using Shape Memory Alloys to Control Vibrations in Flexible Structures.	623-627A	Hydrogen Effects on Low-Cycle Fatigue of the Single-Crystal Nickel-Base Superalloy CMSX-2. The instrument of the Proposition of a Titanium Matrix	2597-2603A
Influence of Microstructure on Centerburst Development in Steel Extrusions.	807-815A	The Anisotropic Mechanical Properties of a Titanium Matrix Composite Reinforced With SiC Fibers.	2975-2984A
Processing Map for Hot Working of Alpha-Zirconium. Ductility and Dynamic Strain Aging in Rapidly Solidified Alu-	629-836A	Stresses See Residual stress	
minum Alloys. High Strain Rate Superplasticity of a 25 wt.% Cr—7 wt.% Ni—3 wt.% Mo—0.14 wt.% N Duplex Stainless Steel.	1021-1028A	Stress intensity	
Prediction of Steel Flow Stresses at High Temperatures and Strain Rates.	1083-1091A 1545-1558A	Stretchability, Temperature effects Nonisothermal Punch Stretching: Measurements and Finite Element Modeling Simulations.	3003-3011A
Application of Analytical Techniques to Stress Relaxation Ex- periments in Commercial Zinc. Dynamic Recrystallization During Hot Deformation of Alumi-	2303-2307A	Stretching Nonisothermal Punch Stretching: Measurements and Finite	
num: a Study Using Processing Maps.	2339-2348A	Element Modeling Simulations.	3003-3011A
Effect of Grain Size on High Strain Rate Deformation of Cop- per.	2349-2357A	Strip See Strip steel	
Strain softening Torsional Hot Workability in 0.47C—0.86Mn—0.5Cr—B		Strip steel, Forming Simulation of the Effect of Texture on Limit Strain in Biaxially	
Steel From 650-870°C. Establishment of a General Formula for Fractional Softening.	469-477A 2160-2162A	Stretched Steel Sheet. Nonisothermal Punch Stretching: Measurements and Finite	2069-2076A
Strengthening (solution)	J. 22 2. 102/1	Element Modeling Simulations.	3003-3011A
See Solution strengthening Stress aging		Strip steel, Rolling The Thermal and Metallurgical State of Steel Strip During Hot	
See Strain aging		Rolling. I. Characterization of Heat Transfer. The Thermal and Metallurgical State of Steel Strip During Hot	307-319A
Stress analysis Simulation of the Effect of Texture on Limit Strain in Biaxially		Rolling. II. Factors Influencing Rolling Loads. The Thermal and Metallurgical State of Steel Strip During Hot	321-333A
Stretched Steel Sheet.	2069-2076A	Rolling. III. Microstructural Evolution.	335-349A

A

The Relationship Between Plastic Anisotropy of Steel Sheet and Temper Rolling Strain.	2156-2160A	Solidification of Undercooled Sn—Sb Peritectic Alloys. II. Heterogeneous Nucleation.	765-773A
Structural hardening		Growth Kinetics of Solid/Liquid Gallium Interfaces. I. Experi- mental.	1259-1270A
See also Dispersion hardening Precipitation hardening		Growth Kinetics of Solid/Liquid Gallium Interfaces. II. Theoretical.	1271-1286A
Secondary hardening Solution strengthening		Containerless Processing and Rapid Solidification of Nb—Si Alloys in the Niobium-Rich Eutectic Range.	2713-2721A
Strain hardening Microstructurally Toughened Particulate-Reinforced Aluminum Matrix Composites.	171-182A	Containerless Processing and Rapid Solidification of Nb—Si Alloys of Hypereutectic Composition. Solidification of Highly Undercooled Fe—P Alloys.	2723-2732A 2761-2768A
NiAl-Based Microstructurally Toughened Composites.	183-189A	Measurements of Rapid Solidification Rate in Highly Under- cooled Melts With a Video System.	2825-2828A
Structural materials See Structural steels		Superheating	EUEU-EUEUN
Structural steels, Mechanical properties Behavior of Acoustic Emission for Low-Strength Structural Steel During Fatigue and Corrosion Fatigue.	2677-2680A	Containerless Processing and Rapid Solidification of Nb—Si Alloys in the Niobium-Rich Eutectic Range. Superlattices	2713-2721A
Structure (atomic) See Atomic structure		The Mechanisms and Temperature Dependence of Superlat- tice Stacking Fault Formation in the Single-Crystal Superal-	0000 00404
Structures (crystalline)		loy PWA 1480. An Investigation of Fe—Ni Order in a Steel.	2309-2318A 2807-2809A
See Crystal structure Grain structure		Superplasticity, Deformation effects	
Microstructure		Recrystallization and Superplasticity at 300°C in an Aluminum—Magnesium Alloy.	1037-1047A
Submerged arc welding Slag—Metal Reactions During Welding. I. Evaluation and Re-		High Strain Rate Superplasticity of a 25 wt.% Cr—7 wt.% Ni—3 wt.% Mo—0.14 wt.% N Duplex Stainless Steel.	1083-1091A
assessment of Existing Theories. Slag—Metal Reactions During Welding. II. Theory.	65-71B 73-81B	Superplasticity, Microstructural effects	1000-1007A
Slag—Metal Reactions During Welding. III. Verification of the Theory.	83-100B	Quantitative Assessment of the Implications of Strain- Induced Microstructural Changes in Superplasticity.	83-96A
Microstructure and Local Brittle Zone Phenomena in High- Strength Low-Alloy Steel Welds.	139-149A	Superplasticity, Stress effects The Shape Memory Effect and Superelasticity in Two-Phase	1479-1490A
Submerged arc welds See Welded joints		Polycrystalline α/β Brasses. Surface analysis (chemical)	1475-14507
Sulfates, Reduction (chemical) The Effect of Reaction Condition on Composition and Proper-		Tribological Behavior and Surface Analysis of Tribodeformed Al Alloy—50% Graphite Particle Composites.	1435-1441A
ties of Ultrafine Amorphous Powders in (Fe,Co,Ni)—B Systems Prepared by Chemical Reduction.	2125-2132A	Surface chemistry The K ₂ ZrF ₆ Wetting Process: Effect of Surface Chemistry on	
Sulfides		the Ability of a SiC-Fiber Preform To Be Impregnated by	2133-2139A
A Comparison of the Fracture Behavior of Two Commercially Produced Heats of HY180 Steel Differing in Sulfide Type.	2277-2285A	Aluminum. Surface defects	2100-2100A
Sulfur, Impurities		Surface Void Nucleation Under the Power-Law Creep Condi-	935-937A
Effect of Temperature and Composition on Surface Tension in Fe—Ni—Cr Alloys Containing Sulfur. Effect of Sulfur Removal on Al ₂ O ₃ Scale Adhesion.	557-560B 739-752A	tion in an Al—3 at.% Mg Solid Solution Alloy. Surface diffusion	935-937A
Sulfur compounds	100 1021	See Diffusion Surface energy	
See Sulfátes Sulfides Sulfur dioxide		Surface Energy Reduction in Fibrous Monotectic Structures. Surface finishing	1881-1886A
Sulfur dioxide, End uses		See Surface pretreatments	
Leaching of Nickel From Supported Nickel Waste Catalyst	775 7040	Surface hardening See also Laser beam hardening	
Using Aqueous Sulfur Dioxide Solution. Sulphur	775-781B	Influence of Cyclic Deformation on Surface Microstructure	1622 16464
See Sulfur		and Hardness of Ion-Implanted Nickel. Surface layer	1633-1646A
Superalloys, Corrosion Fatigue Behavior in the Potentiostatic Passive Corrosion Re-		Brittle Fracture of an Au/Ag Alloy Induced by a Surface Film. Surface pretreatments	531-541A
gime of the Iron-Base Superalloy A-286. Modeling of Corrosion Fatigue Crack Initiation Under Passive Electrochemical Conditions.	513-519A 521-529A	Preliminary Studies on NiAl/Nb ₂ Be ₁₇ Reaction and Effective- ness of BeO as an Interfacial Reaction Barrier.	2535-2538A
Intergranular Stress Corrosion Cracking of Alloy 600 and X-		Surface properties	
750 in High-Temperature Deaerated Water/Steam.	1857-1864A	See also Friction Roughness	
Superalloys, Mechanical properties Quantitative Assessment of the Implications of Strain-		Surface structure	
Induced Microstructural Changes in Superplasticity. Low-Cycle Fatigue Behavior of Nimonic PE16 at Room Tem-	83-96A	Surface temperature Surface tension	
perature. Fracture of Single Crystals of the Nickel-Base Superalloy	499-506A	Tribology Wetting	
PWA 1480E in Helium at 22°C.	731-738A	Surface Composition of Ternary Cu—Ag—Au Alloys. I. Experimental Results.	1833-1840A
Crack Initiation and Propagation During High-Temperature Fatigue of Oxide Dispersion-Strengthened Superalloys.	837-851A	Surface Composition of Ternary Cu—Ag—Au Alloys. II. A Comparison of Experiment With Theoretical Models.	1841-1848A
The Role of the γ/γ' Eutectic and Porosity on the Tensile Behavior of a Single-Crystal Nickel-Base Superalloy.	1443-1451A	Surface roughness	
Development of a Necklace Microstructure During Isotherma Deformation and its Properties Relative to Uniform Micro-		See Roughness	
structures.	1999-2008A	Surface structure, Vibration effects Ultrasound Treatment of Centrifugally Atomized 316 Stain-	
Fracture of Single Crystals of the Nickel-Base Superalloy PWA 1480E in Hydrogen at 22°C.	2031-2038A	less Steel Powders.	3025-3033A
Hydrogen Effects on Low-Cycle Fatigue of the Single-Crysta Nickel-Base Superalloy CMSX-2.	2597-2603A	Surface temperature The Thermal and Metallurgical State of Steel Strip During Hot	
Superalloys, Melting		Rolling. I. Characterization of Heat Transfer.	307-319A
Magnetohydrodynamic and Thermal Behavior of Electroslag Remelting Slags.	111-120B	Surface tension A New Experimental Method for Determining Liquid Density	
Superalloys, Microstructure		and Surface Tension.	27-31B
The Mechanisms and Temperature Dependence of Superlat tice Stacking Fault Formation in the Single-Crystal Superal		The Role of Ledges in Stress Tensor-Mediated Surface Pro- cesses for Silicon and GaAs.	1317-1322A
loy PWA 1480.	2309-2318A	Surface tension, Temperature effects	
Superalloys, Oxidation On the Role of Yttrium During High-Temperature Oxidation of	f	Effect of Temperature and Composition on Surface Tension in Fe—Ni—Cr Alloys Containing Sulfur.	557-560B
an Ni—Cr—Al—Fe—Y Alloy.	1463-1465A	Surfacing	
Superalloys, Welding		See also Hard surfacing In Situ Technique for Measuring the Absorption During Laser	
The Relationship Between Carbon Content, Microstructure and Intergranular Liquation Cracking in Cast Nickel Allo	у	Surface Remelting.	139-141B
718. A Phase Diagram Approach to Study Liquation Cracking in	557-567A	Systems (metallurgical) See Binary systems	
Alloy 718.	887-902A	Quaternary systems	
Supercooling Solidification of Undercooled Sn—Sb Peritectic Alloys.	ı.	Ternary systems Tanks (electrolytic)	
Microstructural Evolution.	753-764A	See Electrolytic cells	

Tantalum, Forming Effect of Processing Variables on Texture and Texture Gradients in Tantalum.	2039-2048A	Structure and Properties of a Rapidly Solidified AI—LI— Mn—Zr Alloy for High-Temperature Applications. II. Spray Atomization and Deposition Processing.	2515-2522A
Tantalum, Microstructure		Shock Densification/Hot Isostatic Pressing of Titanium Aluminide.	2667-2676A
Influence of Initial Ingot Breakdown on the Microstructural and Textural Development of High-Purity Tantalum.	2959-2968A	The Anisotropic Mechanical Properties of a Titanium Matrix Composite Reinforced With SiC Fibers.	2975-2984A
Tantalum compounds, Mechanical properties Mechanical, Elastic, and Structural Properties of Alloys of Ru—Ta High-Temperature Intermetallic Compounds.	129-137A	Tensile strength, Alloying effects The Effect of Copper, Chromium, and Zirconium on the Microstructure and Mechanical Properties of Al—Zn—Mg—	2000 20404
Temper (metallurgical) The Relationship Between Plastic Anisotropy of Steel Sheet and Temper Rolling Strain.	2156-2160A	Cu Alloys. Tensile strength, Cooling effects	2809-2818A
Temper brittleness Comparison of Secondary Hardening Embrittlement in Tung-		Microstructural Engineering Applied to the Controlled Cool- ing of Steel Wire Rod. I. Experimental Design and Heat Transfer.	2769-2778A
sten and Molybdenum Steels. In Situ Fracture Observations on Tempered Martensite Em-	1119-1122A	Microstructural Engineering Applied to the Controlled Cooling of Steel Wire Rod. II. Microstructural Evolution and Me-	0770 07004
brittlement in an AISI 4340 Steel. The Evaluation of In-Service Materials Degradation of Low-Alloy Steels by the Electrochemical Method.	1889-1892A 2097-2106A	chanical Properties Correlations. Microstructural Engineering Applied to the Controlled Cooling of Steel Wire Rod. III. Mathematical Model—Formulation and Predictions.	2779-2790A 2791-2805A
Temper brittleness, Impurity effects Distribution of Antimony Between Carbon-Saturated Iron and Synthetic Slags.	136-139B	Tensile strength, Corrosion effects Microstructure Property Relationships and Hydrogen Effects	
Temper hardening See Secondary hardening		in a Particulate-Reinforced Aluminum Composite. Tensile strength, Environmental effects	2445-2450A
Temperature See also Surface temperature		Fracture of Single Crystals of the Nickel-Base Superalloy PWA 1480E in Hydrogen at 22°C.	2031-2038A
Temperature distribution Temperature gradient Computational Modeling of Stationary Gas-Tungsten-Arc Weld Pools and Comparison to Stainless Steel 304 Experi- mental Results.	243-257B	Tensile strength, High temperature effects On the Embrittlement of a Rapidly Solidified AI—Fe—V—Si Alloy After High-Temperature Exposure. Effect of Long-Term Service Exposure on Microstructure and Mechanical Properties of a CrMoV Steam Turbine Rotor	853-858A
Characterization of the Damping Properties of Die-Cast Zinc—Aluminum Alloys.	617-622A	Steel. Lifetimes and Failure Mechanisms of W/Re Hairpin Fila-	1811-1820A
Influence of Microstructure on Centerburst Development in Steel Extrusions.	807-815A	ments. Tensile strength, Microstructural effects	2077-2084A
Temperature distribution Thermal Behavior of Steel Rolling With Nonconventional Rolls.	1767-1774A	Effect of Hydrogen as a Temporary β Stabilizer on Micro- structure and Brittle Fracture Behavior in a Titanium Alumi- nide Alioy.	71-81A
Temperature field See Temperature distribution		Microstructurally Toughened Particulate-Reinforced Alumi- num Matrix Composites.	171-182A
Temperature gradient		Mechanical Properties and Retained Austenite in Intercriti- cally Heat-Treated Bainite-Transformed Steel and Their Variation With Silicon and Manganese Additions.	489-498A
The Thermal and Metallurgical State of Steel Strip During Hot Rolling. II. Factors Influencing Rolling Loads.	321-333A	The Role of the γ/γ ' Eutectic and Porosity on the Tensile Behavior of a Single-Crystal Nickel-Base Superalloy.	1443-1451A
Temperature measurement Mold Behavior and Its Influence on Quality in the Continuous Casting of Steel Slabs. I. Industrial Trials, Mold Tempera-		Development of a Necklace Microstructure During Isothermal Deformation and Its Properties Relative to Uniform Micro- structures.	1999-2008A
ture Measurements, and Mathematical Modeling. Tempering	861-874B	Effect of Phase Morphology on the Mechanical Behavior of Two Titanium Aluminide Composites.	2009-2019A
See also Quenching and tempering Structures and Tempering Behavior of Rapidly Solidified		Tensile tests See Tension tests	
High-Carbon Iron Alloys. Electron Microscopy Study of the Aging and First Stage of Tempering of High-Carbon Fe—C Martensite.	775-782A	Tensile yield strength	
Microstructural Evolution of Modified 9Cr—1Mo Steel. Low-Temperature Improvement of Mechanical Properties of	797-806A 1049-1058A	See Yield strength Tension tests Development of Deformation Instability in Hot Tensile Test	
AISI 4340 Steel Through High-Temperature Thermome- chanical Treatment. The Tempering of FeNiN Martensite.	1093-1102A 1945-1956A	Specimens. Ternary systems, Phases (state of matter)	2297-2302A
Effects of Intercritical Treatment and Tempering on Fracture Behavior in a Medium-Carbon 2Si—3Ni Steel.	2587-2596A	Representation of Excess Thermodynamic Properties of Ter- nary Systems Using Interaction Parameters. An Assessment of the Fe—C—Si System.	583-591B 2211-2223A
Tenacity See Tensile strength		Calculation of Phase Diagrams and Solidification Paths of Aluminum-Rich Al—Li—Cu Alloys.	2837-2848A
Tensile modulus See Modulus of elasticity		Ternary systems, Reactions (chemical) Activities of Boron in the Binary Ni—B and the Ternary Co—	
Tensile properties See also Elongation		Fe—B Melts.	47-52B
Necking Reduction of area		Tertiary displacements See Displacements (lattice)	
Tensile strength Yield point		Texture See also Rolling texture	
Yield strength Tensile Deformation and Fracture Toughness of		The Origin of Transformation Textures in Steel Weld Metals Containing Acicular Ferrite.	657-663A
2014 + 15 vol.% SiC Particulate Composite. Tensile properties, Alloying effects	113-123A	Simulation of the Effect of Texture on Limit Strain in Biaxially Stretched Steel Sheet.	2069-2076A
Effects of Microalloying Elements and Heat Treatments on Tensile Properties in Cu—23Zn—3.4AI—1Ni—X Alloys.	256-258A	Effects of Transformation on Texture and Iodine Stress Corrosion Cracking Resistance of Zircaloy Sheet.	2247-2256A
Tensile properties, Corrosion effects Accelerated Fracture Due to Tritium and Helium in 21-6-9 Stainless Steel.	879-886A	Texture, Deformation effects Recrystallization and Superplasticity at 300°C in an Aluminum—Magnesium Alloy. Effect of Processing Variables on Texture and Texture Gradi-	1037-1047A
Tensile properties, Heating effects Microstructural Evolution of Modified 9Cr—1Mo Steel.	1049-1058A	ents in Tantalum.	2039-2048A
Tensile properties, Microstructural effects		Thawing See Melting	
Plastic Déformation and Fracture of Binary TiAl-Base Alloys. On Thermal Shock Resistance of Austenitic Cast Irons.	427-439A 1821-1831A	Thermal analysis See Differential thermal analysis	
Tensile shear strength See Shear strength		Thermal conductivity, Microstructural effects On Thermal Shock Resistance of Austenitic Cast Irons.	1821-1831A
Tensile strength In Situ Formation of Three-Dimensional TiC Reinforcements	050 005	Thermal cycling Thermomechanical Fatigue of a Lead Alloy.	1059-1070A
in Ti-TiC Composites. Mechanical Behavior of Cast Particulate SiC/AL (A356) Metal		The Deformation of an Aluminum—Silicon Eutectic Alloy Under Thermal Cycling Conditions.	1113-1115A
Matrix Composites. The Mechanical Behavior of a Hybrid Metal Matrix Composite	1585-1593A	Effects of Thermal Cycling on the Martensitic Transformation in Two-Phase α/β Brasses.	1473-1478A
ite. Structure and Properties of a Rapidly Solidified Al—Li— Mn—Zr Alloy for High-Temperature Applications. I. Ineri	2107-2117A	Thermal expansion Effect of Plastic Deformation on Residual Stresses in	
Gas Atomization Processing.	2503-2514A	Ceramic/Metal Interfaces.	2822-2825A

Thermal expansion, Microstructural effects On Thermal Shock Resistance of Austentic Cast Irons.	821-1831A	Thermodynamics of the Iron Martensitic Transformation and the Ma Temperature of Iron.	1761-1765A
Thermal fatigue Thermomechanical Fatigue of Particulate-Reinforced Alumi-		Thermodynamic Properties of the Fe-Mn-V-C System.	1911-1920A 1921-1935A
num 2xxx-T4. Thermal flux Thermal flux	697-707A	Palladium—Niobium System.	1937-1943A 2162-2165A
See Heat transmission Thermal measurements		tem. Solute Distribution Around a Coherent Precipitate in a Multi-	2187-2198A
See Temperature measurement Thermal properties		component Alloy. An Assessment of the Fe—C—Si System.	2199-2210A 2211-2223A
See Lorenz number Thermal conductivity			2401-2405A
Thermal expansion Thermal stability			2837-2848A
Thermal reduction See Fluidized bed reduction Smelting		Chemical Potential Diagram of Al—Ti—C System: Al ₄ C ₃ For-	3071-3075A 3075-3076A
Thermal resistivity See Thermal conductivity		Thermoelastic properties See also Shape memory	
Thermal shock resistance See Shock resistance		Thermoelastic properties, Heating effects Effects of Thermal Cycling on the Martensitic Transformation	
Thermal spraying See Plasma spraying		in Two-Phase α/β Brasses. Thermoelastic properties, Stress effects	1473-1478A
Spraying Thermal stability		The Shape Memory Effect and Superelasticity in Two-Phase Polycrystalline $\alpha l \beta$ Brasses.	1479-1490A
On the Embrittlement of a Rapidly Solidified Al—Fe—V—Si Alloy After High-Temperature Exposure.	853-858A	Thermoelectricity See Seebeck effect	
Microstructural Evolution in Rapidly Solidified Al—Fe Alloys: an Alternative Explanation.	927-934A	Thermomechanical properties See Thermoelastic properties	
Microstructural and Thermal Stability of a Ti—43Al Alloy Containing Dispersoids of Titanium Di-Boride.	1721-1728A	Thermomechanical treatment	
Thermal stability, Alloying effects The Effects of Chromium Additions to Binary TiAl-Base Al-		Recrystallization and Superplasticity at 300°C in an Aluminum—Magnesium Alloy. High Strain Rate Superplasticity of a 25 wt.% Cr.—7 wt.%	1037-1047A
loys. Thermionic converters	2619-2626A	Ni—3 wt.% Mo—0.14 wt.% N Duplex Stainless Steel. Low-Temperature Improvement of Mechanical Properties of	1083-1091A
See Thermionic generators		AISI 4340 Steel Through High-Temperature Thermome- chanical Treatment.	1093-1102A
Thermionic emission, High temperature effects The High-Temperature Work Function Behavior of Polycrys-		Strength and Ductile-Phase Toughening in the Two-Phase Nb/Nb ₅ Si ₃ Alloys.	1573-1583A
talline Osmium. Thermionic generators	1609-1613A	The Effect of Through-Thickness Anisotropy on the Cryo- genic Mechanical Properties of an Al—Cu—Li—Zr Alloy (Vintage III 2090-T81).	1789-1799A
The High-Temperature Work Function Behavior of Polycrys-	1609-1613A	Development of a Necklace Microstructure During Isothermal Deformation and Its Properties Relative to Uniform Micro-	1709-1799A
Thermochemistry Thermochemical Nature of Minor Elements in Copper Smelt-		structures. Effect of Phase Morphology on the Mechanical Behavior of	1999-2008A
ing Mattes. Thermochemistry of Binary Alloys of Transition Metals: the	677-688B	Two Titanium Aluminide Composites. Effects of Vanadium and Processing Parameters on the Structures and Properties of a Direct-Quenched Low-	2009-2019A
Me—Sc, Me—Y, and Me—La (Me = Silver, Gold) Systems Note on the Enthalpies of Formation of Cu ₃ Si and Cu ₃ Ge.	1103-1111A 2162-2165A	Carbon Mo—B Steel. Structure and Properties of a Rapidly Solidified Al—Li—	2359-2374A
Thermocycling	2102-21007	Mn—Zr Alloy for High-Temperature Applications. I. Inert Gas Atomization Processing.	2503-2514A
See Thermal cycling Thermodynamics		Structure and Properties of a Rapidly Solidified Al—Li— Mn—Zr Alloy for High-Temperature Applications. II. Spray	0545 05004
See also Enthalpy Entropy		Atomization and Deposition Processing. Recrystallization Controlled Rolling and Accelerated Cooling for High Strength and Toughness in V—Ti—N Steels.	2515-2522A 2681-2694A
Heat of formation Heat of mixing		Thermostability	2001-20047
Heat of solution A Thermodynamic Study of Dephosphorization Using BaO—		See Thermal stability Thickness	
BaF ₂ , CaÖ—CaF ₂ , and BaO—CaO—CaF ₂ Systems. Slag—Metal Reactions During Welding. I. Evaluation and Reassesment of Existing Theories.	33-38B 65-71B	The Effect of Through-Thickness Anisotropy on the Cryo- genic Mechanical Properties of an Al—Cu—Li—Zr Alloy	
The Kinetics of S ³⁵ Exchange Between SO ₂ /CO/CO ₂ Gas Mixtures and Copper Sulfide Melts at 1523K.	211-217B	(Vintage III 2090-T81). Thin films, Crystal growth	1789-1799A
Equilibrium Phase Relations and Thermodynamics of the Cr—O System in the Temperature Range of 1500°C to	211-2170	Observations of the Formation and Kinetics of Surface Steps During Evaporation and Condensation.	1299-1304A
1825°C. Application of Thermodynamic Models to the Calculation of	225-232B	Thermodynamical Study of Gas Transport in Thin Film Growth: Application to Bismuth Chalcogenides.	
Solidification Paths of Aluminum-Rich Al-Li Alloys. The Thermodynamic Behavior of Sulfur in BaO—BaF ₂ Slags.	267-271A 333-338B	Tig arc welding	
A Volume-Averaged Two-Phase Model for Transport Phenomena During Solidification.	349-361B	See Gas tungsten arc welding TIG welding	
Injections in the Iron Blast Furnace: a Graphics Study by Means of the Rist Operating Diagrams. Thermodynamic Behavior of Phoephones in Caca-Caca-	363-383B	See Gas tungsten arc welding Time temperature transformation curves	
Thermodynamic Behavior of Phosphorus in CaO—CaF ₂ — SiO ₂ and CaO—Na ₂ O—SiO ₂ Systems. Representation of Excess Thermodynamic Properties of Ter-	499-502B	See TTT curves	
nary Systems Using Interaction Parameters. Thermodynamics of Binary Systems Using Interaction Pa-	583-591B	Tin, Binary systems Thermodynamics of Binary Systems Using Interaction Parameters.	593-605B
rameters. Thermodynamics of Aluminum—Barium Alloys. Peoplet Leviteted in As., H. Coo.	593-605B 607-616B	Tin, Microstructure Solidification of Undercooled Sn—Sb Peritectic Alloys. I.	
Deoxidation Rate of Copper Droplet Levitated in Ar—H ₂ Gas Stream. High-Temperature Thermodynamic Properties of the Vana-	631-639B	Microstructural Evolution.	753-764A
dium Carbides V ₂ C and VC _{0.73} Determined Using a Gal- vanic Cell Technique. Gibbs Energy of Formation of Nickel Chromite.	661-668B 673-675B	Tin base alloys, Casting Behavior of Metal Alloys in the Semisolid State. Numerical Simulation of a Solidifying Pb—Sn Alloy: the Effects of Cooling Rate on Thermosolutal Convection and	269-294B
Thermochemical Nature of Minor Elements in Copper Smelt- ing Mattes. Phase Relations and Thermodynamics of the System Fe—	677-688B	Macrosegregation. Behavior of Metal Alloys in the Semisolid State.	529-540B 957-981A
Cr-O in the Temperature Range of 1600-1825°C (1873-	689-703B	Tin base alloys, Diffusion Determination of Liquid Diffusion Coefficients Along a	
2098K) Under Strongly Reducing Conditions. A Thermodynamic and Experimental Study of the Electrochemically Induced Cooling of the Anode in Hall—Héroult Celle.		Liquidus Phase Boundary. Tin base alloys, Directional solidification	21-26B
Cells. A Thermodynamic Study of the System Fe.O. AloO. SiO. at 1673K	831-837B	Solute Distribution During Steady-State Cellular Growth.	3035-3039A
Fe _x O + Al ₂ O ₃ + SiO ₂ at 1673K. Carbonitride Precipitate Growth in Titanium/Niobium Microalloyed Steels.	839-845B 1511-1524A	Tin base alloys, Mechanical properties Quantitative Assessment of the Implications of Strain Induced Microstructural Changes in Superplasticity.	83-96A

Tin base alloys, Microstructure Solidification of Undercooled Sn—Sb Peritectic Alloys. I.		Shock Densification/Hot Isostatic Pressing of Titanium Aluminide.	2667-2676A
Microstructural Evolution. Solidification of Undercooled Sn—Sb Peritectic Alloys. II. Heterogeneous Nucleation.	753-764A 765-773A	Titanium ores See Ilmenite	2007 201011
Tin nickel alloy plating See Alloy plating		Rutile Tool steels	
Titanium, Alloying additive Effect of Killing Time on the Microstructure and Toughness of the Heat-Affected Zone in Titanium-Killed Steels.	2818-2822A	See also High speed tool steels Tool steels, Powder technology Powder Metallurgy T15 Tool Steel. I. Characterization of Powder and Hot Isostatically Pressed Material.	2733-2745A
Titanium, Alloying elements Carbonitide Precipitate Growth in Titanium/Niobium Microal-	1511 15044	Powder Metallurgy T15 Tool Steel. II. Microstructure and Properties After Heat Treatment.	2747-2759A
loyed Steels. Thermodynamic Consideration of Grain Refinement of Aluminum Alloys by Titanium and Carbon.	1511-1524A 3071-3075A	Topology Ledgewise Vaporization.	1305-1310A
Titanium, Composite materials Microstructurally Toughened Particulate-Reinforced Alumi-		Torsional modulus See Shear modulus	
num Matrix Composites. Reaction of Titanium and Ti—Al Alloys With Alumina. In Situ Formation of Three-Dimensional TiC Reinforcements	171-182A 715-721A	Torsional strength See Shear strength	
in Ti-TiC Composites. Titanium, Diffusion	859-865A	Total heat See Enthalpy	
Correction to "Literature Survey on Diffusivities of Oxygen Aluminum, and Vanadium in Alpha Titanium, Beta Titanium, and in Rutile".	1121-1125A	Toughness See also Fracture toughness Notch toughness Microstructure and Local Brittle Zone Phenomena in High-	
Titanium, Extraction Phase Transformations During Heating of Ilmenite Concentrates.	711-716B	Strength Low-Alloy Steel Welds. Further Study on the Scattering of the Local Fracture Stress and Allied Toughness Value.	139-149A 2287-2296A
Titanium, Powder technology Anomalous Combustion Effects During Mechanical Alloying.	3019-3024A	Toughness, Deformation effects Recrystallization Controlled Rolling and Accelerated Couling	
Titanium, Solubility Solid Solubilities of Manganese and Titanium in Aluminum at 0.1 MPa and 2.1 GPa.	783-786A	for High Strength and Toughness in V—TI—N Steels. Toughness, Heating effects	2681-2694A
Titanium base alloys, Composite materials The Anisotropic Mechanical Properties of a Titanium Matrix		Strength and Ductile-Phase Toughening in the Two-Phase Nb/Nb ₅ Si ₃ Alloys. Toughness, Microstructural effects	1573-1583A
Composite Reinforced With SiC Fibers. Titanium base alloys, Heat treatment Elastic Moduli and Tensile and Physical Properties of Heat-	2975-2984A	A Comparison of the Fracture Behavior of Two Commercially Produced Heats of HY180 Steel Differing in Sulfide Type.	2277-2285A
Treated and Quenched Powder Metallurgical Ti—6Al—4V Alloy.	709-714A	Transferring See Heat transfer Mass transfer	
Correction to "Elastic Moduli and Tensile and Physical Prop- erties of Heat-Treated and Quenched Powder Metallurgical Ti—6AI—4V Alloy".	1129A	Transformations (materials) See Phase transformations	
Titanium base alloys, Mechanical properties Quantitative Assessment of the Implications of Strain- Induced Microstructural Changes in Superplasticity.	83-96A	Transgranular corrosion A Mechanistic Study of Transgranular Stress Corrosion Cracking of Type 304 Stainless Steel.	1453-1461A
High-Damping Metals and Alloys. On the Influence of Microstructure on the Room-Temperature	607-616A	Transgranular fracture Comparison of Fracture Behavior in Intercritically Treated	1.150 7.1011.1
Deformation Behavior of a Naar-α Titanium Alloy. Material Effects in Fretting Wear: Application to Iron, Tita- nium, and Aluminum Alloys.	1122-1125A 1535-1544A	Medium-Carbon Nickel and Silicon Steels. Transgranular fracture, Heating effects	1115-1119A
Micromechanics of Shear Ligament Toughening. The Effects of Chromium Additions to Binary TiAl-Base Alloys.	2021-2029A 2619-2626A	Effects of Intercritical Treatment and Tempering on Fracture Behavior in a Medium-Carbon 2Si—3Ni Steel.	2587-2596A
Titanium base alloys, Microstructure Thickening of Grain-Boundary α Allotriomorphs in a Ti—Cr Alloy by Multiple Sets of Ledges.	1341-1348A	Transition metal alloys See Cobalt base alloys Copper base alloys	
Titanium base alloys, Phase transformations Determination of Equilibrium Solid-Phase Transition Temperatures Using DTA.		Ferrous alloys Manganese base alloys Nickel base alloys Scandium base alloys	
Titanium base alloys, Structural hardening Effect of Phase Morphology on the Mechanical Behavior of Two Titanium Aluminide Composites.		Titanium base alloys Yttrium base alloys Zinc base alloys	
Titanium carbide, Composite materials		Zirconium base alloys Transition metal compounds	
In Situ Formation of Three-Dimensional TiC Reinforcements in Ti-TiC Composites. Titanium compounds	859-865A	See Copper compounds Iron compounds Manganese compounds	
See also Titanium carbide Titanium compounds, Alloying elements		Nickel compounds Titanium compounds Zirconium compounds	
A New Phase in a Rapidly Solidified and Consolidated NbAl ₃ —1TiB ₂ Alloy.	1901-1909A	Transition metals See Cobalt	
Titanium compounds, Casting Evolution of Boride Morphologies in TiAl—B Alloys.	1647-1662A	Copper Iron	
Titanium compounds, Composite materials Creep Deformation of TiB ₂ -Reinforced Near-γ Titanium Al-		Manganese Nickel Titanium	
uminides. Reaction of Titanium and Ti—Al Alloys With Alumina.	447-454A 715-721A	Yttrium Zinc	
Titanium compounds, Heat treatment Microstructural and Thermal Stability of a Ti—43Al Alloy Con- taining Dispersoids of Titanium Di-Boride.	1721-1728A	Zirconium Transmission	
Titanium compounds, Mechanical properties Effect of Hydrogen as a Temporary		See Heat transmission Transmission electron microscopy	
structure and Brittle Fracture Behavior in a Titanium Alumi- nide Alloy.	71-81A	The Use of Transmission Electron Microscopy for the As- sessment of Interphase Boundaries. Electron Microscopy of Transformation Dislocations at Inter-	1139-1144A
The Initiation and Growth of Fatigue Cracks in a Titanium Al uminide Alloy. Plastic Deformation and Fracture of Binary TiAl-Base Alloys	377-391A 427-439A	phase Boundaries. Transuranium metals	1145-1158A
Microstructural Effects on Ambient and Élevated Tempera ture Fatigue Crack Growth in Titanium Aluminide Intermet allics.		See Plutonium	
allics. The Effects of Chromium Additions to Binary TiAl-Base Alloys.	817-828A 2619-2626A	Tribology Tribological Behavior and Surface Analysis of Tribodefor ned Al Alloy—50% Graphite Particle Composites.	1435-1441A
Titanium compounds, Powder technology Dynamic Compaction of Titanium Aluminides by Explosively Generated Shock Waves: Experimental and Materials Systems.		TRIP steels, Mechanical properties Mechanical Properties and Retained Austenite in Intercriti- cally Heat-Treated Bainite-Transformed Steel and Their Variation With Silicon and Manganese Additions.	489-498A

TTT curves The Decomposition of the Beta Phase in the Copper—Tin		V A characteristics See Current voltage characteristics	
System. The Aging Effect on Cu—Zn—Al Shape Memory Alloys With	11-18A	Vacuum degassing	
Low Contents of Aluminum. Influence of Microstructure on Centerburst Development in	25-33A	See Ladle degassing Vacuum refining	
Steel Extrusions. The Effect of the Thermal Path to Reach Isothermal Temper-	807-815A	Kinetics of Removal of Bismuth and Lead From Molten Cop- per Alloys in Vacuum Induction Melting.	447-465B
ature on Transformation Kinetics. Containerless Processing and Rapid Solidification of Nb—Si Alloys in the Niobium-Rich Eutectic Range.	993-999A 2713-2721A	Vanadium, Alloying elements Microstructural Evolution of Modified 9Cr—1Mo Steel. Effects of Vanadium and Processing Parameters on the	1049-1058A
Tubes, Corrosion Delayed Hydride Cracking Behavior for Zircaloy-2 Tubing.	2049-2060A	Structures and Properties of a Direct-Quenched Low-	2359-2374A
Tubing (metal) See Tubes		Vanadium, Binary systems Coherent Phase Equilibrium in Alloys With Congruent Points.	1921-1935A
Tubular goods		Vanadium, Diffusion	
See Tubes Tundishes		Correction to "Literature Survey on Diffusivities of Oxygen Aluminum, and Vanadium in Alpha Titanium, Beta Titanium, and in Rutile".	1121-1125A
Role of Near-Wall Node Location on the Prediction of Melt Flow and Residence Time Distribution in Tundishes by		Vanadium, Quaternary systems	
Mathematical Modeling. Tungsten, Alloying elements	429-437B	Thermodynamic Properties of the Fe—Mn—V—C System. Vanadium carbide, Reactions (chemical)	1911-1920A
The Effect of Tungsten on Dislocation Recovery and Precipitation Behavior of Low-Activation Martensitic 9Cr Steels.	2225-2235A	High-Temperature Thermodynamic Properties of the Vana- dium Carbides V ₂ C and VC _{0.73} Determined Using a Gal- vanic Cell Technique.	661-668B
Tungsten, Coatings Chemical Vapor Deposition Kinetics of Tungsten From WCl ₈ Onto Nickel Plate at Elevated Temperatures.	560-563B	Vanadium compounds See Vanadium carbide	
Tungsten, Reactions (chemical)	000 0000	Vapor deposition	
Discussion of "Evidence for the Existence of Potassium Bub- bles in AKS-Doped Tungsten Wire" and Reply.	2153-2156A	See also Chemical vapor deposition Thermodynamical Study of Gas Transport in Thin Film Growth: Application to Bismuth Chalcogenides.	2401-2405A
Tungsten arc welding See Gas tungsten arc welding		Vaporizing	
Tungsten base alloys, End uses Lifetimes and Failure Mechanisms of W/Re Hairpin Fila-		See also Evaporation Mathematical Modeling of Sulfide Flash Smelting Process. III. Volatilization of Minor Elements.	791-799B
ments.	2077-2084A	Vehicles	701-7000
Tungsten base alloys, Mechanical properties The Reduction of the Interfacial Segregation of Phosphorus		See Spacecraft Veining (cracks)	
and its Embrittlement Effect by Lanthanum Addition in a W—Ni—Fe Heavy Alloy.	2969-2974A	See Cracks	
Tungsten base alloys, Powder technology Gravitational Limit of Particle Volume Fraction in Liquid-		Vessels See Pressure vessels	
Phase Sintering. Tungsten inert gas welding	786-791A	Vibration High-Damping Metals and Alloys.	607-616A
See Gas tungsten arc welding		Characterization of the Damping Properties of Die-Cast Zinc—Aluminum Alloys.	617-622A
Tungsten lamps See Incandescent lamps		Thermal and Mechanical Considerations in Using Shape Memory Alloys to Control Vibrations in Flexible Structures.	623-627A
Tungsten steels, Structural hardening Comparison of Secondary Hardening Embrittlement in Tung-	1110 11001	Development of Vibration-Damping Resins for Room- Temperature Application. Chlorosulfonated Polyethylene: a Versatile Polymer for	629-631A
sten and Molybdenum Steels. Turbine blades, Nondestructive testing	1119-1122A	Damping Acoustic Waves. Vibration Damping Characteristics of Laminated Steel Sheet.	633-640A 653-656A
The Evaluation of In-Service Materials Degradation of Low- Alloy Steels by the Electrochemical Method.	2097-2106A	Video Measurements of Rapid Solidification Rate in Highly Under-	
Turbine disks Development of a Necklace Microstructure During Isothermal		cooled Melts With a Video System. Viscosity	2825-2828A
Deformation and Its Properties Relative to Uniform Microstructures.	1999-2008A	Development of Vibration-Damping Resins for Room- Temperature Application.	629-631A
Turbine disks, Nondestructive testing		Voids	020 00171
The Evaluation of In-Service Materials Degradation of Low- Alloy Steels by the Electrochemical Method. Turbines	2097-2106A	A Comparison of the Fracture Behavior of Two Commercially Produced Heats of HY180 Steel Differing in Sulfide Type. Voids, Corrosion effects	2277-2285A
See Gas turbine engines		Intergranular Stress Corrosion Cracking of Alloy 600 and X- 750 in High-Temperature Deaerated Water/Steam.	1857-1864A
Twinning Accelerated Fracture Due to Tritium and Helium in 21-6-9 Stainless Steel.	879-886A	Microstructure Property Relationships and Hydrogen Effects in a Particulate-Reinforced Aluminum Composite.	2445-2450A
The Crystallography and Atomic Structure of Line Defects in Twin Boundaries in Hexagonal-Close-Packed Metals.		Volatilizing See Vaporizing	
Ultimate shear strength	1100-1100/	Wastes	
See Shear strength Ultimate tensile strength		See Industrial wastes Water	
See Tensile strength		See Salt water	
Ultrafines, Synthesis Preparation of Monosized Ultrafine Particles of Precious Metals Utilizing an Emulsion-Type Liquid Membrane Tech nique.		Water cooling Heat-Transfer Phenomena in Water-Cooled Zinc-Fuming Furnace Jackets.	163-175B
Ultrasonics		Microstructural Engineering Applied to the Controlled Cool- ing of Steel Wire Rod. I. Experimental Design and Heal Transfer.	2769-2778A
An Ultrasonic Method for Reconstructing the Two Dimensional Liquid/Solid Interface in Solidifying Bodies. Ultrasound Treatment of Centrifugally Atomized 316 Stain	467-473B	Microstructural Engineering Applied to the Controlled Cooling of Steel Wire Rod. II. Microstructural Evolution and Mechanical Properties Correlations.	2779-2790A
less Steel Powders. Undercooling	3025-3033A	Microstructural Engineering Applied to the Controlled Cooling of Steel Wire Rod. III. Mathematical Model—	
See Supercooling UP hardfacing method		Formulation and Predictions. Water cooling (cooling of water)	2791-2805A
See Hard surfacing		See Water cooling	
Upset forging See Upsetting		Wear See Frictional wear	
Upsetting Recrystallization and Superplasticity at 300°C in a Aluminum—Magnesium Alloy.	n 1037-1047A	Wear rate Tribological Behavior and Surface Analysis of Tribodeformer Al Alloy—50% Graphite Particle Composites.	1435-1441A
Uranium, Extraction Continuous Precipitation of Uranium Peroxide From High		Wear resistance, Coating effects The Chemistry and Structure of Wear-Resistant, Iron-Bas-	

Weathering steels See Structural steels		White metal (copper matte) See Copper mattes	
Weld defects The Relationship Between Carbon Content, Microstructure, and Intergranular Liquation Cracking in Cast Nickel Alloy 718.	557-567A	Widmanstatten structure On the Influence of Microstructure on the Room-Temperature Deformation Behavior of a Near-α Titanium Alloy.	1122-1125A
A Phase Diagram Approach to Study Liquation Cracking in		Computer Simulation of Morphological Changes of Grain Boundary Precipitates Growing by the Ledge Mechanism.	1235-1245A
Alloy 718. Weld deposited coatings, Mechanical properties The Chemistry and Structure of Wear-Resistant, Iron-Base	887-902A	Wiedemann-Franz law See Lorenz number	
Hardfacing Alloys.	983-991A	Wiedemann-Franz ratio See Lorenz number	
Weld metal Effect of Temperature and Composition on Surface Tension in Fe—Ni—Cr Alloys Containing Sulfur.	557-560B	Wire drawing Dislocation Cell Structures and Mechanical Properties of Oxygen-Free High-Conductivity Copper During Wire Draw-	
Weld metal, Microstructure The Origin of Transformation Textures in Steel Weld Metals Containing Acicular Ferrite.	657-663A	ing at Various Speeds. Correction to "Dislocation Cell Structures and Mechanical Properties of Oxygen-Free High-Conductivity Copper During Wire Drawing at Various Speeds".	258-261A 258-261A
Weld metal, Reactions (chemical) Slag—Metal Reactions During Welding. I. Evaluation and Re- assessment of Existing Theories. Slag—Metal Reactions During Welding. II. Theory.	65-71B 73-81B	Wire rod, Heat treatment Microstructural Engineering Applied to the Controlled Cooling of Steel Wire Rod. I. Experimental Design and Heat	
Slag—Metal Reactions During Welding. III. Verification of the Theory.	83-100B	Transfer. Microstructural Engineering Applied to the Controlled Cooling of Steel Wire Rod. II. Microstructural Evolution and Me-	2769-2778A
Welded joints, Heat treatment Aging Characteristics of Electron Beam and Gas Tungsten Arc Fusion Zones of Al—Cu—Li Alloy 2090. Welded joints, Mechanical properties	903-913A	ing of Steel Wire Rod. II. Microstructural Evolution and Me- chanical Properties Correlations. Microstructural Engineering Applied to the Controlled Cool- ing of Steel Wire Rod. III. Mathematical Model— Formulation and Predictions.	2779-2790A 2791-2805A
Microstructure and Local Brittle Zone Phenomena in High- Strength Low-Alloy Steel Welds.	139-149A	Wolfram	E131-2000A
A Phase Diagram Approach to Study Liquation Cracking in Alloy 718.	887-902A	See Tungsten Work functions, High temperature effects	
Further Study on the Scattering of the Local Fracture Stress and Allied Toughness Value.	2287-2296A	The High-Temperature Work Function Behavior of Polycrys- talline Osmium.	1609-1613A
Welded joints, Microstructure The Origin of Transformation Textures in Steel Weld Metals		Work hardening See Strain hardening	
Containing Acicular Ferrite. Solidification Modeling and Solid-State Transformations in	657-663A	Work softening See Strain softening	
High-Energy Density Stainless Steel Welds. Welded joints, Reactions (chemical)	915-926A	Work strengthening	
Slag-Metal Reactions During Welding. I. Evaluation and Re-	65 74D	See Strain hardening	
assessment of Existing Theories. Slag—Metal Reactions During Welding. II. Theory. Slag—Metal Reactions During Welding. III. Verification of the	65-71B 73-81B	Workability See also Formability Hot workability	
Theory. Welded joints, Thermal properties	83-100B	Characterization of Hot Deformation Behavior of Brasses Using Processing Maps. I. α Brass.	2985-2992A
Effect of Evaporation and Temperature-Dependent Material Properties on Weld Pool Development. Computational Modeling of Stationary Gas-Tungsten-Arc	233-241B	Characterization of Hot Deformation Behavior of Brasses Using Processing Maps. II. β Brass and $\alpha-\beta$ Brass.	2993-3001A
Weld Pools and Comparison to Stainless Steel 304 Experimental Results.	243-257B	Yield point Yielding Behavior of Prestrained Interstitial-Free Steel and 70/30 Brass.	393-401A
Welding electrodes Slag—Metal Reactions During Welding. I. Evaluation and Re-		1000 to 1200K Time-Dependent Compressive Deformation of Single-Crystalline and Polycrystalline B2 Ni—40Al.	1595-1607A
assessment of Existing Theories. Slag—Metal Reactions During Welding. II. Theory. Slag—Metal Reactions During Welding. III. Verification of the	65-71B 73-81B	Yield strain See Strain Yield strength	
Theory. Welding fluxes	83-100B	A Model for the Strain-Rate Dependence of Yielding in Ni ₃ Al Alloys.	125-128A
Slag—Metal Reactions During Welding. I. Evaluation and Re- assessment of Existing Theories.	65-71B	Mechanical Behavior of Cast Particulate SiC/AL (A356) Metal Matrix Composites.	
Slag—Metal Reactions During Welding, II. Theory. Slag—Metal Reactions During Welding, III. Verification of the	73-81B	Stress Concentration at a Notch Tip in Unidirectional Metal Matrix Composites.	
Theory.	83-100B	Dynamic Recrystallization During Hot Deformation of Alumi- num: a Study Using Processing Maps.	2339-2348A
Weldments, Mechanical properties Fracture Toughness Behavior of Ex-Service 2.25Cr—1Mo Steels From a 22-Year-Old Fossil Power Plant.	455-468A	On the Constraint Factor Associated With the Indentation of Work-Hardening Materials With a Spherical Ball. Structure and Properties of a Rapidly Solidified Al—Li—	2375-2384A
Welds See Welded joints		Mn—Zr Alloy for High-Temperature Applications. II. Spray Atomization and Deposition Processing.	2515-2522A
Wettability The Wettability of Carbon/TiB ₂ Composite Materials by Aluminum in Cryolite Melts.	617-621B	Yield strength, Cooling effects Microstructural Engineering Applied to the Controlled Cooling of Steel Wire Rod. I. Experimental Design and Heat	
Wetting Composite Growth in Hypermonotectic Alloys.	339-348B	Transfer. Microstructural Engineering Applied to the Controlled Cooling of Steel Wire Rod. II. Microstructural Evolution and Me	2769-2778A
The K ₂ ZrF ₆ Wetting Process: Effect of Surface Chemistry on the Ability of a SiC-Fiber Preform To Be Impregnated by Aluminum.	2133-2139A	chanical Properties Correlations. Microstructural Engineering Applied to the Controlled Cool-	2779-2790A
Wetting agents The K ₂ ZrF ₈ Wetting Process: Effect of Surface Chemistry on		Formulation and Predictions. Yield strength, Corrosion effects	2791-2805A
the Ability of a SiC-Fiber Preform To Be Impregnated by Aluminum.	2133-2139A	Microstructure Property Relationships and Hydrogen Effects in a Particulate-Reinforced Aluminum Composite.	2445-2450A
Whisker composites, Mechanical properties Dynamic Fracture Behavior of SiC Whisker-Reinforced Aluminum Alloys. White iron, Corrosion	367-375A	Yield strength, Cryogenic effects The Effect of Through-Thickness Anisotropy on the Cryo genic Mechanical Properties of an Al—Cu—Li—Zr Allo (Vintage III 2090-T81).	1789-1799A
Modeling of the Corrosion Behavior and Its Interrelation With the Deformation Behavior and Microstructure in a Newly	2210 0225	Yield strength, Deformation effects The Effect of Plastic Deformation on Al ₂ CuLi (T ₁) Precipita	200 000
Developed 7.5Mn—5Cr—1.5Cu Alloy White Iron. White iron, Metallography	2319-2325A	Yielding Behavior of Prestrained Interstitial-Free Steel and	299-306A
Use of Differential Interference Contrast Microscopy to Detect Duplex Carbides in Alloy White Cast Irons.	1673-1674A	70/30 Brass. Prediction of Steel Flow Stresses at High Temperatures and	
White iron, Microstructure On the Nature of Eutectic Carbides in Cr—Ni White Cast		Strain Mates. Recrystallization Controlled Rolling and Accelerated Cooling for High Strength and Toughness in V—Ti—N Steels.	1545-1558A 2681-2694A
Irons. White iron, Phases (state of matter) Solidification and Phase Equilibria in the Fe—C—Cr—NbC	1709-1720A	Yield strength, Heating effects Elastic Moduli and Tensile and Physical Properties of Heat Treated and Quenched Powder Metallurgical Ti—6AI—4\)	
System.	2181-2186A		709-714A

Correction to "Elastic Moduli and Tensile and Physical Prop- erties of Heat-Treated and Quenched Powder Metallurgical Ti—6AI—4V Alloy".	1129A
Yield strength, High temperature effects Effect of Long-Term Service Exposure on Microstructure and Mechanical Properties of a CrMoV Steam Turbine Rotor	
Steel.	1811-1820A
Yield strength, Microstructural effects Dislocation Cell Structures and Mechanical Properties of Oxygen-Free High-Conductivity Copper During Wire Draw- ing at Various Speeds.	258-261A
Correction to "Dislocation Cell Structures and Mechanical Properties of Oxygen-Free High-Conductivity Copper Dur-	
ing Wire Drawing at Various Speeds". The Role of the γ/γ Eutectic and Porosity on the Tensile Behavior of a Single-Crystal Nickel-Base Superalloy.	258-261A 1443-1451A
Effect of Phase Morphology on the Mechanical Behavior of Two Titanium Aluminide Composites.	2009-2019A
Effect of Grain Size on High Strain Rate Deformation of Cop- per.	2349-2357A
Yield strength, Stress effects Hydrostatic Stresses and Their Effect on the Macroflow Behavior and Microfracture Mechanism of Two-Phase Alloys.	2695-2702A
Yield strength, Temperature effects Establishment of a General Formula for Fractional Softening.	2160-2162A
Yield stress See Yield strength	
Youngs modulus See Modulus of elasticity	
Yttrium, Alloying elements On the Role of Yttrium During High-Temperature Oxidation of an Ni—Cr—Al—Fe—Y Alloy.	1463-1465A
Yttrium base alloys, Reactions (chemical) Thermochemistry of Binary Alloys of Transition Metals: the Me—Sc, Me—Y, and Me—La (Me = Silver, Gold) Sys-	
tems Zinc, Binary systems	1103-1111A
Thermodynamics of Binary Systems Using Interaction Parameters.	593-605B
Zinc, Coatings The Relationship Between Plastic Anisotropy of Steel Sheet and Temper Rolling Strain.	2156-2160A
Zinc, Extraction Heat-Transfer Phenomena in Water-Cooled Zinc-Furning Furnace Jackets.	163-175B
Zinc, Mechanical properties Application of Analytical Techniques to Stress Relaxation Experiments in Commercial Zinc.	2303-2307A
Zinc, Microstructure The Geometry and Properties of Ledges in Interfaces.	1177-1183A
Zinc base alloys, Coatings The Effect of Continuous Heating on the Phase Transformations in Zinc—Iron Electrodeposited Coatings.	1737-1743A
Activation Energy of δ-Γ ₁ Transformation in a Zn—Fe Electro- deposited Coating.	1887-1888A
Zinc base alloys, Mechanical properties Quantitative Assessment of the Implications of Strain- Induced Microstructural Changes in Superplasticity. High-Damping Metals and Alloys.	83-96A 607-616A
Characterization of the Damping Properties of Die-Cast Zinc—Aluminum Alloys.	617-622A
Zirconates, Composite materials Pressure Casting of a Zirconia-Toughened Alumian Fiber-Reinforced NiAl Composite.	3059-3064A
Zirconium, Alloying elements Solidification Microporosity in Directionally Solidified Multi-	
component Nickel Aluminide. Effects of Microalloving Elements and Heat Treatments on	225-234A
Grain Boundary Pest of Boron-Doped Ni ₉ Al at 1200°C. The Effect of Copper, Chromium, and Zirconium on the Mi-	256-258A 1801-1809A
crostructure and Mechanical Properties of Al—Zn—Mg— Cu Alloys.	2809-2818A
Zirconium, Mechanical properties Fracture Initiation at Hydrides in Zirconium.	2327-2337A
Zirconium, Metal working Processing Map for Hot Working of Alpha-Zirconium.	829-836A
Zirconium base alloys, Corrosion Delayed Hydride Cracking Behavior for Zircaloy-2 Tubing. Effects of Transformation on Texture and Iodine Stress Cor-	2049-2060A
rosion Gracking Hesistance of Zircaloy Sheet.	2247-2256A
Zirconium base alloys, Phase transformations Determination of Equilibrium Solid-Phase Transition Temper- atures Using DTA.	1993-1998A
Zirconium compounds See also Zirconates	
Zirconium compounds, Mechanical properties A Simple, Versatile Miniaturized Disk-Bend Test Apparatus for Quantitative Yield-Stress Measurements.	2061-2068A
Zirconium compounds, Microstructure Development of Structure and Porosity in Cast Al ₅ CuZr ₂ and	
Al ₈₈ Mn ₉ Zr ₂₅ Intermetallic Compounds.	2545-2552A



